AERO-HYDRODYNAMIC BEHAVIOUR OF WATER BORNE WIGCRAFT

An Experimental, Numerical Modelling and Simulation Study

By

Pereowei Garrick Ombor

A thesis submitted for the degree of Doctor of Philosophy

School of Engineering

(Marine, Offshore and Subsea Technology Group)

NEWCASTLE UNIVERSITY

August 2023

ABSTRACT

This thesis makes an in-depth investigation on the aerodynamic, hydrodynamic and coupled aero-hydrodynamic behaviors of the water-borne Wing-in-ground effect marine vehicle (WIGcraft) via the development of semi-empirical and numerical tools to evaluate the behaviour of a waterborne WIGcraft model. Semi-empirical models and three potential flow-based numerical simulation models namely, hydrodynamic model for single-/multi-hull planing Outrigger model, ground effect aero-hydrodynamic model for air borne WIGcraft model, and aero-hydrodynamic model for water borne WIGcraft model were developed to investigate the effects associated with coupling wings to a planing boat. The hydrodynamic model was developed by extending the 2.5D theory to non-similar planing hulls. The ground effect aero-hydrodynamic models for air borne and water borne WIGcraft were developed by implementing a numerical slender wing/body theory in a manner analogous to the 2.5D theory to account for the strong nonlinear 3D flows and free surface deformation within the small gap of the WIG-craft moving at constant speed with its wings near undisturbed water surface. As an alternative to the application of image methods commonly used for planar ground effect studies of wings and airfoils, momentum conservation and flow continuity principles were innovatively enforced at the air-water interface through an iterative algorithm. The aero-hydrodynamic models essentially combine the hydrodynamic model and ground effect aerodynamic model at the air-water interface. The three numerical models were validated by means of numerical simulation results obtained from Vortex Lattice Method based Autowing code, as well as with results from captive model experimental tests carried out for an outrigger ship and WIGcraft models. The result from a linear superposition of aerodynamic and hydrodynamic forces and that of a non-linear coupling of the hydrodynamic and aerodynamic models suggest the existence of non-linearities that have a non-negligible effect on the waterborne WIGcraft. This study shows the significance of ground effect, hull generated spray and non-linear coupling effects on the WIGcraft, the correct location, aerodynamics, geometric and structural design of the wings near free surface water, as well as the hull design and stability of a moving water borne WIGcraft.

Acknowledgement

I am immensely grateful to my main supervisor, Professor Zhiqiang Hu who has been patient, encouraging and supportive throughout this study. He introduced me to the rudiments of carrying out a research study and writing out findings as against writing engineering reports. Besides, his invaluable advice, guidance and suggestions concerning the fulfilment of my academic and administrative requirements as a postgraduate student, he made sure the WIGcraft model was built to specification and that I have access to an appropriate towing tank facility. Many thanks to Dr. Yongchang Pu, my co-supervisor, for standing by me during this study. I will never forget to mention the Dean, School of Engineering, the head of school and other administrative staff in Marine, Offshore and Subsea Technology group who ensured the atmosphere on campus is good for research. To all the academic staff and students of the Marine and Offshore and Subsea Technology group at Newcastle University who in one way or the other were helpful to me, thank you.

I also want to acknowledge and appreciate Tertiary Education Trust Fund (TETFund), Nigeria for the grant awarded me between September 2017 and September 2020 of this study. I wish to say thank you to Chief Naval Architect Cotty Fay of Cotty Fay Marine Design Inc., USA for providing the 3D CAD model of the WIGcraft as well as supporting information about the design of the model. I also want to thank Prof. Nikolai Kornev of University of Rostock, Germany for providing me with a free copy of the Autowing code he co-developed. I wish to also say thank you to Dr, Stefan Harries and FRIENDSHIP SYSTEMS AG, Germany for granting me license to access the commercial version of CAESES software. Though the software was not used at the later stage of this study, it will be immensely useful in future studies.

Let me also express my gratitude to Professor Liu of Huazhong University of Science and Technology (HUST), Wuhan, China, who made sure I was granted Chinese visa to carry out the experiment. He also ensured I was comfortable and well taken care of throughout my stay in China. I wish to say thank you to my friends ‘Fish Voyage’, ‘Ablank’ and Fangjuan for all the outings that took off some of the pressures during the period of the experiments in Wuhan. My special thanks also go to Dr. Song who worked tirelessly in the hydrodynamic laboratory at HUST to conduct the experiments as accurately as possible. I will also express my thanks to the HUST hydrodynamic laboratory personnel and postgraduate students, including Dr. Yang, Miss Xiao mei and others who assisted in one way or the other to make sure I successfully completed the experiments on schedule.

To my wife, Oshuare, and mother of my three handsome boys, Pharez, Tamaralayafa and Tarila, words are not enough to express my gratitude for all your patience at the critical times of this study. I wish to also thank members of my family, my mum, Daeria, my siblings Bunnette, Ebikake, Akpobouloukemi, Patricia, and Theresa for all their moral support. Thanks to my friends, A.S. Ebifemi, J.T. Abam, I. Emmanuel and others, too many to mention who were very supportive during this study period.

I am alive today is because God made it possible for the NHS England to diagnose, carry out surgery and support my physical and mental wellbeing during the later part of this study. So, my special thanks to the NHS and the Doctors at Saville Medical Group, Newcastle.

To God Almighty be the glory

Contents

List of Figures

List of Tables

Nomenclature

AoA	Angle of attack.
b_h	Wetted beam.
b_a	Wingspan.
$b_{ah} = b_a\sqrt{\Upsilon}$	Equivalent hydrodynamic surface beam of the wings.
c	Mean aerodynamic chord length of the wings.
${C_{Dchv}}^{eh}$	Viscous drag components on hull bottom pressure area.
${C_{Dhydmod}}^{eh}$	Empirical hydrodynamic pressure lift induced drag component.
${C_{Dhs}}^{eh}$	Whisker's spray drag components.
${C_{Diff}}^{ea}$	Induced drag coefficient of a wing in free flight.
${C_{Dige}}^{ea}$	Aerodynamic lift induced drag of an airborne WIGcraft
$\Delta{C_{Dige}}^{ea}$	Reduction in the free flight aerodynamic lift induced drag caused by the nearness of the wings to the ground surface.
${C_{DOutr}}^{ma}$	Drag coefficient deduced from the measured drag on Outrigger model
C_{Dpoa}	Parasitic drag coefficient of air borne vehicle.
${C_{DWIG}}^{ma}$	Drag coefficient deduced from measured drag on WIGcraft model,
C_{fp}	Friction coefficient for pressure surface area
C_{fr}	Friction coefficient accounting for hull planing surface roughness
$C_{fpr} = C_{fp} + C_{fr}$	
${C_{Lff}}^{ma}$	Measured aerodynamic lift coefficient at free flight,
${C_{Loutrg}}^{ma}$	Lift coefficient derived from the measured lift on the Outrigger model.
C_{Lsp}	Hull generated water spray lift coefficient,
${C_{LWIG}}^{ma}$	Lift coefficient derived from measured lift on the WIGcraft model.
C_{∇}	Savitsky equation correction factor for non-prismatic hulls
d	Operating draught of the vehicle
d_h	Finite depth of seabed
D_{AH}	Multivariate multiple regression expression for aero-hydrodynamic drag
D_{hs}	Total viscous force in the spray area
D_{P0A}	Viscous parasitic (zero lift) drag for subsonic air borne vehicle motion.
D_{TSF}	Total drag force on the accelerating WIGcraft.
G	Green's function

h_{wk}	Height of the trailing edge of wing from the keel.
h_{te}	Height of the trailing edge of the wing from the free surface water.
K_d	Savitsky equation correction factors for non-prismatic hulls.
k_{gc}	Factor which depends on the relative clearance height of the wings
ns1	Constant independent of draught
K_{hsp}	Hull form dependent factor, and its value is independent of operating draught and trim angle.
K_{id}	Proportionality factor regarded as the drag-due-to-lift factor.
K_T	propulsion constant
K_{wsp}	Factor which may be associated with the characteristics of the wings and its location on the spray area of the hull.
$L_{age}{}^{ma}$	Measured aerodynamic lift under pure ground effect (no spray effect)
L_{AH}	Multivariate multiple regression expression for aero-hydrodynamic lift
L_c	Chine wetted length,
L_k	Keel wetted length.
$L_{Outrg}{}^{ma}$	Measured lift on Outrigger model
I	Moment of inertia of the model about the y axis
L_{TSF}	Total steady lift force acting on the accelerating WIGcraft
$L_{WIG}{}^{ma}$	Measured lift on WIGcraft model
l_{wl}	Length of waterline
L_{ws}	Characteristic length of whiskers spray
L_{ZB}	Hydrostatic force on accelerating WIGcraft
M_{AH}	Multivariate multiple regression expression for aero-hydrodynamic moment
m_d	Mass displacement of the WIGcraft model
M_T	Moment of the thrust force.
M_{TSF}	Moment on the accelerating WIGcraft
n_{gc}	Factor associated with the experimental facility/method used to measure aerodynamic lift,
ns1	Constant independent of draught
P	Pressure
P_a	Atmospheric pressure
R_A	Aspect ratio of the wings

R_e, R_{es}	Reynolds number, $R_e = \frac{V_1 \lambda b_h}{\nu}$, $R_{es} = \frac{V_0 L_{ws}}{\nu}$
R_{es_cri}	Critical Reynolds number
S_a	Reference wing area
SCC	Solution control cross plane
S_{wet}	Wetted area of the wing,
S_a	Characteristic (reference) area of the wings.
T_F	Required thrust force on accelerating WIGcraft
U	Boat speed (m/s)
V_0	Whisker spray velocity,
V_1	Average hull bottom velocity
VCG	Vertical centre of gravity
WPA	Water plane area
W_x, W_z	Respective components of the weight of WIGcraft model in the x and z direction of the coordinate system
$x_{ah} = \frac{b_{ah}}{b_h}$	
x_{BM}	Longitudinal buoyancy moment arm
x_c	Chine immersed section
Z_{CH}	Maximum beam
α	Sum of the wing incident angle and the trim angle of the hull
α_0	Zero lift angle of attack of the wings
$\alpha_{eff} = \alpha - \alpha_0$	Effective angle of attack of the wings of the WIGcraft
α_{hyd}	Angle between the stagnation line and the keel
e	Oswald span efficiency factor
ε	Inclination of thrust line relative to keel.
ϵ	Slenderness parameter
$\Delta\lambda_{hs} {b_h}^2$	Effective whisker spray area outside pressure hull bottom
∇	Displacement volume of the hull model
λ	Mean wetted length to beam ratio.
θ_s	Angle between the spray leading edge and the keel
$\Theta = \frac{\theta_s}{\cos\beta}$	
Λ_{LE}	Swept angle
ν	Kinematic viscosity of water.

Υ	Relative air density with respect to water density at the air-water interface.
ρ_a	Air density
ρ_w	Water density
τ	Trim angle
ϕ_1	Velocity potential in water domain
ϕ_2	Velocity potential in air domain
Φ_1	Total potential function in water domain
Φ_2	Total potential function in air domain
ϕ_{IF}	Velocity potential at the air-water interface
ϕ_{1t}	Acceleration potential
ζ	Free surface geometry
λ	Wavelength
Γ	Flow circulation

Superscripts

ma	Measured quantity,
ema	Equivalent hydrodynamic value of the measured aerodynamic quantity.
ea	Empirical aerodynamic quantity
eh	Empirical hydrodynamic quantity.
eha	Equivalent hydrodynamic value of the empirical aerodynamic quantity

Chapter 1: Introduction

1.1 Background and Motivation

The design of a super-fast marine craft with minimal resistance demands the inclusion of aerodynamic lifting components to lift the craft above the water (Yun et al., 2010) . Such hybrid marine crafts are in need for passengers' ferry, search and rescue operations, and conveyance of workers to and from offshore energy fields.

The Wing in Ground effect vehicle (WIGcraft) (see Figure 1.1) is seen to be a powerful vehicle with the potential to effectively combine the advantages of aircraft's speed and comfort together with the high safety, energy efficient and large payload characteristics of ships. The feasibility of an airborne WIGcraft to take advantage of ground effect phenomenon to improve its lift to drag ratio and reduce its fuel consumption and power requirement per payload compared to low-speed free flight airplanes (of the same capacity) have been demonstrated in theory and practice.

Figure 1.1 WIGcraft Model

However, the transport efficiency and economic viability of the WIGcraft has been bedevilled by frequent crashes during its take-off and huge hump drag that must be overcome to lift the boat above the water surface for airborne cruising. (Benedict et al., 2002; Paek, 2006). As a result, the WIGcraft requires a high capital cost to purchase large and more expensive engines, which are mainly needed to provide sufficient thrust to overcome the huge hump drag near take-off. Unlike airplane where more engine power is required at higher altitude, the engine of a WIGcraft becomes under-utilized and operate inefficiently at higher cost margin as soon as the vehicle becomes airborne. Thus, it is apparent that the water borne acceleration mode of the

vehicle prior to take-off plays a major role in the development of a commercial-ready WIGcraft. Several high lift devices have been suggested by aerodynamicists from aerodynamic perspective to improve take-off capability with lesser engine power. However, these devices often fall short to resolve this challenge. There is still a lack of understanding on how to tackle the take-off efficiency problem (Kornev and Matveev, 2013). The take-off and stability challenges can be regarded as a hydrodynamic problem complicated by the presence of aerodynamic forces to varying degree. It thus requires a hydrodynamic model extended by aerodynamic theories to predict the behaviour of the vehicle during its water borne operation. Unfortunately, the study of the dynamics of WIGcraft has largely been reserved for aerodynamicists.

The renewed interest in a new class of WIGcraft vehicle by U.S. Defense Advanced Research Projects Agency (DARPA/TTO, 2021) for addressing challenges encountered by traditional sea and air lift platforms in maritime theatres, attests to the frontier technology behind WIGcraft vehicles. Some of the operational limitations of WIGcrafts stated by DARPA including high sea state and congested water operations may be addressed by a WIGcraft designed to operate efficiently on water just as any conventional high-speed watercraft. In a research project carried out at Cranfield University, UK for the development of future viable marine transport vehicle, the proposed vehicle by the group of researchers was one with combined aerodynamic and hydrodynamic boat weight alleviation. Collu (2008) described this class of hybrid marine vehicle as Aerodynamically Alleviated Marine Vehicle (AAMV) as long as the vehicle possesses the quality of exploiting ground effect aerodynamic lift generated by one or more aerodynamic surfaces during its water borne cruise mode.

Collu's AAMV is essentially a WIGcraft designed to operate with its lower portion submerged on water, such that the weight of the vehicle is alleviated by equal magnitude of aerodynamic and hydrodynamic forces. With the presence of the aerodynamic surfaces, it is expected that the payload efficiency when operating in this water borne mode will be higher than the typical wing-less high-speed marine vehicle due to the improved total lift associated with additional lift generated by the aerodynamic surfaces near the ground. Similarly, the WIGcraft is expected to have a higher payload efficiency in this operational mode compared to a WIGcraft in airborne mode due to the coupled hull-generated hydrodynamic lift and wing-generated ground effect aerodynamic lift. Overall, the transport efficiency and safety of the WIGcraft in the water borne mode is expected to be superior to planing vessels, airplanes of similar size and WIGcraft in airborne operational mode near free surface (Collu, 2008). Interestingly, like the other studies on WIGcraft, the studies on AAMV were mainly directed at investigating the dynamic

longitudinal stability of the hybrid vehicle in calm water and in waves (Collu, 2008; Williams, 2009; Adhynugraha, 2017). This approach to studying the dynamics of ground effect hybrid marine vehicles closely follow that typically used in aircraft flight mechanics and has been the source for the establishment of very important stability and control criteria for WIGcraft.

Beyond any reasonable doubt, the establishment of dynamic stability envelop is crucial for the development of any high-speed hybrid marine vehicle (a vehicle alleviated both aerodynamic and hydrodynamic forces) operating at the air-water interface. It is a well-known fact that a high-speed marine vehicle with adequate static stability may lose its stability while underway as its speed increases, which may result in behaviours such as porpoising, bow diving (submarining effect), unexpected take-off from water surface, chin walking, continuous heeling and other coupled motions which are associated with dynamic instability (ITTC, 2008). On the other hand, a dynamically stable watercraft has inherent static stability. Hence, for a hybrid vehicle such as a WIGcraft with transient aerodynamic and hydrodynamic characteristics, this area of research (WIGcraft stability studies) requires some very serious consideration. Thankfully, a fairly large body of literature and theoretical models for investigating the dynamic stability of hybrid marine vehicle, planing watercraft as well as airborne and water borne WIGcraft do exist (Adhynugraha, 2017; Blount and Fox, 1976; Hicks et al., 1995; Kornev et al., 2010)

It is very important to note that dynamic stability studies of any fluid borne vehicle essentially depend on accurate estimation of the prevailing dynamic forces, from which the stability derivatives are generated (Hicks, 1993; Payne, 1974). An erroneous estimation of the dynamic forces means an incorrect stability prediction. In the linear stability models, the aerodynamic and hydrodynamic derivatives may be combined based on the principle of superposition to study the motions and/or dynamic stability of a fluid borne WIGcraft (Collu, 2008; Collu et al., 2009; James and Collu, 2015). In doing this, the aerodynamic and hydrodynamic stability derivatives may be theoretically estimated from forces derived independently from (linear or nonlinear) separate aerodynamic and hydrodynamic models.

In practice, it is evident that nonlinear effects (ground effects, free surface deformation, hull-generated spray impinging on wings; and draught and trim angle variations) do exists. These nonlinear effects significantly influence the magnitude of the dynamic forces and stability derivatives and can only be better accounted for by nonlinear coupling of the aerodynamic and hydrodynamic models. As a result, it is probable that the independently and separately determined aerodynamic and hydrodynamic forces from which Collu (2008, 2009) and James

and Collu (2015) determined their stability derivatives are inaccurate. As such, the stability derivatives and the results of their stability analysis of the water borne WIGcraft (or AAMV) may be questionable. A similar concern was raised by Adhynugraha (2017); however, his work does not account for the nonlinear effects due to hull-generated spray and aero-hydrodynamic coupling.

A nonlinear coupled aero-hydrodynamic flow modelling and simulation of the rigid body motions is a more holistic approach for studying the dynamic behaviour of the vehicle. From such studies, a more accurate aerodynamic and hydrodynamic stability derivatives may be determined. A comparative study on linear and nonlinear coupling of the aerodynamic and hydrodynamic components of a water borne WIGcraft may be necessary to ascertain the extent of nonlinear effects on the dynamic behaviour of the vehicle.

The focus of this current study is on empirical and numerical modelling, and simulation of a WIGcraft moving at high speed with its hull(s) submerged in water. The wing-in-Ground Effect marine vehicle considered in this study refers to a marine vehicle whose weight can be alleviated by forces generated by its aerodynamic and hydrodynamic surfaces. To the best of the author's knowledge, semi-empirical and potential flow based nonlinear coupled aero-hydrodynamic numerical or analytical model for predicting the dynamic behaviour of water borne WIGcraft is scarcely seen in existing literature. This study attempts to fill this gap. This study for the first time, directly provides a novel model for solving the nonlinear coupled aerodynamic and hydrodynamic flow problem due to wings near a free surface disturbed by the presence of a submerged hull(s) moving at high speed. The coupled aero-hydrodynamic effects on the vehicle are predicted using results generated by the proposed semi-empirical formulations and numerical models.

The original intent of this study is to develop practical and simple-to-implement engineering type theoretical solutions to the aero-hydrodynamic flow problems of a water borne WIGcraft. This basically over-rules the 3D numerical model solutions and effectively reduces the model development choices to either empirical model, 2D numerical or analytical models. The development of empirical and closed form 2D analytical solutions to the aero-hydrodynamic flow problems of WIGcraft operating with part of its hull submerged on water can provide a general insight into the physics of the aero-hydrodynamics of the vehicle at minimal computational cost. The significance of important variables of the problems and their inter-dependence for preliminary design purposes may also be clearly defined. The analytical models in particular are very useful for optimization of vehicle's control system. However, closed form

solutions are more suited for basic sectional geometry of the rigid body, whereas complicated mathematical representation of the flow problem may arise when higher order elements are used to define sectional geometry. Closed form solutions are generally known to have inherent limited application for practical purposes. They break down in situations where the small parameter (e.g., angle of attack and/or ground clearance) and other linear approximations do not apply.

On the other hand, the numerical solution approach is more appropriate, especially when considering the existent nonlinearities in the aero-hydrodynamic flow problems of water borne WIGcraft. The numerical models offer a means to incorporate the nonlinear dynamic effects into the proffered approximate solutions. Nevertheless, it is advantageous to open the solution space to make use of closed form solutions or semi-empirical expressions together with the numerical models where necessary to solve posed aero-hydrodynamic problems. In this thesis, effort is made to formulate empirical and numerical prediction tools to describe the fundamentals of the aero-hydrodynamic problems and the physical characteristics of the solutions to the aero-hydrodynamic problems of a water borne WIGcraft.

1.2 Research Questions and Gaps to fill

Aerodynamics and airplane flight mechanics are very broad research areas, just like hydrodynamics and ship motions studies. The study of a WIGcraft operating on calm water or seaway essentially requires,

- good understanding of aerodynamics and airplane flight dynamics,
- good understanding of hydrodynamics and ship motions in calm water and seaway,
- general knowledge of methods needed to couple both disciplines under appropriate conditions.

It becomes apparent that very extensive studies, careful abstraction of necessary information and critical thinking for practical application of the acquired information are needed to develop theoretical aero-hydrodynamic coupled models for predicting the behaviour of a water borne WIGcraft. Two pertinent questions whose answers form the body of this thesis, and which describes the behaviour of water borne WIGcraft are;

1. What are the compatible theoretical, aerodynamic and hydrodynamic models and their coupling approach required to study the aero-hydrodynamic behaviour of a water borne WIGcraft?

2. Can a reliable and time-efficient nonlinear theoretical model be developed for assessing the aero-hydrodynamic behaviours of a WIGcraft moving on water?

To answer the first question an extensive literature review of various existing aerodynamic and hydrodynamic theoretical models was carried out with a clear objective of identifying robust, adjustable and applicable theoretical models for the development of suitable aero-hydrodynamic empirical and numerical simulation models. A large amount of time and effort in this thesis was spent to carefully study these theoretical models, with a view to finding the suitable models that account for non-linearities and enables easy and reliable coupling of the aerodynamic and hydrodynamic components, and possibly account for the motions of the WIGcraft and free surface. The chosen models are further required to be easily solved with reasonable accuracy, at minimal computational cost and time. These considerations make the process of choosing the suitable models and formulation of the proposed empirical and numerical simulation models of a water borne WIGcraft very challenging and time-consuming during the study.

Using the information gathered from the answers to the first question, attempt was made in answering the second research question by developing a simple semi-empirical model for predicting the total lift and drag forces of a water borne WIGcraft whose wings are subjected to hull-generated spray influence. Three reasonably accurate and computationally efficient numerical simulation models were also developed to directly attack the nonlinear coupled aero-hydrodynamic problem. In the present study, a 2D+t (2.5D) potential flow-based iterative boundary element numerical models were developed to estimate the coupled aero-hydrodynamic forces on the WIGcraft in line with the slender body/wing theory. The models are developed such that their accuracy may be improved by incorporating closed form viscous flow model. The empirical and numerical models provide significant insight into the behaviour of water borne WIGcraft as regards aero-hydrodynamic coupling effects, spray effect and ground effect.

Owing to the fact that it is difficult to come by aerodynamic, hydrodynamic and fluid flow data of a water borne WIGcraft in available literature, fully captive model experiments were conducted (in addition to using the popular vortex lattice method Autowing code) to validate the empirical and numerical models. The results of the experiments were also used together with the appropriate equation of motion to simulate the acceleration to take-off motions of the vehicle (Pereowei et al., 2020).

1.3 Aims, Objectives and Contributions of the Thesis

To improve the transport efficiency of military, search and rescue and commercial water-based transport vehicles in these modern times, it is of primary interest in this study to develop empirical and aero-hydrodynamic tools for predicting the dynamic behaviour of a water borne WIGcraft. The models should be able to capture nonlinearities and coupling effects associated with water borne WIGcraft of arbitrary configurations. Due to the limitations of Reynolds Average Navier-Stokes Equation (RANSE) based CFD solution for the purpose of conceptual/preliminary design and analysis of the aero-hydrodynamic behaviour of fluid borne vehicles with complex fluid flow characteristics, it is desired that the proposed models are robust, reasonably accurate and can be implemented on desktop computers at reasonable computational time expense.

1.3.1 Aims

This thesis aims at contributing to the field of the aero-hydrodynamics of high-speed marine transport vehicles by developing coupled aero-hydrodynamic simulation tools for simulating and evaluating the behaviour, including coupling effects of a water borne WIGcraft of arbitrary configuration.

1.3.2 Objectives

The objectives of the study are to,

1. develop and validate a numerical hydrodynamic model suitable for single-/multi-hull ships such that it can be coupled to an aerodynamic model,
2. develop and validate a numerical aerodynamic model that can be coupled to the hydrodynamic model in item 1 above,
3. couple the proposed numerical aerodynamic and hydrodynamic models in a nonlinear manner to form a nonlinear aero-hydrodynamic model and validate the model,
4. formulate and validate empirical models for predicting the dynamic lift and drag forces on a water borne WIGcraft whose wings are subjected to hull-generated water spray,
5. carry out extensive fully captive model experiments and use the results to validate all the above proposed models,
6. Investigate the existence of nonlinear coupling effects in relation to linear and nonlinear coupling of aerodynamic and hydrodynamic components,

7. Develop a simple simulation model from the experimental data to simulate the acceleration to take-off phase of a water borne WIGcraft.

1.4 Thesis Structure

This study is divided into four parts, namely,

a. extensive literature review on planing watercraft, Air borne, and Water borne WIGcraft (Chapter 2)
b. development and validation of three numerical simulation models for analysis of air borne and waterborne WIGcraft (Chapters 3 to 5, and 7),
c. experimental studies and results analysis (Chapter 6),
d. Formulation and validation of empirical models for the lift and drag forces on planing watercraft, air-borne and water borne WIGcraft (Chapter 6), as well development of a simulation model based on experimental data to predict the acceleration to take-off behaviour of a water borne WIGcraft (Chapter 8).

This section with the aid of Figure1.2 summarizes the details of the remaining chapters of thesis.

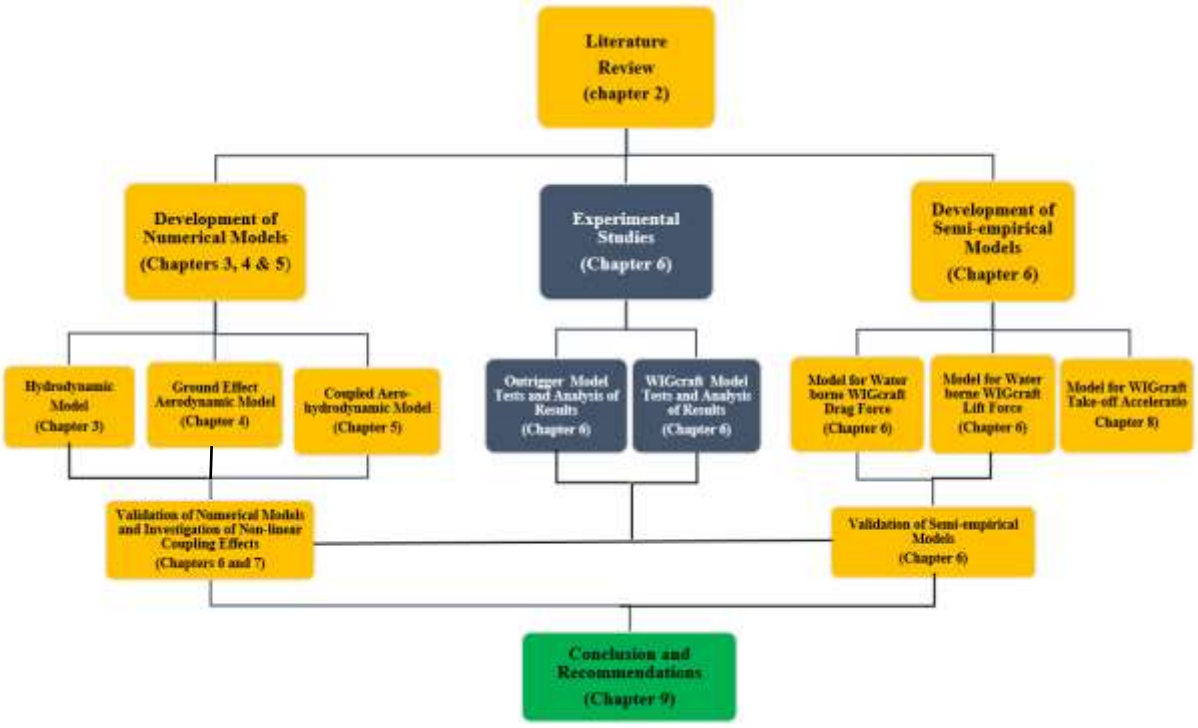

Figure 1.2 Thesis Structure

Chapter 2 reviews existing literatures on WIGcraft developments over the years. The chapter extensively discusses assumptions and salient features of numerous existing analytical, empirical, numerical, and experimental methods available to model the fluid flow characteristics, forces, and dynamic behaviour of related airborne and water borne vehicles. The applicability of these methods for developing water borne WIGcraft simulation models are considered. The literature review is geared towards finding the suitable and computationally less expensive methods that account for non-linearities, enables easy and reliable coupling of the aerodynamic and hydrodynamic components of the boat and capable of giving results to engineering accuracy while elucidating the engineering insights into the design of the vehicle. These considerations make the process of choosing the suitable analysis method and formulation of the simulation model of the WIG boat very challenging and time-consuming during the study. The justification of chosen methods is discussed.

A newly developed 2.5D theory for modelling the hydrodynamic behaviour of a monohull and multi-hull high speed marine vehicles is presented in chapter 3. Boundary element method which accounts for flow separation and spray detachment was used to numerically solve the formulated hydrodynamic potential flow problem of water impacting 2D transverse sections of the experimental model with wings. The model developed is designed to capture non-linearities associated with the moving vehicle, as well as the upstream flow influence on the hydrodynamics of the downstream sections. Hydrodynamic forces and moments of all sections of the vehicle were integrated using Simpson's rule to estimate the total hydrodynamic forces on the vehicle. Adams Bashforth time-stepping method was proposed to simulate the advancement of the free surface. This chapter also presents the solution method to the formulated hydrodynamic problems. The developed numerical model is validated against results from the fully captive model experiments on the model without attached wings is discussed in chapter 7.

In chapter 4, a new ground effect aerodynamic numerical model based on slender wing theory for predicting the behaviour of a low aspect ratio wing with anhedral planform operating near rigid and deformable calm water. To ensure confidence in the validity and application of the model for investigation purposes, results of the numerical model are compared with both captive model experiments on a WIGcraft model, and the popular vortex lattice method based Autowing code. The findings from using the validated numerical model may be used to investigate the free surface deformation and wing performance when moving near the calm water in comparison to free flight.

Chapter 5 presents a newly developed nonlinear aero-hydrodynamic simulation model for investigating the behaviour of the water borne WIGcraft at constant speed. This model is developed by iteratively coupling the ground effect aerodynamic model of the non-planar low aspect ratio wings discussed in chapter 4 and the hydrodynamic model for high-speed multi-hull vessels discussed in chapter 3. The results from this time domain simulation model are also validated against the WIGcraft experimental results in chapter 7.

Alongside the formulation of the empirical models, Chapter 6 presents the fully captured experimental tests on a scaled multi-hull watercraft model with two different configurations, one configuration equipped with wings, the other without wings. The uncertainties associated with the experiments are quantified and discussed. The experimental results are presented in a form of non-dimensional coefficients suitable for summation of the hydrodynamic and aerodynamic component force coefficients by using a newly proposed equivalent hydrodynamic force concept. The aerodynamic contributions to the total lift and drag experienced by the scaled water borne WIGcraft model determined from the experimental results are discussed in relation to the model configuration without wings. This chapter also illustrates how the post-processed results from the experiments are utilized for predicting the effect of the vehicle's running trim angle and draught on the fluid forces acting on both model configurations. To help interpret certain implicit characteristics (such as ground effects, spray effects etc) from the model results, semi-empirical models were formulated. These models were compared with the experimental results. Also discussed in this chapter are the applications of the findings from the semi-empirical models to support the design, safe and efficient operation of WIGcraft moving at constant speed on water.

In chapter 7, results from the Autowing code and the model experiments were used to validate the numerical models developed in the chapters 3, 4 and 5. Results from linear and non-linear coupling of the proposed aerodynamic and hydrodynamic models are compared to examine the veracity of the aerodynamic and hydrodynamic non-linear coupling effect. The discussion on the results of the aero-hydrodynamic model developed in chapter 5 together with the results from the models developed in chapters 3 and 4 provides sufficient insight into the dynamic behaviour of the water borne WIGcraft.

The utilization of the experimental results for simulating the acceleration to take-off phase of the WIGcraft is presented in Chapter 8. A multivariate multiple regression method was used to develop model equations that fits the measured aero-hydro dynamic lift, drag and moment data as a function of draught, speed and trim angle. The Newton's equations of motion were

presented in state-space form and solved using the fourth order Runge Kutta method. The take-off characteristics of the water borne WIGcraft are described with respect to speed and time.

Chapter 9 concludes the thesis. It summarizes the answers to the research questions, aim and objectives and other findings from the study. Recommendations for future studies are also discussed in this chapter.

1.5 Contributions and Findings

The major contributions of this study to the body of existing literature are summarized below.

1. The 2.5D or 2D + t slender body theory was extended to predict the hydrodynamic behaviour of non-similar planing multi-hull ships.
2. The numerical slender wing theory in Drela (2014) was extended by implementing the 2.5D or 2D+ t theory and fluid mass and momentum conservation at the air-water interface to estimate the nonlinear aerodynamic characteristics of a low aspect ratio wing or fluid borne vehicle moving near free surface water.
3. A new numerical model was developed to predict the coupled aero-hydrodynamic behaviour of a waterborne WIGcraft moving on calm water.
4. This study underpins the existence of non-negligible non-linearities associated with linear coupling of the aerodynamics and hydrodynamic components of a waterborne WIGcraft.
5. This study illustrates that hull-generated water spray effect has a significant impact on the aerodynamics of the wings of a waterborne WIGcraft.
6. As against the estimation of the Sub-Aerodynamically Alleviation Zone (Sub-AAZ) proposed by Collu (2008, 2009) which is considered more or less an academic exercise, this current study introduces the *Maximum Efficiency Draught (MED)* as a new and singular most important design parameter crucial for the successful design and efficient operation of a waterborne WIGcraft with wings located at the trajectory of the hull-generated spray.
7. New semi-empirical models for lift and drag coefficients based on a newly introduced equivalent hydrodynamic (submerged hull) beam, and other fundamental aero-hydrodynamic parameters are developed for a water borne WIGcraft. Comparisons between empirical results with experimental data are made using these coefficients.

1.6 List of Published and Unpublished Papers

Published papers.

- Pereowei Garrick O; Hu Z, and Song L. (2020) 'Simulating the Acceleration to Take-Off Phase of a WIGcraft Using Results of a Constrained Experiment', *Proceedings of the ASME 2020 39th International Conference on Ocean, Offshore and Arctic Engineering*. *Volume 6B: Ocean Engineering*. August 3–7, 2020. V06BT06A014. ASME.
- Pereowei Garrick O. (2023) 'On the Maximum Efficiency Draught of a Water borne WIGcraft', *Proc 33rd Int Offshore and Polar Eng (ISOPE) Conf, Ottawa*, ISOPE, pp 4018-4025

Unpublished papers

- Pereowei Garrick O. and Zhiqiang Hu (2023), The dynamic lift characteristics of a water borne WIGcraft. (Under second Review by Ocean Engineering, Elsevier).
- Pereowei Garrick O. (2023) Semi-empirical model for predicting the total drag on a water borne WIGcraft (Unpublished full-length paper)
- Pereowei Garrick O. (2023) An extended 2.5D Numerical Hydrodynamic Model for High-Speed Multihull Ships (Unpublished full-length paper)
- Pereowei Garrick O. (2023) A 2D + t based Numerical Aero-Hydrodynamic Model of Wing in Ground Effect Vehicle near Undisturbed Water Surface (Unpublished full-length paper)
- Pereowei Garrick O. (2023) Coupled Numerical Aero-Hydrodynamic Model of a Water Borne Wing in Ground Effect Vehicle (Unpublished full-length paper)

Chapter 2: Literature Review

2.1 Introduction

Airfoils and wings generate aerodynamic lift due to the pressure difference between their lower and upper surfaces. During free flight, the pressure at the lower surface of the airfoil or wing is much higher than that on the upper surfaces. Moving close to a rigid wall or water surface, the pressure in the lower surface of the airfoil or wing is further increased in comparison to its free flight condition. This is due to the air being trapped with partial leakages underneath the airfoil or wing near the wall or free surface.

As a result, an airfoil or a wing moving in proximity to a rigid ground or deformable free surface experiences greater dynamic pressure difference between its upper and lower surfaces, thereby generating a much higher aerodynamic lift. This increased aerodynamic efficiency was initially observed in airplanes and water-based aircraft's longer flying range or higher payload capacity when operating near rigid or deformable ground and has since been investigated in the early 20^{th} century (Betz, 1912; Raymond, 1921; Wieselsberger, 1922). The presence of the ground near the wing or airfoil obstructs the downwash vorticity generated by the wing. As a result, the induced drag is reduced compared to that during free flight. The increased lift and reduced drag suggest that the aerodynamic efficiency of a wing or airfoil in ground effect is much higher than that in free flight.

This promise of increased aerodynamic efficiency as well as the higher safety associated with vehicles operating on water environment led to the pioneer development of different configurations of 'Wing-In-Ground' Effect Vehicle (WIGcraft). The primary idea behind the development of WIGcraft amidst other advantages was to develop a hybrid water/air borne vehicle that possesses the safe and simple operational characteristics of high-speed ships while using the potential high speed and higher lift promised by ground effect technology to support higher payload compared to conventional airplanes of equivalent size. The dream WIGcraft is expected to possess a superior transport efficiency than cargo planes and fast ships by carrying more payload safely at higher safety levels than cargo airplanes of equivalent size, as well as moving faster with lesser power and fuel consumption cost than fast ships. The promise offered by ground effect technology has also led to the proposal for its application in the development of ground effect trains (Dong et al., 2020; Han et al., 2022) and underwater vehicles (Shi et al., 2021). Nevertheless, it has been shown that the expectations of ground effect aerodynamics with respect to free water surface deformation and increased lift is not easily realizable in reality (Aframeev, 1998).

Till date, only WIGcraft prototypes are available. Commercially existing WIGcraft are generally non-existent. There are primary challenges pertaining to longitudinal stability, excessive take-off power during acceleration runs, unclear coupled aerodynamic and hydrodynamic effects on the behaviour of the vehicle during airborne cruise mode as well as during its motion on water and transition from water to air domains.

Physically, the fluid flow about a WIGcraft moving with its wings above the free surface while portion of its hull is submerged is analogous to the case of a very complicated flow with strong nonlinear coupled aerodynamic, hydrodynamic and hydrostatic effects that occurs in the small gap underneath an airborne plate moving at high speed near a free surface water set in motion by a submerged high-speed moving disturbance. A submerged portion of a hull moving on calm water deforms the free surface significantly, especially around the bow, stern and the spray root regions of the submerged hull. The free surface over which the wing moves, may no longer be described as planar, depending on the free surface deformation characteristics, which is largely a function of the submerged hull form, Froude number and trim angle of the hull, as well as the shape of the lower portion of the wings and its angle of attack.

On one hand, it appears under this scenario, that the characteristics of the coupled aerodynamics, hydrodynamics and hydrostatics of the wings of a water borne WIGcraft is analogous to that of a wing operating near a curved ground. It has been stated that the unsteady effect due to ground curvature of radius equivalent to planar ground clearance is the same order as planar ground effect on aerodynamics (Kwag, 2001; Im & Chang, 2000; Wang, 1991). It is thus essential that any aero-hydrodynamic model developed to investigate the behaviour of AAMV captures these nonlinear unsteady effects. On the other hand, the presence of the wings near the free surface may possibly influence the hydrodynamic characteristics of the hull(s) of the water borne WIGcraft. This is especially true when considering the free surface deformation around the hull(s) due to the influence of the aerodynamically pressurized airflow in the small gap beneath the wings, as well as when envisaging the possible influence of the ground effect aerodynamics on spray generation and spray dynamics around the hull(s) and wings.

2.2 Elemental Hydrodynamic and Aerodynamic Characteristics of a WIGcraft

As noted in Chapter 1, a broad knowledge of the elemental aerodynamic and hydrodynamic characteristics such as running wetted length/area, water spray dynamics, free surface deformation, interference effects/factors, lift, drag, moment, centre of pressure etc., is a pre-requisite for understanding the behaviour of a complex water-borne vehicle as a WIGcraft with multi-hulls. Some elemental hydrodynamic and aerodynamic characteristics relevant to this study are introduced in the following sub-sections.

2.2.1 Dynamic free surface, hull wetted area and length

The running (dynamic) wetted length of a planing watercraft is considered to be the longitudinal distance from the stagnation point at the keel to the stern. Whereas the dynamic (running) wetted area of a planing hull consists of the hull bottom pressure area and other areas wetted by hull-generated water spray. The dynamic wetted area is an important parameter required to determine the lift, drag and moment on the hull. During acceleration of the watercraft, the wetted length and area change as the prevailing forces and moments alter the attitude of the watercraft.

Various empirical expressions have been developed to represent the running wetted length of a planing watercraft (Alourdas, 2016; Bannikov and Lulashevsky, 1976; Savitsky, 1964). Using specific model tests, Alourdas (2016) found out that the wetted length-beam ratio for prismatic hull calculated from the CAHI's (also known as Lyubomirov or TSAGI) method, which was also used in Bannikov and Lulashevsky (1976) and Egorov, (1981) yielded higher mean wetted length-beam ratio than the Savitsky procedure for beam-based speed coefficient $C_{vb} < 3$. However, the predicted drag using both methods were quite in good agreement.

The extent to which the hull area is wetted by solid water is expressed by the dynamic free surface elevation or water rise. The estimation of the dynamic free surface elevation of a planing watercraft is a hydrodynamic problem to which solutions habe been proposed by various researchers using numerical methods (Lai and Troesch, 1996; Zhao et al., 1996). However, convergence issues arise when implementing potential flow based numerical solution for planing watercraft if the dynamics of the spray jet is not properly handled, whereas the RANSE based CFD solutions are computationally very expensive. Empirical expressions which are functions of running wetted length to beam ratios have also been proposed by Savitsky (1964) for planing watercraft. Based on the examination of Savitsky's empirical expression for lift in

the light of the concern raised by (Bertorello & Oliviero, 2007) on the choice of deadrise angle used in the expression, it is suggestive to make appropriate corrections to the Savitsky empirical expression for dynamic wetted length and area before its application for practical purposes.

2.2.2 Free surface deformation

Physical observation of a high-speed airborne WIGcraft moving near calm water reveals the existence of the deformation of the free surface. The nature of the pressure on the free surface underneath the wing depends on the forward speed, relative ground clearance height, power augmentation installation and configuration of the aerodynamic surface(s). Free surface deformation due to nearby wing moving at high speed has been studied since the 1960s and the findings of these studies are substantially reviewed in the section 2.3. The water surface underneath the wings of a water borne WIGcraft may no longer be described as 'free' since it is subjected to, and deformable by air pressure above atmospheric. This deformable free water surface underneath the aerodynamic surface is regarded as *air-water interface* in this study. How the free surface deformation influences the hydrodynamics of planing hulls is relatively unknown since it is difficult to come by such studies (experimental or theoretical) in existing literatures.

For the purpose of hydrodynamic analysis of water-based aircrafts, the effect of the deformation of the free surface is generally assumed negligible, owing to the fact that the density of water is about 800 times the density of air. Nonetheless, studies showing that at planing speed, free surface deformation by gravity is capable of influencing the hydrodynamic characteristics of the hull (Sun and Faltinsen, 2007) raise concerns about the effect of free surface deformation due to ground effect aerodynamics on the hydrodynamics of the hull of the watercraft. As such, it would be useful to verify the validity of this assumption by investigating the extent of the free surface deformation due to ground effect aerodynamics that may possibly influence the hydrodynamics of the hull. Results from such investigations, may help affirm the extent of existence of aerodynamic and hydrodynamic fluid flow coupling at the air-water interface underneath the wings besides the structural coupling of the aerodynamic and hydrodynamic surfaces of a WIGcraft by rigid joints.

2.2.3 Hull generated spray

A review of video footages of available WIGcraft and other water-based aircraft prototypes moving at various speed, trim angle and draught prior to take-off, suggests that spray plays significant role in the hydrodynamics and aerodynamics of the craft (KHMedia, 2011; Panagiotis Zagklis, 2017).

At the lower speed range, the free surface deforms due to relative motion between the planing bottom of the watercraft and the water surface. This leads to the minimal generation of gravity dependent waves similar to that generated by conventional low speed vessels. No spray is generated. A further increment in speed to pre-planing speed range results in generation of a type of *Tollmien–Schlichting* gravity dependent divergent wave from the wetted chine of the hull. As the speed increases towards the planing speed range, the amplitude of these divergent waves at the planing hull bottom and near the wetted chine rises until the waves break up to form whiskers and main sprays. It is seen that at constant trim angle and draught, the flow of water is such that spray generation is a function of the model speed up to a certain speed limit where the spray angle largely remains the same. Watercraft operating at this speed limit may be considered to be fully planing (McBride, 1956).

The design, operation and performance of a water borne WIGcraft is seen to be significantly influenced by its hull generated water sprays which impinges on its aerodynamic surfaces. This statement is pictorially evidenced by Figure 2.1, which shows the extent the hull generated spray can cover the WIGcraft when operating at certain set of speed, trim angle and draught. A large volume of high energy spray can be seen impinging heavily on the upper and lower parts of the wings. This may significantly affect the aerodynamic efficiency of the wings, the motions and stability due to the backward, upward, downward momentum created by the spray impact force on the wings. The impact force of the high-volume, high energy water spray on wings is also capable of preventing or assisting the take-off of the WIGcraft, and may also cause structural failure of the wings, the horizontal tail plane and winglets.

Figure 2.1 Hull generated water spray

Spray effect on a related aerodynamic surface has been experimentally studied by Mcbride (1956) using spray collectors. In one of Mcbride's captive experimental setups without wind screen, the spray collector representing the aerodynamic surface was placed at zero angle of attack angle and at the relative clearance heights of 1.0 and 1.5 beams (from the undisturbed free surface) of the spray generator which had trim angles of 9, 15 and 20 degrees. The lift and drag of the spray generation and spray collector flat regular plates were measured using appropriate electrical strain gage beams and strain gage load cells respectively. The deflection of the strain gage beams was measured visually using galvanometers. Results from this study suggest that hull generated water spray may reduce the aerodynamic efficiency of wings. In a related study, Hansman and Craig (1987) demonstrated that a reduction in aerodynamic lift of rain wetted airfoil sections at low angle of attack may be as high as 25% for certain types of airfoils. By considering that the measured drag of the spray collector was exclusively due to skin friction, Mcbride (1956) showed that there were some measures of correlation between the measured spray skin friction drag and Schoenherr line.

The relative motion between the hull generated spray and the aerodynamic surface results in spray viscous drag on the aerodynamic surfaces. As the air interacts with the water spray, a complex multiphase (possibly foamy air-water mixture) flow with its unique density and viscosity runs in the direction of the spray angle towards the trailing edge of the wings with a velocity different from that of the water spray and the air. Owing to the physical characteristics of the multiphase flow and by stating appropriate flow assumptions, empirical expressions may be necessary to correlate the spray drag and Reynolds number dependent skin friction. A similar approach used by Savitsky et al. (2007) on whisker spray resistance may be used to estimate the spray drag on the wings.

It has been demonstrated that the presence of water sheets on an aerodynamic surface may possibly deflect the air flow over the wings resulting in early trailing edge air flow separation and early stalling of the wings (Valentine and Decker, 1995; Zhang and Cao, 2010). Of course, this may depend on water droplet size from spray breakup, relative speed between air and water spray, and the characteristics of the air-water mixture. Mechanisms for spray breakup has been experimentally studied by many researchers (Axt, 1947; Dundurs and Hamilton, 1954; Latorre, 1983; Latorre and Ryan, 1989). These studies indicated spray breakup is enhanced by increased spray velocity, decreased spray thickness, reduced surface tension, spray turbulence and the spray force caused by the relative motion between the spray and the surrounding air. It can also be seen from Figure 2.1 that the dispersion and reattachment of the hull generated sprays may very well obscure the visibility of the pilot.

There are no standard measurement techniques for measuring the geometry of hull generated spray. Earlier experimental measurement of the geometry of the hull generated spray may be associated to studies on spray effect on the performance of water-based aircraft.

The 'needle method' by Sottorf (1932) and 'cameras method' by Locke (1943) were among the earliest hull generated spray measurement techniques. The unsuccessful measurement of spray geometry by Hugli and Axt (1951) demonstrates the difficulties associated with measuring spray generated by full-scale vessels. A more detailed and successful experimental method for measuring the geometry of hull generated main spray as function of deadrise angle, trim angle and speed was presented by Savitsky and Breslin, (1958) and later by Savitsky and Morabito (2010). The experiments were conducted with and without the presence of a wind screen. Latorre (1983) used electrical contacts approach to measure whisker spray thickness. Using the results from experimental studies on hull generated spray and Green's flat plate and swept wing theories (Green, 1935, 1936a, 1936b), Savitsky and Morabito (2010) presented a computational procedure to describe the origin of hull generated spray as well as estimate the spray geometry, trajectory and location of its apex.

From the foregoing discussion, it is apparent that an investigation on spray characteristics and establishment of limiting criteria to guide WIGcraft design and safe operations thus constitute an essential component in the study of water borne WIGcraft behaviour.

2.2.4 Interference effects and factors

Interference effects occur whenever two structures about which fluid flows are placed adjacent to each other. The performance of a multi-hull water borne WIGcraft is influenced by both

aerodynamic and hydrodynamic related interference effects. The hydrodynamic interaction between hulls in a multi-hull ship can be either constructive or destructive. The interaction effects of a multi-hull ship are largely dependent on factors that influence the hydrodynamic forces and moments of the vessel, such as speed, geometry of the submerged multi-hulls and their configuration (height of cross structure(s), vertical, transverse and longitudinal clearances).

It is of interest to note that available literatures on hydrodynamic related interference effects are commonly associated with wave generation. A high-speed multi-hull starts at a lower speed (length base Froude number, FnL is lesser or equal to 0.3), where viscous drag dominates other drag components of the total drag. Hull interference effect is negligible. As speed increases to a moderate speed level ($0.3 \leq FnL \leq 0.75$), the wave related drag components grows until it dominates the viscous drag and other drag components of the total drag. At this speed range, the interference effect is substantially influenced by the characteristics of ship generated waves (Zaghi et al., 2011). For a further increment in speed to higher speed levels ($0.75 \leq FnL < 1$), viscous drag tends to increase gradually, while the wave drag component reduces and is gradually replaced by hull generated water spray drag. At this speed range, it is difficult to know if the interference is constructive or destructive, and which is the most influential factor on the interference effect. At the planing speed range ($FnL \geq 1$), the spray drag becomes the dominant drag component and the spray dynamics dictate the characteristic of the interference effect. Available models for estimating wave related hull interference effect of multi-hull ships may be applicable for estimating the same for water borne WIGcraft operating at the ($0.3 \leq FnL \leq 0.75$) speed range. However, at higher speed regime, ($0.75 \leq FnL < 1$), such models need to be extended to account for the aerodynamic air pressure effect in the small gap.

At the planing speed regime ($FnL \geq 1$), where spray generation is dominant and hull generated waves are almost absent, the wave related interference expressions become inadequate. During planing, the deformation of the free surface is influenced by the presence of a nearby parallel hull. As a result, the wetted length and beam of the hulls are influenced. It has been shown that the wetted length from the stagnation line to the stern of the watercraft play a significant role in defining the total lift of the planing surface. Multi-hull interference effect may also be associated with variations in the fluid flow velocity around the hulls. This may be considered analogous to the variations in flow direction occurring when high aspect ratio wing fly side by side. Owing to changes in the effective angle of attack, the aerodynamic lift and drag are influenced. A further interference effect may be due to the effect of spray generated by one hull

on the other. Unfortunately, only few studies on interference effects on multi-hull craft operating at planing speed regime are available in literature.

In one of such studies, Savitsky and Dingee (1954) experimentally investigated the type and order of magnitude of the interference effects on lift and wetted surface areas of two parallel flat planing surfaces. Results from the experiment indicated that there is no interference effect on the flat surfaces when they are separated three or more beams apart. At zero spacing, it was found that the wave rise factor associated with the running wetted length to beam ratio used in the hydrostatic lift expression in Savitsky (1964) doubled if the wetted length to beam ratio is not calculated with the total beams of the two planing flat plate surfaces. The water rising factor, however, remains the same as with monohulls if the total combined beams is used for the calculation of the wetted length to beam ratio. Examination of the results further revealed that at zero beam spacing the increment in lift of one planing surface due to the interference of the parallel planing surface may be as high as 47%. This is essentially similar to the lift increment that will result if the beam of a planing surface is doubled. On the other hand, at separation distance beyond three beams, interference of one planing surface has a negligible effect on lift of the other. As separation distance is increased from zero to beyond three beams, the maximum percentage increment in the lift of one planing surface due to the interference of the other, diminishes exponentially to zero.

2.2.5 Drag generated by dynamic surfaces

Drag is generated as a consequence of the relative motion between fluid and an adjacent surface. The total drag experienced by a water borne WIGcraft basically consists of hydrodynamic, and aerodynamic drag components. Sub-components of the hydrodynamic drag include interference drag, separation losses as well as the various drag described in section 2.2.4. The reader may refer to Faltinsen (2006) and Newman (2018) for further details on hydrodynamic drag decompositions. The sub-components of the aerodynamic drag include ground influenced parasitic, induced and water spray drag.

Owing to flow coupling between the aerodynamic and hydrodynamic surfaces, the aerodynamic drag characteristics may be more or less influenced by water spray and ground effects. Conversely, the hydrodynamic drag characteristics may possibly be influenced by the dynamic air pressure within the small gap, especially in certain wetted areas of the hulls such as the chines, stern and other areas where water flow separation occur.

Pereowei et al. (2020) illustrated the increase in the total drag during the acceleration of WIGcraft and the subsequent reduction of the drag as the draught of the vehicle reduces due to dynamic lift as it takes off from calm water. Similar observation was made by Khoo and Koe (2016). From these studies, it may be stated that the hydrodynamic drag is dominant in the acceleration phase while the aerodynamic drag and lift becomes dominant at the take-off stage. This assertion has been verified in a previous experimental work by Collu et al. (2009) where the variations of the aerodynamic, hydrodynamic and hydrostatic percentage contributions to the total forces and moments acting of the water borne WIGcraft was studied.

It is a well-known fact that ground effect reduces the induced aerodynamic drag. As speed increases, there is a reduction of the draught of the vehicle, which implies an increment in the relative ground clearance height of the wings from the free surface. As such, it is safe to assume that at planing to take-off speed regime, the induced aerodynamic drag is likely to increase slightly relative to its value prior to take-off. The slight oscillations observed by Khoo and Koe (2016) near the secondary hump drag which occur at planing speed regimes, may be attributed to the WIGcraft attempting to establish dynamic equilibrium attitude related to the trim and relative clearance height suggested by Collu (2008). Similar oscillatory tendency for a planing monohull overshooting its calm water equilibrium attitude as the boat attempts settle to steady planing has been stated by Vorus (2017).

As the dominance of hydrodynamic and aerodynamic drag components changes at various speed regimes during the acceleration of the WIGcraft, studies have shown that a main (primary) hump drag followed by another lesser (secondary) hump drag may be experienced by the vehicle respectively at the pre-planing and planing speed regimes (Khoo and Koe, 2016). The primary hump drag may be associated to peak wave generation by the hull while the secondary drag is largely influenced by hull generated spray. Savitsky et al. (2007) indicated that the whiskers spray drag may be as high as 15% of the total drag of a planing watercraft. As a result, the region between the pre-planing speed and take-off speed regimes appears to be of prime importance during the design of water borne WIGcraft. This speed region dictates the type of lifting devices and/or lifting surface configuration (type of airfoil, Wing planform, hull form etc) the boat must possess to overcome the hump drag and satisfy its design objectives. In other words, this region defines the configuration and type of WIGcraft vehicle, such as Dynamic Air Cushion Craft (DACC), Power Augmented Ran WIG (PARWIG) craft, Dynamic Air Cushion WIG (DACWIG) craft etc.

Generally, huge engine power is required to overcome the main hump drag observed in this region. Besides longitudinal stability challenges, one of the ultimate design challenges of a

water borne WIGcraft is to device a means to overcome or avoid the hump drag during its acceleration run through take-off by using an engine power no more than the maximum airborne cruise speed power requirement. As such, this region also defines the powerplant systems to be installed and the overall transport efficiency of the aerodynamically supported boat.

The take-off regime of a WIGcraft can be described as the point of unsteady (non-equilibrium) motion of the vehicle where there is a sudden large variation in the aerodynamic and hydrodynamic effort (lift, drag and moment) resulting in a rapid and continuous increase in speed, pitch angle and wing clearance height after overcoming the secondary hydrodynamic hump drag (Cui and Zhang, 2010; Khoo and Koe, 2016). During take-off, the aerodynamic centres of the wing and the hydrodynamic centre of the hull also changes positions suddenly (Yun et al., 2010). To prevent the WIGcraft from crashing, the WIGcraft must be designed such that its stability is maintained as the vehicle transits from hydrodynamic stability to aerodynamic stability. Appropriate measure is required to control the propulsion thrust to yield the right vehicle acceleration to avoid the sudden unsteady attitudinal changes experienced by WIG craft during take-off and landing.

2.2.6 Lift generated by dynamic surfaces

The total lift on a winged boat moving on water includes hydrostatic and hydrodynamic lift (associated with the water submerged portion of a planing hull), and the aerodynamic lift subjected to ground effect (associated with the wings and other parts of the boat not submerged). The WIGcraft moving on water experiences time-dependent variable interactions amongst the hydrostatic, hydrodynamic and aerodynamic efforts depending essentially on the given set of boat speed, trim angle and draught variables. The attitude of the vehicle (variations in trim angle and rise of its centre of gravity or clearance height) changes until it takes off from the water surface.

Collu et al. (2009) investigated the proportions of these forces when the water borne WIGcraft is subjected to rectilinear uniform level motion (RULM). At the start of the acceleration, the hydrostatic force and moment are the dominant efforts that support the weight of the boat. The hydrostatic lift force (buoyancy) of a boat operating at various trim angles is a function of displacement (operating draught), trim angle, mean water wetted length-beam ratio and gravity (Savitsky, 1964).

The hydrostatic force of an accelerating boat has been shown to be lesser than the buoyancy force (equivalent to the weight of the volume of water displaced by the submerged portion of

the hull) due to dynamic suction occurring at certain areas of the submerged hull. As a result, the watercraft experiences a low-speed hump drag (Locke F.W.S Jr., 1948; Payne, 1995). It is of interest to note that the buoyancy force calculated using Archimedes principle is valid for low-speed marine vessels, where the free surface largely remains undisturbed such that it can be linearized without penalties due to nonlinearities.

At higher speed, the small, submerged portion of a transom stern experiences an approximate zero hydrostatic pressure differential relative to atmospheric pressure. In essence, the effective hydrostatic force is equivalent to the difference between the buoyancy due to this portion of the submerged volume and that calculated using Archimedes principle for the total submerged volume. In other words, the difference in height, h_s between the lowest portion of the transom stern and actual free surface is assumed negligible and non-contributory to the actual hydrostatic force because the hydrostatic pressure $\rho g h_s$ at the stern is zero. Consequently, in linearizing the free surface, for hydrostatic force calculation purpose, the fluid flow area around the small, submerged portion (height h_s below the free surface) of the dry transom stern may be assumed to be contiguous with the free surface (Payne, 1995). For triangular shaped watercraft with 'all trailing stern edges or re-entrant pointed stern' as in the case in this study, Wadlin and McGehee (1950a, b) experimental test results suggest no variation of lift coefficient with speed or wetted length, which results in a zero buoyancy at all test conditions. In summary, at planing speeds, the hydrostatic force on the submerged hull with transom stern becomes negligible or equivalent to atmospheric pressure while the hydrodynamic lift force becomes paramount in supporting the weight of the vehicle.

The variation of the hydrostatic forces with speed have been represented by an Archimedes buoyancy factor ranging from 0 to 1 in some studies. For planing speed i.e., when water separates from the transoms and chines and hydrostatic pressure reduces to atmosphere at these parts of the hull, the reduction factor was taken as 0.5 (Savitsky, 1964; Zarnick, 1978). For static and slow speed motion, the reduction factor is approximately 1. It should be noted however, ship motions are sensitive to the value of the reduction factor (Kring, 1978).

At pre-planing speed and depending on the planform area and configuration of the wings, it is generally stated that hydrodynamic forces contribute majorly to the alleviation of the weight of the boat. Hydrodynamic forces are developed as the fluid reacts against the planing hull bottom pressure surface. Prior to planing, a watercraft exerts hydrostatic pressure on the water, as the watercraft moves, it imparts its kinetic energy to the water already subjected to hydrostatic pressure, thereby causing a relative velocity between the hull bottom (high velocity) and the kinetically energised water (low velocity relative to hull bottom velocity) it is in contact with.

By Newton's third law, hydrodynamic normal force is generated over the hull bottom area by the dynamic pressure of the water arising from the relative velocity between the hull bottom area and the water surfaces. The hydrodynamic normal force resolved perpendicularly and tangentially to the direction of motion of the hull are regarded as hydrodynamic lift and drag. Further details on the characteristics of the hydrodynamic pressure and forces relative to forward speed on planing watercrafts can be seen in Kapryan and Boyd (1955); Razola et al. (2014) and Smiley (1951a, b). Various models used to estimate the dynamic pressure forces are reviewed in the later sections of this chapter.

Collu (2008) and Williams et al. (2009) identified a speed regime (Sub-Aerodynamic Alleviation Zone, Sub-AAZ) during the acceleration of a boat where there is equal magnitude of hydrodynamic and aerodynamic forces to alleviate the weight of an AAMV. At further increment in speed beyond the sub-AAZ, the ground effect aerodynamic forces dominate other components of the total lift until the vehicle takes off. In both the pre-planing and planing speed regimes, there is a normal ground effect aerodynamic pressure force generated by the wing in addition to the total pressure force of the hull(s). Physical observation of the towed model shows that the ground effect aerodynamic lift may be heavily influenced by water spray at higher speed depending on the operating trim angle and draught of the watercraft. Further details on ground effect aerodynamic lift are discussed in subsequent sections of this chapter.

Investigation on the simultaneous nonlinear influence of the hydrodynamics and aerodynamics on one another and on the behaviour of the water borne WIGcraft, apparently compels a thorough review of existing literatures on ground effect aerodynamics and hydrodynamic theories in relation to the earlier described elemental characteristics of the water borne WIGcraft. In so doing, a good knowledge on WIGcraft aerodynamic and hydrodynamic components and their appropriate coupling techniques can be developed and utilized to

- formulate the aero-hydrodynamic problems related to water borne WIGcraft vehicle behaviour using appropriate boundary conditions and assumptions,
- develop computational procedures to solve problems and challenges associated with modelling and simulating the behaviour of the water borne WIGcraft vehicle,
- Design a WIGcraft with configurations yielding high transportation efficiency compared to airplanes of similar geometric size.

In the next two sections, Ground effect aerodynamics and watercraft hydrodynamic theories and methods applicable to WIGcraft development are reviewed.

2.3 Ground Effect Aerodynamics Theories/Models related to WIGcraft Development

Advancement in research and development of WIGcraft vehicles over the years are categorized and reviewed in this section.

2.3.1 Steady ground effect aerodynamics of wings/airfoils near planar rigid ground surfaces

Physical observations of ground effect on airplane wings were closely followed by experimental investigations on rigid ground effect phenomenon. The earlier theoretical investigations on ground effect aerodynamics generally follow the application of method of images implemented on the thin airfoil and Prandtl lifting line theories respectively on airfoils and wings moving near planar rigid ground. Results from the application of the theories together with certain parameter-based asymptotic expansion considerations led to the concepts of chord-dominated and span dominated ground effect aerodynamics (Abramowski, 2007). In extreme chord-dominated ground effect aerodynamics, it has been proven that when the ground clearance height of the trailing edge is $\leq 10\%$ of the chord, there is an increase in lift if the lower portion of the wing is not convex shaped, and its angle of attack is not low. Lift coefficients can rise up to unity when air in the small gap underneath the lower portion of the wing experiences stagnation pressure.

The induced drag of a low aspect ratio wing in free flight which is inherently larger than high aspect ratio wing in free flight is reduced due to the ground influence on the vortex shed at the trailing edge. This, off course leads to an overall reduction in the induced aerodynamic drag and a consequential increase in the lift to drag ratio of the low aspect ratio wing in ground effect compared to the free flight scenario. For non-planar ground surfaces (reviewed in later sections of this thesis), the ground curvature and ground clearance height effect are said to be of the same order.

Other related investigations on ground effect that have received enormous attention, lay emphasis on the static and dynamic stability of airfoils and wings. These investigations generally make use of the forces and moments determined from the thin airfoil and lifting line theories. Results from such investigations on the longitudinal stability of WIGcraft led to proposition of stability criteria for wings moving near rigid planar ground surfaces. The popular findings from these investigations suggests that a WIGcraft is at a stable equilibrium state when the aerodynamic centre of pitch is located at a distance behind the centre of gravity of the boat and farther from the leading edge of the wing while the aerodynamic centre of height is ahead

of the centre of gravity (Kumar, 1967; Irodov, 1970; Staufenbiel, 1987; Zhukov, 1993). For water borne WIGcraft, Yang et al. (2015) suggested that stability can be achieved when the aerodynamic entre of height and centre of gravity of the watercraft are ahead of the hydrodynamic centre in heave.

WIGcraft longitudinal stability investigations were mainly carried out by aerodynamicists who largely followed theoretical methods used in studying the aerodynamics of free flight vehicles. These aerodynamic theories, however, were extended to accommodate ground effects. It is of interest to note that the lifting line and thin airfoil theories assume variations in the flow and geometry of the aerodynamic surface along its longitudinal axis are much larger than those in the transverse or cross planes. The Prandtl lifting line theory is particularly suitable for unswept, straight, higher aspect ratio wings of the order ≥ 4.

Studies have shown that anhedral (negative dihedral), forward swept (reverse delta) wing configurations with low aspect ratio of order < 4 are aerodynamically more efficient for wing in ground effect vehicles. These geometric configurations became more or less the de facto standard feature for the WIGcrafts ever since the WIGcraft prototype with low aspect ratio rectangular wing with power augmentation configuration was first designed and tested by Rostislav Evgenievich Alexeyev in Russia and the WIGcraft prototype with negative anhedral delta wing configuration was first designed by Alexander Lippisch in Germany (Rozhdestvensky, 2006; Yun et al., 2010).

Low aspect ratio wings of order < 4 with anhedral and forward sweep configuration are predominant for WIGcrafts. The preference for equipping high speed marine vehicles with low aspect ratio wings with anhedral and forward sweep (or trapezoidal) configuration may be attributed to

- increased aerodynamic lift as the ground is approached compared to other configurations of wing in ground effect,
- Improved reduction of the induced drag from the wings,
- A much higher ground effect aerodynamic efficiency.

A brief consideration on the de facto geometry of WIGcraft wings suggests that the use of lifting line or thin airfoil theories and their various extensions to account for ground effect of practical WIGcraft with low aspect ratio wings appear arguably fundamentally inappropriate. The Prandtl lifting line theory has been extended to what is regarded as the lifting surface theory, which van be used to predict the performance of wings with aspect ratio up to 1. It is instructive

to note that the lifting surface theory still has the inherent straight wing requirements which limits its application for wings with dihedral or anhedral angles.

The slender wing/body aerodynamic theory appears to be a rational choice for investigating the ground effect aerodynamics of a practical low aspect ratio WIGcraft. Unfortunately, a large body of literature appears to limit low aspect aerodynamic theories to pointed triangular wings or bodies of revolution or dirigibles (Anderson, 2016; Katz and Plotkin, 2001). Low aspect ratio aerodynamic theory appears to be reserved for supersonic aerial vehicles.

Studies on the free flight aerodynamics of airborne vehicles with low aspect ratio of order << 1 and triangular planform are commonly available (Jones, 1946). The aspect ratio of surveyed existing WIGcraft prototypes is in the range $1 \leq AR \leq 3$, which appears to contradict the aspect ratio of order << 1 conservative assumption for low aspect ratio aerodynamic theories suggested in most literature. Moreover, the anhedral and forward sweep configuration seems to challenge the justification for applying existing low aspect ratio aerodynamic theories to study the aerodynamics of commonly available WIGcraft. The (Jones 1946) low aspect ratio wing theory is valid for pointed planform wing. For wing configurations that are not monotone increasing laterally from fore to aft (as is common with leading and/or trailing edge forward swept wings of commonly available WIGcraft prototype), Jones (1946) low aspect ratio wing theory breaks down.

Nevertheless, the justification for the choice of low aspect ratio slender wing theory as a tool for investigating ground effects and aerodynamics of an anhedral trailing forward swept/trapezoidal wings of aspect ratio of order ≤2 is not rigorous. It can be related to the physical fluid flow characteristics in the cross plane of the wing, as well as the successful implementation of versions of the slender wing/body theory on rectangular (not pointed triangular planform) wings with aspect ratio greater than unity (Bollay, 1939). This theory has also been used to investigate the aerodynamics of circular wings. The low aspect ratio wing theory also gives greater insight into the flow physics in the small gap. Furthermore, other solutions, such as the lifting surface theory and the vortex lattice methods may be more computationally expensive than the low aspect ratio slender wing/body theory.

Results from Bollay's low aspect ratio wing theory also suggest the possibility of implementing the theory on wings with planform shapes beyond the supersonic cone limit stated by several researchers. Furthermore, the extension of Jones (1946) low aspect ratio wing theory to account for the influence of flow about a section on the flow about downstream sections is analogous to the 2.5D hydrodynamic theory for planing watercrafts. CFD investigations on ground effect

aerodynamics are common in recent times (Abramowski, 2007). Results from these numerical analyses tend to support existing findings about ground effects phenomenon.

2.3.2 Steady ground effect aerodynamics of wings/airfoils near planar deformable (calm water) surfaces

An issue related to existing air borne WIGcrafts theoretical studies concerns operational routes of the vehicle. The primary target for WIGcraft vehicle design and development is to provide a safer and more payload efficient transportation over water than comparable aircrafts in the air, and a faster and more habitable transportation over water than comparable high-speed watercrafts. WIGcraft are not typically designed with the intent to operate over rigid planar and curved ground surfaces. It is concerning to note that there is a huge number of studies on rigid ground effect aerodynamics and only a handful of studies are dedicated to ground effect over deformable free surface water. This may be attributed to the fact that WIGcraft development was initiated by aerodynamicists with minimal knowledge about marine hydrodynamics.

Prior to the proposal for high-speed water-based aircrafts, research in ship hydrodynamics were more focused on generation of gravity waves by high energy winds as well as on water flows at atmospheric air pressure when submerged portion of a watercraft moves. These two research areas forms what is regarded as the classical water wave theory summarized by Wehausen (1960).

Though, modern methods such as BEM, FEA, RANSE etc., for analysing fluid flows about a ship have been developed over time, especially with the continuous improvement in memory and computing power of computers, most of these new methods owe their foundations to the classical water waves theory. Till date, some of the classical theories and methods remains valid.

One common assumption made in conventional numerical ship hydrodynamics is that the free surface flows about a moving ship is subject to atmospheric pressure. As such, the contribution of the air pressure on the free surface to the free surface elevation and ship motions are neglected when satisfying the dynamic boundary condition derived from the Bernoulli pressure equation. This assumption is based on the fact that water is about 800 times denser than air and that the velocity of air during the motion of the ship is significantly less than $\left(\frac{\rho_A}{\rho_W}\right)^{-0.5}$ times that of water. Thus, implying that there is no comparable contribution of dynamic pressure between air and water domains. In other words, there is no air-water coupling effect during the motion

of a ship (Tuck, 1975). The validity of this assumption is challenged when the air pressure above the free surface is significantly lesser or greater than atmospheric. For instance, the strong relative high velocity of air from a static ACV impacting on the free surface has a comparable dynamic pressure contribution to that of water. As a result, there is a coupling between air and water which causes the free surface to deform. Based on this observation, accurate solutions to the aero-hydrodynamic problem of a WIGcraft can be achieved by considering pressure continuity at the air-water interface when coupling the aerodynamics, hydrostatics and hydrodynamics of the vehicle.

Fundamentally, the effect of ground effect aerodynamics on free surface deformation underneath an aerodynamic surface may be related to the effect of incompressible inviscid air (wind) on the interaction between incompressible inviscid free surface water and solid boundaries at shoreline. Tuck (1975) likened the study of high dynamic pressure air over a calm water surface to studying the inverted barometer phenomenon of ocean surfaces, which gives the response of the free surface to variations in prevailing air pressures. By viewing the aerodynamic problem as a negative inversion of the classical gravity water wave problem parameters, Tuck (1975) extended the classical water wave theory to study the 2D nonlinear free surface deformation caused by steady air velocity in excess of 96% of the free surface steady velocity. In other words, the free surface deformation due to the air flows at high speed over a stationary water surface is similar to the static deformation of the free surface by the pressure distribution of a motion-restricted hovercraft hovering above a stationary free surface. Under this scenario, the aerodynamic pressure in the air exceeds the hydrostatic pressure on the water. Neglecting surface tension, Tuck (1975) used the inverted and extended classical steady linear water-waves solutions of planing surfaces to establish a minimum velocity of 6.5m/s for which aerodynamically induced water waves similar to Kelvin-Helmholtz instability will occur. The Hodograph transformation method was used to narrow the flow region before solving the nonlinear air-water interface flow problem. The mathematical approach used to solve the nonlinear free surface problem, however, appears unrealistic for practical problems in ship hydrodynamics.

Following a lead from Widnall and Barrow (1970) who presumed that the 2-dimensional (2-D) channel flow within the small gap between the lower portion of the airfoil and the free surface can be approximated to 1-D channel flow, Tuck (1984a) proposed a 1-dimensional (1-D) theory for an airfoil over stationary water. The 1-D thin wing theory assumes a negligible perturbation to water motion and to a leading order assumes that there is no aerodynamic contribution from the upper part of the airfoil. Tuck (1984a) 1-D theory was based on aerodynamic and hydrostatic

channel flow pressure continuity across the air-water interface. The theory was used to estimate the air flow velocity, pressure and free surface deformation as well as the ground effect forces and moments on the airfoil. The results of the 1-D theory suggests that if the trailing edge is closest to the ground and the clearance height-based Froude number is less than the water to air density ratio, then there is the likelihood that the airfoil will experience increased pressure (greater than that in free flight) in the small gap. This pressure is said to vary as the negative inverse of the clearance height of the small gap and will cause free surface depression which in turn will give rise to a positive net lift. It was seen that the larger the difference between the leading and trailing edge clearances, the more the lift coefficient approaches unity. The free surface deformation was found to be lower near the trailing edge of the airfoil, this is especially true when considering the Kutta condition. It was noted that the free surface deformation decreases at the higher Froude number range as though it is a solid ground.

In a related study by Barber (2007), it was stated that an airborne plate (flat plate, airfoil or wing) moving in close proximity to calm free surface water will develop a reduced air speed and an hydrostatic pressure greater than air pressure hydrostatic pressure in the 'small gap' between the free surface and underneath the plate. Barber (2007) indicated that the airflow underneath the wing is about 1/3 of the free airstream velocity. It is expected that the free surface will deform, resulting in a change in the effective clearance and pressure distribution in the small gap in order to equilibrate the aerodynamic and hydrostatic pressure in the small gap.

Tuck (1984b) stated that most of the dynamic lift will be generated as a result of a rapidly changing flow and pressure distribution in the small gap. The free surface deformation phenomenon by Newton's third law also generates increased pressure lift force on the lower portion of the plate compared to when the plate is in free flight, but lesser when operating near rigid ground surface. It can thus be opined that the interaction between the air and water pressures and the motion of the fluids suggest the existence of a strong nonlinear aerodynamic and hydrostatic coupling effect during the motion of the plate subject to ground effect.

The amount of free surface deformation is a function of dynamic air pressure over the hydrostatic pressure of water in the small gap. The depression of the free surface reduces the blockage of the downwash and trailing vortices. As such, induced drag for wing or airfoil over deformable free surface is expected to be higher than that over rigid ground. From the lift and drag characteristics of a wing in ground effect, it is apparent that a wing or airfoil over deformable free surface is thus slightly less aerodynamic efficient compared to when operating over rigid ground.

In a related study concerning an airfoil moving over a small sloped dynamic free surface, Tuck (1984b) replaced the hydrostatic component in Tuck (1984a) 1-D channel flow theory by a hydrodynamic model with linearized free surface boundary conditions. The free surface deformation due to hydrodynamic pressure distribution on a uniform water stream was determined from the classical water waves solution to the linearized planing surface hydrodynamic problem provided in Wehausen and Laitone (1960). The solution to the resulting 1-D nonlinear theory for the small gap pressure was inconclusive. However, it was found that for parabolic or curved airfoil with fore and aft symmetry, the amplitudes of waves generated tend towards zero as the Froude number approaches zero (the hydrostatic condition).

In a related study, Grundy (1986) considered the free surface deformation due to air moving over a stationary airfoil near a moving free surface. Grundy numerically solved the nonlinear integral equation for the small gap pressure that was derived, by replacing the hydrostatic components in Tuck (1984b) with a linearized free surface hydrodynamic perturbation potential model. The resulting nonlinear theory solves the wing thickness problem and accounts for the aerodynamic contribution of the upper part of the airfoil.

Grundy (1986) demonstrated that at moderate to high Froude number, there is no deformation of the free surface. The ground effect aerodynamics and motion of the airfoil can be computed without considering the motion of water. In other words, the free surface behaves as a rigid ground. This finding has been reaffirmed by Zong et al. (2012) using the lifting line theory. From these results together with the classical waves water assumptions, there is no effect of the air motion on the free surface for wing moving at high speed in ground effect. It can be deduced that there is a specific Froude number range where free surface deformation is caused by an aerodynamic surface moving in close proximity to the free surface beyond which the free surface behaves like a solid ground.

As in Tuck (1984b), Grundy's investigation on the Froude number limit for which the hydrodynamic theory is equivalent to the hydrostatic theory as a function of airfoil geometry yielded inconclusive results. However, it suffices to note that short waves (which tend to invalidate the assumption of linearized free surface boundary condition used in Grundy model) were generated. The hydrodynamic theory for a wide range of airfoil shapes was inconsistent with the hydrostatic theory as the Froude number approached zero. In one group of airfoils with continuous pressure distribution in the small gap for the coupled aerodynamic-hydrostatic theory, the amplitude of short waves generated diminishes as the Froude number tends towards zero. On the other group of airfoil shapes with no continuous pressure distribution in the small

gap, the amplitude of the short waves generated persisted as the Froude number tends towards zero.

The extent of the Froude number range on the deformation characteristics of the free surface remains unclear, especially at the lower Froude number range. The effect on the aerodynamic characteristics of an airfoil or wing moving in proximity to a free surface over the range of free surface deformable Froude number (herein referred to as Critical Froude number) will provide further information needed to accurately predict the behaviour of a winged boat.

2.3.3 Ground effect aerodynamics of oscillating wings/airfoils near rigid/deformable planar surfaces

Studies on ground effect aerodynamics of oscillating wings and airfoils are generally geared towards investigating the wavy and/or deformable free surface effects on the aerodynamics of the wings or airfoil section of the WIGcraft.

Zong et al. (2012) extended the Prandtl lifting line theory to investigate ground effects of a 2-D and 3-D wing near free surface. The 2-D and 3-D wings are replaced respectively by a system of point and horseshoe vortices. By imposing a linear body and free surface boundary conditions, the singularities are also distributed on panels that replace the images of the 2-D and 3D wing. By superposing the air and water velocity potentials on the imposed linear free surface boundary conditions, the effects of the presence of the free surface on the airfoil and the effect of the presence of the airfoil on the free surface were considered in the problem formulation. This study affirms the familiar results of increased lift in chord-dominated ground effect as well as the peak lift coefficients at high Froude number and free surface deformation due to tip vortices earlier studied by Barber (2007) on WIGcraft over rigid and deformable planar surface.

Molina and Zhang (2011) noted that the response frequency of the aerodynamic forces is generally equal to the frequency of the heave motion of an inverted airfoil. As such, the response frequency of the aerodynamic forces of a heaving WIGcraft can be represented by a sinusoidal function. Nevertheless, it was seen that the time histories of the heave motion of the airfoil and the forces were out of phase. The result of the study appears to agree with those of Byelinskyy (1998) for wing flying over a dynamic wavy surface. Relative ground clearance, wing angle of attack and added mass were identified as factors that play significant role in the characteristics of the frequency of oscillation of the aerodynamic forces relative to the frequency of oscillation

of the airfoil in ground effect. The ground effect, wing angle of attack and added mass are the dominant factors respectively in low, medium and high frequency of oscillation.

In a related study, Molina et al. (2016) noted that ground effect increases flow separation at the suction portion of the airfoil undergoing pitching motion. The separation was seen to be more intense and may possibly stall the airfoil for long duration of low frequency of pitching oscillation. The characteristics of the forces on an airfoil undergoing a coupled heave and pitch motion are dominated by the effects of the pitching and heaving motions respectively at low and higher frequencies of oscillation. Depending on the nature of the coupled motions, the aerodynamic forces and performance of the airfoil with regards to stalling may be enhanced or negatively impacted.

2.3.4 Ground effect aerodynamics of wings/airfoils near waves (free surface deformation)

It has been shown that the effects of waves on the aerodynamics of a wing can be measured in a towing tank with good accuracy by replacing the air medium over the wing with water medium and the wavy water surface with an oblique wavy screen at a range of depths below the water submerged wings (Epshtein, 1980; Grebeshov et al., 1976; Panchenkov, 1965). Though this study approach, magnifies the magnitude of the measured effects and the Reynolds number at relatively lower speeds, the replacement of the deformable moving wavy surface with a rigid stationary wavy screen limits the application of this study approach to wings moving at speeds beyond which free surface deformation occurs as discussed previously in this literature. As a result, accurate resolution of the correlation between the moving waves and the stationary wavy screen becomes a great necessity.

Unlike the case of the accurate measurement of the hydrodynamic effects on a wing moving over planar surface in a towing tank, Byelinskyy (1998) stated that there is a reduced accuracy when attempting to measure the effect of non-planar deformable surface water on the characteristics of the forces on the wing moving the near the free surface in a towing tank. On implementing Grebeshov et al. (1976) experimental method, Byelinskyy (1998) noted a non-sinusoidal variation of forces and moment on the wing with respect to the sinusoidal screen of various wavelength and amplitude. Peak values of the forces are attained before the leading edge of the wing reaches the wave crest. The amplitude of oscillation of the lift generated by the wing was seen to increase with angle of attack until it reaches a value equivalent to that of a wing above a flat screen placed at the mean wave height. The values of lift generated by the

wing whose relative clearance height from a flat screen placed at a wave crest was higher than that generated by a wavy screen of equivalent crest height. It was also shown that the wavelength of the screen has an effect on the amplitude of the oscillating lift generated by the wing above the wave crest. The shorter wavelength tends to decrease the lift while the longer wavelength has negligible effect on the lift generated by the wing. In other words, the oscillating amplitude of the lift curve decreases with increasing Strouhal number.

With regards to investigations on free surface deformation due to moving wing/airfoil in proximity, the approach used generally involves linearizing the free surface conditions. As a result, it is not uncommon to find recent studies implementing the method of images as a simple means to solve the boundary value problem (Zong et al, 2012).

In flow problems such as wing/airfoil over certain non-harmonic non-planar ground surfaces or flows around a planing craft where the flow is highly nonlinear, and linearizing the free surface leads to substantial errors, application of the method of images becomes very challenging. Matveev (2015) used appropriate boundary and Kutta condition during the implementation of a potential flow solution to the heave and pitch unsteady motion problem of a WIGcraft flying over sinusoidal wavy surface. Matveev highlighted the importance of controlling the attitude or forward speed of the WIGcraft to avoid resonance frequencies where the WIGcraft amplitude of motion may become excessive. Yang et al. (2010) implemented a RANSE CFD approach to study the effect of a wavy ground on the aerodynamics of a WIGcraft. Yang noted the oscillatory characteristics of the aerodynamic forces as well as a reduction in the total drag.

2.4 High Speed Hydrodynamic Theories/Models related to WIGcraft Development

A planing watercraft moving with forward velocity in calm water develops dynamic pressure which is proportional to the square of the relative velocity between its hull and the water surface. The dynamic pressure over the surfaces of the hull wetted by solid water develops a dynamic lift which carries a fraction or all the weight of the craft depending on its forward speed. The resulting attitude of the watercraft is decided upon by the magnitude/distribution of the dynamic force, and centre and line of action of the force with respect to the centre of gravity of the watercraft. The watercraft as a result experiences motions and accelerations, which are larger and transient when the craft encounters waves. The nonlinear impact loads on the hull due to ship motions and accelerations creates discomfort to crew and passengers. The contribution of

the impact load to the dynamic forces complicates modelling the lift/moment distributions and attitudes of the ship.

The modelling of the forces on a planing craft and its behaviour was motivated by aerodynamicists who had needs for an efficiently designed floats for take-off and landing of water-based aircraft on calm water. The resulting hydrodynamic models were generally adapted from the existing aerodynamic models. Owing to the huge computational cost associated with the implementation of 3D aerodynamic or hydrodynamic models, only 2D models were developed in earlier times. The fluid dynamics problem of moving fluid borne vehicle was viewed from a 2D transverse flow perspective in order to simplify the aerodynamic and hydrodynamic analysis and give practical insight into the physical representation of the problem, as well as aid the structural design of such watercrafts.

2.4.1 Theoretical models

Following the successful implementation of aerodynamic 2D slender body aerodynamic theory for airships by Munk (1924), Theodore Von Karman in 1929 made use of an approximate added mass expression derived from the transverse flow and momentum distribution of a wedge impacting on a calm water surface to estimate the maximum hydrodynamic pressure experienced by the floats of a landing seaplane. The solution to the water entry and impact problem was based on momentum theorem. Three years later, Wagner (1936) began adapting the works of Munk and Von Karman to investigate the hydrodynamics of slender planing surfaces in calm water.

Von Karman (1929) and Wagner (1936, 1948) slender body hydrodynamic solutions offered a means to estimate the 2D sectional transverse loads (forces and moment) on planing watercrafts and represent them as transverse sectional added mass together with their rate of change along the watercraft length. Although, the modelling the flow about a planing surface was highly limited (absence of waves generated, flow separation, wake shape etc) in these early 2D planing craft analytical hydrodynamic models, their hydrodynamic solutions are still relevant for planing watercraft design and behaviour analysis purposes.

2.4.2 Experimental studies

Due to the inadequacies of the early analytical hydrodynamic models, experimental studies which were designed to validate these early hydrodynamic models quickly shifted focus from water-based aircraft to the study of planing phenomenon of various watercraft configurations under sea conditions. (Fridsma, 1969; Sottorf, 1944; Shoemaker, 1934; Sottorf, 1932). Fridsma experimental studies in 1969 is usually credited as the most popular experimental studies on a systematic series of high-speed vessels. Results from the experiments are still in use today to valid theoretical models.

Several experimental studies on planing boats, flying boats and other water-based aircrafts have been carried out since after Fridsma work in accordance with ITTC recommended practices (de Luca & Pensa, 2017; Khoo and Koe, 2016; Grigoropoulos and Loukakis, 1995; Kowalyshyn and Metclaf, 2006; Keuning, 1994). Free running model, self-propulsion model or full-scale tests are primarily used to investigate the behaviour of planing watercrafts. Captive model tests are generally used to estimate steady components of the hydrodynamic characteristics of planing watercrafts.

It is believed that the results of these experimental studies contributed most significantly to the knowledge of high-speed planing craft behaviours in calm water and in waves. Till date experimental methods are deemed the most reliable method to investigate planing phenomena. Nevertheless, experimental tests are very expensive and time consuming to carry out. The applicability of the test results is more or less restricted to the hullform of the parent hull. As a results, model tests are often recommended for after-preliminary design purposes and are also reserved for validating theoretical models. Studies to solve the hydrodynamic problems without carrying out model experiments led to the development of semi-empirical and statistical models which were derived from the results of a large number of experiments.

2.4.3 Empirical and statistical models

Results from several of these experimental studies including those of Perring and Johnston (1935); Sottorf (1944); Locke Jr. (1949) and others provided the foundation upon which several researchers including the Savitsky (1964) semi-empirical models for hydrodynamic design of planing craft were developed.

The Savitsky (1964) model relates empirically developed equations for lift, drag, wetted area, centre of pressure and porpoising stability limits to speed, trim angle, deadrise angle and loading

to describe the hydrodynamic characteristics and behaviours, such as power requirement, running attitude, draught and porpoising stability of prismatic planing hulls. The Savitsky semi-empirical method is far simpler and less computational compared to other 3D hydrodynamic models. However, as common with most empirical models to define boundaries of applicability, the Savitsky method has inherent restricted applicability to prismatic hulls with constant deadrise, moving at planing speed with a trim angle range between 2 to 14 degrees. Notwithstanding, the Savitsky (1964) semi-empirical model has been modified over the years to account for the effect of non-prismatic hullform (Bertorello and Oliviero, 2007; Oliviero, 2010; Schachter et al., 2016) and spray drag (Savitsky et al., 2007). The semi-empirical model in all of its modified forms arguably remains the most popular hydrodynamic model for planing craft design and analysis till date. Its commonly used to validate other theoretical planing watercraft hydrodynamic models (Fu et al., 2014; Zhao et al., 1997).

The form of the empirical equations developed in the Savitsky model were essentially adapted from considerations and formulations used in aerodynamic theories and models. It thus appears to hold a huge promise for practical and reliable aero-hydrodynamic modelling of water borne WIGcraft Vehicles. A very robust Savitsky based model for the aero-hydrodynamic design of WIGcraft and performance prediction may be developed by the inclusion of elemental spray dynamic characteristics together with ground effect aerodynamics into existing extended Savitsky models.

Statistical hydrodynamic models are also used to predict the performance of high-speed marine vessels. Popular among this class of models are Holtrop-Mennen model (Holtrop and Mennen 1978, 1982) and the Mercier and Savitsky (1973) model for pre-planing phase of high-speed boats. These models are based on linear and nonlinear regression analysis of extensive experimental data. In recent times, artificial neural networks are being used to develop statistical models (Radojčić, 2019; Radojcic and Kalajdzic, 2017; Radojcic et al., 2014). Like the semi-empirical and other asymptotic models, statistical hydrodynamic models are not universal in character and must be used within the limits of their applicability, otherwise incorrect results may be generated.

The cost of experimental model tests and restrictive applicability of semi-empirical and statistical hydrodynamic models encouraged researchers to develop alternative mathematically oriented solutions to planing hydrodynamic problems.

2.4.4 Low aspect ratio slender body hydrodynamic theory

The slender body theory originally discovered by Max Munk in 1924 for bodies of revolution at subsonic speed and later extended by Robert Jones for wings in 1946 is a special branch of aerodynamic flow modelling method. The Robert Jones (1946) low aspect slender wing theory has been primarily used for studies regarding the flow characteristics of delta-shaped (pointed) aircrafts and projectiles travelling at supersonic speed as long as the configuration of the vehicle lies within the bounds of the Mach cone from its apex. This has led to the general impression that the low aspect ratio slender wing theory is reserved for very high-speed fluid-borne vehicles with low aspect ratio lifting surface. On this premise, and with some correction for 3D effects, the low aspect ratio slender wing theory has been successfully applied to predict planing craft hydrodynamics and spray generation (Savitsky and Morabito, 2010; Garme and Rosen, 2003; Tulin, 1957).

It can be seen that, what is regarded as high speed in hydrodynamics of water borne vehicles (watercrafts) is basically a low-speed aerodynamics of air borne vehicles (aircrafts). Whereas, aircrafts are regarded as low speed when their speed is below Mach 0.8 (980km/hr), the fastest boat on Guinness book of record (the jet powered hydroplane named Spirit of Australia) reached a speed of 511.km/hr (or 344.86mph or 300knots) without crashing on 20 November 1977.

In this regard, when the motion of a WIGcraft on the surface of water is below Mach 0.8, the water borne WIGcraft vehicle may be described as high-speed motion of its hull and low speed motion of its wings. While the hydrodynamic description of the high-speed hull motion on water of the WIGcraft using low aspect ratio slender body theory seems appropriate, the aerodynamic description of the wing near the water surface using the same theory somewhat appears to contradict the notion that low aspect ratio slender body theory is reserved for other than low speed aircrafts. It becomes imperative to define the limits of applicability of the slender body theory. Unfortunately, the term ‘slender’ is quite ambiguous without a definitive parameter that defines how slender the body is. In both aerodynamics and hydrodynamics, the specific definition of the slenderness parameter, ϵ is usually avoided, especially where matched asymptotic expansion method is considered.

However, Aspect ratio which is basically the ratio between the transverse and longitudinal dimensions (wingspan to chord and wetted hull beam to mean wetted length ratios); and speed in terms of Mach number (ratio between vehicle speed and sound speed) in aerodynamics and Froude number (ratio between inertia and gravity force) in hydrodynamics are usually considered respectively as primary and secondary parameters that define the limit of the correct

application of slender body/wing theory. The application of the low aspect ratio slender wing theory is said to be restrictive for objects moving at supersonic speed within the bounds of the Mach cone and less restrictive for hull, fuselage, and wing at the subsonic (Mach No < 0.8) speed regime (Adams and Sears, 1952; Jean Ross, 1961; Ogilvie, 1967) In fact, Munk (1924) used the theory in investigating the aerodynamics of a bluff airship body at subsonic speed.

Meanwhile for hydrodynamic application, speed range generally falls within the subsonic region in aerodynamic theory. The correct application of the theory within this subsonic speed range is influenced by the gravity-based Froude Number, $F_{nL} = \frac{U}{\sqrt{gL_{wet}}}$, which is more or less a controlling parameter for the characteristics of waves generated by the ship. Ogilvie (1967) categorised the application of slender body theory into four free surface related hydrodynamic problems as $\epsilon \rightarrow 0$, namely

1. Problems associated with gravity dominating the entire water domain. $g = O(\epsilon^{-1})$ and $F_{nL} = O(\epsilon^2)$
2. Ship wave resistance problems associated with near field gravity waves and mean gravity waves at large distances from the body. $g = O(1)$ and $F_{nL} = O(\epsilon)$
3. Far field problems associated with near field gravity waves and vanishing influence of gravity at large distances from the body. $g = O(\epsilon)$ and $F_{nL} = O(1)$
4. Planing problems associated with negligible gravity everywhere. $g = O(\epsilon^2)$ and $F_{nL} = O(\epsilon^{-1})$

a. Linear strip theory

The linear strip theory which is an applied form of the slender body theory in marine hydrodynamics is an established method used to provide reliable solutions to the first two problems. In practice, the strip theory is the most widely used method for predicting ship motions of slow-moving marine vessels. The approach does not require a rigorous mathematical justification for its application to provide reliable solutions to linear ship hydrodynamic problems. In the two degrees of freedom frequency domain strip theory originally developed by Korvin-Kroukovsky (1950) and Korvin-Kroukovsky and Jacobs (1957) and extended by Ogilvie and Tuck (1969), Salvesen et al. (1970) and Beck and Løken (1989) to six degrees of freedom, the amplitude of the wave excitation force and the ship's response are linear (i.e. directly proportional) and harmonic with the encounter frequency of the incident wave. In other

words, the ship's response occurs harmonically with its frequency of encounter with the incident wave.

Radiation forces due to ship motions are expressed in terms that are proportional to the ship motion variables (accelerations, velocities, and displacements). These variables are associated respectively with frequency dependent added mass, damping, and restoring hydrodynamic coefficients. The determination of the appropriate exciting force and hydrodynamic coefficients is crucial for a successful implementation of the strip theory to specific ship motions problems. It has been suggested that with the right choice of values of the hydrodynamic coefficients, the linear strip theory may still be used to predict the behaviour of a ship in less severe waves. This approach has been reported to give reasonably accurate results in cases where nonlinearities in the ship motions are minimal (Gerritsma & Beukelman, 1967)

However, for cases such as large amplitude waves, green water shipping and low frequency high forward speed or accelerating boats, where strong nonlinearities are observed, the linear strip theory have been shown to be inadequate. Time domain strip theory was later developed to capture nonlinear ship responses. Cummins (1962) introduced a convolution integral to account for memory effects during large ship motions, as such was able to transform the frequency domain strip theory into a time domain strip theory. Ever since, several nonlinear time domain potential flow models that satisfy the exact free surface and/or hull surface conditions have been developed for predicting large relative ship motions of vessels with non-planing hullforms.

It can be seen that the generic strip theory does not rationally account for high-speed effect. As such, there appears to be no justification for its use for predicting the behaviour of planing watercraft and hydrodynamics, and consequently water borne WIGcraft dynamic behaviour.

Blok and Beukelman (1984) made use of the linear strip theory to predict the heave and pitch motions of for high-speed displacement ship.. They found that the linear strip theory was quite successful up to a length-based Froude number of 1.14. A more rigorous mathematical formulation was developed by Gerritsma et al. (1974) in an attempt to account for the influence of speed on Added mass and damping distribution over the length of the hull. However, like Korvin-Kroukovsky and Jacobs (1957) model, the associated nonlinearities that arise as a result of the variations of steady state equilibrium trim angle and sinkage common with planing crafts were not accounted for.

b. Nonlinear strip theory

Some challenges negating the application of the conventional displacement ship hydrodynamic models, such as the linear frequency or time domain strip theory to investigate the performances (payload and dynamic efficiencies, dynamic trim and sinkage, stability, hump drag characteristics etc) of planing watercrafts were extensively discussed by Keuning (1994) and Renilson (2007). The primary reasons for these challenges can be attributed to nonlinearities associated with the variations in running trim angle and sinkage, leading to changing submerged volume and form coefficient as the boat accelerates to higher speeds. Moreover, the hullform for watercrafts designed for planing are very different from those of the conventional ships. As such, the flow characteristics around the planing hulls both in calm water and in waves also differ. Due to the above-mentioned operational characteristics and challenges of ships supported by dynamic forces, it becomes apparent that the well-established principles for investigating resistance, powering, dynamic stability, seakeeping and manoeuvrability of conventional displacement ships are inadequate for predicting the behaviour of planing craft without some form of modifications. The Savitsky (1964) method is similarly found to be inadequate for the specific purpose of including variations in trim angle and sinkage during the acceleration of the watercraft.

The 2D + t and other nonlinear strip theories for planing crafts both of which are extensions of the linear strip theory are well known for their successes in providing modelling and simulation solutions to the last two marine hydrodynamic problems identified by Ogilivie (1967) as discussed previously in this section. These last two categories of problems are of particular interest to this study and the 2D+t and nonlinear strip theories for their solutions are hereby reviewed.

Martin (1978) and Zarnick (1978) extended the linear strip theory to study the nonlinear motions of planing monohull boats in waves. For planing craft in regular deep-water waves of small slopes and large wavelengths compared to the crafts length, Zarnick (1978) developed a nonlinear hydrodynamic model by adapting a low aspect ratio wing theory and a Wagner 2D expanding wedge impact analysis based linear strip theory to account for the aforementioned flow and motion phenomena. Zarnick's theory ignores hull generated waves and forces associated with the unsteady circulatory flow (wave diffraction is neglected). The values of the coefficients in the resulting equations of motion derived from less rigorous theoretical and empirical relations do not appropriately represent the hydrodynamic conditions around the submerged portion of some of the given sections along the hull length. The Zarnick's model mentioned and crudely accounted for hydrostatic force component of the total hydrodynamic

force by using Shuford (1957) disputed empirical corrected factor (Tventies, 2001; Kring, 1988; Payne, 1974). Zarnick stated the important role played by the added mass distribution on hydrodynamic lift generation. The Zarnick model was validated using results from Fridsma (1969) systematic experimental study on planing monohull boats performance.

Keuning (1994) extended the existing Zarnick's nonlinear strip theory by including nonlinearities associated with trim angle and draught changes due to increasing planing speed of the boat in calm water. Empirical expressions for sinkage (steady state heave) and trim angle (steady state pitch) variations due to hydrodynamic effects derived from existing and new experiments were used to estimate the appropriate buoyancy correction factor and added mass of the model in order to account for the nonlinearities. Solution to the linear equations of ship motions yield results that are in reasonable agreement with ship motions experiments. Nevertheless, it was observed that distribution of loadings along the ship varied widely from experimental values at high Froude number, 1.14. This may be related to poor prediction of hull sectional loads at higher speeds (inherent with the strip theory) which a may have a negative influence on the accuracy of the structural design of the boat.

An alternative approach that reduces the computational burden of the iterative method suggested by Keuning (1994) was implemented by Garme and Rosen (2003). Garme and Rosen implemented Tulin (1957) and Tulin and Hsu (1986) slender body theory-based potential flow solution to a 2-D wedge section impact problem, together with Pierson (1950) splash-up expression, also used by Payne (1994) to determine the pressure distribution and added mass for the various sections of the hull. Garme and Rosen (2003) used similar database approach by McGregor et al. (1990) to store the hydrodynamic forces and coefficients and implemented a prediction-correction computational procedure to solve the nonlinear equations of ship motions of a planing craft moving with constant forward speed in head seas. Though, the results obtained by Garme and Rosén (2003) and Garme (2005) were said to be in good agreement with captive model and full-scale test after correction for 3D effect, the mathematical formulation used to express the nonlinear spray phenomenon do not describe the actual characteristics of the spray.

The quest for mathematical procedure that accounts more precisely for nonlinear effects such as free surface deformation and dynamic characteristics of water spray from the submerged multi-hull negates the choice of the reviewed nonlinear strip theories, as well as their alternative forms proposed by Ghadimi et al. (2013); Ruscelli (2009; Payne (1994); Hicks et al. (1993) and Hicks (1993) as appropriate hydrodynamic models to be coupled to a ground effect aerodynamic model in order to predict the behaviour of a water-borne WIGcraft.

2.5 2D + t (2.5D) Theory

The 2D+t or 2.5D theory is a popular method for predicting the hydrodynamic behaviour (including spray jet generated) of planing watercrafts. Spray jet generation is a phenomenon that occurs at higher speed regimes typically unsuited for the conventional strip theory application. Obviously, the strip theory and its various available extensions, often with empirical expressions for the hydrodynamic coefficients do not rigorously investigate the evolution of the jet spray and its effect on the hydrodynamics of the hull.

An elaborate review of the evolution of the 2D+t theory can be seen in Fontaine and Tulin (1998). It is typically implemented following the boundary element method-based solution of the 2-D water entry problem of wedge- or arbitrary- shaped ship sections. In this theory, the trajectory and geometry of hull generated spray are predicted on cross planes normal to keel line of the watercraft. This is contrary to the swept wing analogy approach proposed by Savitsky and Morabito (2011), where cross planes normal to the stagnation or spray root line are used to determine the trajectory, geometry and apex location of the hull-generated spray. Using a simple analytical approach, Morabito (2010) demonstrated that in using cross planes normal to the keel line, the 2D+t theory overpredicts the spray velocity, especially at high trim angles due to the inclusion of substantial horizontal component velocity.

For sharp wedge sections with small deadrise angles, upon which there is a rapid rise of water as the wedge penetrate the free surface, the 2D+t theory has been found to yield incorrect results. The results for such sections may be improved by using a high-resolution scheme during the numerical analysis. Which, of course, is computationally expensive. It has also been shown that the accuracy of the results of the 2D+t theory diminishes as the trim angle of the watercraft is increased (Morabito, 2010). Nevertheless, the application of the 2D+t theory for predicting the pressure forces on planing/semi-displacement hulls as well as waves and the trajectory and geometry of hull generated spray to engineering accuracy has been demonstrated by several researchers (Lugni et al., 2004; Zhao et al., 1997) A comparative study involving experimental validation of spray prediction methods using planes normal to the stagnation line and planes normal to the keel line would provide helpful information for planing craft researchers and designer.

It is of interest to note that in some versions of the 2D+t numerical hydrodynamic potential flow theories, the local jet flow near its intersection with the 2D hull sections (i.e., near the apex of the water splash) is commonly assumed to be negligible with respect to hull impact dynamics. In other words, jet flow separation is not accounted for and therefore the geometry of the hull

generated spray is not predicted (Zhao and Faltinsen, 1993). Investigations on the influence of ground effect on the spray cannot be carried out using such models. Zhao et al. (1996) and Mei et al. (1999*)* proposed approximate solutions to the global (outer flow) water entry initial boundary value problem with flow separation at fixed points via partial linearization of the free surface boundary conditions. The proposed approach considered the exact dynamic free surface condition to be less important but satisfied the exact body boundary condition and partial linearized free surface boundary conditions on the horizontal plane at the splash up height near its intersection with the 2D hull section. This model accounts for separation from fixed separation points. In 1997, Zhao extended Zhao et al. (1996) model to predict the nonlinear hydrodynamic behaviour of a planing craft in calm water.

It can be hypothesized that, the effect of the aerodynamic flow on the free surface elevation, the jet flow near its intersection with the hull and the rapidly changing nonlinear separated water flow (at apex of the jet flow) beneath the wings will completely change the geometry and dynamic characteristics of the jet flow, with a resultant effect on the hydrodynamics of the hull, as well as on the aerodynamics of the wings. Acceptance of this hypothesis suggests that Zhao et al. (1996, 1997) hydrodynamic models may be adequate for the formulation of the coupled aero-hydrodynamic model of a water borne WIGcraft transverse section.

Where the hypothesis is null, a simple aero-hydrodynamic model can be developed by coupling any of the following hydrodynamic models, Hascoët et al. (2019); Mei et al. (1999); Tassin et al. (2014); Wagner (1936) and Yettou et al. (2007) together with the method of images generally used for investigating wing section near planar ground (e.g., Zong et al., 2012).

2.6 Coupled Aero-hydrodynamic Models and Methods for Water borne WIGcraft

Besides the availability of few experimental studies on WIGcraft (reviewed later in this section), there is a general scarcity of studies on the coupled aero-hydrodynamic behaviour of a WIGcraft moving on water, and where they exist, these studies are largely directed more at investigating the longitudinal stability and equilibrium attitude of the vehicle. In one such study, Collu (2008) investigated the stability of AAMV operating in the sub-AAZ where there is equivalent magnitude of contribution of the aerodynamic and hydrodynamic forces and moment. It remains unclear how the linearly combined aerodynamic and hydrodynamic coefficients used in developing the mathematical model were determined (Adhynugraha, 2017).

Collu et al. (2009) developed a mathematical model to predict the equilibrium attitude and static/dynamic stability of Aerodynamically Alleviated Marine Vehicle (AAMV) or water borne WIGcraft by using interpolation method to combine the hydrodynamics of planing boats based on modified Savitsky (1964) semi-empirical method and the aerodynamics of wings near ground based on Betz (1912) and Wieselberger (1921) semi-empirical methods. The resulting model was however not experimentally validated. Collu et al., (2009a) illustrated the benefits of aerodynamic alleviation by determining, analysing and comparing the equilibrium attitude of and forces and moments acting on an AAMV and a planing boat (with similar hullform, hydrodynamic and inertia characteristics).

In a related study, a mathematical model was also developed by Yang et al. (2015) to predict the aero-hydro dynamic attitude of an aerodynamically alleviated planing catamaran. This model is based on combining a modified Savitsky (1964) semi-empirical model (for predicting the hydrodynamics of the planing surfaces) with Rozhdestvenski (2000) asymptotic analysis method (for predicting the aerodynamics of 1-D plate in extreme ground effect). The authors suggested that to avoid crashing as a result of longitudinal static instability during take-off from water to air cruise mode, the hydrodynamic centre in heave should be located downstream of both the aerodynamic centre in height and centre of gravity. This can be achieved by placing sponsons in front of the centre of gravity. It should be noted that these criteria and suggestions made from the results of the mathematical model are yet to be validated. Amiri et al., (2015) also developed a semi-empirical method to evaluate the hydro-aerodynamic performance of an AAMV at various regimes during its acceleration phase. The model developed used a simplified relation to account for the hydrodynamic drag due to spray effect. The model indicated encouraging agreement with experimental results at the lower speed range and reasonable deviation at higher speed.

A common denominator amongst these studies is the fact that they do not investigate the nonlinear coupled air-water flow characteristics at the air-water interface underneath the wings during the motion of the water borne WIGcraft. These mathematical models could be regarded as inadequate in that they do not include the strong water spray effect on the aerodynamics of the boat during its motion in this regime. Water spray effect is generally assumed negligible by most researchers engaged in the hydrodynamics of aerodynamically supported boats. However, the effect of the water spray on the aerodynamics may be very significant. As such, spray effect requires considerable attention.

Free to trim and heave semi-captive model or free-running model acceleration testing facilities are generally recommended for experimental investigations of unconventional planing

watercraft (ITTC, 2017; Peter Van Oossanen, 1984; Renilson, 2007). Free to heave and pitch semi-captive experimental tests on a scaled model without wings was popular in the earlier years of seaplane and flying boat hydrodynamic investigations (Hugli and Axt,1951). Using this method, the aerodynamics of the wings are modelled by parabolically unloading the model as speed increases during the experimental runs, while the aerodynamic contribution of the craft tail to pitching moment during the experimental runs may be modelled using an oil damper system (Chu, 1923). The aerodynamic coefficients of the wings were assumed to be constant.

The experimental investigation conducted by Khoo and Koe (2016) like that of James and Collu (2015) closely follows the work by Hugli and Axt (1951). The results of these investigations appear to be not completely satisfactory because of the fairly broad assumptions made about the parabolic aerodynamic alleviating (unloading) caused by the wings. Experience with WIG craft model experiments indicates that the unloading created by wings operating under ground effect is influenced by several factors including spray effect, pitch motions etc. Moreover, the aerodynamic contributions were pre-determined prior to conducting the experiments. These experiments do not adequately and explicitly investigate the aerodynamic contributions to the vehicle dynamics and resistance at various operational conditions.

Even when using facilities suitable for semi-captive or free running tests, the variations in trim and submerged volumes makes estimation of residual resistance and up-scaling more laborious and difficult since the form factor varies with vessel speed. Another challenge encountered when using these experimental approaches is the smaller physical model requirement to accommodate speed and size limitations of most existing towing tank generally built for testing the larger displacement hull models. Errors in up-scaled performance data may be reduced by correctly modelling appendages and other structure that may influence trim angle and sinkage. Towing tanks not equipped with mechanisms that allow acceleration runs and/or free to heave and trim may not necessarily be ideal for the experimental investigation of the dynamic attitude (trim and sinkage) of this class of watercrafts.

While experimental methods are considered the most reliable method for investigating the behaviour of WIGcrafts, the limitations of its use as described in this section and in section 2.4.2 compels the need for reasonably accurate theoretical simulation model for WIGcraft behaviour.

A brief consideration of the geometry, kinematics, and dynamics of the practical water borne WIGcraft with anhedral and reverse delta configuration suggests the 3D numerical approach as the most appropriate to solve the unsteady nonlinear coupled aero-hydrodynamic flow problem.

On this premise, the potential flow vortex lattice method (VLM) and the volume of flow RANSE method appears to be the priority choice for more accurate predictions.

The Vortex Lattice Method (VLM)is a more robust extension of the Prandtl lifting line theory. It is a popular numerical method used in computational fluid dynamics to investigate the flow characteristics around fairly complex geometry of fluid borne vehicles. The versatility of the vortex lattice method for preliminary investigation of the aerodynamics of various wing configurations has been demonstrated in several studies. The VLM has also found applications in 3D planing hull hydrodynamics (Lai & Troesch, 1996; Migeotte et al., 2005). However, the time taken to complete the simulation is rather too long.

The Autowing code is a simple, fast, and reliable parametric modelling tool that is based on the vortex lattice method co-developed by Prof. Kornev Nikolai. It is one of the very few dedicated software for modelling ground effect aerodynamics of wings/airfoils. It can also be used to assess the hydrodynamics of submerged hydrofoils. However, it lacks the capability for spray prediction and does not have provisions for nonlinear coupling the aerodynamic and hydrodynamics of a WIGcraft operating on water at planing Froude number. In this thesis, Autowing code will be used to validate the low aspect ratio slender wing model developed for predicting the performance of dihedral wing in ground effect.

Williams (2009) presented a study that attempted to investigate the behaviour of a WIGcraft moving on water. He analysed the performance of KUDU II with demi-hulls and a quadrimaran hull vehicle using CFD. When investigating the pressure distribution around the submerged hull, this study modelled the flow separation in the form of vortices shed at the transom of the watercrafts. Physical insight into the nonlinear coupling of the hydrodynamics of the hull and the aerodynamics of the cross platform is lost due to the method used in this study. Moreover, no attempt was made to model or investigate most of the nonlinear phenomena such as spray generation, the air-water interface deformation, variations in trim angle and sinkage that are hallmarks of planing watercrafts, such as a water borne WIGcraft. As such, the CFD procedure proposed by Williams is unsuitable to model and/or simulate the behaviour of realistic planing watercrafts with aerodynamic surfaces.

It is important to note that using high fidelity CFD method to model and simulate planing watercraft spray generation and complex multi-phase dynamics is difficult, very computationally expensive and may prove too much for today's desktop computers to handle. For practical purposes, it is thus inappropriate to use RANSE based CFD for conceptual design or preliminary investigation of the complex non-linear flow underneath the wings of a WIGcraft

operating on water. An idea of the huge computational expense required to model and simulate the behaviour of planing craft including spray (without aerodynamic coupling) can be got from a study presented by Fu et al., (2014), where Numerical Flow Analysis (NFA) CFD code was implemented on high performance computing (HPC) system.

Nevertheless, various types of volume of fluid RANSE CFD based methods are increasingly being used to study various aspects of fluid borne vehicles, including ground effects. (Hosseini et al., 2021; Khoo and Koe, 2016).

With the increasing computational power of modern desktop computers, the RANSE CFD solutions may well become the primary tool for investigating the behaviour of fluid borne vehicles in the future. The downside common with CFD based solution besides the computational cost, is that insight into the physics of flow of a planing watercraft is typical lost when they are implemented. This major concern is described in detail by Katz, (2019)

The computational burden of RANSE CFD is usually lowered by assuming an ideal fluid in a potential flow solution, in which the contribution of fluid viscosity, turbulent eddies and surface tensions are ignored. The justification for potential flow method is based on the fact that at high Reynolds number flows, usually experienced by hard chine planing crafts, the effect of the hull boundary layer viscous force on the pressure distribution around the hull is negligible (Faltinsen, 2006). As a result, the potential flow theory may be used to mathematically describe the pressure distribution around the hull while ignoring the prevailing viscous forces. Nevertheless, the accuracy of the potential flow prediction model for the aero-hydrodynamic behaviour of a WIGcraft may be enhanced by incorporating a viscous boundary layer model.

This thesis marks the first time, an effort based on potential flow theory is being made to provide an engineering solution to the coupled aero-hydrodynamics and flow characteristics problems in the small gap underneath the wings, and in between the hulls of a water borne WIGcraft. In this study, the 2.5D approach is implemented together with the slender wing/body theory to couple the ground effect aerodynamics of the wing and the hydrodynamics of the submerged portion of the hull(s). The justification of this proposed approach is based on:

- The accuracy of the 2.5D theory in predicting the hydrodynamics and spray characteristics of planing boats.
- The acceptable applicability of the slender wing theory in predicting the ground effect aerodynamics for low aspect ratio wings operating at speeds independent of Mach number.

- The practicality of the 2D transverse strip approach used during the design, development, construction and structural assessment of marine vessels. This is in clear contrast to the chordwise longitudinal strip theory used in airplane wing loading analysis. As a result, the approach used in this study offers the ship designer and constructor the opportunity to adapt and utilize existing (traditional) boat building methods for the production of WIGcraft capable of free flight and wing-in-ground effect operations with portions of its hull submerged on water.

The proposed aero-hydrodynamic simulation model is capable of capturing nonlinearities and coupling effects associated with water borne WIGcraft. The model, which is fast, robust, reasonably accurate and can be executed on desktop computers also predicts effects of the aerodynamics of the wings on the free surface and the hull generated spray generated.

Chapter 3: Development of a Hydrodynamic Simulation Model for Planing Monohull and Multi-hull Watercrafts

3.1 Introduction

This chapter proposes the development of a 2.5D hydrodynamic model for predicting the behaviour of an outrigger watercraft model with one main hull and two smaller side hulls (sponsons) moving at high forward speed. The shapes of the side hulls are identical. Each hull has variable deadrise angle and beam along the length of the watercraft model. The proposed numerical model is also applicable for predicting the hydrodynamic behaviour of monohedral and polyhedral planing watercraft with variable deadrise angles and beams along its length. Details of the formulation and numerical solution of the hydrodynamic problem of the watercraft moving at high forward speeds are described in various sections of this chapter. Comparison of the results from the computational implementation of the proposed hydrodynamic model with those from a captive model experiment on an Outrigger model are presented in Chapter 7 of this thesis.

3.2 General Fluid Flow Assumptions

The characteristics of fluid flow caused by a rigid body motion on the fluid are principally governed by the interaction of gravitational, inertial and viscous forces. Dimensional analysis of these forces yields Reynolds Number, Froude number and Mach Numbers as three nondimensional coefficients that can be used to describe the fluid flow. Based on the small aspect ratio and high-speed characteristics of a typical planing watercraft, Reynolds number for their flow characteristics ranges between intermediate (transitional flow) and high (Turbulent flow) while their Froude number are usually very high. As a result, Viscous forces are typically lesser than inertial forces and for flow regions outside the thin boundary layer close to the vehicle, viscosity may be neglected. If water and air compression during ship section entry into water are neglected, the fluid flow outside the thin boundary layer near the hull may be considered as inviscid, homogeneous, incompressible and irrotational. The flow about these areas satisfies the time-dependent continuity (or conservation of mass) equation and time-dependent conservation of momentum equations. As such, fluid flow outside the thin viscous boundary layer near the hull may be described using the potential flow theory.

3.3 Coordinate Systems

The description of the position or motion of a fluid particle or rigid body without defining a reference coordinate system is almost meaningless. The full potential flow equations used to describe the flow field generally consist of time dependent variables defined in coordinate reference systems with three spatial coordinates. To illustrate the application of these variables in describing the flow fields and motion of the planing watercraft moving at a steady high forward velocity, three spatial reference systems (space-fixed, local geometric and hull-fixed reference systems) are considered for the hydrodynamics and motions of the hull as shown in Figure 3.1.

3.3.1 Earth- or space-fixed coordinate system $O - xyz$

In this global coordinate system denoted by the position vector $\boldsymbol{\chi} = (x, y, z)^T$, the axes directions are fixed in space. with origin O at the point the main hull intersects the undisturbed free surface. The $O - xy$ plane coincides with the calm water surface. The x axis points in a direction opposite to the forward velocity **U** = $(-U_\infty,0,0)$ motion of the boat while the y axis points in the port direction. The z axis is upward and perpendicular to the calm water surface. The boundary value problem (BVP) of the hydrodynamics of the ship sections is solved in this reference frame.

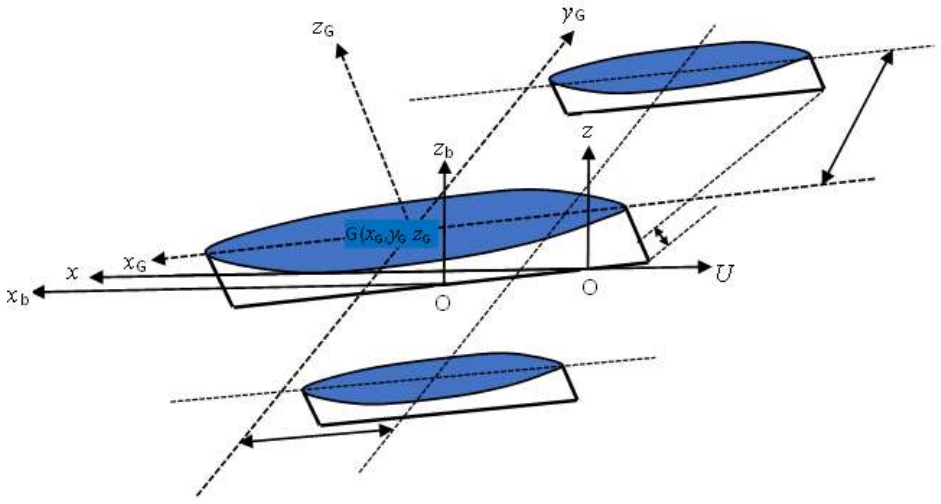

Figure 3.1 Coordinate system of Outrigger Model

3.3.2 Local geometric coordinate system coordinate system $O - x_G y_G z_G$

This moving coordinate system is denoted by the position vector $\boldsymbol{\chi_G} = (x_G, y_G, z_G)^T$. The direction of the x_G, y_G, z_G axes of this reference frame are parallel to that of the space-fixed coordinate system except that its origin O traces the keel line of the main hull as shown in Figure 3.1. At the initial time, $\boldsymbol{\chi_G}$ has its origin coincident with that of the space-fixed coordinate system, where the main hull intersects the undisturbed free surface. The wetted surface of the model is defined and the 2.5D theory is implemented in the local geometric reference frame.

3.3.3 Hull (body)-fixed coordinate system $G - x_b y_b z_b$

In this moving coordinate system, the origin G which is at the centre of gravity of the main hull of the model is denoted by the position vector $\boldsymbol{\chi_b} = (x_b, y_b, z_b)^T$ as shown in Figure 3.1. The G$-x_b z_b$ plane lies at the longitudinal plane of symmetry located at the main hull of the symmetric vehicle. The x_b-axis is parallel to the baseline of the model, always positive sternward and parallel to the longitudinal axis of the vehicle. The y_b-axis is perpendicular to the $O - x_b z_b$ plane and is positive in the starboard direction. The z_b-axis is perpendicular to the baseline and is positive upward. In this coordinate system, the system of equations of motion of the watercraft model is solved.

3.4 Formulation of the Problem

Based on the potential flow assumptions stated in section 3.2 of this chapter, the water flow about the hulls may be described using a scaler function of the velocity field coordinates, termed the total potential function Φ_1, which satisfies the 3D Laplace equation (eq.3.1) everywhere in the fluid domain, subject to the domain boundary conditions.

$$\nabla^2 \Phi_1(\boldsymbol{\chi}, \mathrm{t}) = 0 \tag{3.1}$$

Where the total velocity potential Φ_1 for the water flow about the 3D hull based on linear superposition principle, comprises of the steady perturbation velocity potential $\phi_1$on the hulls and the free stream velocity potential $U_\infty x$. The total velocity potential is given as

$$\Phi_1(\boldsymbol{\chi}, \mathrm{t}) = \phi_1(\boldsymbol{\chi}, \mathrm{t}) + U_\infty x \tag{3.2}$$

$$\nabla^2 \Phi_1(\boldsymbol{\chi}, \mathrm{t}) = \nabla^2 \phi_1(\boldsymbol{\chi}, \mathrm{t}) = 0 \tag{3.3}$$

It can be seen that both $\phi_1(\chi, \mathrm{t})$ and $U_\infty x$ also satisfy the Laplace equation in the water domain.

For slender, low aspect ratio ships moving at high speeds, it can be assumed that the longitudinal variation in hull geometry and fluid flow are negligible in comparison to the transverse and vertical variations and may be of the order of magnitude $O\left(\epsilon^{-\frac{1}{2}}\right)$ in comparison to the ship length, which is $O(1)$. Here, ϵ is a small (perturbation) parameter which may be considered equivalent in magnitude to the slenderness ratio (beam/length or draught/length) of the watercraft.

It can be shown that upon implementing a series expansion on the steady perturbation velocity potential using the small (perturbation) parameter, ϵ, the 3D Laplace equation for the perturbation velocity potential reduces to a 2D Laplace equation (eq.3.4), subject to certain boundary conditions.

$$\nabla^2\phi_1(y, z, \mathrm{t}) = 0 \qquad (3.4)$$

The 2D Laplace equation describes flow continuity in the transverse planes (cross planes) of the watercraft transverse sections, subject to the boundary conditions described below.

3.4.1 The boundary value problem (BVP)

In slender body theory, the analysis of water flow over 2D transverse sections of the hull planing through an earth fixed transverse (cross planes) planes (yz) is generally considered analogous to that of the time dependent surface water penetration of successive 2D sections of the hull (Wagner, 1936). Because of the peculiar geometric characteristics of the Outrigger ship hulls, this study considers the shape (height, beam, deadrise angle, local trim angle etc) of the transverse sections of the hulls to vary with time, as the sections advance and move vertically downward. As a result, the flow about the sections of the hulls cannot be precisely described as self-similar. Neither is the section water entry speed steady. The problem is more of an unsteady 2D time domain problem with time varying hull transverse section geometry in the space fixed reference frame.

For the model moving with a steady forward speed U in a direction parallel to a decreasing x-axis in the earth-fixed coordinate system, the vertical fluid velocities V of successive 2D transverse sections of the ship entering the water at small local trim angles $\tau(x)$ may be given as

$$V(x) = U_\infty sin\tau(x) \qquad (3.5)$$

The local trim angle of a section for a curved keel line consists of the global trim angle and the keel camber angle. It may be expressed as the local gradient of the keel line curve at specific locations of the sections along the x_b-axis in the local reference frame. i.e.

$$\tau(x) = -\frac{dz_G}{dx_G} \tag{3.6}$$

For straight keel line as in prismatic hull, the local trim angle is equivalent to the global trim angle of the ship.

One of the major problems encountered when mathematically describing the fluid flow field about a hull section penetrating the water surface is to determe the velocity potential that satisfies the two-dimensional Laplace equation and the specified conditions on the various fluid boundaries of the decomposed flow domain. In the following paragraphs the decomposition of the flow domain into boundary segments and their associated boundary conditions are described.

a. Fluid domain decomposition

The domain occupied by the fluid flowing about the multi-hull ship transverse section in the 2D cross plane may be decomposed into boundary segments with differing conditions as shown in Figure 3.2. It is seen from the figure that the water flow domain Ξ_1, for a given planing outrigger model ship hull transverse section is bounded by the following boundary segments, viz,

- multi-hull cross section Ξ_B,
- free surface, Ξ_{FS},
- seabed, Ξ_{SB},
- far field at two vertical walls adjacent to the multi-ship cross section, Ξ_{FF}.

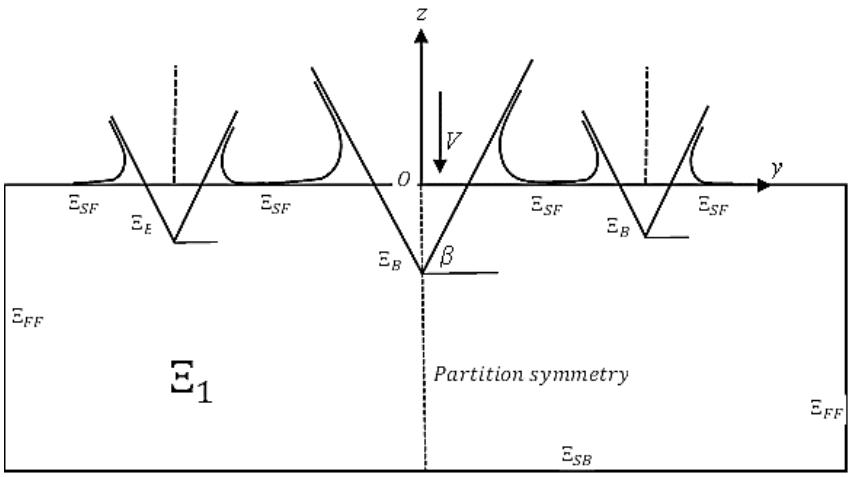

Figure 3.2 2D Flow domain decomposition

Since the multi-hull is symmetric about the longitudinal axis of the main hull, one half of the flow domain about multi-hull ship section may be considered for the hydrodynamic analysis. The half domain may be reflected to yield the hydrodynamic solution of the other half. Similar idea has been expressed by Kashiwagi (2018) for investigating wave-body interactions of multi-hull ships. However, in this case, it is assumed that the hulls are far enough from each other such that their interactive effect at high Froude number can be neglected.

It should be noted that for outrigger ships with vertical clearances between the main and outrigger hulls, at certain draught (especially draught during planing motion) only the main hull is in contact with the free surface water. In this circumstance, though the side hulls are wetted by spray from the main hull, the hydrodynamic analysis approach is generally similar to that of planing monohull ship.

b. Boundary conditions

The uniqueness of the 2D potential solution to the boundary value hydrodynamic problem of a ship section entering water is subject to the conditions specified on these boundary segments. The boundary segments and their respective necessary conditions applicable for a water entry problem of a given Outrigger transverse section are described below.

c. Kinematic boundary condition of the transverse section of the moving hulls

A kinematic boundary condition requiring no fluid flow penetration condition into the submerged rigid hull sections is enforced. The fluid flow velocity v_1 is tangential to the surface contour of the ship section. In other words, the normal component of the fluid perturbation velocity on the 2D hull section surface equals the velocity $\boldsymbol{V}$ of a point on the hull section in the normal direction of its surface.

$$\frac{\partial \phi_1}{\partial n} = V_n \qquad \text{on } \Xi_B(\text{t}) \tag{3.7}$$

Where,

n is the 2D unit normal vector pointing into the fluid domain.

V_n is the velocity of a point on the hull in the normal direction of the hull surface.

Ξ_B(t) is the wetted hull below the instantaneous free surface elevation $\zeta(y;t)$

In this study, the Neumann boundary (no fluid flow penetration on surface of hull sections) condition stated in equation 3.7 is satisfied on the exact wetted surface of the submerged hull sections.

d. Free surface boundary condition

The kinematic and dynamic boundary conditions of the free surface must be satisfied for the flow solution to be unique. The kinematic boundary condition demands fluid particles to remain on the free surface, whose geometry is defined by its elevation (eq.3.8) with respect to the origin of the space fixed coordinate system.

$$\zeta(y;t) - z = 0 \tag{3.8}$$

The kinematic condition of the nonlinear free surface on the 2D cross plane Ξ_{FS}(t) may be expressed in the Mixed Euleran Lagrangian (MEL) form of the fluid flow (Longuet-Higgins & Cokelet, 1976). Thus

$$\frac{D\zeta}{Dt} = (\phi_1)_z \qquad \text{at } z = \zeta(y;t) \text{ on } \Xi_{FS}(\text{t}) \tag{3.9}$$

$$\frac{Dy}{Dt} = (\phi_1)_y \qquad \text{at } z = \zeta(y;t) \text{ on } \Xi_{FS}(\text{t}) \tag{3.10}$$

Where,

$\frac{D}{Dt} = \frac{\partial}{\partial t} + \nabla\phi_1.\nabla$ is the material derivative.

The dynamic condition of the flow on the 2D cross plane requires that the pressure on free surface is constant and satisfies Bernoulli's equation.

If the effect of surface tension and air compression underneath the section is assumed to be negligible and and no air pocket is formed during the impact, the dynamic condition of the ideal fluid enclosed within the 2D boundary is satisfied in accordance with the mixed Euleran-Lagrangian form of momentum conservation equation for potential fluid flow, viz,

$$\frac{D\phi_1}{Dt} = \frac{1}{2}|\nabla(\phi_1)|^2 - g\zeta \qquad \text{on } z = \zeta(y;t) \quad \text{on } \Xi_{FS}(\text{t}) \qquad (3.11)$$

e. Far field Boundary Condition

At distances outside the free surface near the outbound side of the outrigger section, it is assumed that there is no disturbance to the fluid flow. As such, the velocity potential may be assumed to be zero.

$$\phi_1 = 0 \qquad \text{at } \sqrt{y^2 + z^2} \quad \text{on } \Xi_{FF} \qquad (3.12)$$

It is stated that where the solution procedure to the boundary value problem (BVP) is defined as an initial value problem (IVP), the far field condition may not be necessary to obtain a steady state unique solution. As time tends towards infinity, the solution to the initial boundary value problem (IBVP) will generally satisfy the far field radiation condition as the fluid vanishes everywhere (Finkelstein A., 1957).

f. Seabed boundary condition

It may be assumed that the seabed is a regular horizontal planar rigid surface at deep water at finite depth, d_h. Since the seabed is assumed to be rigid and immobile, the no fluid flow penetration condition can be implemented on the seabed boundary.

$$\frac{\partial\phi_1}{\partial n} = \nabla\phi_1.\boldsymbol{n} \cong \frac{\partial\phi_1}{\partial z} = 0 \qquad \text{At } z = -d_h \text{ on } \Xi_{SB} \qquad (3.13)$$

The approximation, $\frac{\partial \phi_1}{\partial z} = 0$ simplifies the numerical solution of the boundary value problem of each ship transverse section. This deep-water approximation is based on the well-known fact that as long as the water depth is not less than half the length, λ of waves generated by a planing vessel ($\lambda > 2d_h$), the seabed will have minimal effect on the fluid flow about the hull.

3.5 Numerical Solution Method

The hydrodynamic flow field due to vertical water entry of ship transverse sections may be represented by the superposition of potential functions on the various segments of the flow domain. Using the Green's second identity, the solution to the boundary value problem (BVP) defined above, which satisfies both the Laplace equation and the prescribed boundary conditions may be expressed for a point (y, z) as

$$\vartheta\phi_1(y,z) = \int_{\Xi} \left[G(y,z;\eta,\zeta) \frac{\partial \phi_1(\eta,\zeta)}{\partial n(\eta,\zeta)} - \phi_1(\eta,\zeta) \frac{\partial G(y,z;\eta,\zeta)}{\partial n(\eta,\zeta)} \right] d\Xi(\eta,\zeta) \qquad (3.14)$$

Where,

ϑ is the solid angle interior to the domain between the tangents of corner points on the domain.

$$\delta = \begin{cases} \theta & \text{interior angle} \\ \pi & \text{semi} - \text{circled singularity point} \\ 2\pi & \text{for singularity point within domain} \end{cases}$$

The total boundaries of the fluid domain Ξ comprises of the section contour Ξ_B, exact free surface contour Ξ_{FS}, seabed contour Ξ_{SB}, and far field contour Ξ_{FF}. The Green's function $G(y,z;\eta,\zeta) = lnr$, where r is the distance between singularity and field point.

3.5.1 Domain boundaries discretization

It is considered that the integral over the far field boundary segment (Ξ_{FF}) is non-contributory to the solution of the boundary integral equation. By implementing the double body consideration (image method) with respect to the seabed at $-d_h$, the seabed boundary condition can be satisfied. It can be seen in Figure 3.2 that the free surface contour consists of inner and outer parts. The jet flow, water rise and the flow intersection with the body are studied in the inner part of the free surface.

The outer part of the free surface contour shown in Figure 3.2, which is far from the hull section up to infinity generally behaves like a vertical dipole with singularity at the centre of hull section. The dipole field decreases rapidly with respect to r from near its free surface intersection with the hull to the outer flow part. The contribution of the integral of the outer part of the free surface in an infinite fluid on the velocity potential is zero and $A(t)\frac{z}{y^2+z^2}$ when the free surface elevation is at z=0 and otherwise respectively. Different starting positions of the outer free surface boundary segments may be tested to ensure conservation laws are satisfied where necessary.

Where only one-half symmetry of the fluid domain is studied, then the symmetry line of partition must be discretized using constant elements. The boundary discretization approach is such that, on Ξ_B and other boundaries (including the partition line of symmetry) near the hull section, elements of equal size are used. However, it is preferable that the size of the elements is increased gradually as the distance between the boundaries and the hull section increases. In essence, a greater number of smaller sized elements are used on the hull section and boundaries near it.

The unknowns in stated boundary integral equation are ϕ_1 on Ξ_B and $\frac{\partial \phi_1}{\partial n}$ on Ξ_{SF} as well as A(t) which is determined as part of the solution of equation 3.14. To determine numeric values of these unknowns, the various boundary segments are discretized into small straight-line elements connecting each other at nodes such that the linked elements follow the contour of the boundaries of the domain.

3.5.2 Discretization and solution of the boundary integral equation (BIE)

In this thesis, boundary element method (BEM) is used to solve the BVP earlier described. Boundary element method (BEM) is a numerical method that is popularly used to solve the boundary value problem involving flow continuity about complex flow shapes in marine hydrodynamics. As such, this thesis will concentrate more on the application of the BEM to solve the BVP described earlier without repetition of details of the BIE discretization procedure. Details of the BEM method may be found in several aerodynamic and hydrodynamic textbooks including Hess and Smith (1967), Pozrikidis (2002) and Volker Bertram (2012).

The boundary integral equation (BIE) eq.3.14, is discretized and applied at the centre node on the midpoint of each element in turn for the boundary segments. The discrete solutions to the BIE at each segment are assumed to be constant over the small length of each element. The

choice of the constant elements takes out a layer of mathematical rigorousness associated with the use of higher order boundary element schemes, without so much sacrifice on the accuracy of the results for academic purpose, especially where smaller sized elements are used. It reduces the complexity of the numerical challenge posed at the point of intersection between the hull section and the free surface.

The discretized boundary integral equation for all points (y, z) at central nodes of the Neumann and Dirichlet boundary elements may be expressed in matrices form as a set of N number of linear algebraic equations for the midpoint nodes on N number of elements making up the domain boundaries,

$$\begin{bmatrix} A_{ij} & C_{ij} \\ B_{ij} & D_{ij} \end{bmatrix} \begin{Bmatrix} \dfrac{\partial \phi_1}{\partial n}_j \\ \phi_{1_j} \end{Bmatrix} = \begin{Bmatrix} f_i \\ g_i \end{Bmatrix} \tag{3.15}$$

In a more compact form, inclusive of the special case where the grid at the discontinuity point of hull-free surface intersection is modified for the purpose of accounting for the different values of the $\frac{\partial \phi_1}{\partial n}$ on the free surface and on the hull section, the system of linear equation may be expressed as

$$[A]\{X\} = \{Y\} \tag{3.16}$$

In equation 3.16, $[A]$ may be regarded as the influence coefficients of the unknown terms $\{X\}$, including the unknown $\frac{\partial \phi_1}{\partial n}$ on the free surface where it intersects with the hull section. $\{Y\}$ contains all the known terms including $\frac{\partial \phi_1}{\partial n}$ on the hull section where it intersects the free surface. Using matrix inversion technique, the unknown terms $\{X\}$ may be determined. Thus, the velocity potential and its normal derivative become known at the midpoints of all the elements of the domain.

3.5.3 Free surface evolution

After evaluation of the velocity potential and its normal derivatives on the elements constituting the domain, the new position and velocity potential of particles on the free surface may be determined by implementing Adams-Bashforth-Moulton (ABM) prediction-correction time stepping integration on equations 3.9, 3.10 and 3.11.

The y and z coordinate derivatives of the velocity potential may be determined from the normal and tangential derivatives ($(\phi_1)_n \; and \; (\phi_1)_s$) respectively of the velocity potential, thus,

$$(\phi_1)_y = (\phi_1)_s n_z + (\phi_1)_n n_y \tag{3.17}$$

$$(\phi_1)_z = (\phi_1)_s n_y - (\phi_1)_n n_z \tag{3.18}$$

The normal derivative of the velocity potential on both the hull section and the free surface are known from the solution of the BVP, while the tangential velocity on each element on the free surface may be determined by numerically differentiating the velocity potential along the free surface contour.

In the free surface evolution procedure, for the unknown vector, $\boldsymbol{Y} = \langle\{y\},\{z\},\{\phi_1\}\rangle$ on the free surface, the fourth-order Adams-Bashforth-Moulton (ABM4) integration method is first initialized by implementing a fourth order Runge Kutta $(RK4)$ numerical integration method on the time derivatives of the unknown vector,

$$\frac{dY}{dt} = f(\boldsymbol{Y}, t) \tag{3.19}$$

For unconstrained hulls, the velocity and displacement of the hull are included as members of the unknown vector **Y**. By fitting a polynomial curve over the $f^{-3}, f^{-2},$ and f^{-1} values, the fitted polynomial curve may be extrapolated to f^0 at the next time step, $t = t_0 = 0$. The superscripts denote the time step for which the values of **Y** are considered.

With the values of f^{-3}, f^{-2}, f^{-1} and f^0, the fourth order Adams-Bashforth-Moulton time stepping scheme may be iteratively implemented by predicting the values of the unknown functions at the next time step $t = t_0 + \Delta t$

$$Y^{1p} = Y^0 + \frac{\Delta t}{24}(55f^0 - 59f^{-1} + 37f^{-2} - 9f^{-3}) \tag{3.20}$$

and correcting it with

$$Y^{1c} = Y^0 + \frac{\Delta t}{24}(9f^{1p} + 19f^0 - 5f^{-1} + f^{-2}) \tag{3.21}$$

The solutions are considered acceptable where the remaining error in Y^{1c} is less than

$$\frac{|Y^{1c} - Y^{1p}|}{} \leq 20$$

This scheme is adopted because it involves iteration and error checking of the free surface evolution and hull variation at each time step. As a result, it is crucial for controlling the accuracy of the free surface evolution and hull displacement at each time step, as well controlling the time interval for introducing the time-varying geometric hull sections during the implementation of the 2.5D theory for solving the water entry problem. At each time step, the

evolution of the free surface is checked to ensure compliance with the mass, momentum and energy conservation laws.

Mass is said to be conserved when the mass flow rate of the free surface above the undisturbed water level is equal to the time rate of the mass fluid displaced of the submerged portion of the hull section. Momentum is conserved when the heave force on the hull section is equal to time rate of change of the added mass of the fluid in the heave direction. Finally, energy is conserved when the kinetic energy of the fluid is equal to the rate of work done by the fluid on the hull section.

3.5.4 Smoothing and regriding

The development of saw-tooth appearance of the free surface has earlier been identified by Longuet-Higgins and Cokelet (1976), who were the first to introduce the Mixed Euleran Langragian (MEL) method for predicting the evolution of the free surface. A smoothing method was presented by them to correct this numerical instability for equally spaced points on the free surface. In this study, after each time step, the saw-tooth numerically instability noticed on the free surface contour with unequally spaced nodes was removed by implementing an adaptive digital smoothing technique. Details of the smoothing method may be found in Taylor and Nicolas (1989) and Orfanidis (1996).

The removal of the numerical instability on the free surface process is followed by regriding the updated free surface contour as well as other domain boundaries. It is of interest to note that more elements are introduced in areas of high curvature such as the spray root region during the regriding process after each time step.

Additional details on the free surface treatment and regriding procedure in other to accommodate a new geometrically dissimilar hull section will be described later the 2.5D theory section of this chapter.

3.5.5 Water jet and spray cut-off models

The physics of main spray blisters and whiskers spray generated by a planing hull and hull section impacting on water has been extensively discussed by Savitsky (1964) and Vorus (2017). Numerically, modelling the jet flow resulting from the water entry of a hull section requires exercising some caution when following the fluid particle during the solution of the

free surface evolution equations. This is especially necessary for points on the free surface near the hull section, which are likely to breach the hull section boundary segment during the free surface evolution process and cause numerical breakdown of the calculation.

Zhao and Faltinsen (1993) and Kihara (2004) specified a limiting angle (dependent on deadrise angle) between the free surface jet and the hull beyond which the jet tip cut-off is specified. Sun and Faltinsen (2007) suggested an alternative cut-off model that employed the use of a threshold distance between the jet and the hull section. This model was said to allow prolonged evolution of the jet in other to simulate the influence of gravity on the free surface, especially, at the top of the jet. Sun and Faltinsen (2007) associated the generation of the thin spray mainly with gravity effect and to a lesser extent to surface tension. The thin spray emanating from the water jet after a while is cut-off before impacting on the free surface after overturning to avoid numerical breakdown of the BEM. The cut-off element originating from the midpoint of the overturned spray is directed normal to the introduced element intersecting the hull section and the free surface. It was stated that though the cut-off portion was influenced by gravity, it has no effect on the free surface geometry or forces on the hull section.

In each of these cut-off models, a new element normal to the hull section is introduced to close the flow domain in other to satisfy the condition required to implement the BEM. It is worth noting that from a practical point of view, after a while the jet is likely to break up into droplets under certain conditions such as reduced surface tension, velocity difference between spray and surrounding air and jet turbulence (Dundurs and Hamilton, 1954). As a result, more than one element may be introduced to intersect the free surface and the hull section and the direction of these sections does not need to be normal to the hull section but freely chosen (Kihara, 2006).

Since the hull sections in this thesis are non-similar, the spray at times does not always exactly exhibit the monotonous spray characteristics beyond the highly curved spray root region towards the spray edge. The contact angle made between the free surface and the hull section contours are also unknown a priori.

As such, in other to implement a jet and spray cut-off model that allows gravity and other prevailing effect on the spray and the stagnation pressure to be examined in this study, a limiting distance between the free surface jet and hull section contours beyond the spray root area is specified equivalent to the order of magnitude of the free surface grid. For distance beyond this threshold, the spray is cut-off and a new element connecting the hull section to the first node on the second element of the free surface is introduced. The first element on the free surface is discarded.

3.5.7 Pressure and force distribution on transverse section

It is seen that by using the Mixed Eulerian-Lagrangian method and the free surface evolution equations, the water-rise and trajectory of the jet spray can be determined. At each time step, if ϕ_{1t} is known, the sectional hydrodynamic pressure on a wetted hull section can be determined by evaluating the Bernoulli's equation,

$$P - P_a = -\rho_1 \left(\phi_{1t} + \frac{1}{2} |\nabla \phi_1(y,z)|^2 + gz \right) \qquad (3.22)$$

The hydrodynamic forces and moment on the instantaneous wetted areas of any given section of the hull in the vertical plane can be determined by numerically integrating the pressure on the surface of the hull section.

$$f_i = \int_{\Xi_B} (P - P_a) n_i d\Xi \qquad i = 1,3,5 \qquad (3.23)$$

f_1, f_3 *and* f_5 are surge force, heave force and pitching moment respectively on the section.

The sectional hydrodynamic force together with the speed influenced hydrostatic and other external forces on a given hull section causes the section to accelerate at each time step. As such, the velocity, and the position of both the unconstrained hull section and the free surface changes at each time step during the solution of the water entry boundary value problem (BVP). It is of interest to note that for accurate modelling of the hydrodynamic forces on the hull for successive time steps during investigation on ship motions (seakeeping) and passenger comfort level, it is expedient that the distribution of sectional acceleration along the hull is determined. However, for a fully captive model moving at constant speed at a given attitude (draught and trim angle), the ship motions are constrained (i.e., the attitude of the ship is maintained) while the prevailing dynamic forces and moments on the hull are measured as the free surface and spray jets evolves and propagates.

The relationship between the sectional dynamic forces generating the accelerations and motions of a given ship section in the vertical plane may be determined from Newton's equation of rigid body motion implicit in time in the space-fixed reference frame,

$$m_i a_i = f_i \qquad \text{for } i = 1,3,5 \qquad (3.24)$$

Where,

m_i for $i = 1,3$, are the sectional mass components in surge and heave motions respectively and for $i = 5$, is moment of inertia components relative to the centre of mass of the section about the y

a_i are the accelerations of the section in the ith direction.

f_i are the forces acting on the section in the ith direction and consist of the hydrodynamic, hydrostatic and other external forces and moment.

Equations 3.22 and 3.23 show the mutual dependence of the acceleration and the hydrodynamic force on the hull section. If one of these parameters is known, the other can easily be solved and the solution to the defined BVP can proceed. Interestingly, these two parameters are unknown beforehand. Propositions such as finite difference methods (which are generally unsuitable for time stepping BVP, where hull and free surface motions are unknown a priori) and definition of BVP for an auxiliary or artificial function related to the acceleration field have been made to estimate the value of ϕ_{1t} (Greco M, 2001; Tanizawa K., 1995; Cointe et al., 1990). As a result, it became possible to uncouple the mutual dependence between the fluid and body motions to proceed with the numerical solution of the defined boundary value problem.

In this thesis, an approach which reduces the computational expense required to evaluate the forces acting on the hull sections by allowing parallel computation of the velocity potential and the auxiliary function is proposed. The approach used is derived from the formulation presented in Cointe et al. (1990); Tanizawa (1995,1996); van Daalen (1993); Wu et al. (2004); Wu G.X. and Eatock Taylor (1996). From the proposed formulation, it can be shown that the sectional forces may be given in the body-fixed reference frame as

$$f_i = -\sum_{j=1}^{5} N_{ij} a_j + f_{Bi} \tag{3.25}$$

where,

f_{Bi} includes weight of hull section and other non-acceleration related components

the sectional added mass N_{ij} is given as

$$N_{ij} = -\int_{\Xi_B} n_j \varphi_{1i} d\Xi \tag{3.26}$$

Using the popular added mass identity, $N_{ij} = N_{ji}$, for $i = j = 1,3,5$, equation (3.26) becomes

$$N_{ij} = -\int_{\Xi_B} \varphi_{ji} n_i d\Xi \tag{3.27}$$

For $i = 5$, $n_i = \boldsymbol{r} \times \boldsymbol{n}$

3.6 2.5D Theory

The traditional slender wing theory is analogous to the traditional strip theory in hydrodynamics, which is recognised to fall short when used to predict nonlinear hydrodynamics of high-speed watercraft. The theory assumes that flow about a transverse section do not have influence over adjacent downstream sections. As a result, the theory does not account for the 3D non-linear characteristics of the flow about the hull moving at high speed. This shortcoming of the traditional slender body theory is addressed by implementing the 2.5D theory. In the 2.5D theory, the 2D boundary value problem is solved together with the 3D free surface boundary conditions. This section illustrates the details of the 2.5D theory for studying the hydrodynamics of a high-speed watercraft.

A hull moving with a velocity U and each hull transverse section (hereafter, referred to as just hull sections) with x_b-varying geometry is seen to impact on the free surface with a vertical velocity $V(x_G)$ on a cross plane fixed in space. The depth of water entry of a section after a given time t may be given as

$$d(x_G, t) = V(x_G)t = Utsin\tau(x_G) \tag{3.28}$$

Meanwhile, in the local reference frame, the depth of the section at a given x_G location relative to the undisturbed water surface is given as

$$d(x_G) = x_G tan\tau(x_G) \tag{3.29}$$

equations 3.28 and 3.29 may be non-dimensionalized with the maximum beam (Z_{CH}) at chine position of the section, then it can be seen that for the same section, $x_G(t)$

$$\frac{Utsin\tau(x_G)}{Z_{CH}} = \frac{x_G tan\tau}{Z_{CH}} \tag{3.30}$$

and $x_G(t) = Ut$

In essence, the velocity field for a section that enters the water at a time t with velocity V(x_G) is the same as the velocity field of a section at x_G location. As a result, the 3D planing hydrodynamic BVP of flow about a submerged hull with variable geometric sections (i.e., variable local trim and deadrise angles along its length) may be solved as a time stepping 2D unsteady impact problem in a solution control cross (SCC) plane in a space-fixed coordinate system at uneven spatial intervals along the ship model length. The 2D unsteady water entry problem studied in this thesis involves section geometry that changes at each interval along the

length of the ship. The solution procedure to the 2D unsteady impact problem of the 3D hull may still be anchored on the slender body theory if it satisfied the necessary conditions.

The slender body theory assumes that the transverse variations of the hull geometry and flow field about the hull moving with a velocity U is larger than the variations in the longitudinal direction by an order of magnitude. As a result, it can be stated that flow perturbations about the hull transverse sections are not influenced by the conditions of the flow about hull sections in downstream cross planes. Rather, the hull sections downstream move with the velocity U into the trailing edge of the upstream hull sections. On this basis, solutions to the hydrodynamic BVP in a cross plane may be seen as an initial boundary value problem (IBVP) in the solution control cross (SCC) plane located initially at the point of intersection between the stem of the ship's bow and the undisturbed water surface. Using the transformation equation, $x_G = Ut$ the solutions in the SCC plane at any time may be stepped to the next hull section downstream in time interval equal to the corresponding time interval appropriate for accurate prediction of the free surface evolution (see section 3.5.3 for discussion on free surface evolution) until it reaches the stern or transom section.

3.6.1 2.5D theory procedure

For the purpose of implementing the 2.5D procedure, the hull may be divided into three regions as shown in Figure 3.3 and described below.

- the fore sections region (Section A-A) which begins slightly ahead of the stem intersection with the undisturbed water surface and ends at the section immediately downstream of where the stem intersects the free surface. In other words, this region begins at time $t = t_0$ and ends at time $t = t_1$
- The Chine unwetted region (Section A-B) which begins from where the fore region ends and ends at the point of chine immersion into the water.
- The chine wetted region (Section B-B) which begins after chine immersion and ends at the rooster's tail ending position beyond the transom.

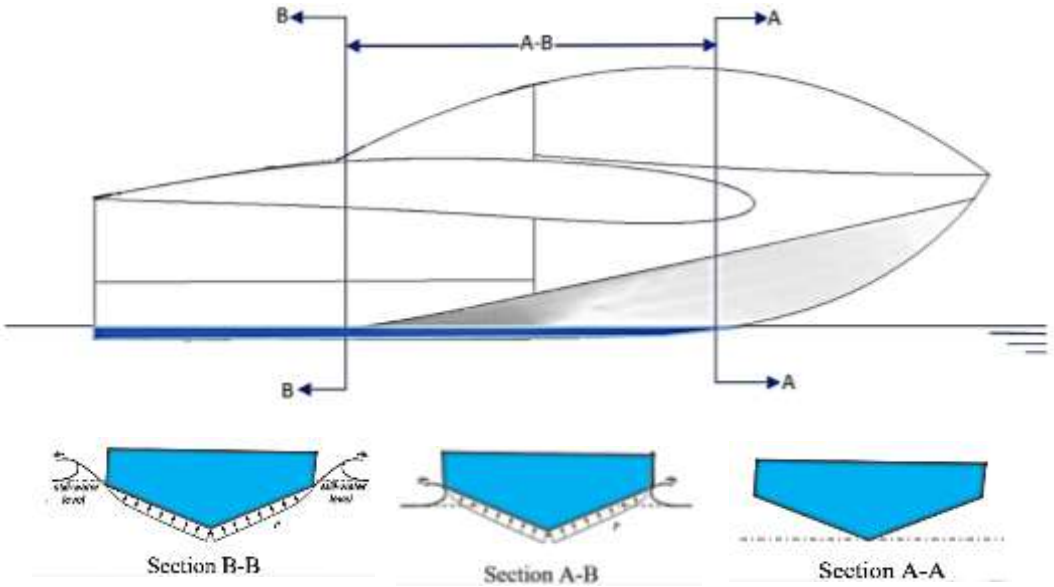

Figure 3.3 Hull regions for implementing 2.5D theory.

Separate hydrodynamic considerations are required for each of these hull regions. The first two regions are of primary interest in this study. The chine wetted region is considered to contribute less to the hydrodynamics pressure force on the hull and consequently, the lift dynamics of the watercraft.

a. Fore sections region and initial boundary value problem (IBVP)

The problem defined in section 3.4.1 is solved as an initial boundary value problem (IBVP) beginning at the fore region (section A-A in Figure 3.3). The SCC plane is initially placed at a longitudinal location $x(t_0)$ relative to the hull as shown in Figure 3.4.

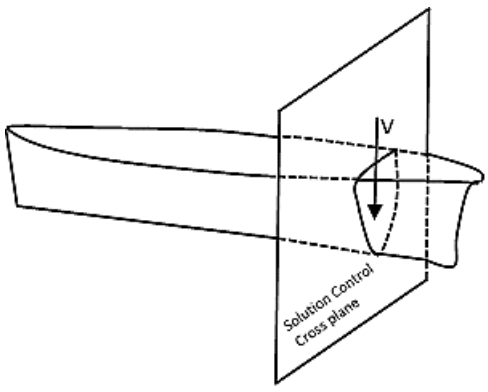

Figure 3.4 Solution Control Cross Plan

Prior to $t = t_1$, it is assumed that only a small portion of the hull section at the stem has penetrated the free surface. Depending on the deadrise angle, this region is characterised by a rapid rise of water on the first hull section contour. The flow characteristics is equivalent to the flow situation described by Ogilvie (1967) where the effect of gravity is absent everywhere in the flow domain. As such, violates the slender body assumption and solutions to the BIE defined in this thesis may give erroneous results. Suggested solution to the BVP in this region includes Mackie (1962) analytical solution for the BVP of a wedge section with large deadrise angle and Wagner (1936) outer domain solution to the BVP of a section with low deadrise.

For the apex of the transverse section of a typical planing watercraft which has large deadrise angle β penetrating the free surface with velocity **V**, Mackie's analytical solution to the initial value problem on the free surface about the section is given as

$$\phi_1 = \frac{\beta}{2\pi}\int_0^1 ln\frac{y^2 + (z+\zeta)^2}{y^2 + (z-\zeta)^2} \tag{3.31}$$

$$\zeta(t) = \frac{\beta}{\pi}\left[ln\left(1 + \frac{1}{y^2}\right) + 2ytan^{-1}\left(\frac{1}{y}\right) - 2\right] \tag{3.32}$$

The wetted width may be approximated from Wagner (1936) similarity solution as

$$y(t) = \frac{\pi\zeta(t)}{2tan\beta} \tag{3.33}$$

b. Chine unwetted downstream hull sections on the solution control cross plane

The solution to the IBVP solved on the SCC plane at $x(t_0) = 0$ is used as the new boundary conditions on the next time t_1 in the A-B sections in Figure 3.3. The SCC plane with updated boundary conditions is stepped downstream to the next longitudinal position at $x(t_1) = x_1$. A new non-similar hull section is introduced to the SCC plane and the BVP is solved on the SSC plane at $x(t_1) = x_1$, subjected to the free surface boundary condition at the SCC plane and the new hull section boundary condition. The stepping process is repeated until the SCC plane reaches the longitudinal location $x(t_c) = x_c$, where the chine is immersed.

Figure 3.5 shows the location of x_c on the hull bottom. The spray root line is formed by joining the points on the hull sections where a line normal to the planing bottom but tangential to the spray root curve intersects the hull section.

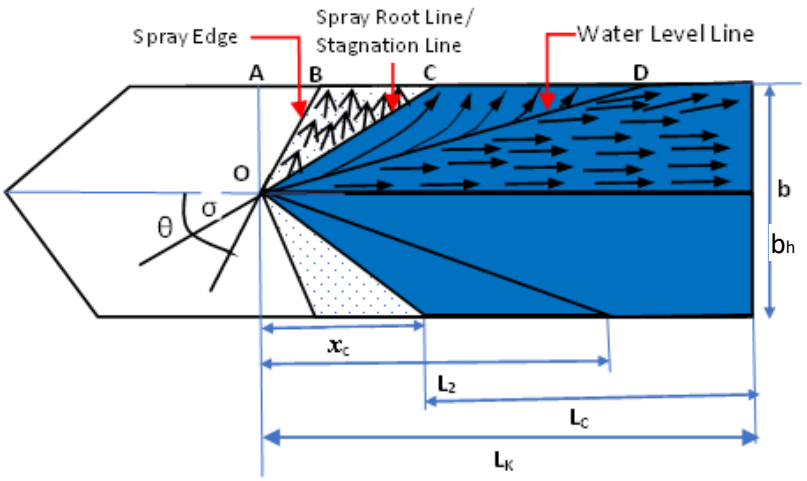

Figure 3.5 View of planing bottom

it can be seen from Figure.3.3, that,

$$x_c = L_K - L_c \tag{3.34}$$

Where,

L_c is the chine wetted length,

L_k is the keel wetted length.

If l_{wl} are b_h are defined respectively as the mean wetted length and beam, then for a hull with variable deadrise angle operating at a trim angle, the mean wetted length ratio beam ratio may be approximated from the Bannikov and Lulashevsky (1976) wetted length to beam ratio as

$$\lambda_w = d_{te}\left(\frac{1+\sqrt{1+1.6B\tau}}{2B\tau}\right) = \frac{L_K + L_c}{2B} \tag{3.35}$$

d_{te} is the draught at transom.

By solving equations (3.34) and (3.35), L_K and L_c can be determined.

At the chine, the flow separates from the section with an acceleration much greater than acceleration due to gravity. As such, there is no need to account for the effect of gravity on the flow characteristics. The flow can be viewed as a localized flow problem that alters the geometry of the free surface. A localized analytical solution such as that presented by Bao et al. (2016) and Zhao et al. (1996) is thus required for the flow separation problem. Subject to the Kutta condition which requires that fluid flow with finite velocity leaves the chine tangentially and that at the point flow detachment the pressure is atmospheric. Zhao et al. (1996) demonstrated that the velocity potential at the separation point with local polar and local cartesian coordinates (r, θ) and (s, n) respectively may be expressed as

$$\phi_{loc} = A_0(t) + U_s(t) + A_{\frac{3}{2}}(t) r^{\frac{3}{2}} cos\left(\frac{3}{2}\theta\right) \qquad (3.36)$$

Where,

$U_s(t)$ is the tangential velocity at the free surface and A_i are constants.

By equating the tangential derivatives of the velocity potentials at points on a fictitious body continuation near the chine to that of the free surface near the chine, as well as equating the normal derivative of their respective velocity potential, the constants can be evaluated as part of the solution of the boundary integral equation 3.14 less of two linear equations for nodes near the flow detachment point. Subsequently, the velocity potential at the point of separation on the hull section surface can be determined. More information on the procedure can be seen in Zhao et al. (1996).

The pressure on the point of separation along the chine may be expressed as

$$P - P_a = -\rho_1 \frac{\partial}{\partial t}\left[A_0(t) + U_s(t) + A_{\frac{3}{2}}(t) r^{\frac{3}{2}}\right] - \frac{1}{2}\rho_1 \left[U_s(t) - \frac{3}{2} A_{\frac{3}{2}}(t) r^{\frac{1}{2}}\right]^2 \qquad (3.37)$$

and the forces on the point of separation is given by equation 3.23.

3.6.2 Numerical treatments on the solution control cross plane

The introduction of a new non-similar hull section requires the apex of the hull section to be maintained at the local origin relative to the centre plane of symmetry of the main hull and that the free surface element near the hull is adjusted or new element introduced where necessary to accommodate the geometry of the hull. At each time step, all numerical treatments of the free surface and hull section boundaries are carried out such that the fluid flow conservation laws are satisfied.

The adjustment of the discrete element of the free surface near the hull or introduction of new elements is especially necessary when the time interval is large. It should be noted that fluid variables are not evaluated at nodes located at the point of intersection between the hull and the free surface because of the confluence of the hull and free surface boundary conditions at that point. These control measures, however, creates numerical instabilities which are normally reduced when the time step for solving the BVP is small.

It is of interest to note that the shape and velocity (rate of expansion) of the spray root and the spray are determined everywhere by the shape, position and penetration velocity of the hull section. In self-similar hulls, the water rise, and spray shape are uniquely defined by the shape of the self-similar hull. As the section penetrates further, the shape of the water-rise and spray remains the same, however, their sizes changes. On the other hand, for non-similar, time varying section geometries, both the shape and size of the wave rise and spray changes continuously and nonlinearly as hull penetration progresses. The changes in the shape of the free surface may be minimized by using small time steps or spatial intervals between sections during the analysis.

Generally, for self-similar slender hull geometry, after solving the BVP of a hull section and updating both the section and free surface conditions, the first point on the free surface may not coincide with the hull section boundary element and certain adjustment are made to the first node (or element) on the free surface (Zhao and Faltinsen, 2003; Sun and Faltinsen, 2007). This observation is also true for hulls with time varying geometry when the space interval between adjacent hull sections is small. In other words, the hull is made to be slowly varying with the help of the prediction-correction integration method used in the free surface evolution. Similar idea for using small space interval in the numerical computation of the hydrodynamics of more general non-similar planing hulls was suggested in Vorus (2017).

Prior to when the free surface and hull section contours become parallel to each other, any gap between the updated free surface and hull section are closed by projecting the first node of the free surface to the hull surface as suggested in Sun and Faltinsen (2007). However, in the event where the first node on the updated free surface breaches the boundary of the non-similar hull section, then the second node is extended to intersect while the first node that breached the hull section boundary are discarded. Where more than one free surface element breaches the hull section boundary, the length scale of the free surface boundary elements may be contracted.

It is important to ensure that the free surface nodes never breach the boundary of newly introduced non-similar hull sections. This is normally prevented by using small space interval between sections along the longitudinal axis during the implementation of the Adams-Bashforth-Moulton numerical integration method.

3.6.3 Total Hydrodynamic forces on the hulls

In the absence of viscous and other external forces, the total hydrodynamic forces and moment on wetted hull surface due to free surface rise (solid water) may be determined by numerically integrating the sectional forces distribution along the wetted length of the hull.
The total hydrodynamic force F_{TH} on the ship model is

$$F_{TH} = \int_{l_{wl}} f_i \, dx \tag{3.38}$$

Where,

$i = 1$ for horizontal components, $i = 3$ for vertical force components

l_{wl} denotes the entire wetted length of the main hull or outrigger boundary.

3.7 Chapter Summary

The development of a 2.5D theory for predicting the hydrodynamic loads on a non-similar monohull and multi-hull high speed watercraft has been described in this chapter. The formulated hydrodynamic problem was solved as an initial boundary value problem using the boundary element method (BEM). Careful numerical treatments of the free surface evolution and jet spray are required for successful implementation of the BEM. Details of the numerical treatments are presented. A method to uncouple the mutual dependence between the fluid and body motions was developed to allow the numerical evaluation of the time dependent velocity potential ϕ_{1t} in the unsteady Bernoulli's equation. The sectional and total loads on the hulls were determined by numerically integrating the solutions of the formulated boundary value problem.

Chapter 4: Development of an Aero-Hydrodynamic Simulation Model for an Air Borne WIGcraft

4.1 Introduction

It has been theoretically proven that a wing moving near rigid ground or undisturbed water surface has a superior aerodynamic performance over a wing in free flight in terms of higher lift to induced drag ratio due to ground effect. As the proximity of the wing to the water surface increases, the aerodynamic and hydrodynamic components of the flow field become nonlinear and more strongly coupled. This flow coupling in addition to the 3D geometric variations of the small gap clearance underneath the wings may result in a significant variation on the dynamic behaviour of the wings and the free surface elevation. This coupling effect may be associated to the variations in the dynamic air pressure on both the wings and the free water surface. The flow problem at the air-water interface may thus be viewed as the mutual effect the air has on the water surface, vice versa.

In this chapter, a coupled aero-hydrodynamic flow model of an anhedral cambered wing with finite thickness attached to a hull moving at an angle of incidence near undisturbed free surface is developed based on potential flow assumptions.

Due to the high Reynolds number (attached) flows outside the thin boundary layer surrounding typical subsonic airplanes and WIGcraft, the complex momentum and continuity equations of the Navier Stokes equation may be respectively reduced to simple Bernoulli and Laplace equations in order to provide important features of the flow field without loss of generality. The spatial derivative of the potential function (or the solution) of the Laplace equation yields the outer-flow velocity distribution about the airborne vehicle. By solving the Bernoulli equation, the outer-flow pressure distribution may be estimated.

Since high Reynolds number fluid flow occur about the surfaces of the air borne WIGcraft model considered in this Chapter, the potential flow theory becomes applicable in the development of a numerical model to predict the forces on the model. The potential flow-based solutions may be improved by coupling a viscous flow model. The potential flow theory also offers the advantage of a simple and cost-effective computational means to nonlinearly couple the aerodynamic and hydrodynamic flow domains at the air-water interface of both air borne and water borne WIGcrafts via a 2.5D theory in each domain together with a fluid momentum exchange principle.

The aerodynamic problem under consideration is formulated based on the basic flow assumptions of the slender wing theory, which is valid for rectangular wing of aspect ratio of order <2. The solution to the BVP of wings with low aspect ratio of order >2 using the slender wing theory is generally first order accurate in comparison to solutions derived from theories that assume flow along the longitudinal plane of the wing. Higher order terms of the solution may be neglected. (Ashley and Landahl, 1965; Bollay, 1939).

This study extends Drela, (2014) numerical slender wing theory by implementing the 2.5D theory to rationally account for moderate to high forward speed effect and the strong nonlinear 3D character at the air-water interface in the small gap underneath the wing. Against the method of images, which is popularly used to account for ground effects on wings in proximity to planar surfaces and linearized free surfaces, this study proposes an alternative approach based on flow velocity and pressure continuity at the interface to account for non-planar and nonlinear ground effects.

Owing to the complex combined wing-body geometry and the proposed method of coupling the air and water flow considered in this study, the popular Douglas-Neumann panel method, first proposed by Hess and Smith (1967) which is based on distributions of source and vortex singularities on straight-line panels representing airfoils and wings surfaces in free flight is rendered inappropriate. To solve the BVP for the coupled air and water flow in the small gap, this study implements an alternative boundary element method (BEM) based on Green's second identity, which is applicable for the solution of general Neumann exterior boundary value problems via evaluation of potential functions and its normal derivatives on the elements comprising the boundaries of the domain. A related Green's function method has earlier been proposed by Morino Luigi and Kuo Ching-Chiang (1974) for 3D arbitrary wing with finite thickness in subsonic and unsteady flows in free flight.

Comparison of the results from the computational implementation of the proposed model developed in this chapter with those from Autowing vortex lattice code and experimental data is presented in Chapter 7 of this thesis.

4.2 General Assumptions

As with most Newtonian fluids, the flow characteristics about the moving rigid wings is generally governed by the interaction of gravitational, inertial, and viscous forces. For high Reynold's number attached flow over a wing moving at high speed near free surface, the modelling of the fluid flow and forces on a wing may be carried out based on similar general

flow assumptions made in section 3.2. On neglecting air compressibility and viscosity effect, the flow fields on the water and air domain may be described using the potential flow theory subject to boundary conditions on the wings and the undisturbed water surface. At the air-water interface underneath the wings, the flow field may be described using the potential flow theory with boundary conditions that couple the potential functions in both air and water domains.

4.3 Coordinate System

The position of the wing and the fluid are defined by the space-fixed ($O - xyz$), local geometric ($O - x_g y_g z_g$) and body-fixed ($G - x_b y_b z_b$) coordinate systems. These coordinate systems are similar to that described in chapter 3. However, the location of the origin space-fixed and local geometric coordinate system differs from their corresponding coordinate systems described in chapter 3. The body-fixed coordinate system is the same as described in chapter 3.

The origin of the space-fixed coordinate system may be arbitrarily located at any position in space. In this chapter, the origin of the space-fixed coordinate system is located on the free surface with its longitudinal position at the leading edge of the wing as shown in Figure 4.1. The x −axis points towards the tail of the vehicle in the reverse direction of the forward motion of the vehicle. the $O - xy$ plane lies on the undisturbed water surface while the $O - xz$ plane is perpendicular to the undisturbed free surface. The origin of the local geometric coordinate system is the same as described in chapter 3. However, in this chapter, its origin at the leading edge of the fuselage and it follows the baseline of the fuselage.

It is important to note that the aerodynamic BVP is solved in the space-fixed reference frame, the 2.5D theory is implemented on a local geometric reference frame and the equation of motion of the wing is specified and solved in the body-fixed reference frame.

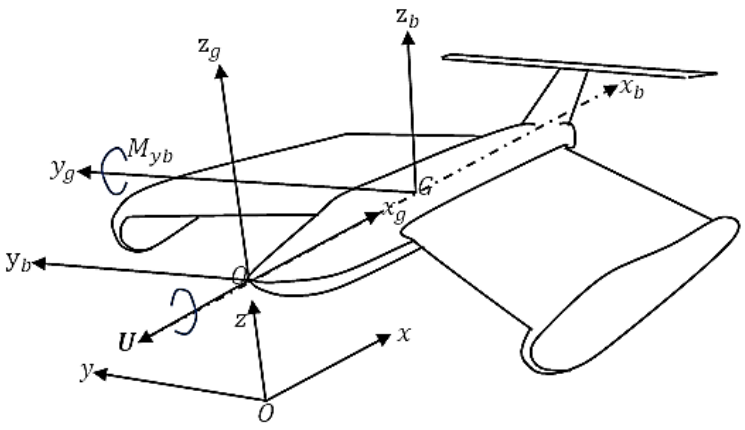

Figure 4.1 Coordinate systems

4.4 Formulation of the Problem

The anhedral low aspect ratio wing is considered to move with an attitude near water surface and on a straight course at a constant velocity $\boldsymbol{U}$ in the forward direction opposite the $x - axis$ direction in the space-fixed reference frame. The fluid flow underneath the wing is seen to exhibit a strong nonlinear 3D character at the air-water interface. Based on the assumptions stated in section 4.2 of this chapter, the flow fields everywhere in the air and water domains may be described by the velocity potentials $\Phi_i(\boldsymbol{\chi}, \mathrm{t})$ which satisfy the 3D Laplace equation

$$\nabla^2 \Phi_i(\boldsymbol{\chi}, \mathrm{t}) = 0 \qquad \text{on } \Xi_i(\mathrm{t}) \tag{4.1}$$

Where,

Subscript $i = 1$ on water domain and 2 on air domain.

$$\Phi_i(\boldsymbol{\chi}, \mathrm{t}) = \phi_i(\boldsymbol{\chi}, \mathrm{t}) + U_\infty x \tag{4.2}$$

As a result,

$$\nabla^2 \phi_i(\boldsymbol{\chi}, \mathrm{t}) = 0 \qquad \text{on } \Xi_i(\mathrm{t}) \tag{4.3}$$

The fluid velocities in the air and water domains may be expressed as

$$u_i = \nabla \phi_i(\boldsymbol{\chi}, \mathrm{t}) + U_\infty \quad \text{on } \Xi_i(\mathrm{t}) \tag{4.4}$$

The velocity of the air-water interface may be taken as the mean of the fluid velocities in the air and water domains,

$$w = \frac{\nabla \phi_1(\boldsymbol{\chi}, \mathrm{t}) + \nabla \phi_2(\boldsymbol{\chi}, \mathrm{t})}{2} + U_\infty \qquad \text{on} \qquad \Xi_{IF}(\mathrm{t}) \tag{4.5}$$

To simplify the solution to the 3D Laplace equation such that it can account for nonlinearities, the solution to the Laplace equation may be expanded with respect to perturbation parameters in accordance with the traditional slender wing theory. The relative ground clearance, $\left(h_c = \frac{height\ of\ wing from\ ground}{wing\ chord}\right)$ and the aspect ratio $\left(R_{WA} = \frac{wing\ span}{wing\ chord}\right)$ of the wing are two general mutually exclusive perturbation parameters for wings moving near rigid or deformable surface.

In span dominated ground effect, ground effect persists even when the clearance height is equal to the span of the wing. In chord dominated ground effect, extreme ground effect is noticed when the ground clearance is 10% of the chord length. The aspect ratio R_{WA} of the wings of a typical WIGcraft is generally low and is of the same order as the relative ground clearances h_c

at which ground effect noticeably influences the dynamic forces on the WIGcraft. As a result, the perturbation expansion may be carried out with respect to either of these two parameters.

It can be shown that upon implementing a series expansion on the steady perturbation velocity potential with respect to the ground clearance perturbation parameter, the 3D BVP is reduced to a set of 2D nonlinear BVP in crossflow planes along the chord of the wing. The flow field about the wing transverse sections in each of these crossflow planes may be described using the 2D Laplace equation (4.5) subjected to certain boundary conditions.

$$\nabla^2\phi_1(y,z,\mathrm{t}) = 0 \qquad (4.5)$$

The 2D Laplace equation describes flow continuity in the transverse planes (crossflow planes) of the transverse sections of the wing, subject to the boundary conditions described later in this section.

4.4.1 The 2D boundary value problem (BVP)

For a wing moving with constant velocity $\boldsymbol{U}$ and an angle of attack α, an observer on an earth-fixed reference frame, will see portions of the wing pass through a transverse plane fixed in space in a time dependent manner. Owing to the variations of the width, incident and anhedral angles, the motion of the wing is seen as a time-dependent vertical displacement and vertical velocity $V(x_w) = U_\infty sin\alpha(x_w)$ of its variable geometric section on the fixed transverse plane. It is noteworthy that the vertical displacement and variation in wing transverse section geometry along the chord of the wing in passage of time results in an unsteady flow about the wing-body.

The unsteady flow causes the added mass of the wing to change by an amount equivalent to the increase in aerodynamic lift per unit length (Keuning, 1994; von Karman, 1930). In other words, pressure difference arises between corresponding points on the upper and lower portion of the wing. Due to the presence of the water surface near the lower portion of the wing, the pressure on this part of the wing increases further, which may lead to further increase in the pressure difference and lift compared to wings in free flight.

The motion of the wing can also be seen to be analogous to that of an inverted variable deadrise hull. As a result, the 2.5D theory for non-similar, time varying section geometries described in chapter 3 becomes applicable for studying the aerodynamic problem of the wing subject to free surface effects. The solution to the 2D boundary value problem of the wing in ground effect is made unique when subjected to the boundary conditions of both the air and water domains.

a. Air and water domain decomposition

The BVP is seen as two different boundary value problems for air and water domains that are coupled together at the air-water interface. The air and water domain boundaries enclosing the wing section coincide at the air-water interface. The air-water interface is assumed to have zero thickness. It is required that the flow field in the air domain enclosing the upper and lower surfaces of the transverse wing section be continuous for correct application of BEM. As such, the air domain boundary surface is designed such that a branch-cut is inserted to make the domain simply connected and the flow solution single-valued as shown in Figure 4.2. The resulting air and water domains may be decomposed into boundary segments with differing conditions. The air and water domains setup and their respective boundary segments are shown in Figure 4.2.

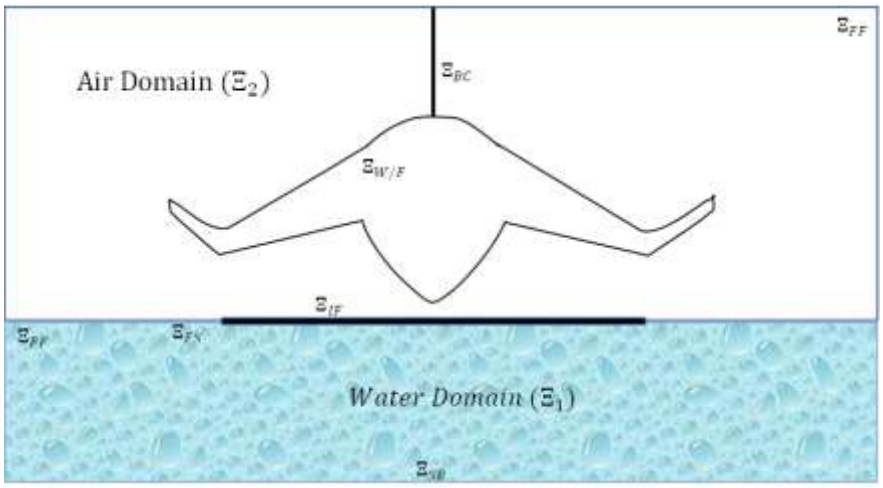

Figure 4.2 Domain decomposition for airborne WIGcraft

It is seen from Figure 4.2 that the air flow domain Ξ_2, for a wing transverse section is bounded by the following boundary segments, viz;

- wing-Fuselage cross section $\Xi_{w/F}$,
- far field at two vertical walls adjacent to the wing transverse section and one horizontal wall above the wing cross section Ξ_{FF},
- branch-cut with two-sided barrier surfaces Ξ_{BC} connecting the wing section to the vertical far field wall. The branch-cut is inserted to sandwich the discontinuities in the velocity potential and prevent circumnavigation of the wing transverse section.
- Air-water interface Ξ_{IF}, subjected to aerodynamic and atmospheric pressure.

Meanwhile, the water domain Ξ_1 is bounded by

- air-water interface boundary segment, Ξ_{IF}, subjected to aerodynamic and atmospheric pressure.
- a free surface boundary segment Ξ_{FS}, subjected to atmospheric pressure and adjacent to the air-water interface,
- far field boundary segments Ξ_{FF} at two vertical walls adjacent to the wing transverse section,
- seabed boundary segment Ξ_{SB} below the air-water interface and the free surface.

b. Boundary value problem in the air domain

The local geometry of a wing section and the air water interface are respectively prescribed by

$$h^{\pm}(y;t) - z = 0 \qquad \text{on } \Xi_w(\text{t}) \tag{4.6}$$

$$\zeta^{\pm}(y;t) - z = 0 \qquad \text{on } \Xi_{IF}(\text{t}) \tag{4.7}$$

Where plus and minus superscripts mean upper and lower portions of the surface respectively.

The kinematic boundary condition on the wing transverse section surface is given by,

$$\frac{\partial \phi_2}{\partial n} = \boldsymbol{V_{1n}} \qquad \text{on } z = h^{\pm}(y;t) \text{ on } \Xi_w(\text{t}) \tag{4.8}$$

In the steady flow boundary value problems, the velocity potential is continuous along the Ξ_{BC} and discontinuous across the branch-cut. The jump in the velocity potential across the branch-cut shown in Figure 4.2 is simply the difference in potential at points P_1 and P_2 where Ξ_W intersects Ξ_{BC}.

$$\Delta\phi_2 = \phi_{P2} - \phi_{P1} \tag{4.9}$$

Since the perturbation velocity is continuous off the body, it can be assumed that on the branch-cut, the tangential velocity potential (rate of change of the velocity potential along Ξ_{BC}) is continuous across the branch-cut. It can thus be shown that velocity potential jump along the Ξ_{BC} is constant.

$$\Delta\frac{\partial \phi_2}{\partial t} = \frac{\partial}{\partial t}\Delta\phi_2 = 0$$

$$\Delta\phi_2 = constant \tag{4.10}$$

The continuity of the tangential velocity potential across the branch-cut may be related to the constant potential jump along Ξ_{BC} via the velocity potentials at the points of intersection P_1 and P_2,

$$\Delta\phi_2 = \phi_{P2} - \phi_{P1} \qquad \text{on } \Xi_{BC}(t) \tag{4.11}$$

It can thus be seen that the velocity potential jump across the branch-cut is equal to flow circulation along the branch-cut.

$$\Delta\phi_2 = \phi_{P2} - \phi_{P1} = \oint_{P_1}^{P_2} \nabla\phi_2 \,.\, d\Xi = \Gamma \qquad \text{on } \Xi_{BC}(t) \tag{4.12}$$

$\Delta\phi_2$ has a constant value Γ all along the branch-cut.

Meanwhile, the normal component of the velocity potentials on the two sides of the branch cut are equal and opposite. As such, they cancel out and contribute nothing to the fluid flow in the domain.

The air flow on the far field and free surface boundaries outside the small gap are considered non-contributory to the total air flow in the air domain. The free surface is maintained at atmospheric pressure.

$$\nabla\phi_2 \to 0 \qquad \text{on } \Xi_{FF}(t) \text{ and } \Xi_{FS}(t) \tag{4.13}$$

The contribution of the flow in the air-water interface boundary to the total flow in the air domain is described below.

c. Air-water interface boundary conditions

At the interface, the continuity of normal velocity across the upper and lower portions of the interface should be satisfied. This continuity condition is satisfied by equating the normal derivative of the velocity potential on both sides of the interface. As a result, it can be assumed that the normal displacement velocity of the air-water interface is equal to the normal derivative of the velocity potential of fluid on either side of the interface,

$$\frac{\partial\phi_{IF}}{\partial n} = \frac{\partial\phi_1}{\partial n} = \frac{\partial\phi_2}{\partial n} \qquad \text{on } \Xi_{IF}(t) \tag{4.14}$$

The kinematic condition of the interface requires that fluid particles remain on the surface. As such, geometric evolution of the interface follows the position of the fluid particles on its surface at each time step. The air-water interface evolution equation may be given as

$$\frac{D\zeta}{Dt} = \frac{1}{2}(\phi_{1z} + \phi_{2z}) \quad \text{at } z = \zeta(y;t) \text{ on } \Xi_{IF}(\text{t}) \tag{4.15}$$

$$\frac{Dy}{Dt} = \frac{1}{2}(\phi_{1y} + \phi_{2y}) \quad \text{at } z = \zeta(y;t) \text{ on } \Xi_{IF}(\text{t}) \tag{4.16}$$

Where

$$\frac{D}{Dt} = \frac{\partial}{\partial t} + \frac{1}{2}\left(\sum_{i=1}^{2} \nabla\phi_i\right).\nabla$$

is the material derivative.

The dynamic boundary condition on the air-water interface requires pressure continuity across the interface to satisfy the momentum conservation law. In this study, the effect of the dynamic air pressure in the small gap on the free surface displacement is considered not negligible. Dynamic air pressure sets the free surface into dynamic motion. Unlike the studies in Grundy (1986), Liang et al. (2013a, 2013b) and Zong et al. (2012), the free surface is not linearized. A fully non-linear free surface hydrodynamic problem coupled to the aerodynamic problem at the interface is solved.

The dynamic condition (momentum conservation) of the ideal fluid on the air-water interface in the small gap can be satisfied following the MEL form of Bernoulli's equation for potential flow, which accounts for the dynamic and hydrostatic pressure on the interface,

$$\frac{D\phi_1}{Dt} = \frac{\rho_2}{\rho_1}\left[\frac{1}{2}|\nabla(\phi_2)|^2\right] + \frac{1}{2}\left(1 - \frac{\rho_2}{\rho_1}\right)(\nabla\phi_1.\nabla\phi_2) - g\zeta \quad \text{at } z = \zeta(y;t) \text{ on } \Xi_{IF}(\text{t}) \tag{4.17}$$

This equation (4.17) is valid if it is assumed that the effect of surface tension and air compression underneath the section is assumed to be negligible and and no air pocket is formed in the small gap.

d. Boundary value problem in the water domain

The free surface boundaries adjacent to the air-water interface boundaries are considered to be undisturbed and subjected to atmospheric pressure. As such, the velocity potential in these boundaries is zero. The far field and seabed boundary conditions are exactly similar as described in chapter 3 of this thesis. The boundary conditions of the air-water interface and the effects the flow on air-water interface has on the total water flow in the water domain are described in the preceding sub-section.

4.5 Numerical Solution Method

The aero-hydrodynamic coupled BVP can be solved as an initial value problem by iteratively coupling at the interface, the separate solutions of the boundary value problems in the air and water domains.

4.5.1 Numerical solution to BVP in water domain

The solution of the BVP in the water domain may be obtained by superposing the potential functions and its normal derivatives on the boundaries of the water domain subject to the boundary conditions described in the preceding section of this thesis. The value of the velocity potential and its normal derivative at any point (y, z) on the boundaries of the water domain where ϕ_1 is a continuous solution of the flow continuity equation, may be determined using the Green's second identity,

$$\vartheta\phi_1(y,z) = \int_{\Xi_1} \left[G(y,z;\eta,\zeta) \frac{\partial \phi_1(\eta,\zeta)}{\partial n(\eta,\zeta)} - \phi_1(\eta,\zeta) \frac{\partial G(y,z;\eta,\zeta)}{\partial n(\eta,\zeta)} \right] d\Xi_1(\eta,\zeta) \qquad (4.18)$$

Where,

ϑ is the solid angle interior to the domain between the tangents of corner points on the domain.

$$\delta = \begin{cases} \theta & \text{interior angle} \\ \pi & \text{semi} - \text{circled singularity point} \\ 2\pi & \text{for singularity point within domain} \end{cases}$$

The water domain Ξ_1 comprises of the interface contour Ξ_{IF}, free surface contour Ξ_{FS}, seabed contour Ξ_{SB}, and far field contour Ξ_{FF}. The Green's function $G(y,z;\eta,\zeta) = lnr$, where r is the distance between singularity and field point.

Water domain boundaries discretization

The integral over the far field (Ξ_{FF}), seabed (Ξ_{SB}), and free surface (Ξ_{FS}) boundary segments are considered non-contributory to the solution of the boundary integral equation.

Given that ϕ_1 on Ξ_{IF} can be determined from equation 4.17, the unknown in stated boundary integral equation is $\frac{\partial \phi_1}{\partial n}$ on Ξ_{IF}. To determine numeric values of this unknown, the various boundary segments are discretized into small straight-line elements connecting each other at nodes such that the linked elements follow the contour of the boundaries of the domain. The

boundary discretization approach may be such that, on the air-water interface boundary, smaller elements of equal size are used. Whereas for the other boundaries, larger sized elements whose size is further increased gradually as the distance between the boundaries and the wing section increases are used.

Discretization and solution of the boundary integral equation (BIE)

As in chapter 3, the boundary integral equation (BIE) eq.4.18, is discretized and applied at the centre node on the midpoint of each element in turn for the boundary segments. The discrete solutions to the BIE at each segment are assumed to be constant over the small length of each element. The discretized boundary integral equation for all points (y, z) at central nodes of the boundary elements may be expressed in matrices form as a set of N number of linear algebraic equations for the midpoint nodes on N number of elements making up the water domain boundaries,

$$[A]\{X\} = \{Y\} \tag{4.19}$$

$[A]$ is the influence coefficients of the unknown terms $\{X\}$ i.e. the unknown $\frac{\partial \phi_1}{\partial n}$ on the air-water interface in the small gap underneath the wing. $\{Y\}$ contains all the known terms of ϕ_1 on the air-water interface. Using matrix inversion technique, the unknown terms $\{X\}$ may be determined. Thus, the velocity potential and its normal derivative becomes known at the midpoints of all the elements of the air-water interface boundaries as well as other boundaries of the water domain.

4.5.2 Numerical solution to BVP in air domain

The solution of the BVP in the air domain may also be obtained by superposing the potential functions and its normal derivatives on the boundaries of the air domain subject to the boundary conditions described in the preceding section of this thesis. The value of the velocity potential and its normal derivative at any point (y, z) on the boundaries of the water domain may be determined using the Green's second identity,

$$\vartheta\phi_2(y,z) = \int_{\Xi_2} \left[G(y,z;\eta,\zeta) \frac{\partial \phi_2(\eta,\zeta)}{\partial n(\eta,\zeta)} - \phi_2(\eta,\zeta) \frac{\partial G(y,z;\eta,\zeta)}{\partial n(\eta,\zeta)} \right] d\Xi_2(\eta,\zeta) \qquad (4.20)$$

Where,

ϑ is the solid angle interior to the domain between the tangents of corner points on the domain.

$$\delta = \begin{cases} \theta & \text{interior angle} \\ \pi & \text{semi} - \text{circled singularity point} \\ 2\pi & \text{for singularity point within domain} \end{cases}$$

The boundaries of the air domain Ξ_2 comprises of the wing section contour, the branch-cut barriers Ξ_{BC}, air-water interface contour Ξ_{IF}, free surface contour Ξ_{FS}, and far field contour Ξ_{FF}. The Green's function $G(y,z;\eta,\zeta) = lnr$, where r is the distance between singularity and field point.

Discretization of domain boundaries

The integral over the far field (Ξ_{FF}) and free surface Ξ_{FS} boundary segments are considered non-contributory to the solution of the boundary integral equation. Since the normal derivative across the branch-cut cancels out, the integral over the branch-cut becomes,

$$-\Gamma \int_{\Xi_{BC}} \left[\frac{\partial G(y,z;\eta,\zeta)}{\partial n(\eta,\zeta)} \right] d\Xi_2(\eta,\zeta) \qquad (4.21)$$

Given that $\frac{\partial \phi_2}{\partial n}$ on Ξ_{IF} is assumed known from equation 4.14 while Γ on Ξ_{BC} can be determined from equation 4.12, the remaining unknowns in the stated boundary integral equation are ϕ_2 on Ξ_W and ϕ_2 on Ξ_{IF}. To determine numeric values of these unknowns, the various boundary segments are discretized into small straight-line elements connecting each other at nodes such that the linked elements follow the contour of the boundaries of the domain. In the discretization of the boundaries, the boundary Ξ_W of the wing and other boundaries such as Ξ_{IF} and Ξ_{BC} near the wing section, elements of equal size are used. However, for improved numerical accuracy, it is preferable that the size of the elements is increased gradually as the distance between the boundaries and the wing section increases. In essence, a greater number of smaller sized elements are used on the wing section and boundaries near it.

Discretization and solution of the boundary integral equation (BIE)

A similar BIE discretization scheme described in the previous sections of this thesis is implemented on the boundaries of the air domain to yield N number of linear algebraic equations.

$$[B]\{\mathfrak{X}\} = \{\Upsilon\} \tag{4.22}$$

$[B]$ is the influence coefficients of the unknown terms $\{\mathfrak{X}\}$ i.e. the unknown ϕ_2 on wing and air-water interface boundaries. $\{\Upsilon\}$ contains all the known terms of $\frac{\partial \phi_2}{\partial n}$ on the wing and air-water interface boundaries. the unknown terms in $\{\mathfrak{X}\}$ may be determined using matrix inversion technique. Thus, the velocity potential and its normal derivative becomes known at the midpoints of all the elements of the air-water interface boundaries as well as other boundaries of the air domain.

4.5.3 Coupling algorithm and solution to aero-hydrodynamic BVP

The steps taken to implement this coupling algorithm and solve the resulting aero-hydrodynamic BVP are described below.

a. *Determination of $\frac{\partial \phi_1}{\partial n}$ on the interface in the water domain*

   At the initial time $t_0 = 0$, ϕ_1 is assumed to be zero on the interface and free surface. Equation 4.19 is solved to obtain a tentative value for $\frac{\partial \phi_1}{\partial n}$ on the interface.

b. *Determination of ϕ_2 on the interface and wing section in the air domain*

   Using normal velocity continuity equation 4.14, $\frac{\partial \phi_2}{\partial n}$ on the interface in the air domain can be evaluated. Equation 4.22 is then solved to obtain ϕ_2 on the interface and wing section.

c. *Determination of new value of ϕ_1 on the interface in the water domain*

   By knowing the velocity potentials on the interface in the air domain in the preceding step, the pressure continuity equation 4.17 across the interface is evaluated using using the 4th order Runge Kutta numerical method to obtain a new value of ϕ_1 on the interface in the water domain. A similar procedure was carried out when evaluating the velocity potential on the free surface in chapter 3, howbeit, Adams Bashforth Moulton method was implemented during the evaluation process.

d. Convergence condition

The new value of ϕ_1 calculated in step (c) becomes the new tentative value of ϕ_1 on the interface in the water domain and step (a) is repeated to obtain a new value for $\frac{\partial \phi_1}{\partial n}$ on the interface in the water domain. Steps (b) to (d) are repeated until the current and previous values of $\frac{\partial \phi_1}{\partial n}$ on the interface converges. This iteration procedure is carried out at each time step prior to introducing the next wing-fuselage transverse section.

4.5.4 Air-water interface evolution

On achieving convergence during the solution of the coupled aero-hydrodynamic BVP in time t, the values of ϕ_1 and ϕ_2 on the interface obtained from the previous section, are used in the evaluation of the air-water interface evolution by solving equations 4.15 and 4.16 using the 4th order Runge Kutta numerical method to obtain the geometry of the air-water interface. As a result, the effect of the wing on the geometry of the free surface can be described. Similar procedure was carried out when evaluating the free surface evolution in chapter 3, howbeit, Adams Bashforth Moulton method was employed during the evaluation process.

4.5.5 Loading on wing transverse sections

It can be seen that the aerodynamic BVP of the wing-body combination in proximity to the free surface is seen to be analogous to that of the hydrodynamic BVP of planing watercraft. As a result, a similar method described in chapter may be employed to evaluate the pressure and force loading on transverse sections of the wing-body combination. The sectional aerodynamic pressure on the wing-fuselage transverse section moving at constant forward speed near disturbed water surface can be determined by evaluating the unsteady Bernoulli's equation,

$$P_{F/W} - P_a = -\rho_2 \left(\phi_{2t} + \frac{1}{2} |\nabla \phi_2(y,z)|^2 \right) \tag{4.23}$$

The sectional aerodynamic loading coefficient on the wing-fuselage section moving at constant forward speed near disturbed water surface may be expressed as

$$\sigma_p = \frac{P_l - P_u}{\frac{1}{2}\rho_2 U_\infty} \tag{4.24}$$

Where P_l and P_u are the pressure on the lower and upper portion of the wing-fuselage.

The aero-hydrodynamic forces and moment on any given section of the wing and/or fuselage on the vertical plane can be determined by numerically integrating the pressure on the surface of the section using the equation below,

$$f_{w/Fi} = \int_{\Xi_{W/F}} (P_2 - P_a) n_i d\Xi \qquad i = 1,3,5 \tag{4.25}$$

$f_{F/W1}, f_{F/W3}\ and\ f_{F/W5}$ are surge force, heave force and pitching moment respectively on the section.

In the traditional slender wing/body theory of free flight vehicles, where the air-water flows are not coupled, ϕ_{2t} in equation 4.23 may be evaluated by using the finite difference method. Using the transformation equation $x = ut$, ϕ_{2t} may be expressed as

$$\phi_{2t} = U_\infty \nabla \phi_2(x) \tag{4.26}$$

U_∞ is the free stream velocity.

However, for the 2.5D theory where the 3D unsteady nonlinear flows are accounted for in the small gap underneath the ground effect vehicle, the evaluation of ϕ_{2t} poses similar challenge as in the hydrodynamic case described in chapter 3. The ideal procedure for evaluating ϕ_{2t} would be to use an auxiliary velocity potential function and ϕ_{2t} together with the boundary conditions of the convergent solution of the BVP of given sections in the air domain. It can thus be shown that the sectional forces and pitch moment may be given in the body-fixed reference frame as

$$f_{W/Fi} = -\sum_{j=1}^{5} N_{ij} a_j + f_{Bi} \qquad \text{on wing-fuselage} \tag{4.27}$$

where,

f_{Bi} includes weight of wing-fuselage section and other non-acceleration related components. The sectional added mass N_{ij} is given as

$$N_{ij} = -\int_{\Xi_B} n_j \varphi_{1i} d\Xi \tag{4.28}$$

Using the popular added mass identity, $N_{ij} = N_{ji}$, for $i = j = 1,3,5$, equation (4.27) becomes

$$N_{ij} = -\int_{\Xi_B} \varphi_{ji} n_i d\Xi \tag{4.29}$$

For $i = 5$, $n_i = \boldsymbol{r} \times \boldsymbol{n}$

By assuming that the motions and accelerations of the wing-fuselage and air-water interface evolution is far less than that of the hull motions and free surface evolution described in chapter 3, finite difference approach can be used to estimate the value of ϕ_{2t} to a reasonable accuracy and without many difficulties.

4.6 2.5D Aero-hydrodynamic Theory

The traditional slender wing or body theory does not consider the effect of flow on one transverse wing section on adjacent sections. As a result, the slender wing-body theory is unsuitable to account for the 3D nonlinear effects associated with wings moving near water surface. As noted earlier in section 4.4.1, that in the passage of time, in a crossflow plane fixed in space, the wing-body combination under consideration in this thesis behaves in an almost similar manner to that of a non-similar or variable geometry hull described in chapter 3. It is of interest to note that the traditional slender body theory in aerodynamic assumes the unsteady flow may be approximated as a steady flow due to the fact that pressure propagates through incompressible air at an infinite rate. This approximation implies flow about a wing-body transverse section do not have influence over adjacent sections.

For wings moving near water surface, it is obvious that in the small gap between the lower portion of the wing and the air-water interface, the pressure propagation through the air is restrained and may no longer be infinite. As a result, the coupled flow about a wing-body section will influence the flow about downstream wing-body sections. On this note, the traditional slender wing-body theory fails to account for the effects of the strong nonlinear 3D coupled air-water flow in the small gap underneath the wings.

To account for the nonlinear 3D effects on the air-water interface and the wing-body combination, this study proposes the implementation of the 2.5D theory described in chapter 3 to extend of the traditional slender wing-body theory for wing-body combination in free flight. The flow problem is considered as an initial boundary value problem (IBVP), which is solved in a space-fixed solution control cross (SCC) plane following similar procedure described in Chapter 3.

4.6.1 2.5D theory procedure

To implementing the 2.5D procedure, the wing-body may be divided into three regions namely,

- the fore fuselage region which begins slightly ahead of the leading edge of the fuselage and ends near the leading edge of the foremost chord of the wing. This region begins at time $t = t_0$ and ends at time $t = t_{WLE-1}$
- The coupled wing-fuselage region which begins the leading edge of the wing and ends at the aft-most trailing edge of the wing. This region begins at time $t = t_{WLE}$ and ends at time $t = t_{WTE}$
- The aft fuselage section region which begins after the coupled wing-fuselage region and ends at the trailing edge of the fuselage. This region begins at time $t = t_{WTE+1}$ and ends at time $t = t_{FTE}$

Separate aero-hydrodynamic considerations are required for each of these regions. The coupled wing-fuselage region is of primary interested in this study. The fuselage only (fore and aft fuselage) regions contribute less to the aerodynamic lift of the airborne vehicle and consequently to the dynamics of the vehicle. The boundary value problem formulated for the coupled wing-body region and solved in the preceding sections of this chapter are applicable also to the fuselage only regions of the vehicle. However, the integrals over the wings are excluded from the solution of the formulated boundary value problem.

The solutions to the aero-hydrodynamic BVP in a cross plane may be seen as an initial boundary value problem (IBVP) in the solution control cross (SCC) plane, which is located initially slightly aft of the leading edge of the fuselage $x_g(t_0)$. Using the transformation equation, $x_g = Ut$ the solutions of the BVP in the SCC plane at any time may be stepped to the downstream sections of the wing-body downstream at equal time interval until it reaches the trailing edge of the fuselage. Because the 2D boundary value problem of the wing-body is solved together with a 3D interface boundary condition, the solution process is regarded as 2.5D theory.

At, $t = t_0$, it is assumed that an infinitesimal portion of the fuselage is located on the SCC. Since subsonic flow is considered and air compressibility is neglected, the velocity potential at the air-water interface may be initiated as tentative and used together with other initial boundary conditions to kick-start the iteration solution to the BVP of the section in the SCC as described in section 4.5.3. After convergence, the solution to the IBVP solved on the SCC plane at $x_g(t_0) = 0$ is used as the new boundary conditions on the next time t_1. The SCC plane with updated boundary conditions is stepped downstream to the next longitudinal position at $x_g(t_1) = x_{g_1}$. A new non-similar fuselage section is introduced to the SCC plane and the BVP is solved (as described in section 4.5.3) on the SSC plane at $x_g(t_1) = x_{g_1}$, subjected to the air-

water interface boundary conditions at the SCC plane and the new fuselage section boundary condition.

The stepping process is repeated after convergence of the solution at each station along the longitudinal axis of the hull, until the SCC plane reaches the longitudinal location $x(t_{WLE-1}) = x_{g_{t_{WLE-1}}}$, prior to where the coupled wing-fuselage region begins. The interface geometry and the fore fuselage loading are evaluated in accordance with sections 4.5.4 and 4.5.5 of this chapter for all the sections in this region.

The SCC plane enters the coupled wing-fuselage region with updated air-water interface boundary conditions at time $t = t_{WLE}$ where the BVP of the first section with its unique boundary conditions in this region is solved following section 4.5.3 until convergence is reached. The SCC plane stepping process continues to downstream wing-fuselage sections whose BVP are solved until $x_g(t_{WTE}) = x_{g_{t_{WTE}}}$, prior to where the aft fuselage region begins. The air-water interface geometry, the wing and the fuselage loading are evaluated in accordance with sections 4.5.4 and 4.5.5 of this chapter for all the sections in this region.

Following similar routine as described in the last paragraph, the BVP of the various sections in the aft fuselage region are solved at the respective positions of the SCC plane with updated interface boundary conditions until the section at the trailing edge of the fuselage is reached. The air-water interface geometry and the aft fuselage loading are evaluated in accordance with sections 4.5.4 and 4.5.5 of this chapter for all the sections in this region.

4.7 Total Force on Wing and Fuselage

The distribution of the transverse loads along the longitudinal axis of the vehicle may be evaluated from the results of the 2.5D theory for all transverse sections of the air borne WIGcraft vehicle. The total aero-hydrodynamic forces on the vehicle may be determined by integrating the load or sectional lift distribution beginning from the leading edge of the fuselage over the entire length of the vehicle,

4.8 Chapter Summary

In this chapter, the Drela (2014) numerical slender wing-body theory has been extended to account for the strong nonlinear 3D flows within the small gap of an air-borne vehicle moving at constant speed near undisturbed water surface. The proposed aero-hydrodynamic numerical model is analogous to the 2.5D hydrodynamic theory and can be used to account for ground effects on a non-planar aerodynamic surface moving at constant speed near a nonplanar rigid or deformable surface.

Separate boundary value problems were formulated for the flows in the air and water domains. The BVPs are coupled together at the air-water interface in the small gap underneath the wing-fuselage using velocity and pressure continuity equations. The boundary value problems were solved as an initial boundary value problem using the BEM and an iterative scheme in a solution control cross plane, until the solution converges. Evolution equations were presented to determine the air-water interface geometry during the passage of the vehicle. The rational for the 2.5D theory for the aero-hydrodynamic problem and the procedure for implementing the theory were discussed.

The proposed model allows the effect of the free surface on the wing-fuselage to be accounted during the evaluation of the loadings on the wing-fuselage. A similar method developed for the temporal derivative of velocity potential in chapter 3 was suggested to give accurate results for the temporal derivative of the velocity potential in the air domain. An alternative approximate method based on finite difference method was also presented to evaluate the temporal derivative of the velocity potential in the air domain. Finally, formula for calculating the total load on the vehicle were also presented.

Chapter 5: Development of a Numerical Aero-Hydrodynamic Simulation Model for a Water Borne WIGcraft

5.1 Introduction

This chapter proposes a nonlinear numerical model to evaluate the coupled aero-hydrodynamic characteristics of a WIGcraft moving at constant speed near calm water surface. The proposed model is based on the combination of the hydrodynamic model for a high-speed watercraft developed in chapter 3 and the aero-hydrodynamic model of an air-borne WIGcraft developed in chapter 4. The same coordinate systems in chapter 4 are used in this chapter. In extending the model developed in chapter 4 to account for the effect of the free surface deformation caused by the submerged hull of the WIGcraft, the BVP of the water domain in chapter 4 is replaced by the BVP of the water domain in chapter 3. A two-step iterative procedure is proposed to couple the air and water domains. Details of the air and water domain coupling procedure, and numerical treatments are presented in this chapter.

5.2 Formulation of the Problem

The WIGcraft model is considered to move with an attitude near water surface and on a straight course at a constant velocity $\boldsymbol{U}$ in the forward direction opposite the $x - axis$ direction in the space-fixed reference frame as shown in Figure 4.1. Based on the assumptions stated in section 4.2 of this chapter, the flow fields everywhere in the air and water domains may be described by the velocity potentials $\Phi_i(\boldsymbol{\chi}, \mathrm{t})$ which satisfy the 3D Laplace equation

$$\nabla^2 \Phi_i(\boldsymbol{\chi}, \mathrm{t}) = 0 \qquad \text{on } \Xi_i(\mathrm{t}) \tag{5.1}$$

Where,

Subscript $i = 1$ on water domain and 2 on air domain.

$$\Phi_i(\boldsymbol{\chi}, \mathrm{t}) = \phi_i(\boldsymbol{\chi}, \mathrm{t}) + U_\infty x \tag{5.2}$$

As a result,

$$\nabla^2 \phi_i(\boldsymbol{\chi}, \mathrm{t}) = 0 \qquad \text{on } \Xi_i(\mathrm{t}) \tag{5.3}$$

The fluid velocities in the air and water domains may be expressed as

$$u_i = \nabla \phi_i(\boldsymbol{\chi}, \mathrm{t}) + U_\infty \quad \text{on } \Xi_i(\mathrm{t}) \tag{5.4}$$

The fluid velocity on the air-water interface in the small gap underneath the wings may be taken as the mean of the fluid velocities in the air and water domains,

$$w = \frac{\nabla\phi_1(\chi,\mathrm{t})+\nabla\phi_2(\chi,\mathrm{t})}{2} + U_\infty \quad \text{on} \quad \Xi_{IF}(\mathrm{t}) \qquad (5.5)$$

Based on the slender wing-body assumptions discussed in chapter 3 and 4, the 3D BVP is reduced to a set of 2D nonlinear BVP in crossflow planes along the longitudinal axis of the vehicle. The flow field about the wing transverse sections in each of these crossflow planes may be described using the 2D Laplace equation (5.6) subjected to certain boundary conditions.

$$\nabla^2\phi_i(y,z,\mathrm{t}) = 0 \qquad (5.6)$$

The 2D Laplace equation describes flow continuity in the transverse planes (crossflow planes) of the transverse sections of the submerged hull and/or wing-fuselage, subject to the boundary conditions described later in this section.

5.2.1 The 2D boundary value problem (BVP)

The BVP for the vehicle in a cross-flow plane can be viewed as a combination of non-similar wedged-shaped hull section and non-similar inverted wedged shaped wing-fuselage body section moving with vertical displacement and velocity in spaced-fixed cross-flow plane in an unsteady manner. As a result, the 2.5D theory for non-similar, time varying section geometries discussed in chapter 3 and 4 becomes applicable for studying the aerodynamic problem of the wing-fuselage and the hydrodynamic problem of the submerged hull. Both BVPs are mutually inclusive, subject to the air-water interface conditions. The solution to the 2D boundary value problem of the wing-fuselage section in ground effect and/or the submerged hull section is made unique when subjected to the air-water interface and other boundary conditions in both the air and water domains.

a. Air and water domain decomposition

The BVP is seen as two different boundary value problems for air and water domains that are coupled together at the air-water interface. The air and water domain boundaries enclosing the wing-fuselage and/or the submerged hull sections coincide at the air-water interface. Unlike Figure 4.2 in chapter 4, in this chapter, part of the hulls is considered to penetrate the air-water interface. The interface is assumed to have zero thickness. It is required that the flow fields in the air and water domains which respectively enclose the transverse wing-fuselage and

submerged hull section be continuous for correct application of BEM as shown in Figure 5.1. Details of the insertion of a branch-cut in the air domain are discussed in chapter 4 and also shown in Figure 5.1.

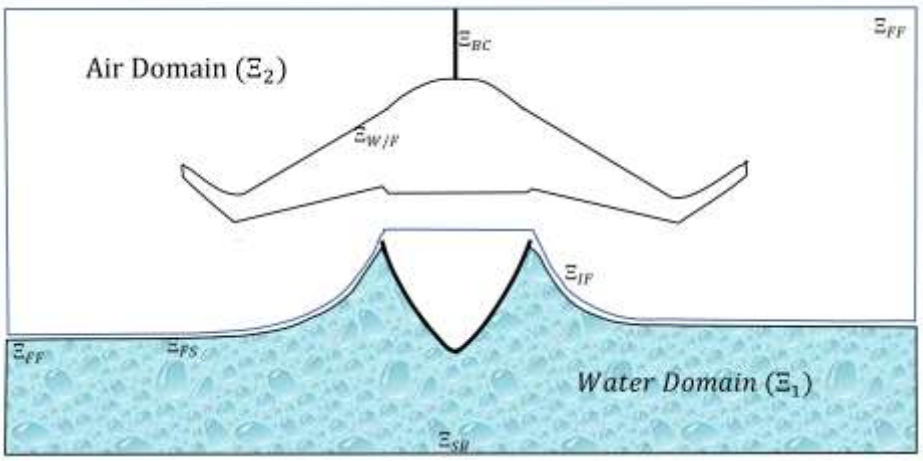

Figure 5.1a Domain decomposition for monohull WIGcraft section on free surface

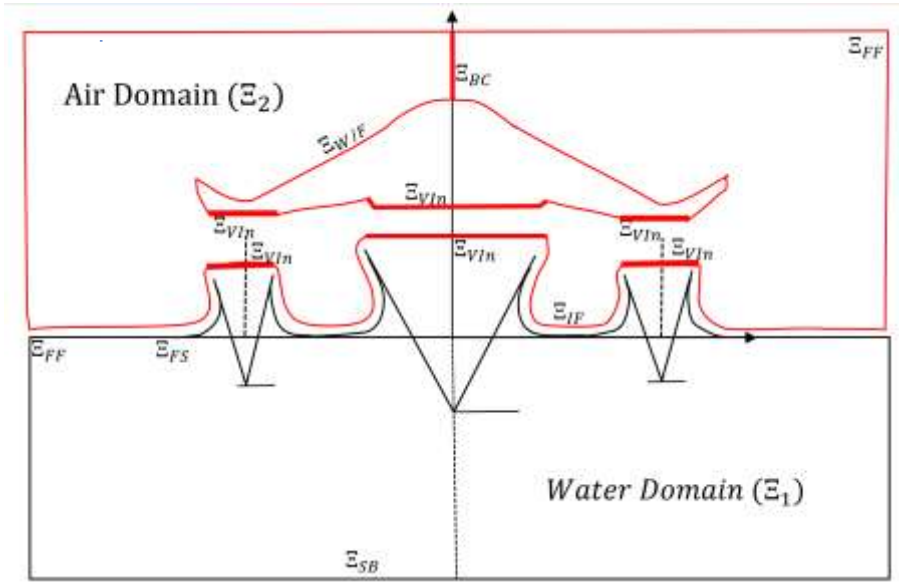

Figure 5.1b Domain decomposition for multihull WIGcraft section on free surface

It can be seen in Figure 5.2 that an internal boundary segment Ξ_{VIn} is introduced to split the vehicle body near the wing root into hull and wing-fuselage sections in other to ensure the air and water domains are separated and closed. As a result, the BEM can be applied to solve the BVP in each domain separately. These internal boundaries are virtual, and their velocity potential may be chosen arbitrarily. On these virtual internal boundary segments Ξ_{VIn}, the velocity potential on the internal and external parts are assumed equal. The normal derivative

of the velocity potential on the internal and external parts of Ξ_{VIn} are also assumed equal. As a result, the velocity potential, and its normal derivative on Ξ_{VIn} are non-contributory to the total solution in each of the domains.

Figure 5.2 illustrates that the air-water interface boundary in the small gap is located on either side of the main hull while the free surfaces is located on the outer sides of the sponsons. Figure 5.2 further shows that the air-water interface is dynamic and nonlinear due to the forward motion and perturbations of the submerged hull. Otherwise, it can be stated that the boundaries of the air domain in Figure 4.2 is the same as that of Figure 5.2. It can also be seen that the boundaries of the water domain in Figure 3.2 is the same as that of Figure 5.2, however, the elevation and boundary conditions of the water surface are different due to the dynamic air pressure from wings.

b. Boundary value problem in the air domain

The local geometry of a wing-fuselage section and the air water interface are respectively given as

$$h^{\pm}(y;t) - z = 0 \qquad \text{on } \Xi_{W/F}(\text{t}) \tag{5.7}$$

$$\zeta^{\pm}(y;t) - z = 0 \qquad \text{on } \Xi_{IF}(\text{t}) \text{ and } \Xi_{FS} \tag{5.8}$$

Where plus and minus superscripts mean upper and lower portions of the surface respectively.

The kinematic boundary condition on the wing transverse section surface is given by,

$$\frac{\partial \phi_2}{\partial n} = \boldsymbol{V_{1n}} \qquad \text{on } z = h^{\pm}(y;t) \text{ on } \Xi_{w/F}(\text{t}) \tag{5.9}$$

The velocity potential jump across the branch-cut is given as

$$\Delta\phi_2 = \phi_{P2} - \phi_{P1} = \oint_{P_1}^{P_2} \nabla\phi_2 \,.\, d\Xi = \Gamma \qquad \text{on } \Xi_{BC}(\text{t}) \tag{5.10}$$

$\Delta\phi_2$ has a constant value Γ all along the branch-cut.

The normal component of the velocity potential on the two sides of the branch-cut cancels out and contributes nothing to the fluid flow in the domain. The air flow on the far field above and below the wing-fuselage in the air domain are considered non-contributory to the total air flow in the air domain.

The air particles on the free surface boundaries on the outer part of the sponsons in the air domain are not dynamic and are considered non-contributory to the total air flow in the air domain. The free surface is steadily maintained at atmospheric pressure always. Thus,

$$\nabla\phi_2 \to 0 \qquad \text{on } \Xi_{FS}(t) \tag{5.11}$$

The evolution of the free surface Ξ_{FS}(t) on the outer part of the sponsons in the air domain are dictated by the free surface evolution equations in the water domain discussed in chapter 3 and later in this section.

The contribution of the flow in the air-water interface boundary Ξ_{IF}(t) to the total flow in the air domain is described below.

c. Air-water interface boundary conditions

As in chapter 4, it is assumed that the normal displacement velocity of the air-water interface is equal to the normal derivative of the velocity potential of fluid on either side of the interface,

$$\frac{\partial\phi_{IF}}{\partial n} = \frac{\partial\phi_1}{\partial n} = \frac{\partial\phi_2}{\partial n} \qquad \text{on } \Xi_{IF}\text{(t)} \tag{5.12}$$

The air-water interface evolution equation may be given as

$$\frac{\tilde{D}\zeta}{Dt} = \frac{1}{2}(\phi_{1z} + \phi_{2z}) \quad \text{at } z = \zeta(y;t) \text{ on } \Xi_{IF}\text{(t)} \tag{5.13}$$

$$\frac{\tilde{D}y}{Dt} = \frac{1}{2}(\phi_{1y} + \phi_{2y}) \quad \text{at } z = \zeta(y;t) \text{ on } \Xi_{IF}\text{(t)} \tag{5.14}$$

Where

$$\frac{\tilde{D}}{Dt} = \frac{\partial}{\partial t} + \frac{1}{2}\left(\sum_{i=1}^{2}\nabla\phi_i\right).\nabla$$

is the material derivative.

As in chapter 4, the dynamic condition (momentum conservation) of the ideal fluid on the air-water interface is given by

$$\frac{D\phi_1}{Dt} = \frac{\rho_2}{\rho_1}\left[\frac{1}{2}|\nabla(\phi_2)|^2\right] + \frac{1}{2}\left(1 - \frac{\rho_2}{\rho_1}\right)(\nabla\phi_1.\nabla\phi_2) - g\zeta \quad \text{at } z = \zeta(y;t) \text{ on } \Xi_{IF}\text{(t)} \tag{5.15}$$

This equation (5.15) is valid if it is assumed that the effect of surface tension and air compression underneath the section is assumed to be negligible and and no air pocket is formed in the small gap.

d. Boundary value problem in the water domain

The far field and seabed boundary conditions are exactly similar as described in chapter 3. The boundary conditions of the air-water interface and the effects the flow on air-water interface has on the total water flow in the water domain are described in the preceding sub-section.

The kinematic and dynamic boundary conditions of the free surface Ξ_{FS}(t) on the outer side of the sponsons in the water domain are expressed in the mixed Euleran-Lagrangian form as in chapter 3,

$$\frac{D\zeta}{Dt} = (\phi_1)_z \quad \text{at } z = \zeta(y;t) \text{ on } \Xi_{FS}(\text{t}) \tag{5.16}$$

$$\frac{Dy}{Dt} = (\phi_1)_y \quad \text{at } z = \zeta(y;t) \text{ on } \Xi_{FS}(\text{t}) \tag{5.17}$$

$$\frac{D\phi_1}{Dt} = \frac{1}{2}|\nabla(\phi_1)|^2 - g\zeta \quad \text{on } z = \zeta(y;t) \quad \text{on } \Xi_{FS}(\text{t}) \tag{5.18}$$

Where,

$\frac{D}{Dt} = \frac{\partial}{\partial t} + \nabla\phi_1.\nabla$ is the material derivative.

5.3 Numerical Solution Method

The aero-hydrodynamic coupled BVP may be solved as an initial value problem by iteratively coupling at the free surface and air-water interface, the separate solutions of the boundary value problems in the air and water domains.

5.3.1 Numerical solution to BVP in water domain

The solution of the BVP in the water domain may be obtained by superposing the potential functions and its normal derivatives on the boundaries of the water domain subject to the boundary conditions described in the preceding section of this thesis. The value of the velocity potential and its normal derivative at any point (y, z) on the boundaries of the water domain where ϕ_1 is a continuous solution of the flow continuity equation, may be determined using the Green's second identity,

$$\vartheta\phi_1(y,z) = \int_{\Xi_1} \left[G(y,z;\eta,\zeta) \frac{\partial \phi_1(\eta,\zeta)}{\partial n(\eta,\zeta)} - \phi_1(\eta,\zeta) \frac{\partial G(y,z;\eta,\zeta)}{\partial n(\eta,\zeta)} \right] d\Xi_1(\eta,\zeta) \quad (5.19)$$

Where,

ϑ is the solid angle interior to the domain between the tangents of corner points on the domain.

$$\delta = \begin{cases} \theta & \text{interior angle} \\ \pi & \text{semi} - \text{circled singularity point} \\ 2\pi & \text{for singularity point within domain} \end{cases} \quad (5.20)$$

The water domain Ξ_1 comprises of the hull contour Ξ_H, interface contour Ξ_{IF}, free surface contour Ξ_{FS}, seabed contour Ξ_{SB}, and far field contour Ξ_{FF}. The Green's function $G(y,z;\eta,\zeta) = lnr$, where r is the distance between singularity and field point.

Water domain boundaries discretization

The integral over the far field (Ξ_{FF}) boundary segment is considered non-contributory to the solution of the boundary integral equation. By implementing the double body method with respect to the seabed at $-d_h$, the seabed boundary condition (Ξ_{SB}) can be satisfied.

The free surface contour Ξ_{FS} which consists of inner and outer parts is restricted to the outer part of the sponsons. The inner and the outer parts of the free surface are similar in character to the free surface described in chapter 3. As a result, the discretization of the free surface contour follows the approach used in chapter 3.

The water surface on either side of the main hull as well as that on the inner part of the submerged sponsons may not be regarded as 'free' since it is subjected to aerodynamic pressure from the wings. In this chapter, the water surface in the small gap underneath the wings is regarded as the air-water interface. The air-water interface contour Ξ_{IF} is the boundary segment where the aerodynamic fluid flow about the wing-fuselage and hydrodynamic fluid flow about the submerged hull are primarily coupled. The air-water interface also consists of inner and outer parts, both subjected to aerodynamic pressure.

The jet flow, wave rise and the flow intersection with the submerged main hull and inner part of the submerged sponson, which are subject to aerodynamic pressure are studied in the inner part of the air-water interface, while the outer part of the air-water interface of the submerged main hull and sponsons, behaves like a vertical dipole subjected to aerodynamic pressure. The discretization of the air-water interface contour follows the same discretization scheme used for

the free surface contour in chapter 3. That is, the boundary discretization approach is such that, on Ξ_H and other boundaries near the multi-hull section, elements of equal size are used. However, for more numerical accuracy, it is preferable that the size of the elements is increased gradually as the distance between the boundaries and the hull section increases. In essence, a greater number of smaller sized elements are used on the hull section and boundaries near it.

The unknowns in stated boundary integral equation are ϕ_1 on Ξ_H, $\frac{\partial \phi_1}{\partial n}$ on Ξ_{FS}, $\frac{\partial \phi_1}{\partial n}$ on Ξ_{IF} as well as A(t) which is determined as part of the solution of equation 5.19. To determine numeric values of these unknowns, the various boundary segments are discretized into small straight-line elements connecting each other at nodes such that the linked elements follow the contour of the boundaries of the domain.

Discretization and solution of the boundary integral equation (BIE)

As in chapter 3, the boundary integral equation (BIE) equation 5.19, is discretized and applied at the centre node on the midpoint of each element in turn for the Neumann and Dirichlet boundary segments. The discrete solutions to the BIE at each segment are assumed to be constant over the small length of each element. The discretized boundary integral equation for all points (y, z) at central nodes of the boundary elements may be expressed in matrices form as a set of N number of linear algebraic equations for the midpoint nodes on N number of elements making up the water domain boundaries,

$$[A]\{X\} = \{Y\} \tag{5.21}$$

$[A]$ is the influence coefficients of the unknown terms $\{X\}$ i.e. the unknown $\frac{\partial \phi_1}{\partial n}$ on the inner and outer free surface on the outer part of the sponsons, $\frac{\partial \phi_1}{\partial n}$ on the inner and outer part of the air-water interface in the small gap underneath the wing and ϕ_1 on the submerged hulls.

$\{Y\}$ contains all the known terms of ϕ_1 on the inner and outer free surface contour, ϕ_1 on the inner and outer air-water interface contour and $\frac{\partial \phi_1}{\partial n}$ on the hull contours. Using matrix inversion technique, the unknown terms $\{X\}$ may be determined. Thus, the velocity potential and its normal derivative becomes known at the midpoints of all the elements of the hull, free surface and air-water interface boundaries as well as other boundaries of the water domain.

5.3.2 Numerical solution to BVP in air domain

The solution of the BVP in the air domain may also be obtained by superposing the potential functions and its normal derivatives on the boundaries of the air domain subject to the boundary conditions described in the preceding section of this thesis. The value of the velocity potential and its normal derivative at any point (y, z) on the boundaries of the water domain may be determined using the Green's second identity,

$$\vartheta\phi_2(y,z) = \int_{\Xi_2} \left[G(y,z;\eta,\zeta) \frac{\partial \phi_2(\eta,\zeta)}{\partial n(\eta,\zeta)} - \phi_2(\eta,\zeta) \frac{\partial G(y,z;\eta,\zeta)}{\partial n(\eta,\zeta)} \right] d\Xi_2(\eta,\zeta) \tag{5.22}$$

Where,

ϑ is the solid angle interior to the domain between the tangents of corner points on the domain.

$$\delta = \begin{cases} \theta & \text{interior angle} \\ \pi & \text{semi} - \text{circled singularity point} \\ 2\pi & \text{for singularity point within domain} \end{cases} \tag{5.23}$$

The boundaries of the air domain Ξ_2 comprises of the wing-fuselage section contour, the branch-cut barriers Ξ_{BC}, air-water interface contour Ξ_{IF}, free surface contour Ξ_{FS}, far field contour Ξ_{FF} and the virtual internal contours Ξ_{VIn}. The Green's function $G(y,z;\eta,\zeta) = lnr$, where r is the distance between singularity and field point.

Discretization of domain boundaries

The integral over the far field (Ξ_{FF}), the free surface Ξ_{FS} and the virtual internal (Ξ_{VIn}) boundary segments are considered non-contributory to the solution of the boundary integral equation. As in chapter 4, the integral over the branch-cut is given as

$$-\Gamma \int_{\Xi_{BC}} \left[\frac{\partial G(y,z;\eta,\zeta)}{\partial n(\eta,\zeta)} \right] d\Xi_2(\eta,\zeta) \tag{5.24}$$

Given that $\frac{\partial \phi_2}{\partial n}$ on Ξ_{IF} is assumed known from equation 5.12 while Γ on Ξ_{BC} can be determined from equation 5.10, the remaining unknowns in the stated boundary integral equation are ϕ_2 on $\Xi_{W/F}$ and ϕ_2 on Ξ_{IF}.

The values of these unknowns are obtained by discretizing the boundary segments into small straight-line elements connecting each other at nodes such that the linked elements follow the contour of the boundaries of the domain. In the discretization of the boundaries, the boundary

$\Xi_{W/F}$ of the wing-fuselage and other boundaries such as Ξ_{IF} and Ξ_{BC} near the wing section, elements of equal size are used. However, as was stated for the water domain, it is preferable that the size of the elements is increased gradually as the distance between the boundaries and the wing/fuselage section increases.

Discretization and solution of the boundary integral equation (BIE)

A similar BIE discretization scheme described for the wing/fuselage in chapter 3 of this thesis, is implemented on the boundaries of the air domain to yield N number of linear algebraic equations.

$$[B]\{\mathfrak{X}\} = \{\Upsilon\} \tag{5.25}$$

$[B]$ is the influence coefficients of the unknown terms $\{\mathfrak{X}\}$ i.e. the unknown ϕ_2 on wing/fuselage and air-water interface boundaries. $\{\Upsilon\}$ contains all the known terms of $\frac{\partial \phi_2}{\partial n}$ on the wing/fuselage section and air-water interface boundaries. the unknown terms in $\{\mathfrak{X}\}$ are determined using matrix inversion technique. Thus, the velocity potential and its normal derivative becomes known at the midpoints of all the elements of the air-water interface boundaries as well as other boundaries of the air domain.

5.3.3 Procedure for Coupling the Air and Water Domains

The approach implemented to couple the aerodynamic and hydrodynamic boundary value problems and solve the resulting aero-hydrodynamic BVP in chapter 4 are modified to account for the presence of the hull section and its effects on the evolution of the air-water interface and free surface, and the resultant aero-hydrodynamic coupling effects on both the hull and wing/fuselage sections. The following steps are implemented to couple the aerodynamic and hydrodynamic BVPs,

a. *Determination of $\frac{\partial \phi_1}{\partial n}$ on the free surface and air-water interface in the water domain*
   At the initial time $t_0 = 0$, ϕ_1 is determined from the Mackie's analytical solution to the initial value problem on the free surface and interface as discussed in chapter 3. Equation 5.19 is solved to obtain a tentative value for $\frac{\partial \phi_1}{\partial n}$ on the free surface and the air-water interface.

b. *Determination of ϕ_2 on the air-water interface and wing section in the air domain*

   Using normal velocity continuity equation 5.12, $\frac{\partial \phi_2}{\partial n}$ on the interface in the air domain can be evaluated. Equation 5.22 is then solved to obtain ϕ_2 on the air-water interface and wing section.

c. *Determination of new value of ϕ_1 on the free surface and air-water interface in the water domain*

   By knowing the velocity potentials on the air-water interface in the air domain in the preceding step, the pressure continuity equation 5.15 across the air-water interface is evaluated using using the 4th order Adams Bashforth Moulton method to obtain a new value of ϕ_1 on the interface in the water domain. The new value of ϕ_1 on the free surface in the water domain is obtained from equation 5.18 in the next time step using the 4th order Adams Bashforth Moulton numerical method discussed in chapter 3.

d. *Convergence condition on the air-water interface*

   On the air-water interface, the new value of ϕ_1 calculated in step (c) becomes the new tentative value of ϕ_1 on the interface in the water domain and step (a) is repeated to obtain a new value for $\frac{\partial \phi_1}{\partial n}$ on the air-water interface in the water domain. Steps (b) to (d) are repeated until the current and previous values of $\frac{\partial \phi_1}{\partial n}$ on the air-water interface converges. This iteration procedure is carried out at each time step prior to introducing the next WIGcraft transverse section.

5.4 Free Surface and Air-water Interface Evolution, Smoothing and Regridding

On achieving convergence during the solution of the coupled aero-hydrodynamic BVP in time t, the values of ϕ_1 and ϕ_2 on the air-water interface obtained from the preceding section are used in the evaluation of the air-water interface evolution equations 5.13 and 5.14, by implementing the 4th order Adams Bashforth Moulton numerical method to obtain the geometry of the air-water interface for the next time step. As a result, the effect of the wing on the geometry of the free surface can be described. Similarly, on the free surface, the value of ϕ_1 on the free surface obtained from the preceding section are used in the solving the free surface evolution equations 5.16 and 5.17, by employing the Adams Bashforth Moulton method to obtain the geometry of the free surface for the next time step. The evaluation of the free surface and air-water interface evolution follows the same methods used in section 3.5.3 of chapter 3 in compliance with mass, momentum and energy conservation laws. A smoothing and regriding

procedure similar to that described in section 3.5.4 is implemented to remove numerical instabilities on the interface and free surface and prepare the boundaries of these surfaces for the next time step.

5.5 Water jet and spray cut-off models

Main spray blisters and whiskers spray has been discussed in chapter 3 of this thesis for free water surface.

The presence of the wing over the free surface requires extra caution when following the fluid particle during the solution of the free surface evolution equations. Three possibilities that may cause the numerical breakdown of the BEM calculation include,

- Points on the free surface near the hull section breaching the hull section boundaries during the free surface evolution process. The procedure to avoid this follows similar treatments described in chapter 3.
- The thin spray emanating from the water jet impacting on the free surface and/or air-water interface after overturning at its apex location. The jet cut-off procedure described in chapter 3 was found suitable to prevent this from occurring.
- Main spray and whiskers spray hitting on the wing-fuselage section surface prior to reaching the apex its trajectory. A jet cut-off procedure is implemented prior to the spray or wave rise reaching any part of the wing-fuselage section. A local empirical model can be introduced to describe the trajectory of the spray on the wings-fuselage.

It was noted in chapter 3 that because, the sections are non-similar, there is the possibility of the spray to exhibiting the monotonous spray characteristics beyond the curved spray root towards the spray edge and that contact angle between the free surface and the hull section contours is unknown a priori. To account for gravity effect, the jet spray cut-off model implemented in this chapter is similar to that described in chapter 3. However, the jet is cut-off before it reaches the adjacent hulls and the wings in the interface without considering the limiting distance between the water jet and the hull section contour. A new element connecting the hull section to the first node on the first element of the free surface is introduced to close the flow domain in other to satisfy the condition required to implement the BEM.

5.6 Pressure, Forces and Pitching Moment on Hull Transverse Section

The values of ϕ_1 on the hull surfaces may be inserted into equation 5.26 to determine the aerodynamic influenced hydrodynamic pressure on the submerged main hull section as well as that on the inner part of the submerged sponsons. Similarly, the values of ϕ_1 on the outer part of the submerged sponson can also be inserted into equation 5.26 to determine the hydrodynamic pressure on that part of the sponsons.

$$P_H - P_a = -\rho_1 \left(\phi_{1t} + \frac{1}{2} |\nabla \phi_1(y,z)|^2 \right) \tag{5.26}$$

ϕ_{1t} is evaluated in the water domain as described in chapter 3, by using the boundary conditions of the solution of BVP for given sections in the water domain.

The hydrodynamic forces and moment on the hull section which consists of the main hull Ξ_{H1} and inner part of the sponsons Ξ_{H2} section boundaries as well as on the outer part of the sponsons Ξ_{H3} boundary on the vertical plane may be determined by numerically integrating the pressure on the surface of the hull boundaries,

$$f_{Hi} = \int_{\Xi_{H1}} (P_1 - P_a) n_i d\Xi_{H1} + \int_{\Xi_{H2}} (P_1 - P_a) n_i d\Xi_{H2} + \int_{\Xi_{H3}} (P_1 - P_a) n_i d\Xi_{H3} \tag{5.27}$$

$i = 1,3,5$, f_{H1}, f_{H3} and f_{H5} are surge force, heave force and pitching moment respectively on the hull section.

The representative form of equation 5.27 ensures that the pressure on the submerged main hull and inner part of the sponsons due aerodynamic effect can be isolated and evaluated with respect to when there is no aerodynamic pressure from the wing.

Alternatively, ϕ_{1t} may be evaluated such that the sectional forces and pitch moment on the submerged hull are determined directly in the body-fixed reference frame as

$$f_{Hi} = -\sum_{j=1}^{5} N_{ij} a_j + f_{bi} \qquad \text{on submerged hulls} \tag{5.28}$$

where,

f_{bi} includes weight of wing-fuselage section and other non-acceleration related components

The sectional added mass N_{ij} is given as

$$N_{ij} = -\int_{\Xi_H} n_j \varphi_{1i} d\Xi \tag{5.29}$$

Using the popular added mass identity, $N_{ij} = N_{ji}$, for $i = j = 1,3,5$, equation (4.27) becomes

$$N_{ij} = -\int_{\Xi_H} \varphi_{ji} n_i d\Xi \tag{5.30}$$

For $i = 5$, $n_i = \boldsymbol{r} \times \boldsymbol{n}$

This alternative approach is less computational expensive because ϕ_{1t} and ϕ_1 can be evaluated simultaneously. However, it does not readily isolate the aerodynamic effect on the hydrodynamics of the hull.

5.7 Loading, Forces and Moment on Wing-Fuselage Transverse Section

The sectional aerodynamic pressure $P_{F/W}$ on the wing-fuselage transverse section near disturbed water surface can be determined by evaluating the unsteady Bernoulli's equation,

$$P_{F/W} - P_a = -\rho_2 \left(\phi_{2t} + \frac{1}{2} |\nabla \phi_2(y,z)|^2 \right) \tag{5.31}$$

The sectional aerodynamic loading coefficient on the wing-fuselage section moving at constant forward speed near disturbed water surface may be expressed as

$$\sigma_p = \frac{P_l - P_u}{\frac{1}{2}\rho_2 U_\infty} \tag{5.32}$$

Where P_l and P_u are the pressure on the lower and upper portion of the wing-fuselage section.

The procedure for evaluating ϕ_{2t} follows the procedure described in Chapter 4. The aerodynamic forces and moment on any given section of the wing-fuselage near the disturbed water surface on the vertical plane can be determined by numerically integrating the pressure on the surface of the section using the equation below,

$$f_{w/Fi} = \int_{\Xi_{W/F}} (P_2 - P_a) n_i d\Xi \qquad i = 1,3,5 \tag{5.33}$$

$f_{F/W1}, f_{F/W3}$ *and* $f_{F/W5}$ are surge force, heave force and pitching moment respectively on the section.

ϕ_{2t} may also be evaluated such that the sectional forces and pitch moment may be determined directly in the body-fixed reference frame as

$$f_{W/Fi} = -\sum_{j=1}^{5} N_{ij} a_j + f_{gi} \qquad \text{on wing-fuselage} \tag{5.34}$$

where,

f_{gi} includes weight of wing-fuselage section and other non-acceleration related components

The sectional added mass N_{ij} is given as

$$N_{ij} = -\int_{\Xi_B} n_j \varphi_{1i} d\Xi \tag{5.35}$$

Using the popular added mass identity, $N_{ij} = N_{ji}$, for $i = j = 1,3,5$, equation (4.27) becomes

$$N_{ij} = -\int_{\Xi_B} \varphi_{ji} n_i d\Xi \tag{5.36}$$

For $i = 5$, $n_i = \boldsymbol{r} \times \boldsymbol{n}$

5.8 2.5D Aero-hydrodynamic Theory

The nonlinear 3D effects on the air-water interface, the wing-fuselage combination and the hull is accounted for by implementing the 2.5D theory described in Chapter 4. The flow problem is considered as an initial boundary value problem (IBVP), which is solved in a space-fixed solution control cross (SCC) plane following similar procedure described in Chapter 4.

5.8.1 2.5D theory procedure

For the purpose of implementing the 2.5D procedure, the WIGcraft may be divided generally into six regions namely,

- the fuselage fore region which begins slightly ahead of the leading edge of the fuselage and ends slightly ahead of the stem intersection with the undisturbed water surface. This region begins at time $t = t_0$ and ends at time $t = t_{HLE-1}$. This region is applicable for WIGcraft where the wings are located aft of the water entry point of the stem section of the hull.
- The hull fore sections region which begins slightly ahead of the stem intersection with the undisturbed water surface and ends at the section immediately downstream of where the stem intersects the free surface. In other words, this region begins at time $t = t_{HLE}$ and ends at time $t = t_{H0}$
- The chine unwetted region which begins from where the hull fore region ends at time $t = t_1$ and ends at the leading edge of the foremost chord of the wing at time $t = t_{WLE}$

- The coupled chine unwetted-wing-fuselage region, which begins the leading edge of the wing at time $t = t_{WLE}$ and ends at the point of chine immersion into the water at time $t = t_C$
- The coupled chine wetted-wing-Fuselage region, which begins just after chine immersion at time $t = t_C$ and ends at the aft-most trailing edge of the wing at time $t = t_{WTE}$
- The chine wetted region which begins after chine immersion at the aft-most trailing edge of the wing at time $t = t_{WTE}$ and ends at the rooster's tail ending position beyond the transom at time $t = t_{HTE}$ for WIGcraft with wing trailing edge located afore the transom.

Separate aero-hydrodynamic considerations are required for each of these regions. The coupled chine unwetted-wing-fuselage region is of primary interested in this study. The fuselage-only (fore and aft fuselage) regions contribute less to the aerodynamic lift of the airborne vehicle and consequently to the dynamics of the vehicle. The boundary value problem formulated for the coupled wing-fuselage region and whose solution is described in the preceding sections of this chapter are applicable also to the fuselage-only regions of the vehicle. However, the integrals over the wings are excluded from the solution of the formulated boundary value problem.

The solutions to the aero-hydrodynamic BVP in a cross plane may be seen as an initial boundary value problem (IBVP) in the solution control cross (SCC) plane, which is located initially slightly aft of the leading edge of the fuselage $x_g(t_0)$. Using the transformation equation, $x_g = Ut$ the solutions of the BVP in the SCC plane at any time may be stepped to the downstream sections of the wing-body downstream until it reaches the trailing edge of the fuselage. Because the 2D boundary value problem of the wing-body is solved together with a 3D interface boundary condition, the solution process is regarded as 2.5D aero-hydrodynamic theory.

At, $t = t_0$, it is assumed that an infinitesimal portion of the fuselage is located on the SCC. Since subsonic flow is considered and air compressibility is neglected, the velocity potential at the air-water interface may be initiated as zero tentatively and used together with other initial boundary conditions to kick-start the iterative solution process of the BVP of the section in the SCC, as described in section 4.5.3. After convergence, the solution to the IBVP solved on the SCC plane at $x_g(t_0) = 0$ is used as the new boundary conditions on the next time t_1. The SCC plane with updated boundary conditions is stepped downstream to the next longitudinal position at $x_g(t_1) = x_{g_1}$. A new non-similar fuselage section is introduced to the SCC plane and the

BVP is solved (as described in section 4.5.3) on the SSC plane at $x_g(t_1) = x_{g_1}$, subjected to the air-water boundary conditions at the SCC plane and boundary conditions at the new hull section.

The stepping process is repeated after convergence of the solution at each station along the longitudinal axis of the hull, until the SCC plane reaches the longitudinal location $x(t_{HLE}) = x_{g_{t_{HLE}}}$, prior to where the hull intersects the free surface and continues to the chine unwetted region. The BVP of the hull fore section and the chine unwetted regions and the procedures for their solution are described in Chapter 3 of this thesis. The free surface geometry and submerged hull section loading are evaluated in accordance with the procedure described in chapter 3 for all the sections in this region.

The SCC plane is advanced aft-ward until it enters into the coupled chine-unwetted wing-fuselage region located at $x(t_{WLE}) = x_{g_{t_{WLE}}}$. With updated air-water interface boundary conditions, the BVP of the first section in this region with its unique boundary conditions is solved following the procedure described in the preceding sections of this chapter until convergence is reached. The air-water interface geometry, the wing-fuselage and hull loading are evaluated in accordance with procedures described in chapters 3 and 4 for all the sections in this region.

Following similar routine as described in the last paragraph, the BVP of the various sections in the coupled chine-unwetted wing-fuselage region and beyond are solved at the respective positions of the SCC plane with updated air-water interface boundary conditions until the section at the trailing edge of the hull and fuselage is reached. The air-water interface geometry and the wing-fuselage loading for all the sections are evaluated as described in Chapters 3 and 4.

5.8.2 Total aero-hydrodynamic forces on the water borne WIGcraft

The distribution of the transverse loads along the longitudinal axis of the water borne WIGcraft vehicle may be evaluated from the results of the 2.5D theory for all transverse sections of the vehicle. In the absence of viscous and other external forces, the total hydrodynamic forces on the WIGcraft due to free surface rise (solid water) may be determined by numerically integrating the sectional forces (equations 5.27) distribution along the wetted length of the hull and chord of the wing.

5.8 Chapter summary

In this chapter, the aero-hydrodynamic model developed in chapter 4 for air-borne WIGcraft moving near undisturbed water surface has been extended by replacing the BVP of the water domain in chapter 4 with the BVP of the water domain in chapter 3.

A two-step iterative approach has been developed to couple the air and water domains and to estimate the coupling effects on the hull, wing-fuselage and water surface. In the first step, the BVP in the water domain which couples the free surface with the hull is first solved following chapter 3 to determine the hydrodynamic load on the hull and free surface geometry and dynamics. In the second step, the BVP in the air domain which couples the resulting nonplanar geometry and nonlinear dynamics of the free surface, and the wing-fuselage is then solved in an iterative manner following chapter 4. The effect of the dynamic air pressure on the air-water interface in the small gap may alter its geometry and velocity field from that in the initially calculated in the first step. As a result, the solutions in the first and second steps are iterated until the free surface geometry and velocity field converges. Formula for calculating the load distribution on the hull and the wing-fuselage were presented.

Chapter 6: Experimental Studies and Empirical Modelling on WIGcraft Dynamic Behaviour

6.1 Introduction

This chapter begins by introducing a novel experimental approach involving fully captive model tests for quantitative measurement of the hydrodynamic, aerodynamic and aero-hydrodynamic forces on a WIGcraft model moving with constant forward speed on calm water. Empirical models are formulated and validated alongside the analysis of the experimental results. The behaviour of the water borne WIGcraft model is examined in comparison with those of an Outrigger of the same submerged hull surface geometry.

6.2 Experimental Approach

The objectives for carrying out the experimental studies on waterborne WIGcraft is to build a database of forces which can be used to validate the theoretical models developed in this thesis. The experiments also give physical insight into the relatively unknown fluid flow characteristics and motions behaviour of the water borne WIGcraft moving with constant forward speed.

The idea behind the experimental approach was derived from the procedure used in Maskalik and Rozhdestvensky (1998). Analogous experiments for measuring the aerodynamic forces on marine vehicles by towing the model slightly above the water surface are described in Belynsky (1997), Hugli and Axt (1951), ITTC (2017) and Khoo and Koe (2016).

Fully captive model tests for the watercraft model configurations with and without the aerodynamic surfaces were conducted in a towing tank to measure the prevailing forces on the models. During the experiment, the model is locked in draught and trim angle (which are systematically varied for each running speed), and a database of dynamic forces is developed by measuring and recording the forces. The hydrostatic force may be calculated from hullform parameters. For the model configuration with wings, the aerodynamics of the wings towed slightly above the free surface is measured together with hydrodynamics of the wetted hull. In this thesis, this combined aerodynamic and hydrodynamic forces are referred to as aero-hydrodynamic forces.

The difference between the coupled aero-hydrodynamics of the model configuration with wings (henceforth, referred as WIGcraft model) and the hydrodynamics of the model configuration

without wings (henceforth referred to as Outrigger model) yields the experimentally determined total aerodynamic contribution to a planing watercraft equipped with wings. The appropriateness and validity of this approach in estimating the aerodynamic characteristic from a comparative study between a WIGcraft and an Outrigger in this study have been previously demonstrated in a related study by Maskalik and Rozhdestvensky (1998) for power augmented WIGcrafts and Lin & Day (1974) for SWATH ships and also discussed in Peter Van Oossanen, (1984).

The downside to this experimental approach is the lengthy and often tedious data fitting and mathematical modelling required before the experimental results can become useful for prediction implicit characteristics of the towed model. However, this empirical modelling exercise is key to understanding the behaviour of a water borne WIGcraft.

To develop new empirical models, as much information that can be gathered to understand the behaviour of the waterborne WIGcraft is required. The proposed experimental approach offers the advantage of providing various information associated with the performance of the model beyond the capability of the semi-captive or free running model experimental methods typically used to investigate the behaviour of planing watercrafts. This unique advantage compels its use in this study.

The results from the experiments are used to develop empirical expressions for the total lift and drag on the water borne WIGcraft model, as well as to validate the proposed numerical models developed in the earlier chapters of this thesis. It is necessary to state here that ground effect aerodynamic results from Autowing code which was developed based on the vortex lattice method are compared with corresponding results from both the experiments and the proposed numerical models.

6.3 Model Description and Configurations

The model used for the experimental study is a scaled 1m model of an 8m stepless conceptually designed WIGcraft. The model size was chosen based on the speed limit of the towing tank carriage, and to minimize scale and towing tank wall interference effect. The model was built of wood finely finished and painted yellow with high gloss enamel coating to make visible the draught marks at the lower part of the wings and the transom. The principal particulars and lines drawing of the model are given in Table 6.1 and Figure 6.1 respectively while the constructed models are shown in Figure 6.2.

Table 6.1 Particulars of WIGcraft and Outrigger Models

	WIGcraft model		**Outrigger model**	
Description	**Main**	**Sponson**	**Main**	**Sponson**
Overall Length: (m)	1	0.566	1	0.566
Beam: (m)	0.29	0.055	0.29	0.055
Overall Beam (incl. lateral clearances): (m)	1.021		1.021	
Maximum draft (m)	0.065		0.065	
Lateral Clearance (m)	0.511			
Longitudinal Clearance (m)	0.243			
Longitudinal Centre of Gravity from Aft: (m)	0.39		0.39	
Vertical Centre of Gravity from keel	0.122		0.178	
Wings incident angle (degrees)	0		N/A	
Mean Aerodynamic Chord (m)	0.613		N/A	
Wing Aspect Ratio	1.33		N/A	

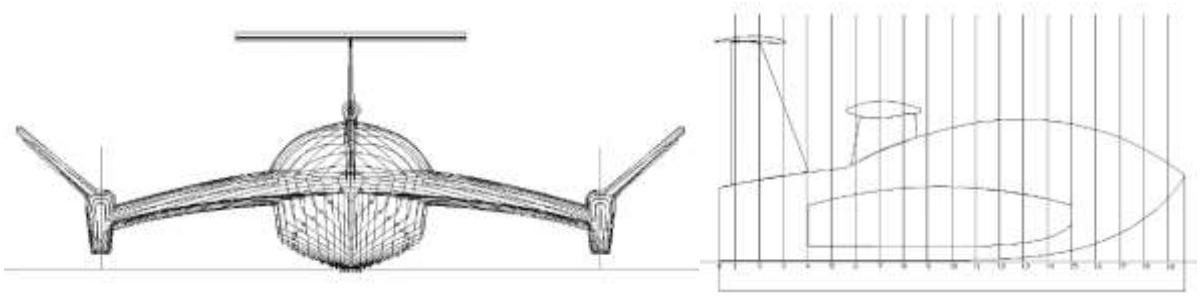

Figure 6.1 Lines of the experimental experimental WIGcraft model

One of the model configurations is a complete WIGcraft (see Figure 6.2a) whose geometry consists of the hard chine main hull, thin hard chine side-hull endplates (regarded as sponsons or outriggers), wings, winglets, and a vertical and horizontal tail plane.

(a) WIGcraft model configuration

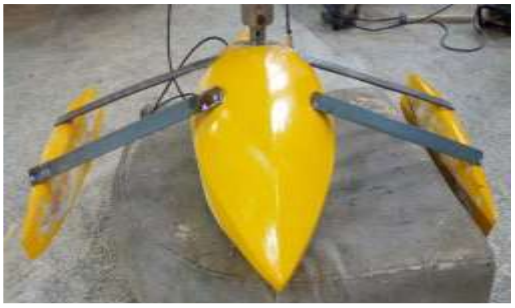

(b) Outrigger model configuration

Figure 6.2 Experimental model configurations

The hulls have a warped hullform with variable deadrise angles from bow to stern. It is important to note that transom sterns are more or less a hallmark of high-speed marine vehicles (HSMV). However, since the prototype and the model of the watercraft will not be fitted with water-based propulsion system, the model was not equipped with a transom stern. To ensure the flow is streamlined so as to minimize turbulence in the boundary layer downstream of the hull, and with the objective of improving flow separation characteristics, thereby minimizing the resultant flow separation and wake drag, the stern part of the model is designed such that the ratio between the stern section area and the maximum sectional area is less than 0.01. The height of the chine line with respect to the keel line varied elliptical from the bow where the chine height is maximum to the stern where it joins the keel.

The other model configuration (the Outrigger model) is more like a trimaran configuration similar in hullform to the WIGcraft model but differs in the sense that the aerodynamic lift enhancing surfaces (wings, winglets, and tail) are detached from the WIGcraft configuration (See Figure 6.2b). The main fuselage-hull is rigidly connected to two small sponsons by means of crossbars, such that the positions of the sponsons from the fuselage are the same with that of the WIGcraft model.

6.4 Experimental Facilities Set-up

The fully constrained model experimental tests were carried out in the towing tank of the hydrodynamics laboratory at Huazhong University of Science and Technology (HUST), China. The towing tank is 175m x6m x 6m in dimension. The carriage which is controlled electronically has a speed range from 0 to 7m/s. The towing tank is equipped with Computarized Position Mechanism (CPM) which is attached to and driven by the main carriage of the towing tank. The mechanism which has independent drives for the individual six degree of freedom

position is coupled to a vertical tube frame which is rigidly fixed at the centre of gravity of the model. This setup allows the towing tank operator to remotely fix the model to any trim angle or draught position for any given run. In this experiment only the draught and trim angles of the model were varied for the specified speed range.

The CPM mechanism is equipped with a six-axis force/torque sensor to measure and record the six degrees of freedom forces and torque efforts acting on the boat being towed. However, for this study which concerns longitudinal motion behaviour of the waterborne WIGcraft, only longitudinal and vertical forces are considered. The idea of decoupling the vertical and lateral plane motions from the total motions of a planing watercraft is a well-established procedure for ship motions study. The coordinate system of the sensor is aligned with axis of the model, so that output readings are in the hull-fixed coordinate system with origin at the centre of gravity of the main hull of the model.

Data sampling rate is 20Hz. The analogue signals sensed passes through multi-channel amplifiers and filters to an analogue-to-digital signal converter and it is recorded by a desktop computer in real time and displayed graphically. The digital signal is converted and stored automatically to Microsoft Excel spreadsheet file format. Prior to conducting the experiment, the measuring system was calibrated to ensure there is a linear relationship between the output voltage and the physical quantity being measured. Other accessories available and used in the hydrodynamic laboratory include high-definition video camara, wave maker, a beach system for absorbing the waves.

6.5 Experimental Test Programme

The experiments were conducted following the experimental matrix shown in appendix A. The test matrix was selected to reflect the possible attitudes the model may attain as speed is increased to the expected take-off speed value. The experimental matrix considered five draught positions (0.065m, 0.035m, 0.015m, 0.00m and -0.006m) measured from the keel at the transom. The -0.006m draught position implies the model was above the calm water surface. The draught positions may be used to give an indication of the clearance height of the lowest part of the wing of the WIGcraft above the calm water surface. The draught positions were also chosen to represent the variations in the displacement and transition regime of the model as a result of the action of aero-hydrodynamic effort during its motion.

Four trim angles (0º, 2º, 4º and 6º bow up) were also considered to evaluate trim effects of the dynamics of the watercraft. The trim angles indirectly give a measure of the angle of attack of the wings and tail of the WIGcraft since the incidence angle of the wings is zero degree. A carefully selected speed range to cover the most important part of the transition regimes including the flaring and predicted take-off regimes was implemented. The speed range covered by the experiment are 2.0m/s, 2.5m/s, 3.0m/s, 4.0m/s, 4.5m/s, 5.0m/s and 5.5m/s. This speed range was selected to correspond with the full-size speeds of the WIGcraft prototype as well as satisfy the speed limit of the towing carriage.

6.6 Testing Conditions and Procedure

The tests are performed in restricted calm water with standard ambient temperature, density and kinematic viscosity of water. The test runs followed a random order to minimize experimental errors. Measurements of the six axis forces and moments were recorded after a steady state run were recorded. Runs whose readings are found to be inconsistent with expected values were repeated. The measuring system was reset to zero after each run. A waiting time of about 15minutes was exercised after each run to allow the water return to its undisturbed state. To properly ascertain that the model moves in even keel as well as capture the water spray characteristics, video recording of each run was made and reviewed before the next experimental run. Physical insights as well as qualitative and quantitative information on the flow characteristics about the models were gathered during the experiments and reviewed from the video recordings.

6.7 Presentation of Experimental Results

Each computed coefficient of the measured force data represents the average of the force coefficients. At pure planing, the computed average coefficients are essentially independent of speed (McBride,1956; Shuford, 1957; Savitsky, 1964; Doctors, 1985). The measured forces on the Outrigger and WIGcraft models are expressed in non-dimensionalised lift and drag coefficients in the form,

$$C_{LDiv} = \frac{F_{LDiv}}{0.5\rho_w U^2 {b_h}^2} \qquad (6.1)$$

Where,

F_{LDiv} is the measured lift or drag force.

The uncertainties associated with the experiments are first estimated in percentages prior to the presentation and analysis of the experimental lift and drag results. The effects of the trim angle, speed coefficients and draught and relative ground clearances on the behaviour of the dynamic forces on the experimental models are discussed. Comparison is made between the experimental models equipped with wings (WIGcraft) and that without wings (Outrigger). For consistency in summing the hydrodynamic and aerodynamic coefficients, alternative hydrodynamic coefficients (whose hydrodynamic force values are equal to the aerodynamic force values) are proposed to replace the aerodynamic coefficients.

For convenience in describing the behaviour of the models, draught and relative ground clearance are two parameters used to describe the vertical position of the models with respect to the space-fixed reference frame. The relationship between both parameters is tabulated as part of Tables A2 and A3 in appendix A.

6.8 Experimental Imperfections and Uncertainties

The accuracy and reliability of the measured results from captive model tests is generally influenced by imperfections of the facilities and experimental technique employed. The uncertainties associated with measured results are assessed and discussed below in accordance with ISO-GUM (1995) and recommended procedures and guidelines stated in the International Towing Tank Conference (ITTC, 2002, 2014a, b) where necessary.

Though the 6 axis load cells measured the 3 geometric axial forces and moments about them directly from the captive model experiment, in this study which concerns the coupled aero-hydrodynamic forces in the vertical plane, only the forces on the Outrigger and WIGcraft models measured in the vertical plane are considered as the measurands for the uncertainty analysis.

The standard uncertainty U_i associated with a given measurand or parameter i composed of jth component is herein denoted by $U_{i,j}$. For a given parameter, the total standard uncertainty due to the various uncertainty components may be estimated as

$$U_i = \sqrt{\left(U_{i,j}\right)^2 + \left(U_{i,j+1}\right)^2 + \cdots + \left(U_{i,j+n}\right)^2} \qquad \text{j = 1, 2…, n} \qquad (6.2)$$

Potentials sources (parameters) of uncertainties associated with the captive model experiments carried out in this study include temperature (U_T), density (U_ρ), blockage effect (U_{bk}) of towing tank, towing speed (U_V), wetted beam of submerged hull (U_{b1}) at specified experimental draught, measured lift ($U_{\hat{F}}$) and lift coefficient ($U_{C_{\hat{F}}}$).

It is expected that there will be some definite bias in the hull fairing between workshops using multi-axis computerised numerical controlled (CNC) milling machines, which may yield slightly different values of the beam and displacement volume of the model, and consequently influence the measured force and calculated lift coefficient. Owing to the possible ±1mm manufacturing error in all co-ordinates and 2mm bias limit in model beam obtained from a high-quality Vernier Calliper which corresponds with the bias limit stated in ITTC (2002) Procedure 7.5-01-01-01 Rev 01, an uncertainty $U_{bh,mod}$, arises in the nominal wetted beam obtained from the 3D CAD ship model.

The Type B wetted beam relative standard uncertainty $U'_{bh,mod}$ associated with construction of the watercraft model geometry can simply be estimated as

$$U'_{bh,mod} = \frac{\delta b_h}{b_h} \tag{6.3}$$

δb_h is the error associated with the beam measurement.

Installation related uncertainties such as hull model trimming, alignment of the centreline of the hull model, the load cells and the towing force in the straight-line ahead direction of the of the motion of the towing carriage may influence the measured wetted beam, draught, forces and the respective coefficients of the measured forces. Owing to the fact that the hull model installation and testing were carried out in a well-controlled manner by an experienced laboratory personnel, installation uncertainties $U_{b1,inst}$ are assumed to be negligible. The total wetted beam uncertainties U_b may be obtained by using equation 6.2.

The measured temperature of the water during the experiments in the indoor towing tank facility varied slightly from a mean temperature of 19°C. The density of water in the towing tank at recorded temperature for each experimental run is calibrated according to ITTC (1999) Procedure 7.5-02-01-03, Rev 00, thus,

$$\rho = 1000.1 + 0.0552T_w + 0.0077{T_w}^2 + 0.00004{T_w}^3 \tag{6.4}$$

Given that the temperature of water in the tank is measured by a thermometer with a guaranteed accuracy of ±0.1%, which is 0.067% of the nominal temperature of 15°C, temperature

calibration uncertainty $U'_{T,Cal}$ arises. The corresponding measured uncertainty ($U'_{\rho,Cal} \cong 0.002\%$) of the water density due to uncertainties in the temperature measurement is negligible, while the corresponding uncertainty for the kinematic viscosity water is about $U'_{\upsilon,Cal} \cong 0.2\%/\sqrt{3} \cong 0.1\%$. The deviation of water temperature thus has effect on viscosity and consequently on the Reynolds number and frictional drag but may be neglected for dynamic lift force measurement during then captive model test. The uncertainty in the viscosity has negligible effect on dynamic lift.

Owing to the poor heat conductivity and low coefficient of thermal expansion ($5 \times 10^{-5}/°C$) of wood material, thermal deformation of the model hull geometry (and its related standard uncertainty, $U'_{T,mod}$) due to temperature changes in the time and place of manufacture and during the experimental test in the laboratory are considered negligible. The total temperature standard uncertainty $U'_{T,}$ can be obtained as the root sum square of the accuracy of temperature using equation 6.2.

From experience using the towing tank facility, it was reported that the towing carriage yields negligible errors when operating at speed range below 6m/s. As a result, velocity standard uncertainties, $U'_{V,DAS}$ associated with the data acquisition system of the towing speed measurement device is not considered in this study where the maximum speed is 5.5m/s. Given that speed data are measured to an accuracy of 0.05%, the towing speed relative standard Type B uncertainty $U'_{V,Cal}$ associated with the calibration of the speed measuring device is considered to be the ratio between the half unit variation of the smallest significant figure of the speed parameter for a given test run.

$$U'_{V,Cal} = \frac{\delta V}{V} \tag{6.5}$$

The total speed uncertainties U'_V may be obtained by using equation 6.2.

Owing to the relatively large length, breadth and depth of the towing tank with respect to the model size, the uncertainties associated with the blockage effects of the boundaries of the towing tank are considered negligible and the measured components of the dynamic force in the vertical plane do not need corrections to account for blockage effects. Measurement errors due to misalignment of the hull model were minimized by ensuring the geometry of the hull generated water spray on both sides of the hull model are identical for each experimental run. As a result, the standard uncertainty $U_{F_i,Mis}$ of measured component i of the dynamic force (in the vertical plane of symmetry of the hull) due to misalignment are considered negligible. Temperature variation may influence the measured forces through density and viscosity of the

water in the towing tank. The earlier stated value of the density uncertainty due to uncertainty in the temperature measurement suggests it has negligible effect on the measured force. Meanwhile, the Reynolds number and the frictional force are reasonably affected by the viscosity uncertainty, especially for displacement vessels. As a result, measured drag has to be corrected to account for the slight variation of measured temperature from the mean temperature of the tests or nominal temperature (15°C). The uncertainty in the drag propagated from the viscosity uncertainty may be estimated from

$$U'_{\hat{F}_i,\upsilon T} = \frac{C_{fr}}{C_D} \cdot \frac{0.87}{log_{10}Re-2} \cdot \frac{\delta\upsilon}{\upsilon} \quad \text{in turbulent flow regimes} \tag{6.6}$$

Where,

C_{fr} is the friction coefficient,

C_D is the total measured drag,

Re is the Reynolds number.

υ is the kinematic viscosity of water.

The uncertainty in the viscosity which was earlier stated to be of the order of 0.1% due to temperature measurement leads to a standard uncertainty of order of < 0.05% in the drag and may be regarded as negligible. Similarly, the uncertainty in the viscosity is considered to have negligible effect on dynamic lift.

The relative uncertainty components of the model resistance related to model geometry is generally of the order of 0.05% which may be regarded as negligible. (ITTC, 2014b).

For a planing water-based aircraft about which flow is generally turbulent, the viscosity minimally influences the dynamic lift force on the planing hull and wings. Consequently, there was no need to adjust the measured force at temperature T_i for each measured force F_i to that at the mean temperature before the data analysis is performed. The propagation of temperature uncertainty into the measured dynamic forces through changes in density and viscosity may be obtained from

$$U'_{\hat{F}_i,T} = \sqrt{\left(U'_{\hat{F}_i,\rho T}\right)^2 + \left(U'_{\hat{F}_i,\upsilon T}\right)^2} \tag{6.7}$$

The first term in equation 6.7 $U'_{\hat{F}_i,\rho T} = \frac{U'_T}{\rho}\frac{\delta\rho}{\delta T}$ which is the uncertainty in the measured force due to effect of temperature variation on water density is generally negligible. $\frac{\delta\rho}{\delta T}$ for a given experimental test run may be derived from equation 6.4.

The second term in equation 6.7 is the uncertainty in the measured force due to effect of temperature variation on viscosity. This term may lead to standard uncertainty of the order <0.05% in lift uncertainty and may also be neglected for measurement of lift forces in the vertical plane during captive model test.

The load cells and other measuring instruments were tested and calibrated with the help of data acquisition system (DAS) before each experimental run. The Newton weight calibrated load cells generally have a negligible uncertainty of 0.001% which leads to the measured forces having a negligible calibrated uncertainty $U_{F_i,cal}$.

For a low pass filtered time history of each experimental run, the average of the dynamic force $\widehat{F_i}$ in the vertical plane read by the DAS is obtained thus,

$$\widehat{F_i} = \frac{1}{n}\sum_{m=1}^{n}\tilde{F}_{im} \tag{6.8}$$

Where $\tilde{F}_{im}$ is the *m*th data points of the measured component i of the force within the filtered time history of the time interval $\Delta t = \frac{n}{f_s}$ for *n* number of data points sampled at a rate f_s. The standard and relative standard uncertainty of the average of the force read by the DAS can be respectively estimated from ITTC (2014b) general guideline for Type A uncertainty analysis as

$$U_{\widehat{F_i},DAS} = \frac{\hat{s}}{\sqrt{n}},\ U'_{\widehat{F_i},DAS} = \frac{\hat{s}'}{\sqrt{n}} \tag{6.9}$$

$\hat{s} = \sqrt{\frac{1}{n-1}\sum_{m=1}^{n}\left(\widehat{F_i} - \tilde{F}_{im}\right)^2}$ and $\hat{s}' = \frac{\hat{s}}{\widehat{F_i}}$ are respectively the standard and relative standard deviation of the filtered time history of the measured data.

Analogous to ITTC (2014b) 7.5-02-02-02, the relative standard Type B uncertainty in the towing speed propagates into the dynamic force $\widehat{F_i}$ in the vertical plane through the dynamic pressure on the hull model,

$$U'_{\widehat{F_i},V} = \frac{\delta\widehat{F_i}(V)}{\widehat{F_i}} \approx \frac{\partial\widehat{F_i}}{\partial(\rho V^2)}.\frac{\partial(\rho V^2)}{\partial V}.\frac{\partial V}{\widehat{F_i}} = 2\frac{\delta V}{V} = 2U'_V \tag{6.10}$$

Similarly, since the measured dynamic force in the vertical plane is a function of the wetted beam as stated in equation 6.1, the relative standard Type B uncertainty in the wetted beam propagates into the force as the wetted beam square and can be estimated as follows.

$$U'_{\widehat{F}_i,b_h} = \frac{\delta \widehat{F}_i(b_h)}{\widehat{F}_i} \approx \frac{\partial \widehat{F}_i}{\partial (b_h{}^2)} . \frac{\partial (b_h{}^2)}{\partial b_h} . \frac{\partial b_h}{\widehat{F}_i} = 2\frac{\delta b_h}{b_h} = 2U'_{bh,mod} \quad (6.11)$$

Generally, the adjustment of the measured forces and its coefficient due to propagation of uncertainty in the wetted beam from variation in the temperature of the water in the towing tank to the corresponding forces and coefficients at the nominal temperature at 15C are very small. Moreover, it is stated in ITTC (2014b) that there is no analytical relationship between a non-unform deformation of hull geometry with the forces on the hull. As a result, the uncertainty associated with this measured force and its coefficient data reduction are not considered in this paper.

The relative standard uncertainty in a measured component of the average dynamic force $\widehat{F}_i$ in the vertical plane may be estimated from equation 6.12 in a manner analogous to ITTC (2014b) general guideline for uncertainty analysis in resistance tests,

$$\left(U'_{\widehat{F}_i}\right)^2 = \left(U'_{\widehat{F}_i,T}\right)^2 + \left(U'_{\widehat{F}_i,V}\right)^2 + \left(U'_{\widehat{F}_i,DAS}\right)^2 + \left(U'_{\widehat{F}_i,b_h}\right)^2 \quad (6.12)$$

The results of the analysis of the significant uncertainty components related to the measured lift coefficient of both model configurations for test run at 0.035m draught, 4° trim angle and considered speed range in this study are summarised in Table 6.2. Complete listing of the mean combined uncertainties in the measured lift and drag for other sets of draught and trim angle test conditions for the WIGcraft and Outrigger models are summarised in Tables A2 and A3 of Appendix A.

Table 6.2 Contributions to Overall Uncertainty in measured aero-hydrodynamic lift for 0.035m Draught and 4° Trim Angle

Uncertainty Components	Relative Uncertainty for Outrigger Model (%)							Relative Uncertainty for WIGcraft Model (%)						
	2.0 (m/s)	2.5 (m/s)	3.0 (m/s)	4.0 (m/s)	4.5 (m/s)	5.0 (m/s)	5.5 (m/s)	2.0 (m/s)	2.5 (m/s)	2.5 (m/s)	4.0 (m/s)	4.5 (m/s)	5.0m (m/s)	5.5 (m/s)
Wetted beam (0.239m)														
$U'_{b1,mod}$	0.21	0.21	0.21	0.21	0.21	0.21	0.21	0.21	0.21	0.21	0.21	0.21	0.21	0.21
$U'_{b1,inst}$	<0.05	<0.05	<0.05	<0.05	<0.05	<0.05	<0.05	<0.05	<0.05	<0.05	<0.05	<0.05	<0.05	<0.05
Total wetted beam relative Uncertainty, U'_{b1}	0.21	0.21	0.21	0.21	0.21	0.21	0.21	0.21	0.21	0.21	0.21	0.21	0.21	0.21
Temperature (19°C)														
$U'_{T,\rho}$	0.002	0.002	0.002	0.002	0.002	0.002	0.002	0.002	0.002	0.002	0.002	0.002	0.002	0.002
$U'_{T,v}$	0.1	0.1	0.1	0.1	0.1	0.1	0.1	0.1	0.1	0.1	0.1	0.1	0.1	0.1
$U'_{T,mod}$	<0.05	<0.05	<0.05	<0.05	<0.05	<0.05	<0.05	<0.05	<0.05	<0.05	<0.05	<0.05	<0.05	<0.05
$U'_{T,Cal}$	0.263	0.263	0.263	0.263	0.263	0.263	0.263	0.263	0.263	0.263	0.263	0.263	0.263	0.263
Total Temp. R. Uncertainty U'_T	0.263	0.263	0.263	0.263	0.263	0.263	0.263	0.263	0.263	0.263	0.263	0.263	0.263	0.263
Water Density														
$U_{\rho,Cal}$	0.002	0.002	0.002	0.002	0.002	0.002	0.002	0.002	0.002	0.002	0.002	0.002	0.002	0.002
U'_{ρ}	0.002	0.002	0.002	0.002	0.002	0.002	0.002	0.002	0.002	0.002	0.002	0.002	0.002	0.002

Towing Speed														
$U_{V,DAS}$	n.a	n.a	n.a	n.a	n.a	n.a	n.a	n.a	n.a	n.a	n.a	n.a	n.a	n.a
$U'_{V,Cal}$	0.025	0.020	0.0133	0.0125	0.011	0.010	0.0091	0.025	0.020	0.0133	0.013	0.011	0.010	0.0091
U'_{V}	0.025	0.020	0.0133	0.0125	0.011	0.010	0.0091	0.025	0.020	0.0133	0.013	0.011	0.010	0.0091
Lift Force														
$U'_{F_i,Mis}$	<0.05	<0.05	<0.05	<0.05	<0.05	<0.05	<0.05	<0.05	<0.05	<0.05	<0.05	<0.05	<0.05	<0.05
$U'_{F_i,Load}$	<0.05	<0.05	<0.05	<0.05	<0.05	<0.05	<0.05	<0.05	<0.05	<0.05	<0.05	<0.05	<0.05	<0.05
$U'_{\widehat{F_i},DAS}$	8.7299	6.312	2.6645	0.9747	1.093	0.537	1.435	2.169	0.842	1.051	4.63	1.59	3.90	1.69
$U'_{\widehat{F_i},V}$	0.05	0.04	0.033	0.025	0.022	0.02	0.018	0.05	0.04	0.033	0.025	0.022	0.02	0.018
$U'_{\widehat{F_i},b_1}$	0.418	0.418	0.418	0.418	0.418	0.418	0.418	0.418	0.418	0.418	0.418	0.418	0.418	0.418
$U'_{\widehat{F_i},T}$	0.0001	0.0001	0.0001	0.0001	0.0001	0.0001	0.0001	0.0001	0.0001	0.0001	0.0001	0.0001	0.0001	0.0001
Combined Uncertainty $U'_{\widehat{F_i}}$	±3.03	±6.33	±2.70	±1.06	±1.17	±0.68	±1.50	±2.21	±0.94	±1.13	±4.65	±1.65	±3.92	±1.74
Expanded Uncertainty $U'_{\widehat{F_i}exp}$	±6.06	±12.66	±5.40	±2.12	±2.34	±1.36	±2.99	±4.42	±1.88	±2.26	±9.29	±3.29	±7.84	±3.48
Mean Combined Uncertainty in Lift Coeff.	**±2.35**							**±2.32**						
Mean expanded Uncertainty in Lift Coeff.	**±4.70**							**±4.64**						

It is seen in Table 6.2 that the combined uncertainties of the measured lift forces for the test cases are of the order less than 10%. For some unclear reasons, Table A2 in the appendix shows a relatively higher percentage uncertainty at the 2° trim angles at all draught positions for both the WIGcraft and Outrigger models. It is also seen that the uncertainty associated with the use of the data acquisition system (DAS) to acquire the forces on the models is by far the largest contributor to the total uncertainty in all cases.

6.9 Analysis of Lift Results and Formulation of Empirical Model for Total Lift

In this section, the lift results of the experiments will be analysed alongside the formulation of a semi-empirical model to predict the total dynamic lift on a waterborne WIGcraft with spray influence.

The total measured lift on a water borne WIGcraft moving on calm water consists of the hydrostatic and hydrodynamic lift components (associated with the water submerged part planing hull), and the aerodynamic lift subjected to hull-generated spray and ground effect (associated with the wings and other parts of the boat not submerged). The magnitude of the hydrodynamic and aerodynamic lift forces depends essentially on the given set of boat speed, trim angle, and draught variables.

The components of the hydrodynamic and aerodynamic lift forces on the water-borne WIGcraft which are represented by their respective non-dimensionalised hydrodynamic C_{LH} and aerodynamic lift coefficients C_{LA} (consisting of free flight lift, C_{Lff}; ground effect lift, C_{Lge}; and spray lift, C_{LSP}) are shown in Fig.6.3.

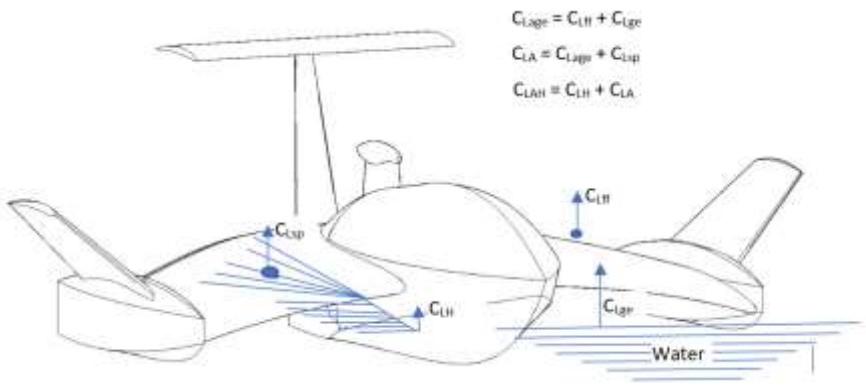

Figure 6.3 Components of lift forces on water borne WIGcraft

6.9.1 Equivalent Hydrodynamic Lift Coefficient, $C_{LA\rightarrow Heq}$

Using the Morrison's equation, the dimensionless coefficient of a given lift force component is expressed thus,

$$C_{Li} = \frac{L_i}{0.5\rho_i S_i U^2} \tag{6.13}$$

Where subscript i represents for hydrodynamic, aerodynamic or coupled aero-hydrodynamic lift components.

L_i is the lift generated by hydrodynamic or aerodynamic surface,

ρ_i is the density of water or air,

S is the wetted area of hulls or wings,

U is the speed of the vehicle,

It is possible to represent the lift coefficient of a water-borne WIG craft with the sum of the lift coefficients associated with aerodynamic and hydrodynamic lift generating surfaces as,

$$C_{LAH} = C_{LH} + C_{LA} = \frac{L_H}{0.5\rho_w S_w U^2} + \frac{L_A}{0.5\rho_a S_a U^2} \tag{6.14}$$

Where,

C_{LH} is the component of the lift coefficient of the lift generated by the hull (i.e., hydrodynamic submerged hull surface) as shown in Figure 6.3,

C_{LA} is the component of the dynamic lift coefficient of the lift generated by the aerodynamic surface. C_{LA} is the sum of the coefficients of the free flight lift (C_{Lff}), lift specifically due to ground effect (C_{Lge}) and hull generated spray lift (C_{Lsp}) as indicated in Figure 6.3

C_{LAH} is the coupled aero-hydrodynamic coefficient for the water-borne WIGcraft. It entails the combination of the aerodynamic and hydrodynamic lift coefficients of the hull(s) and wings respectively.

During fully constrained water borne WIGcraft model experiments, the hydrodynamic and aerodynamic lift components are measure simultaneously. The aerodynamic and hydrodynamic lift generating surfaces are inextricably bound in generating the coupled aero-hydrodynamic lift force. It is important to note that in the expression of the coupled aero-hydrodynamic lift

coefficient presented in equation 6.14, the accurate determination of the dynamic wetted area of the hull presents a unique challenge. As a result, it is not unusual to find the dynamic wetted hull surface area replaced by the beam square (${b_h}^2$) of the submerged portion of the hull. The hydrodynamic lift coefficient may thus be simplistically given as

$$C_{LH} = \frac{L_H}{0.5\rho_w {b_w}^2 U^2} \tag{6.15}$$

Following the alternative form of the hydrodynamic lift coefficient stated in equation 6.4, the coefficient of the coupled aero-hydrodynamic force stated in equation 6.3 may be concisely expressed as

$$C_{LAH} = \frac{L_{AH}}{0.5\rho_{ah} {b_{ah}}^2 U^2} \tag{6.16}$$

Where,

L_{AH} measured coupled aero-hydrodynamic lift force,

ρ_{ah} is considered to be an imaginary fluid with perfect mix of air and water,

b_{ah} is considered to the beam of an imaginary coupled aero-hydrodynamic lift generating surface exposed to a fluid of perfect air and water mixture.

It is important to note that the inconsistent wetted area and density parameters associated with the aerodynamic and hydrodynamic lift coefficients of the wings and hulls respectively in equation 6.16, makes it cumbersome to express the coefficient of the coupled aero-hydrodynamic force of a water-borne WIGcraft in the format presented in equation 6.16. For convenience and consistency in expressing the coefficient of the coupled aero-hydrodynamic forces of a water-borne WIGcraft in a form similar to equation 6.16, an equivalent hydrodynamic coefficient is herein proposed to represent the aerodynamic lift coefficient of the wings of span, b_a in equation 2. The equivalent hydrodynamic coefficient is derived from the aerodynamic force (generated by the aerodynamic surface with span, b_a) whose value equals the value of hydrodynamic force generated by some hypothetical hydrodynamic hull surface with submerged beam equal to $b_{a\rightarrow heq}$.

The usual aerodynamic lift coefficient $C_{LA} = \frac{L_A}{0.5\rho_a S_a U^2}$ generated by the wing surface of a water-borne WIGcraft may be transformed into an equivalent hydrodynamic lift coefficient $\mathrm{C_{LA\rightarrow Heq}}$ by using the transformation factor $\left(\frac{{x_{ah}}^2}{R_A}, x_{ah} = \frac{b_{a\rightarrow heq}}{b_h}\right)$ as shown in Figure 6.4.

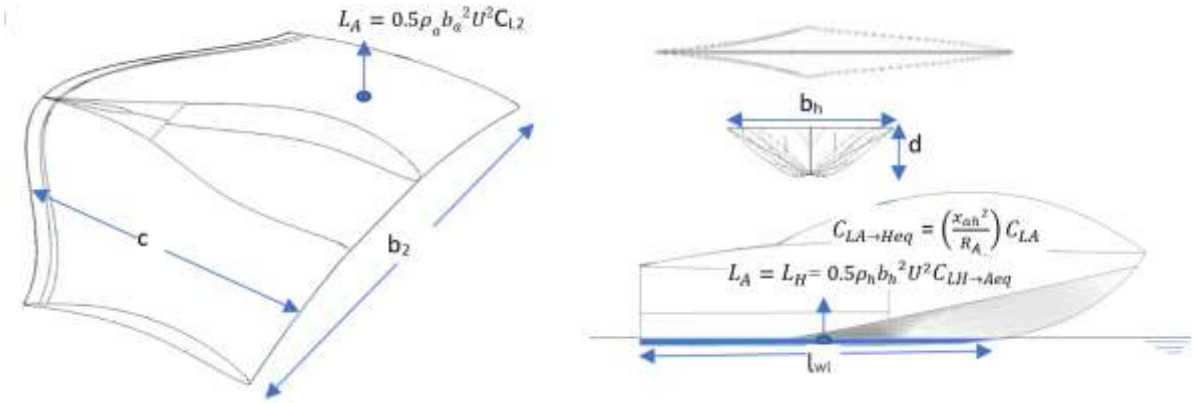

(a) Aerodynamic lift on wing surface with span b_a and aspect ratio R_A

(b) submerged hull portion (shaded blue) generating Hydrodynamic lift equal to the Aerodynamic Lift of the wing in Figure 6.4a

Figure. 6.4 Equivalent hydrodynamic lift coefficient concept: Relating wingspan and planing hull beam in lift generation.

At a given draught *d*, the equivalent hydrodynamic lift coefficient $C_{LA\rightarrow Heq}$ is the lift coefficient necessary for a hypothetical hydrodynamic surface with submerged beam, $b_{a\rightarrow heq}$ to generate lift force of value equal to that generated by an aerodynamic surface with span, b_a and aspect ratio R_A. While the value of the forces generated by the hypothetical hydrodynamic surface equals that generated by the wings, $C_{LA} \neq \mathrm{C_{LA\rightarrow Heq}}$ and $\mathrm{b_{a\rightarrow heq}} \neq \mathrm{b}_a$.

The hypothetical beam, $\mathrm{b_{a\rightarrow heq}}$ is related to submerged beam of the hull model, b_h by

$$x_{ah} = \frac{b_{a\rightarrow heq}}{b_h}, \text{ valid for } b_h > 0 \qquad (6.17)$$

On the other hand, the hypothetical hydrodynamic lift generating beam, $\mathrm{b_{a\rightarrow heq}}$ replacing the aerodynamic lift generating surface of the wings of the watercraft is related to the span, b_a of the wings by

$$b_{a\rightarrow heq} = b_a\sqrt{\Upsilon} \qquad (6.18)$$

$\Upsilon = \frac{\rho_a}{\rho_h}$ is air to water density ratio at the air-water interface.

The equivalent hydrodynamic lift coefficient may be mathematically expressed as,

$$C_{LA\rightarrow Heq} = \frac{L_A}{0.5\rho_h {b_h}^2 U^2} = \left(\frac{{x_{ah}}^2}{R_A}\right) C_{LA} \qquad (6.18)$$

Equation 6.6 is valid for $b_h \geq 0$, and is such that the aerodynamic lift,

$$L_A = 0.5\rho_a S_a U^2 C_{L2} = 0.5\rho_h {b_h}^2 U^2 C_{LA\rightarrow Heq} \quad (6.19)$$

This lift coefficient as presented in equation 6.18 is not typical in aerodynamics. However, it helps to simplify the coupling of lift coefficients from aerodynamic and hydrodynamic surfaces of different sizes in the coupled aero-hydrodynamic lift coefficient expression of a waterborne WIGcraft. The coupled aero-hydrodynamic coefficient stated in equation 6.14 may now be presented as,

$$C_{LAH} = C_{La} + C_{LA\rightarrow Heq} = \frac{L_H}{0.5\rho_h {b_h}^2 U^2} + \frac{L_A}{0.5\rho_h {b_h}^2 U^2} \quad (6.20)$$

And the coefficient of the coupled aero-hydrodynamic lift forces may now be expressed in the concise form similar to equation 6.16, thus,

$$C_{LAH} = C_{LH} + C_{LA\rightarrow Heq} = \frac{L_H + L_A}{0.5\rho_h {b_h}^2 U^2} = \frac{L_{AH}}{0.5\rho_h {b_h}^2 U^2} \quad (6.21)$$

Equation 6.21 shows the coefficients of the aerodynamic and hydrodynamic lift generated by their respective wetted surfaces and surround fluid properties are superposed to form a coupled aero-hydrodynamic lift coefficient associated with only the parameters of the submerged hull and its surrounding fluid. Thus, a single coupled aero-hydrodynamic force coefficient of a water-borne WIGcraft may be estimated given the geometric parameters of the wings and submerged portion of the hull, and the fluid properties surrounding the waterborne WIGcraft moving at a given speed.

The results of the measured coupled aero-hydrodynamic forces of the WIGcraft and the empirical expressions for estimating the components that constitute the coupled aero-hydrodynamic lift coefficients of a waterborne WIGcraft are described in the following sub-sections.

6.9.2 Experimental results of measured coupled aero-hydrodynamic lift of a water borne WIGcraft

Figure 6.5 shows the measured dynamic lift coefficient $C_{L,i} = \frac{L_i}{0.5\rho_w U^2 {b_h}^2}$ characteristics of both the Outrigger and WIGcraft model configurations placed side by side for draught ≥ 0. Where

b_h is the static wetted beam of the submerged hull and subscript iv represents lift component generated by the hydrodynamic, aerodynamic or coupled aero-hydrodynamic lifting surfaces of the outrigger or WIGcraft. This form of non-dimensional aerodynamic lift coefficient is not typically used in aerodynamic studies of airplanes and WIGcraft, which in most studies are airborne. This form of the lift coefficient was devised for convenience and to ensure consistency when comparing the types of dynamic lift forces generated by the aerodynamic and hydrodynamic lifting surfaces, as well as when both types of lifting surfaces are coupled as in the case of a waterborne WIGcraft.

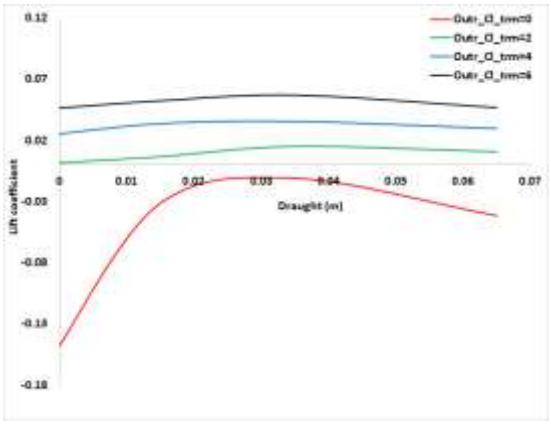

a. Lift coefficient vs draught (Outrigger)

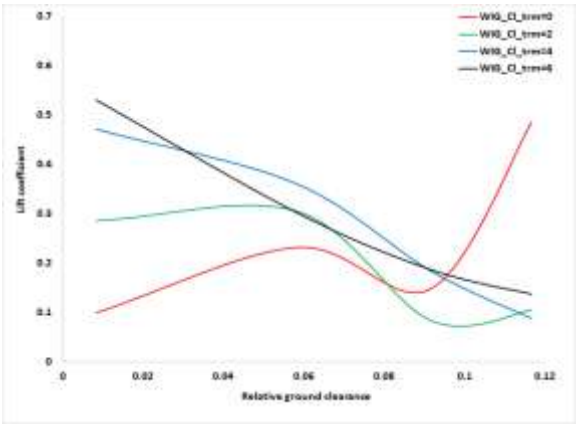

b. Lift coefficient vs draught (WIGcraft)

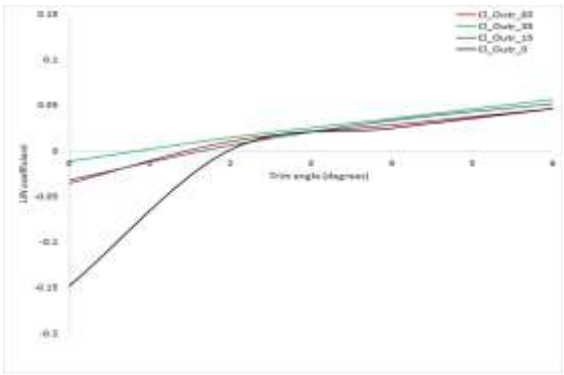

c. Lift coefficient vs trim angle (Outrigger)

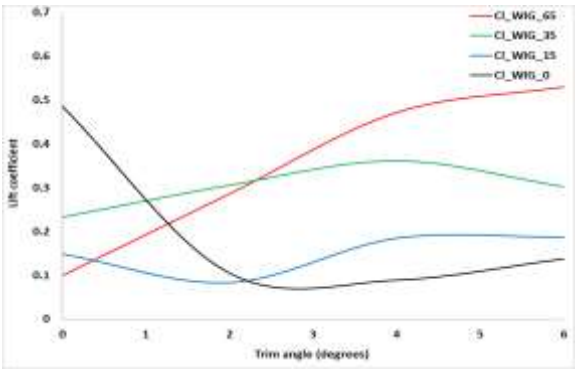

d. Lift coefficient vs trim angle (WIGcraft)

Figure 6.5 Measured dynamic lift coefficients of WIGcraft and Outrigger model configurations

It is seen in Figure 6.5b that for the WIGcraft model, at the higher angle of attack range (AOA = 4° and 6° in this case), the lift coefficient decreases as the relative ground clearance increases. It is to be noted that the lift coefficient at the highest AOA (6° in this study) has the steepest slope. On the other hand, for the lower AOA (0° and 2° in this case), though the general trend is downward, a more oscillatory lift coefficient characteristic which tends to increase at the transition region from extreme ground effect $\left(\frac{h}{c} \leq 0.1 chordlength\right)$ to a general ground effect

$\left(0.1chordlength \leq \frac{h}{c} \leq 0.2chordlength\right)$ is noted as the ground clearance increases. These findings agree with the results of the classical works of Tomotika et al. (1933) and Serebriyskiy (1939) which indicated that at higher AOA, the additional lift due to ground effect diminishes more (in comparison with the lower AOA) as the relative ground clearance increases. In other words, *as the WIGcraft transitions from extreme ground effect, higher lift can be achieved when the vehicle is operated at the lower trim angle*. This finding is relevant for accurate stability analysis and motion control of a WIGcraft during take-off from water. The lift characteristics in this transition region may significantly influence the dynamic stability characteristics of the WIGcraft. Though the works of Boschetti et al. (2017, 2022) and Kornev, (2019) did not specifically mentioned this characteristic of the lift coefficient of an airborne WIGcraft at the transition from extreme ground effect, their findings gave clear insight into the significance of such lift coefficient characteristics on the stability of WIGcraft and airplanes flying at low altitudes, such as during landing. Meanwhile, for the outrigger model, the effect of trim angle variation on lift appears to be more significant than draught effect as shown in Figure 6.5a. The outrigger model dynamic lift coefficient is seen to be generally independent or less sensitive to draught changes, especially at higher trim angles. From the foregoing discussion, can thus be stated that the wing geometry and attitude, and its proximity to the free surface water significantly influence the fluid flow about the airborne or waterborne WIGcraft and its resultant dynamic force characteristics.

Figures 6.5c and d show the lift coefficient curve of the outrigger and WIGcraft models respectively. For trim angles beyond 2°, the lift curve of the outrigger and WIGcraft models follow the typical shape of the lift coefficient curve of lifting surfaces that are predictable using the linear lifting line theory. This theory, however, will fail to predict the nonlinear effects correctly at higher trim (> 4° in this case). At the lower trim angle range (< 2°), the convex and concave shapes of the lift curve at the extreme draught positions (outside design draught range), i.e., 0.065m and zero draughts respectively are to be noted. The departure of the dynamic lift curve below 2° trim angle may be interpreted as consequences of higher experimental errors as can be seen in Appendix A2.

6.9.3 Dynamic lift of Outrigger model, $C_{Lhydmod}{}^{eh}$

The dynamic lift (total lift void of buoyancy) on a planing prismatic surface derived from the semi-empirical equation for lift in Savitsky (1964) method is given by,

$$C_{Lhyd}{}^{eh} = 0.12\lambda^{\frac{1}{2}}\tau^{1.1} - 0.0065\beta\left(0.012\lambda^{\frac{1}{2}}\tau^{1.1}\right)^{0.6} \quad (6.22)$$

This expression is valid for single chine prismatic hulls with transom stern undergoing uniform rectilinear motion in calm water and at constant draught. Other restrictions for the applicability of equation 6.13 include deadrise angle $\beta \leq 30°$, trim angle $2° \leq \tau \leq 15°$, mean wetted length to beam ratio, $\lambda \leq 4$, speed range $0.6 \leq Cv \leq 13$ and no convex surface. In equation 6.22 and other equations in this thesis, the superscript *eh* represents an *empirical hydrodynamic* quantity.

The Savitsky (1964) semi-empirical equation for lift has also been applied in professional practice for the prediction of the lift of non-monohedral hull with variable deadrise angle and chine along the length of the hull (Bertorello and Oliviero, 2007). The deadrise angle, β of a non-prismatic hull to be used in the application of Savitsky (1964) equation has been a subject of debate, especially as regards its effect on the longitudinal trim and total resistance of the watercraft (Bertorello and Oliviero, 2007; Blount and Fox, 1976; Savitsky et al., 2007). The deadrise angle at transom, at ¼ of the ship length from stern and that at the longitudinal centre of gravity have been suggested for use in the Savitsky equation for non-prismatic hulls. In this thesis, an empirical expression (equation 6.23) obtained from the mean wetted length expressions in Savitsky (1964) and Bannikov and Lulashevsky (1976) is proposed to estimate a suitable deadrise angles, β, that also accounts for the warped and non-prismatic submerged multi-hulls of a waterborne WIGcraft,

$$tan\beta = 2\pi tan\tau\left[\frac{d}{b_h sin\tau} - \frac{h_{te}}{2\tau b_h}\left(1 + \sqrt{\left(1 + 1.6\tau\frac{b_h}{h_{te}}\right)}\right)\right] \quad (6.23)$$

d and b_h are respectively the draught and wetted beam of the submerged portion of marine vehicle moving at trim angle, $\tau > 0$.

h_{te} is the height of the trailing edge of the wing. For a planing hull, h_{te} may be taken as zero. A flat planing surface corresponds to when the deadrise angle $\beta = 0$.

It is important to state that the application of the Savitsky (1964) method for warped hulls and for more extensive operational range in practice requires some form of modification of the coefficients in the equation. Such modifications may be carried out based on the known effects of the hull form on the characteristics of the fluid flow about the wetted hull surfaces and

dynamic forces generated by the surfaces. The Savitsky equation for dynamic lift and its other derivatives were developed following the swept wing analogy which entails predicting the dynamic lift from linear dynamic lift, cross flow drag related lift and leading-edge suction lift components. The crossflow drag related lift is known to be independent of trim angle and mean length but varies with deadrise along the ship length. Meanwhile, the leading-edge suction depends on the geometry of the leading edge at each draught.

For warped hulls with pointed re-entrant non-transom stern shown in Figure 6.6a, it is obvious that hull bottom pressure area behind the stagnation line is reduced by about a little above two-third in comparison to the typical transom sterns of planing boats of the same wetted length.

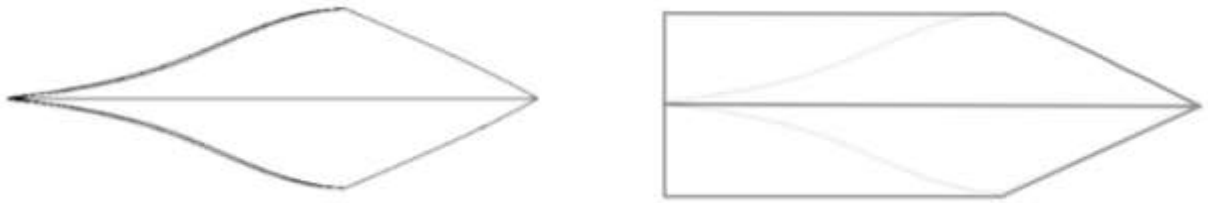

(a) Pointed re-entrant stern *(b) Transom stern*

Figure 6.6 Water plane area (WPA) geometry of a typical warped main hull with pointed re-entrant stern

The smaller hull bottom pressure area over the draught of boats with pointed sterns, leads to a significant reduction of the linear and cross flow drag related lift components and ultimately as well as the hydrodynamic lift coefficient predicted using the Savitsky (1964) lift equation. The operating draught which dictates the mean wetted length and chine wetted or unwetted condition, plays a significant role on the value of the hull bottom pressure area, as well as the characteristics of velocity field and the dynamic pressure lift distribution on this area as illustrated in Figure 6.7.

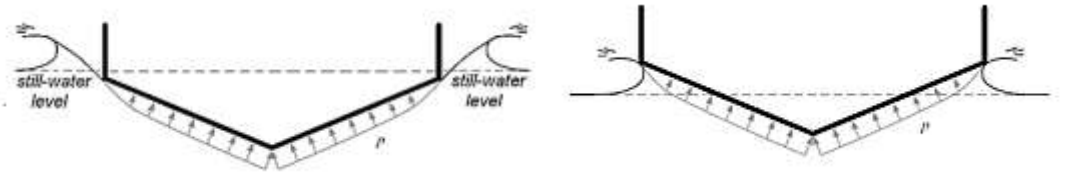

(a) Chine wetted hull section (b) Chine unwetted hull section

Figure 6.7. Pressure distribution on bottom hull sections at different draught

As a result, it is essential that for a given planing hull configuration with pointed (all trailing) stern, the dynamic lift coefficient of equation 6.22 be modified to get a better agreement with experimental data viz,

$$C_{Lhydmod}{}^{eh} = 0.12C_{\nabla}\lambda^{\frac{1}{2}}\tau^{1.1} - 0.0065\beta\left(0.012\lambda^{\frac{1}{2}}\tau^{1.1}\right)^{0.6} \quad (6.24)$$

Where,

$$C_{\nabla} = \frac{\sum(WPA \times d)}{\sum(l_{wl} \times b_h \times K_d)} \quad \text{for displacement volume, } \nabla > 0 \quad (6.25a)$$

$$C_{\nabla} = \frac{C_{\mathrm{WPA}}}{K_d} = \frac{\sum(WPA)}{K_d \sum(l_{wl} \times b_h)} \quad \text{for flat surface with displacement volume } \nabla \cong 0 \quad (6.25b)$$

$\sum(l_{wl} \times b_h)$ is the sum of the product of the wetted length and beam of the submerged portion of the hull(s).

$\sum WPA$ is the sum of the water plane area of submerged portion of the hull(s).

K_d is a factor that may be associated with cross-flows and the effects the variation of the Water Plane Areas (WPAs) with draught has on the hydrodynamic lift. Due to the warped nature of the hullform, the cross-flow effect of the fluid about the cross sections for chine immersed and chine-non-immersed hulls varies. As a result, the K_d will also be different for each draught.

Figure 6.8 compares the proposed semi-empirical hydrodynamic lift coefficients (equation 6.24) with the measured hydrodynamic lift coefficient $\left(C_{LH} = C_{LOutrg}{}^{ma} = \frac{L_{Outrg}{}^{ma}}{0.5\rho_w U^2 {b_h}^2}\right)$ of the Outrigger model at all draught positions for the considered trim angle range 2° to 6°. Figure 6.8a shows this comparison for draughts 0.035m and 0.065m. At these draught conditions, both the main hull and the sponsons are submerged in the water and are thus representative conditions for planing multi-hulls. Table 6.3 shows the difference between the experimental and semi-empirical results are in the order of 10% at the 0.035m and 0.065m draught conditions.

Table 6.3 Percentage difference in hydrodynamic lift coefficient between experimental data and proposed empirical equation 6.24.

Percentage difference between measured and equation 6.16.					Percentage difference between Wadlin and McGehee (1950) and equation 6.16.				
Draught (m)	Trim Angle (deg)	λ	K_d	Difference (%)	Draught (m)	Trim Angle (deg)	λ	K_d	Difference (%)
0.065	2	2.87	0.700	10.84	0.12	4	4.00	31.2	9.07
	4	2.80		7.93		8			1.48
	6	2.73		2.35		12			0.85
0.035	2	3.26	0.325	8.39	0.08	4	4.00	19.2	9.67
	4	3.04		0.72		8			5.23
	6	2.86		0.91		12			6.65
0.015	2	4.20	0.170	150.89					
	4	3.51		0.66					
	6	3.10		3.60					
Zero	2	4.93	15.000	603.73					
	4	3.81		6.69					
	6	3.41		7.78					

Except at the lowest trim angle limit for Savitsky's lift equation (i.e., at 2°) for the 0.065m draught condition, the percentage differences between the measured results and those from the proposed empirical expressions for the dynamic lift at draught 0.035m and 0.065m are generally below 8% as can be seen in Table 6.3. Because the differences between the results and the uncertainty (shown in Table A2 in appendix A) associated with the measured hydrodynamic lift coefficients at draughts 0.035m and 0.065m are low, it can be stated that there is a good agreement between the measured data and the results of the proposed empirical expressions, especially at trim angles beyond 2°.

Figure 6.8b compares the measured lift coefficients with those of the proposed semi-empirical equation at draughts 0.015m and zero metres. Both zero and 0.015m draught positions represent hydrodynamic situations similar to single planing hulls. Due to the vertical clearance between the main hull and the sponsons, the sponsons are not submerged. At the zero and 0.015m draught positions, $K_d = 5.000\ and\ 0.170$ respectively. Except at the lower trim angle (2°), the percentage differences between the measured results and those from the proposed empirical expressions for the dynamic lift for the zero and 0.015m draught conditions are respectively below 9% and 5% at the higher trim angles ($\tau > 2°$) as can be seen in Table 6.3.

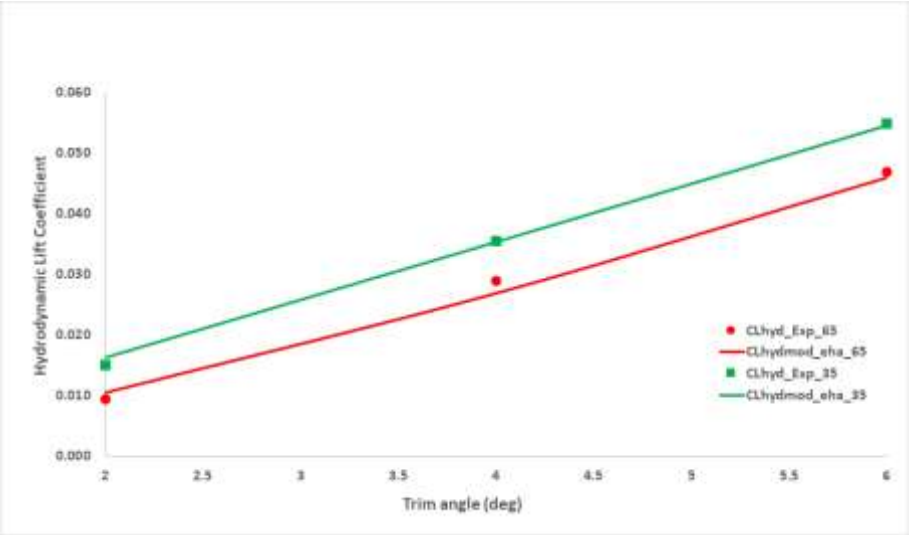

a 0.065 and 0.035m draught positions

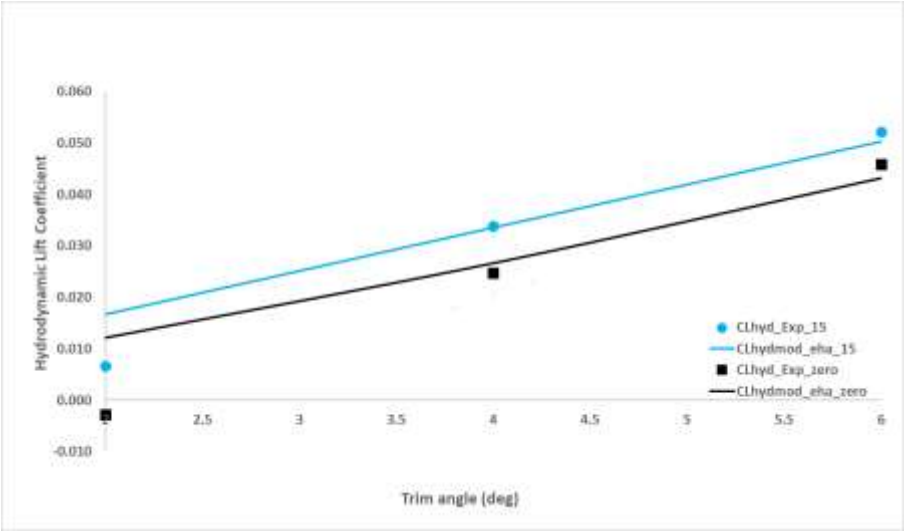

b zero and 0.015m draught positions

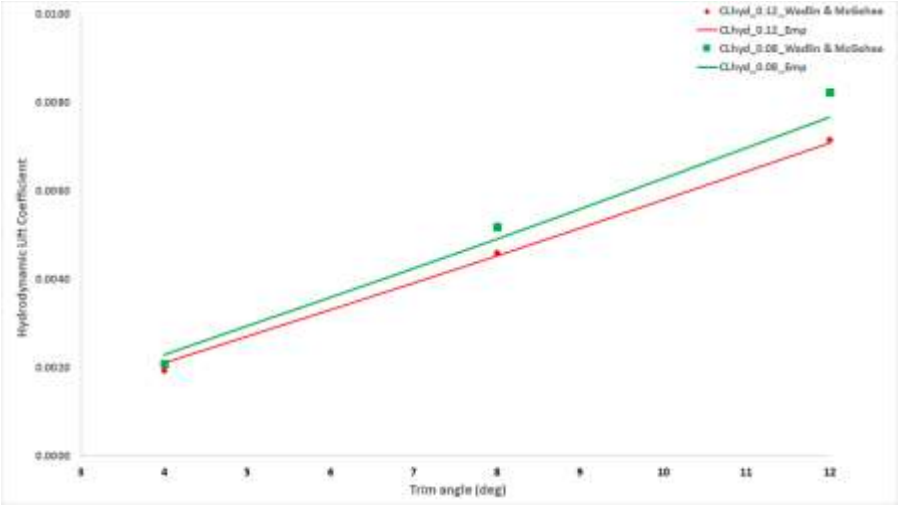

c Wadlin and McGehee data comparison

Figure 6.8 Measured and proposed semi-empirical hydrodynamic lift coefficient

For the draught conditions (especially where the chine is not fully immersed, i.e., at zero and 0.015m draught), Table 6.3 shows the existence of a large percentage difference between the measured data and the proposed semi-empirical expression at 2° trim angle, which is the lower trim angle limit specified for the Savitsky (1964) semi-empirical expression for hydrodynamic lift of planing hulls. At these draught positions and 2° trim angle, the lift coefficients estimated from the proposed empirical equation lies outside the upper uncertainty limits of the measured lift coefficient. However, from the uncertainty values of the measured lift compared with other trim angle attitudes for all the considered draught positions (especially at zero and 0.015m draughts) shown in Table 2A in the appendix A, it can be suggested that the large percentage differences between the results of the proposed empirical model and the experiments are not unconnected to the uncertainties associated with the results obtained from carrying out model tests at 2° trim angles.

It is important to note from Table 6.3 that at the 2° trim angles for the zero and 0.015m draught positions, the empirical formula is applied to experimental data generated for a hull model having a length to beam ratio of about $\lambda = 4.9$ and 4.2 respectively, which is beyond the mean wetted length to beam ratio upper limit required for appropriate application of the Savitsky (1964) semi-empirical expression for hydrodynamic lift of planing prismatic hulls. A mean wetted length to beam ratio beyond 4.0 is indicative of warped planing hulls operating at low draught and generally with chine non-immersed.

At this 2° lower trim angle limit, the large percentage difference between the proposed empirical model and experimental results may be attributed partly to the much higher uncertainty (30.42% at d = 0.015m and 27.99% at d = 0 for the Outrigger model) associated with the measured data at these test conditions. The large discrepancies may also be partly due to the fact that the proposed empirical expression is applied outside the limits of its wetted length to beam ratio, and that it does not adequately account for the influence the chine geometry and condition (immersion characteristics) has on the hydrodynamic lift generated by the submerged hull surfaces at the planing speed regime. Shuford (1957) noted that the influence of chine characteristics on hydrodynamic lift is difficult to quantify. Though, the constant K_d value estimated in this study yields acceptable lift results at the trim angles considered for each draught position, the K_d value may be adjusted for this lower trim angle and draught limits to better account for the influence of the chine conditions. It may be helpful to note that planing boats are generally operated at ≥4° (not 2°) in practice.

It is also seen from Table 6.3 that the value of K_d is independent of trim angle at each of the draughts and generally decreases with draught. The higher value of K_d and higher percentage difference between the experimental and semi-empirical results noticed at the zero draught condition does not necessarily negates the stated characteristics of K_d with respect to trim angle and draught. The zero draught condition represents a unique draught extreme limit case for application of the proposed semi-empirical model.

A comparison of the lift coefficient results calculated from equation 6.24 and from previous experimental data of model 250E re-entrant pointed stern in Wadlin and McGehee (1950b) is given in Fig.6.8c and the percentage differences are given on the right-hand side of Table 6.3. Model 250E has a flat bottom (i.e., zero deadrise) and triangular plan form with a longitudinal taper ratio of 4:1, and extreme upper limit of mean wetted length to beam ratio of 4.0. As previously noted for the measured results in this study, the results of the equation 6.24 also correlate well with experimental data of Wadlin and McGehee (1950b). The maximum difference between the experimental data and the empirical expression is below 10%. It is to be noted that the correlation between equation 6.24 and the experimental data from Wadlin and McGehee (1950b) was achieved with a much higher K_d value than those stated for the planing hull model tested in this study. This higher K_d value may be associated to the characteristics of the hull form and the experimental test facility used.

The findings from this study suggests that Equation 6.24 is applicable for predicting the hydrodynamic lift of a fully planing hull at displacement-based Froude Number $Cv \geq 3$, trim angle, $2° \leq \tau \leq 12°$, mean wetted length, $\lambda \leq 4$ and draught, $d \geq 0$. The proposed empirical expression (equation 6.24) for estimating the hydrodynamic lift coefficient is, however, more accurate and applicable to larger draught and higher trim angle conditions where the lift is minimally influenced by chine conditions. Using equation 6.24, the lift coefficient of various configurations of warped hulls can be estimated by changing the value of K_d. Since the values of K_d is largely independent of trim angles > 2°, by carrying out a single model test of a hull model at a given draught and trim angle greater than 2° to determine K_d value, the lift coefficient of warped planing mono- or multi- hulls at the tested draught for a range of trim angles can be estimated using equation 6.24.

6.9.4 Free surface (ground) effects on aerodynamic lift, $C_{Lage}{}^{eha}$

In Figure 6.5d, it is seen that the lift curve of the WIGcraft is a function of its trim angle (or AOA) and draught (or relative ground clearance height). In an alternative interpretation with respect to Figure 6.5b, it can be stated that Figure 6.5d illustrates the increase in dynamic lift of a waterborne WIGcraft with draught at trim angles beyond 2°. This tendency is further illustrated in Figure 6.12 (see later pages), where it is shown that the stalling angle of the wings is not the same as the stalling angle of the WIGcraft. It is seen in Figure 6.12 that the wings stall earlier than the WIGcraft itself. For instance, at the 0.035m draught the stalling angle of the wing is near 3° while that of the WIGcraft is delayed beyond 4°. The waterborne WIGcraft generally, appears to stall near 4° trim angle (or AOA) which corresponds to the stalling angle of most very fast airplanes and planing boats.

The stalling angle of the WIGcraft, however, indicates the limited envelop for linear increment in lift with trim angle (or AOA) as the draught varies during the acceleration of the watercraft to take-off. This lift characteristics gives a glimpse into the stability challenges and control difficulties a WIGcraft pilot will encounter when accelerating or when on waves due to variations in trim angles as the watercraft accelerates. In essence, the WIGcraft may not be suitable for slow cruise or slow take-off acceleration run where larger stalling angle (typically 15°) is required.

Overall, the shape of the lift curve in Figure 6.5 generally follows the nonlinear lifting line theory. The nonlinearities may be associated with certain dynamic effects of the vehicle, notably, hydrodynamic suction pressure at planing bottom, free surface proximity of the wings (ground effects) and hull-generated spray impinging on the wing surfaces. To delineate the aerodynamic related nonlinear effects (i.e., ground effects) from the coupled aero-hydrodynamic lift curve of the waterborne WIGcraft, it is expedient to formulate empirical expressions for the lift characteristics for the WIGcraft model in both airborne and waterborne modes.

In 1946, R.T. Jones proposed the following empirical expression for the low aspect ratio lift curve from experimental tests on elliptical and rectangular wings in free flight,

$$\frac{\partial C_{Lff}}{\partial \alpha} = \frac{2\pi R_A}{R_A+3} \tag{6.26}$$

As noted elsewhere in this thesis, wings moving close to free surface water creates ground effects sufficient to reasonably change the fluid flow, dynamic forces and motion behaviours

of an otherwise free flight vehicle. On consideration of the characteristics of the lift coefficients in Figure 6.5 and existing ground effect theories stated in Mantle (2016), which suggests that the lift curve slope varies with the relative ground clearance and asymptotically approach out of ground effect, the increment in free flight aerodynamic lift coefficient of the WIGcraft model as a function of angle of attack and its proximity to the free surface water may be empirically expressed by modifying the lift expression proposed by Jones (1941), thus,

$$\Delta C_{Lage}{}^{ea} = \frac{2\pi R_A}{R_A+3}\frac{\alpha_{eff}}{\tanh\left(\frac{n_{gc}}{3}\alpha_{eff}\right)}\left(k_{gc}e^{-20\left(\frac{h_{te}}{c}\right)}\right) \qquad (6.27a)$$

Valid at $2° \leq \alpha_{eff} \leq 10°$ for air borne WIGcraft

superscript *eh* represents an *empirical aerodynamic* quantity.
h_{te} is the height of the trailing edge of the wing from the free surface water as earlier defined.
R_A is the aspect ratio of the wings,
c is the mean aerodynamic chord length of the wings

The effective angle of attack which accounts for changes in the trailing edge vortices due to the presence of the ground is given by $\alpha_{eff} = \alpha - \alpha_0$, $\alpha_{eff} > 0$
α is the sum of the wing incident angle and the trim angle (AOA) of the hull,

α_0 is zero lift angle of attack.

n_{gc} is a factor associated with the experimental facility/method used to measure the free flight aerodynamic lift, especially at the lower trim angle range. Its value which typically range; $n_{gc} \leq 3$ depends on the relative clearance height of the trailing edge of the wings from the ground surface.

k_{gc} is a factor which depends on the relative clearance height of the wings from the ground.

By multiplying equation 6.27a by the equivalent hydrodynamic lift coefficient transformation factor, $\frac{x_{ah}{}^2}{R_A} = \frac{b_a{}^2}{b_h{}^2}\frac{\Upsilon}{R_A}$ in section 6.9.1, the increment in aerodynamic lift of a waterborne WIGcraft due to ground effect may be expressed as,

$$\Delta C_{Lage}{}^{eha} = \left(\Delta C_{Lage}{}^{ea}\right)\frac{b_a{}^2}{b_h{}^2}\frac{\Upsilon}{R_A} = \frac{2\pi}{R_A+3}\frac{b_a{}^2}{b_h{}^2}\Upsilon\frac{\alpha_{eff}}{\tanh\left(\frac{n_{gc}}{3}\alpha_{eff}\right)}\left(k_{gc}e^{-20\left(\frac{h_{wk}-d}{c}\right)}\right) \qquad (6.27b)$$

Valid for waterborne WIGcraft at draught > 0, $2° \leq \alpha_{eff} \leq 10°$

Superscripts ea and eha respectively represent the proposed empirical aerodynamic quantity and its equivalent hydrodynamic value.

h_{wk} is the height of the trailing edge of wing from the keel,
d is the operating draught of the vehicle

Thus, the pure ground effect aerodynamic lift coefficient of the WIGcraft near the free surface water may be represented by

$$C_{Lage}{}^{ea} = \frac{2\pi R_A}{R_A+3}\frac{\alpha_{eff}}{\tanh\left(\frac{n_{gc}}{3}\alpha_{eff}\right)}\left(1 + k_{gc}e^{-20\left(\frac{h_{te}}{c}\right)}\right) \qquad (6.28a)$$

Valid for air borne WIGcraft.

In equation 6.28a, the increment in the free flight aerodynamic lift coefficient due to ground effect was expressed as a fraction of the free flight aerodynamic lift coefficient of the vehicle using exponential function.

The hydrodynamic equivalent of $C_{Lage}{}^{ea}$ is given as

$$C_{Lage}{}^{eha} = \frac{2\pi}{R_A+3}\frac{{b_a}^2}{{b_h}^2}\Upsilon\frac{\alpha_{eff}}{\tanh\left(\frac{n_{gc}}{3}\alpha_{eff}\right)}\left(1 + k_{gc}e^{-20\left(\frac{h_{wk}-d}{c}\right)}\right) \qquad (6.28b)$$

Valid for waterborne WIGcraft at $b_h > 0$

Unlike equation 6.28a which is not related in any form to the submerged hull, equation 6.20b as presented, enables easy summation of the ground effect aerodynamic lift coefficient of the wings and the hydrodynamic lift coefficient of the submerged hull surface.

For the WIGcraft investigated in this thesis, the lift due to ground effect (i.e., lift due to nearness of wings to the free surface water) is isolated from the lift due to hull-generated water spray on the wings, by considering only experimental test cases where hull-generated water spray does not flow about the wings of the WIGcraft. These cases are when the WIGcraft model trim angles are 0, 2, 4 and 6 at zero draught and 0, 2, 4 trim angles when the keel of the WIGcraft model is above the water surface by 6mm.

Following from section 6.9.1, the measured ground effect aerodynamic lift coefficient ${C_{Lage}}^{ma} = \left(\frac{{L_{WIG}}^{ma} - {L_{Outrg}}^{ma}}{0.5\rho_a {b_a}^2 U^2}\right)$of the wing surface is transformed into its hydrodynamic equivalent,

$${C_{Lage}}^{ema} = \frac{{x_{ah}}^2 {C_{Lage}}^{ma}}{R_A} = \frac{{L_{WIG}}^{ma} - {L_{Outrg}}^{ma}}{0.5\rho_w {b_h}^2 U^2} \quad (6.29)$$

$${C_{LOutrg}}^{ma} = \frac{{L_{Outrg}}^{ma}}{0.5\rho_w U^2 {b_h}^2} \quad (6.30)$$

$${C_{LWIG}}^{ma} = \frac{{L_{WIG}}^{ma}}{0.5\rho_w U^2 {b_h}^2} \quad (6.31)$$

Subscripts ma and ema are respectively the measured aerodynamic quantity and its equivalent hydrodynamic value.

${C_{LWIG}}^{ma}$ is the lift coefficient derived from measured lift ${L_{WIG}}^{ma}$, on the waterborne WIGcraft model.

${C_{Loutrg}}^{ma}$ is the lift coefficient derived from the measured lift ${L_{Outrg}}^{ma}$, on the Outrigger model.

Equations 6.30 and 6.31 are equivalent to equations 15 and 21 respectively in subsection 6.9.1

Table. 6.4 and Figure 6.9 (below) show the agreement between the proposed empirical expression for the lift coefficient ${C_{Lage}}^{ea}$ and the measured lift coefficient ${C_{Lage}}^{ma}$ when the tested WIGcraft model with aspect ratio, $R_A = 1.333$ is towed at relative ground clearances $\frac{h_{te}}{c} = 0.114$ (i.e. zero draught) and 0.124 (i.e., 6mm above the free surface water).

Table 6.4 Comparison between measured vs proposed empirical aerodynamic lift coefficients.

R. ground clearance height	Aspect Ratio	Trim Angle (deg)	${C_{Lage}}^{ma}$	${C_{Lage}}^{ea}$	${C_{Lage}}^{ema}$	${C_{Lage}}^{eha}$	Difference (%)
0.114 (Zero draught)	1.333	0	0.3082	Undefined	0.0362	Undefined	Undefined
		2	0.6484	0.6308	0.0422	0.0410	2.70
		4	1.0478	1.1084	0.0554	0.0586	5.78
		6	1.6920	1.6499	0.0819	0.080	2.49
0.124 (6mm above free surface water)	1.333	0	0.1244	Undefined	n.a*	n.a*	-
		2	0.3410	0.3188	n.a*	n.a*	0.90
		4	0.5764	0.5905	n.a*	n.a*	3.01

n.a means not applicable.*

For the general ground effect conditions, where $0.1 < \frac{h_{te}}{c} \leq 0.2$, the percentage difference between the proposed semi-empirical expression and the measured data of the anhedral trapezoidal wings at all trim angles was in the order of 5% when the value of $k_{gc} = 70$ and n_{gc} = 0.667.

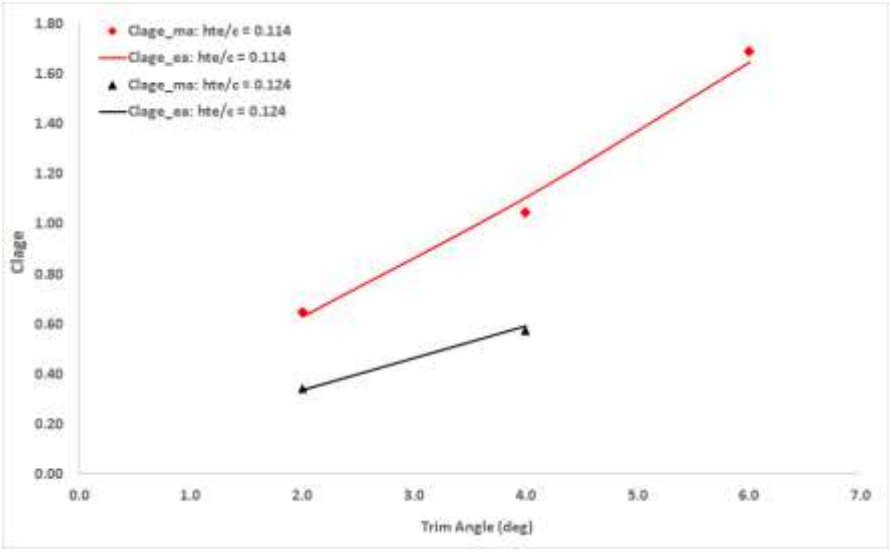

Figure 6.9 Comparison between measured and proposed empirical aerodynamic lift coefficients.

This result reaffirms the report of Belynsky and Zinchuk (1998) that towing tank facilities can be used to measure ground effect aerodynamic forces on towed models to pinpoint accuracy in calm water.

To further verify the validity of the empirical equation, equation 6.28a was applied to the experimental lift data of an anhedral trapezoidal wings from Fink and Lastinger (1961). Figure 6.10 compares the experimental lift data from Fink and Lastinger (1961) with the proposed empirical equation for two different aspect ratios ($R_A = 1, 2$) and relative clearance heights ($\frac{h_{te}}{c} = 0.042, 0.083, 0.167$), while Table 6.5 shows the percentage difference between their results.

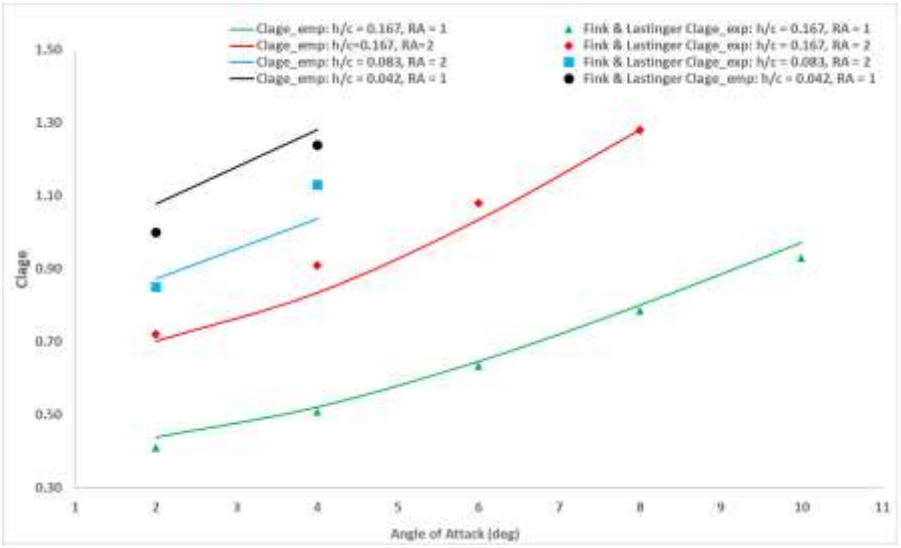

Figure 6.10 Comparison between Fink and Lastinger (1961) lift data and proposed empirical aerodynamic lift coefficients.

The Figure also suggests that for general ground effect conditions where $0.1 < \frac{h_{te}}{c} \leq 0.2$, the value of $k_{gc} = 70$, irrespective of the aspect ratio. For extreme ground effect where $\frac{h_{te}}{c} \leq 0.1$, the value of k_{gc} equals 17.5 (i.e., a quarter of the k_{gc} value of the wings for general ground effect condition). For the general ground effect conditions, $0.1 < \frac{h_{te}}{c} \leq 0.2$, the value of n_{gc} equals 0.233. At $0.2 < \frac{h_{te}}{c} \leq 1.00$, the value of n_{gc} was found to decrease by half when the aspect ratio of the wings was doubled following the implementation of equation 6.28 on Fink and Lastinger (1961) wing data.

Table 6.5 Disparity in ground effect lift coefficient between Fink and Lastinger (1961) and the proposed empirical equation

Relative ground clearance height	Aspect Ratio	Angle of Attack (deg)	Difference (%)	Relative ground clearance height	Aspect Ratio	Angle of Attack (deg)	Difference (%)
0.167	1	2	6.90	0.167	2	2	0.72
		4	2.23			4	0.91
		6	1.85			6	1.08
		8	2.02			8	1.28
		10	4.57			-	-
0.043	1	2	5.01	0.083	2	2	2.57
		4	0.74			4	7.39

The above comparative analysis shows that the proposed semi-empirical expressions stated in equations 6.28 correlates well with the Fink and Lastinger (1961) wind tunnel experimental data, as well as with the towing tank experimental data obtained in this study. Though the empirical expression has been verified for limited test data, they reinforce the estimation of pure ground effect aerodynamic lift (with no water spray effect) on an air borne and water borne WIGcraft from towing tank experiments (Belynsky and Zinchuk, 1998).

6.9.5 Hull-generated spray effect on aerodynamic lift, $C_{Lsp}{}^{eha}$

Hull-generated spray effect is important for the correct location and design of the wings of a water-borne WIGcraft. The upward moving hull-generated water spray induces a vertical force component on the hull and the wings. However, this spray lift on the hull may be considered negligible compared to the spray lift on the wings. The aerodynamics of most water borne WIGcraft is significantly influenced by the dynamic pressure of the hull-generated water spray impinging on it. For a typical planing hull surface, the whiskers spray which is bounded by the spray edge and the stagnation line are observed to rise and move sideways (transverse direction), sometimes beyond the chine and impinging on the wings. The energy and consequently velocity of the water spray is reduced over the distance between the spray root and wing leading edge and wing surface due to; flow turbulence as it mixes with air, thermal dissipations, and oscillations of disintegrated spray particles. Since the turbulent spray over the wing is a mixture of water and air, its density becomes a composite of both air and water.

If the two-phase air-water mixture in the spray are in equilibrium but energy and mass are not conserved, then there can be no approximate constant spray velocity. Thus, the velocity varies along the trajectory of the spray from the spray region to the leading edge of the wing and over the wing top and bottom surfaces. In this paper, at each position along the spray trajectory, mass and energy are assumed conserved and the spray velocity is assumed constant. The magnitude of impinging pressure of the water spray on the upper and lower surfaces of the wings (see Figure 2.1) then depends on

- the hull form (primarily hull deadrise angle (β) and operational parameters such as trim angle (τ) and speed (f_{nB}). These parameters also dictate the volumetric flow rate and trajectory of the hull generated spray as investigated and described in detail by Morabito (2010).

- the geometry (b_a) and location (h_{te}) of the wings with respect to the keel from the free surface (d) of the hull(s), as well as the orientation (α_{eff}) of the wings with respect to the spray direction.

By considering how the various aforementioned parameters influencing the dynamic pressure on the wings of the WIGcraft model, a simplified semi-empirical expression for the spray lift coefficient of the wings of a water borne WIGcraft may be given as

$$C_{Lsp}{}^{eha} = b_a{}^2 \left(K_{wsp} \alpha_{eff}{}^{ns1} f_{nB}{}^2 \left(\frac{d}{h_{te}}\right)^{0.4} - K_{hsp} \beta \tau^{-0.1} \frac{\left(\frac{d}{h_{te}}\right)^{0.11}}{f_{nB}{}^2} \right) \tag{6.32}$$

Valid for all ground clearance and draught for which water spray impinges on the wings.

The first term in equation 6.32 accounts for how the size, location and orientation of the wings influence the dynamic pressure of hull-generated spray on the wings of a water borne WIGcraft. This term is suggestive of the fact that the approach used to estimate the spray lift is analogous to that used to estimate the aerodynamic lift on low aspect ratio swept wings. Similar consideration was implemented by Savitsky (1964) in developing the semi-empirical expression for the hydrodynamic lift of planing hulls. Superscript $ns1$ is draught independent constant. Generally, the superscript $ns1$ in equation 6.32 is in the limit $0.9 \leq ns1 = 1.1$.

The draught to wing clearance height $\frac{d}{h_{te}}$ which is analogous to the mean wetted length to beam ratio in Savitsky's hydrodynamic lift expression indicates the significance of the location of the wings with respect to the operating draught of the watercraft. K_{wsp} is a factor which may be associated with the characteristics of the wings and its location on the spray area of the hull.

The second term in equation 6.32 accounts majorly for the effect of the hull deadrise and operating trim angles on spray generation and the trajectory of the spray from chine exit point on the hull, and ultimately on the spray lift. The trim angle and the deadrise angle play critical role in the volume and direction of the hull generated spray. Depending on the combination of both the deadrise and trim angles, the spray may possess high forward velocity without impinging on the wings, move athwartship without a longitudinal component or move perpendicular to the chine of the hull.

K_{hsp} is a hull form dependent factor, and its value is independent of operating draught and trim angle.

Physical observation of hull generated water sprays characteristics informs that the free surface/water spray geometry deforms until at certain high-speed regime (herein regarded as the planing speed regime) when the free surface/water geometry remains relatively constant (McBride,1956). Beyond this planing speed, Kelvin-Helmholtz instability occurs, and the glassy spray blister disintegrates into droplets at reduced breakup distance (Dundurs and Hamilton, 1954, 1955). As a result, the water spray impact on the wings is reduced. The first and second terms in equation 6.32 capture this impact characteristics of the hull generated spray on the wings as the speed of the WIGcraft model is increased or decreased.

The first and second terms in equation 6.32 also account for the fact that as the operating draught of the WIGcraft model reduces to zero, the relative ground clearance of the wings increases, the spray volume generated by hull also decreases to zero and the spray is less likely to impinge on the wings and contribute to the dynamic lift of the WIGcraft model. The reverse is the case for increasing draught.

The measured lift of the waterborne WIGcraft less the measured lift generated by Outrigger and the pure ground effect lift wings at equal ground clearance gives a quantitative value of the spray effect on the aerodynamic lift of the waterborne WIGcraft. Thus,

$$C_{Lsp}{}^{ma} = C_{LWIG}{}^{ma} - C_{LOutrg}{}^{ma} - C_{Lage}{}^{eha} \qquad (6.33)$$

$C_{LOutrg}{}^{ma}$ and $C_{LWIG}{}^{ma}$ are defined in equations 6.30 and 6.31 respectively.

Figure 6.11 illustrates the characteristics of the deduced hull-generated water spray lift on the wings for all speed and trim angles considered in this study. The results from the empirical expression (equation 6.32) for spray lift coefficient is seen to correlate well with the experimentally deduced spray lift coefficient data of the waterborne WIGcraft model (equation 6.33).

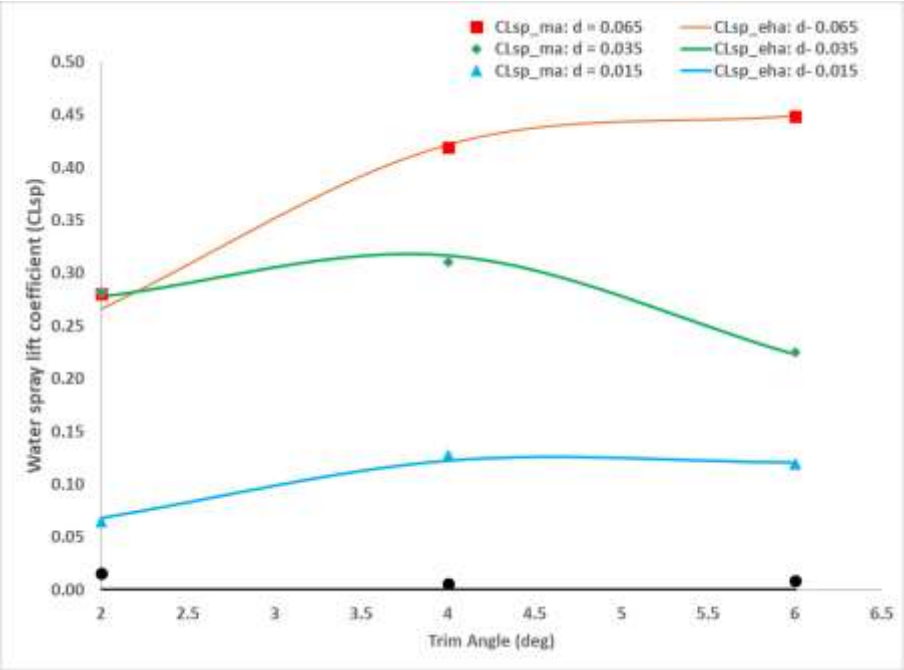

Figure 6.11 Experimental vs empirical spray lift factors

The fact that the hull generated water spray is seen to increase with trim angle up to a peak point before decreasing suggests the significance of the influence of both speed and trim angle on the spray lift coefficient in an analogous manner to that of Savitsky (1964) lift coefficient. It is obvious that the main spray contributes positively to the total lift even though at times it moves over the top of the wings.

Table 6.6 shows good agreement between the empirical expression (equation 6.32) for estimating the spray lift and that derived from the measured lift coefficient of the water borne WIGcraft model (equation 6.33). The percentage difference between the empirical model and the experimental data are in the order of 5% in almost all cases.

Table 6.6 Comparison between ${C_{Lsp}}^{ma}$ and ${C_{Lsp}}^{eha}$

Draught (m)	K_{wsp}	Trim Angle (deg)	Difference (%)	Draught (m)	K_{wsp}	Trim Angle (deg)	Difference (%)
0.065	0.0040	2	5.02	0.035	0.0150	2	5.7288
		4	0.72			4	4.2607
		6	0.31			6	1.0288
0.015	0.0029	2	1.30	0	0.0000	2	-
		4	1.95			4	-
		6	0.89			6	-

As with K_d values for the hydrodynamic lift equation 6.24, the value of K_{wsp} is independent on the operating trim angle. At zero draught, there is no spray formation and impingement on the wings and $K_{wsp} = 0$. The value of K_{hsp} equals 0.0062 for the hull used in this study. K_{hsp} is independent of operating draught and trim angle. The superscript $ns1$ in equation 6.32 is in the limit $0.9 \leq ns1 = 1.1$, with the upper limit applicable for $\alpha_{eff} \cong \tau \leq 4°$.

From Figure 6.11, it is seen that the draught plays a very significant role in dictating the contribution of the hull generated spray to the total lift of the WIGcraft. As the draught tends towards zero, the spray effect on the lift diminishes to zero. Except at zero draught, the spray characteristics are similar for all draught positions. At the zero-draught position, there is no spray effect (because no spray impinges on the wings). These zero spray characteristics is well depicted by the empirical model. The small values for spray lift coefficient noted in the Figure for the experimental data may be attributed to experimental error from the data acquisition system, especially at the 2° trim angle where Table A2 in the appendix show relatively high uncertainty percentage. The lesser percentage difference shown in Table 6.6 between the experiment data and the results of the empirical spray lift expression in spite of the high uncertainty percentage at 2° trim angle at the zero-draught position, may be associated with cancellation of the experimental errors (in the measured data of the WIGcraft and Outrigger models) that occurred when deducing the experimental spray lift coefficient by implementing equation 6.33.

6.9.6 Dynamic lift characteristics of the wings

Waterborne WIGcrafts are essentially boat hulls equipped with wings subjected to ground effects. As stated earlier, the wings of a waterborne WIGcraft are subjected to not only ground effects but also hull-generated water spray effect. To examine the dynamic lift characteristics on the wings fitted to the Outrigger model, the difference between the measured lift coefficients of the WIGcraft and the outrigger model configurations are plotted in Figure 6.12 alongside the dynamic lift coefficients of both the WIGcraft and the Outrigger models.

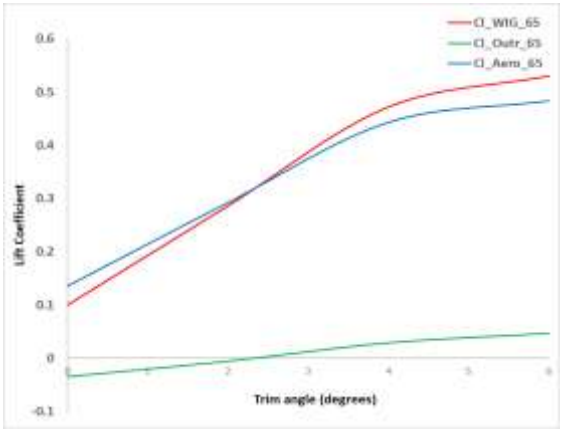

a. at draught 0.065m (h/c = 0.008)

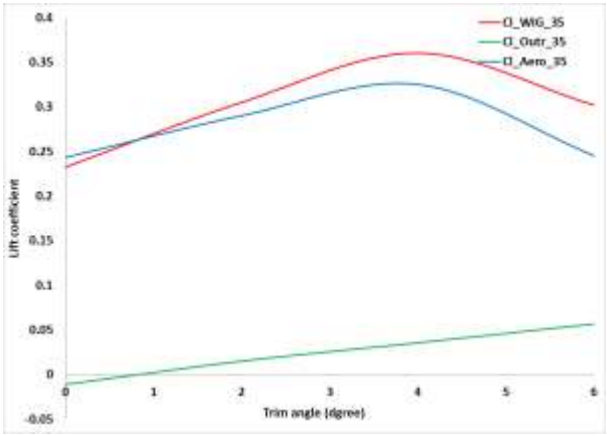

b. draught 0.035m (h/c = 0.058)

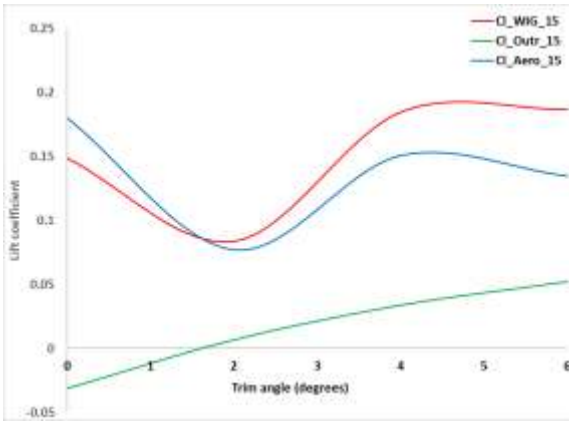

c. at draught 0.015m (h/c = 0.092)

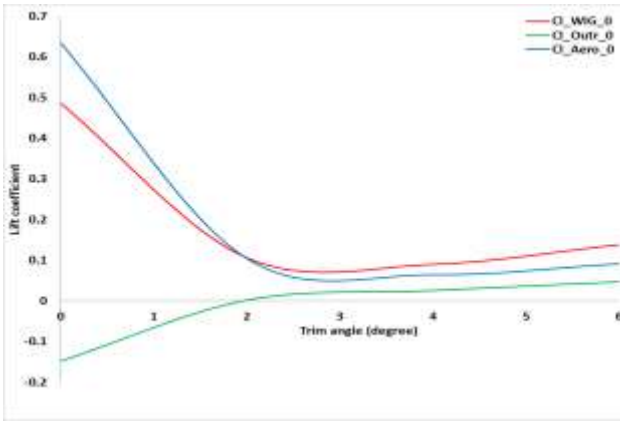

d. at zero draught (h/c = 0.114)

Figure 6.12 Dynamic lift characteristics of wings fitted to outrigger model configuration

At all draught positions and especially at trim angles beyond 2°, the planing Outrigger model exhibits minimal nonlinear lift characteristics. thereby indicating that the Outrigger model is less sensitive to trim angle changes in comparison with the WIGcraft model.

The almost linear relationship between the lift coefficients and the trim angle for the Outrigger model is notable, especially at the higher draughts and trim angle beyond 2°. Whereas the WIGcraft model and the hull-generated water spray influenced wings near the free surface water exhibits a highly nonlinear lift characteristic. Notwithstanding, it is seen that beyond 2° trim angle (AOA), the lift coefficient of the wings and WIGcraft is similar to typical lift coefficients in free flight aerodynamics. This suggests that with corrections for the nonlinearities the popular lifting line theory is likely to hold true for the water spray wetted wings of the waterborne WIGcraft model used in this study. Hence, it can be stated that the presence of the free surface has a reasonable effect on the aerodynamic lift of the isolated wing at the relative ground clearance heights considered in this study. It is to be noted that for a range

of draughts where hull-generated water spray impinges on the wings of the WIGcraft, the presence of the free surface has a more significant effect on the lift as the ground clearance increases. This observation may be attributed to the water spray trajectory, spray energy and the spray impacted areas of the wings.

From the foregoing, the aerodynamic lift coefficient of the near free surface wing of a water borne WIGcraft and its hydrodynamic equivalent may simply be expressed as,

$$C_{Lwing}{}^{ea} = C_{Lage}{}^{ea} + C_{Lsp}{}^{eha} \tag{6.34a}$$

$$C_{Lwing}{}^{eha} = C_{Lage}{}^{eha} + C_{Lsp}{}^{eha} \tag{6.34b}$$

6.9.7 *Dynamic lift on a waterborne* WIGcraft

By combining the expression for change in aerodynamic lift inclusive of ground and spray effects (equations 6.28b and 6.32) together with the hydrodynamic lift (equation 6.24) generated by the submerged hulls, the empirical relation for the dynamic lift of a waterborne WIGcraft may be expressed in the following form,

$$C_{LWIG}{}^{eha} = C_{Lhydmod}{}^{eh} + C_{Lage}{}^{eha} + C_{Lsp}{}^{eha} \tag{6.35}$$

This expression is valid for trim angle in the range $2 \leq \tau \leq 10$, and at all draught positions and relative ground clearance heights.

Figure 6.13 compares equation 6.35 with the measured dynamic lift coefficient (see $C_{LWIG}{}^{ma}$ in equation 6.31) at various draught or relative clearance height. From Figure 6.13, it is seen that there is a good agreement between the proposed empirical expression and the measured dynamic lift coefficient.

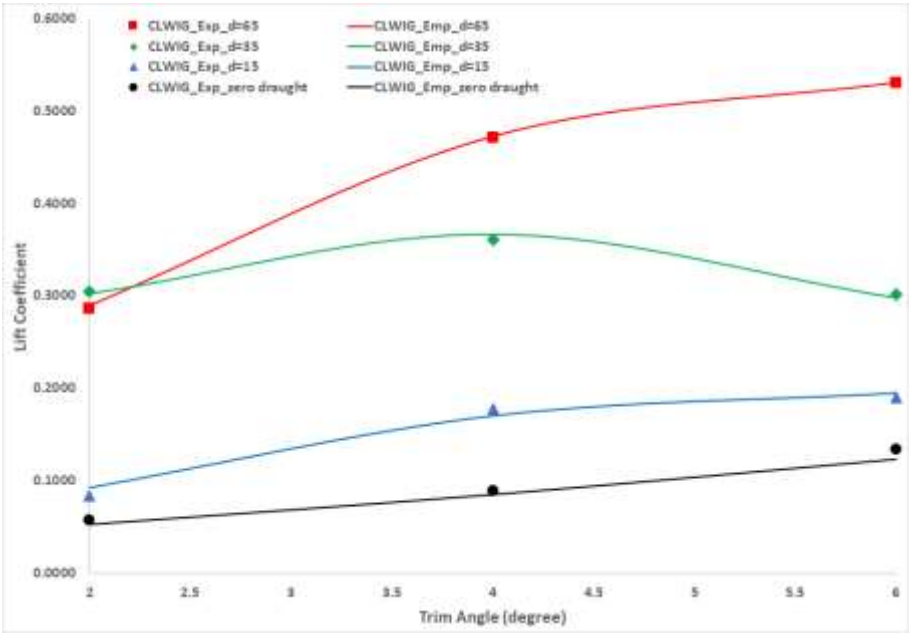

Figure 6.13 Dynamic lift curve of a water borne WIGcraft

Figure 6.13 also shows that the total dynamic lift increases nonlinearly with trim angle and draught. In other words, the total dynamic lift is seen to increase with decrease in the relative ground clearance height of the trailing edge of the wings. This suggests that the contribution of hydrodynamic lift and hull generated spray lift components to the total dynamic lift is much larger than the lift contribution from ground effect. As a result, for water borne WIGcraft operating at large draughts with water spray impinging on its wings, the effect of the wings' proximity to the free surface water may be regarded as secondary.

The percentage difference between the experimental and proposed empirical results are shown in Table 6.7.

Table 6.7 Comparison between $C_{LWIG}{}^{ma}$ *and* $C_{LWIG}{}^{eha}$

Draught (m)	Trim Angle (deg)	Difference (%)	Draught (m)	Trim Angle (deg)	Difference (%)
0.065	2	1.37	0.035	2	0.74
	4	0.18		4	1.64
	6	0.11		6	1.21
0.015	2	9.44	0	2	7.79
	4	3.88		4	4.52
	6	2.73		6	8.34

At the larger draught positions (0.065m and 0.035m), Table 6.7 shows that the percentage difference between the proposed semi-empirical model and measured results is below 2%. At 0.015m and zero draught (especially at the 2° trim angle), the proposed model shows a slightly higher percentage difference between the proposed model and the experimental lift data. This higher percentage difference suggests that the differences in results between the semi-empirical models (for the hydrodynamic lift, ground effect aerodynamic lift and the spray), and those derived from the experiments are transmitted to the proposed semi-empirical model for the coupled aero-hydrodynamic lift of the water borne WIGcraft.

It is also to be emphasized that equation 6.35 is composed of three lift force components. Therefore, the possibility that the good agreement between the proposed semi-empirical expression (equation 18) and the experimental data of the water borne WIGcraft model may have been aided by the cancellation of the differences between the lift components and their corresponding experimental data when the lift components are summed cannot be over-ruled.

Because the constants in the proposed semi-empirical expressions were derived from a limited test data, it can be stated that the proposed semi-empirical model tools developed in this section provide a good basis for predicting the hydrodynamic lift of multi-hull vessels, ground effects and hull-generated water spray effects on the aerodynamics of the WIGcraft model as well as the total lift of a water-borne WIGcraft pending further validation from a more extensive sets of test data on waterborne WIGcraft of various configuration and operational range.

6.10 Analysis of Drag Results and Formulation of Empirical Model for Total Drag

In this section, the drag results of the experiments are analysed alongside the formulation of a semi-empirical model to predict the drag on a waterborne WIGcraft with spray influence.

Similar form of coefficients for the measured force data used for the dynamic lift in the previous section will be implemented.

$$C_{D,i} = \frac{D_i}{0.5\rho_w U^2 {b_h}^2} \tag{6.36}$$

For the WIGcraft, it is shown in Figure 6.14b and d that the measured drag coefficient of the WIGcraft model is dependent on both the trim angle and ground clearance. The drag coefficient on the WIGcraft decreases as the clearance height is increased, while increasing the trim angle

causes a slight increment in drag. A hump drag is noticeable near the take-off position where there is a transition from hydrodynamic to aerodynamic drag forces.

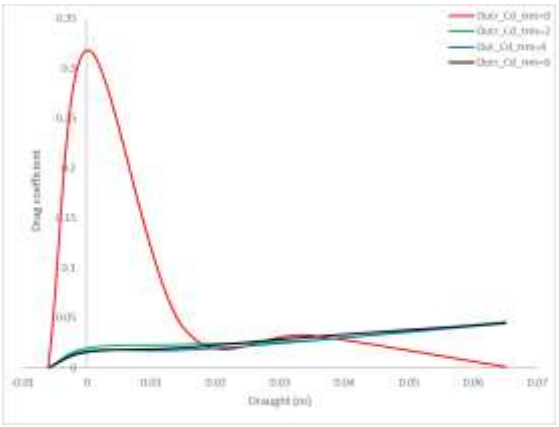

a. Trim angle effect on Outrigger model Drag

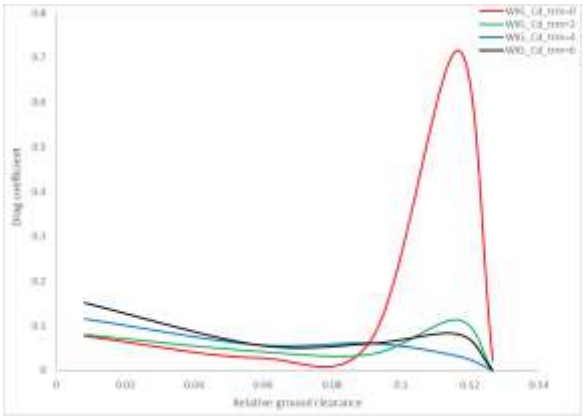

b. Trim angle effect on WIGcraft model Drag

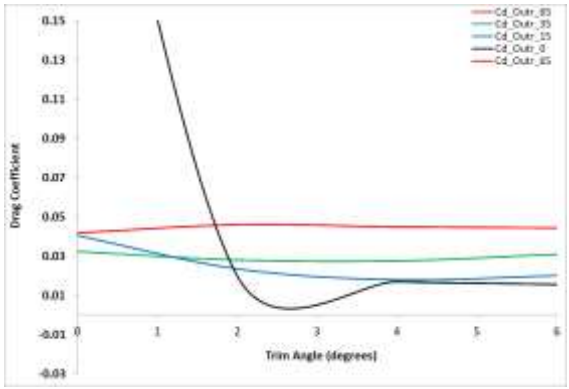

c. Draught effect on Outrigger model Drag

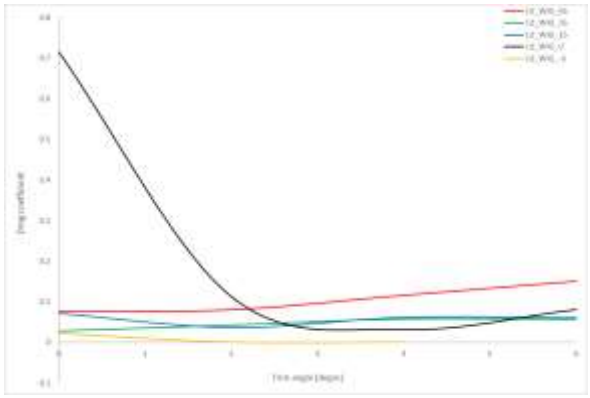

d. Draught effect on WIGcraft model Drag

Figure 6.14 Measured drag coefficient on the WIGcraft model

Figures 6.14 a and c, show the increase in drag with draught for the Outrigger model, howbeit, the drag is less dependent on trim angle beyond 2 degrees.

The total drag on the planing Outrigger model basically comprises of the whiskers spray drag, hydrodynamic pressure lift induced drag and viscous drag components acting on the pressure bottom area of the hull. Whereas the drag on the WIGcraft consists of ground effect aerodynamic lift induced drag, parasitic drag and hull generated water spray drag on wings components in addition to the Outrigger drag components earlier stated. These elemental components of the total drag on the models are discussed in the following subsections.

6.10.1 Drag components on Outrigger model

Empirical or statistical expressions for estimating the drag components of a planing monohulls are well established as discussed in Chapter 2 of this thesis. For the fully constrained Outrigger

model experiments in this study, the weight of the model is fully suspended by the carriage of the towing tank. As such, only the hydrodynamic pressure and viscous force components responsible for creating the hydrodynamic drag are measured.

a. Hydrodynamic pressure lift induced drag component, $C_{Dhydmod}{}^{eh}$

The component of the hydrodynamic lift induced drag created by the hydrodynamic pressure acting normal to the bottom of the hull(s) (see Figure 6.15), may simply be expressed mathematically and in coefficient form as,

$$C_{Dhydmod}{}^{eh} = \left(C_{Lhydmod}{}^{eh}\right)tan\tau \qquad (6.37)$$

Where $C_{Lhydmod}{}^{eh}$ is the hydrodynamic lift coefficient described in section 6.9.3,

b. Hydrodynamic viscous drag components

The viscous drag on the hull(s) is composed mainly of drag forces acting tangentially to the

- bottom of the hull(s),
- whiskers spray area shown in Figure 6.14 and
- all other spray wetted areas on the hull referred to as side wetting and neglected in Savitsky (1964) and Savitsky et al. (2007)

The viscous drag on the bottom of the hulls and the whiskers spray area have been rigorously investigated and described in Savitsky (1964) and Savitsky et al. (2007).

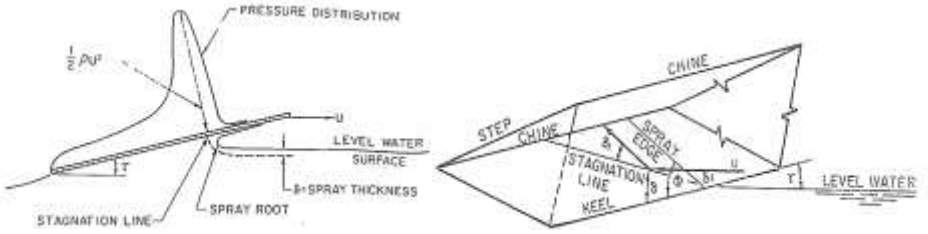

(a) Pressure distribution and flow directions on planing surface

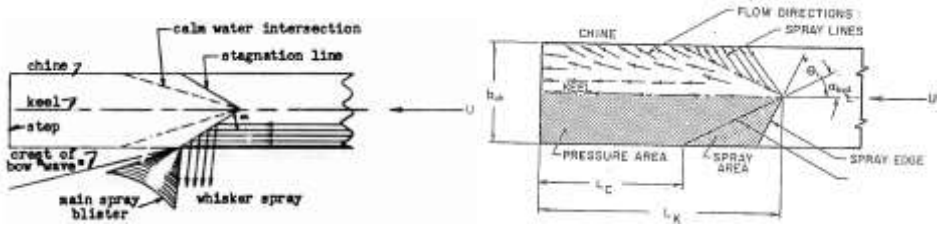

(b) view of planing hull bottom on plane parallel to keel

Figure 6.15 Flow direction along planing hull and extent of spray area

bi. Viscous drag components on hull bottom pressure area, ${C_{Dchv}}^{eh}$

The empirical formula for the component of the hydrodynamic viscous drag on the pressure bottom area of the hull(s) given in Savitsky (1964) may be expressed in coefficient form as

$$ {C_{Dchv}}^{eh} = \frac{{V_1}^2}{U^2}.\frac{\lambda C_{fpr}}{cos\beta cos\tau} \tag{6.38} $$

$C_{fpr} = C_{fp} + C_{fr}$

$C_{fr} = 0.0004$ friction coefficient accounting for hull planing surface roughness

C_{fp} =friction coefficient for pressure surface area, estimated from ITTC 1957 or Schoenherr turbulent friction coefficient defined for Reynolds number, $R_e = \frac{V_1 \lambda b_h}{\nu}$

ν is the kinematic viscosity of water.

V_1 is the average bottom velocity which is usually less than the forward velocity of the planing boat due to higher pressure at the planing bottom than free stream pressure. This higher pressure slows down the forward velocity at this bottom area. V_1 is estimated in Savitsky (1964) by using Bernoulli's principle between the free stream conditions and dynamic pressure conditions and may be expressed in alternative form as a function of the hydrodynamic lift coefficient,

$$ V_1 = U\sqrt{1 - \frac{{C_{Lhydmod}}^{eh}}{\lambda cos\tau}} \tag{6.39} $$

U is the boat speed (m/s)

bii. Whisker's spray drag components, ${C_{Dhs}}^{eh}$

The component of the whiskers spray drag coefficient ahead of the stagnation line may be estimated from Savitsky et al. (2007) expression for whiskers spray drag,

$$ {C_{Dhs}}^{eh} = \Delta\lambda_{hs} C_{fhsr} \tag{6.40} $$

Where

$C_{fhsr} = C_{fhs} + C_{fr} = \frac{D_{hs}}{0.5\rho_w U^2 \Delta\lambda_{hs} {b_h}^2}$

D_{hs} is total viscous force in the spray area.

$\Delta\lambda_{hs} {b_h}^2$ is the effective whisker spray area outside pressure hull bottom and may be determined from chart presented in Savitsky et al., (2007) or from the expression.

$$ \Delta\lambda_{hs} = \frac{cos\Theta}{4sin2\alpha_{hyd}cos\beta} = \frac{cos\left(\frac{\theta_s}{cos\beta}\right)}{4sin2\alpha_{hyd}cos\beta} = \frac{2\alpha_{hyd}}{cos\beta} \tag{6.41} $$

$$\alpha_{hyd} = tan^{-1}\frac{\pi tan\tau}{2tan\beta} \quad (6.42)$$

$$\Theta = \frac{\theta_s}{cos\beta} \quad (6.43)$$

$$\theta_s = 2\alpha_{hyd} \quad (6.44)$$

C_{fhs} is the viscous friction coefficient in spray area calculated following the method described in Savitsky et al. (2007).

$C_{fr} = 0.0004$ friction coefficient accounting for hull planing surface roughness

It should be noted that at high trim angles, a high-volume spray with forward velocity greater than the boat speed is possibly generated. According to Weinstein and Kapryan (1953), the portion of the wetted hull that experiences relative motion with the high-volume forward spray, appears to have a reversely directed relative velocity. In reality, especially for full scale boats, the viscosity of fluid (basically air/water mixture) will also differ owing to their different fluid densities and mixing proportions.

The Reynold number is thus different (possibly higher) from that on the hull bottom surface and pushing the flow towards turbulent regime. As such, the friction force component on this portion of the boat increases. The friction force is however, likely acting in the forward direction of the boat motion, thereby reducing the overall viscous drag acting against the forward motion of the boat.

The viscous friction resistance coefficient C_{fs} of the whiskers spray area may be calculated from the following approximate formula given in Savitsky et al. (2007):

Blasius skin friction formular for laminar flow, $R_{es} < 1.5 \times 10^6$ for models.

$$C_{fs} = \frac{1.328}{\sqrt{R_{es}}} \quad (6.45a)$$

Prandtl-Schlichting skin friction line for transitional flow. $1.5 \times 10^6 \leq R_{es} \leq 1.5 \times 10^7$ for models.

$$C_{fs} = \frac{0.074}{\sqrt[5]{R_{es}}} - \frac{4800}{R_{es}} \quad (6.45b)$$

Schoenherr friction correlation (ATTC) line for full-scale boat

$$\frac{0.242}{\sqrt{C_{fs}}} = log_{10}(R_{es}C_{fs}) \quad (6.45c)$$

Or 1957 ITTC

$$C_{fs} = \frac{0.075}{[log_{10}R_{es} - 2]^2} \quad (6.45d)$$

Where,

$R_{es} = \frac{V_0 L_{ws}}{\nu}$

V_0 is the whisker spray velocity,

Kinematic viscosity $\nu = \frac{\mu}{\rho_w} = 1\ centistoke\ (1 \times 10^{-6}\ m^2/s)$

For 50% air to water flow over the wing or hull surfaces, Pavlov (2020) suggested that the fluid ρ_w, density may be reduced to 0.5 when calculating the Reynolds number and spray drag.

Critical Reynolds number which indicates the transition from laminar to turbulent flow in the whisker spray area has a range: $3 \times 10^5 < R_{es\_cri} < 3 \times 10^6$ for model tests.

For full scale boat motion where $R_{es} > 1.5 \times 10^7$, V_1 is used as the velocity in the Reynold number.

$l_{ws} =$ Characteristic length of whiskers spray calculated as half the length of the forward spray edge in the plane of the hull bottom i.e.

$$l_{ws} = \frac{1}{2} \times \frac{b_h/2}{sin2\alpha cos\beta} \tag{6.46}$$

The total drag on the Outrigger model may thus be approximated as

$$C_{DOutrg}{}^{eh} = C_{Dhyd}{}^{eh} + C_{Dchv}{}^{eh} + C_{Dhs}{}^{eh} \tag{6.47}$$

Figure 6.16 compares the calculated and measured drag coefficient of the Outrigger model. The Figure shows a good correlation between the experimental results and the results predicted by the semi-empirical expression for the Outrigger model. In almost all the draught cases considered, the trim angle has a minimal effect on the drag characteristics of planing hull.

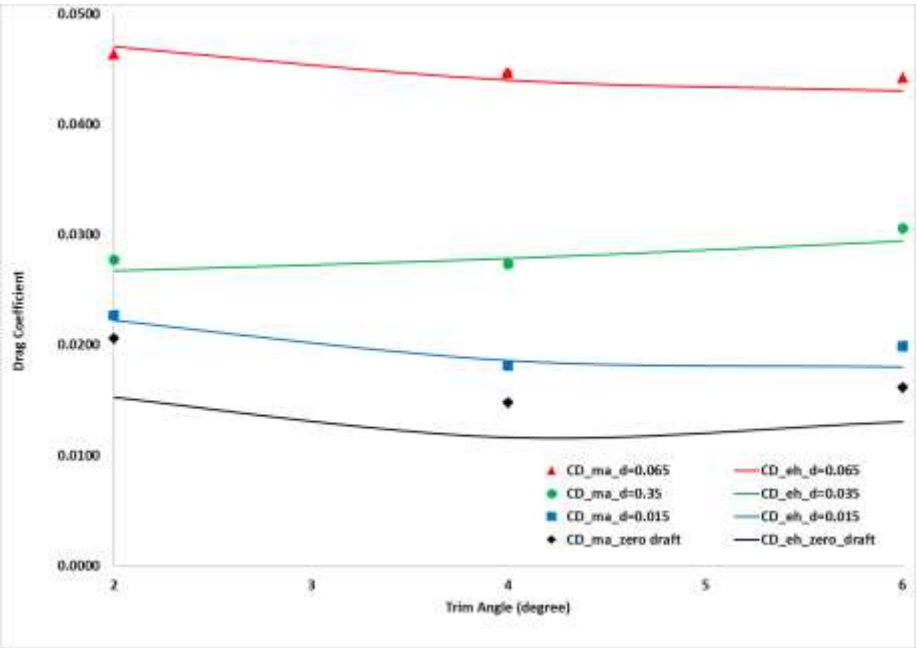

Figure 6.16 Calculated drag vs measured drag on Outrigger model

In Table 6.8, The empirical expression for the drag on the Outrigger model is compared to of the experimental data. Except for the zero draught conditions, the percentage difference between the results of the semi-empirical expression and that of the experiments are generally below 5% at all draught and trim angle conditions.

Table 6.8 Comparison between $C_{DOutrg}{}^{ma}$ *and* $C_{DOutrg}{}^{eh}$

Draught (m)	Trim Angle (deg)	Difference (%)	Draught (m)	Trim Angle (deg)	Difference (%)
0.065	2	1.44	0.035	2	3.67
	4	1.55		4	1.84
	6	2.78		6	3.90
0.015	2	2.04	0	2	26.11
	4	2.51		4	21.63
	6	9.43		6	17.53

The low uncertainty values at these draught conditions suggests the reliability of the experimental data and gives a measure of validity for the results obtained by implementing the Savitsky (1964) and Savitsky et al. (1997) semi-empirical drag models to estimate the drag on the Outrigger model.

The higher percentage difference between model and experimental results noted at the zero draught conditions appears to be commensurate with the experimental uncertainties associated with the drag measurement at the zero draught conditions (see Table A3 in the appendix). As a

result, the higher percentage difference between the model and experimental results may be attributed to experimental errors mainly from the data acquisition system.

6.10.2 Ground effects (due to wings near free surface) on aerodynamic drag

The induced drag is as a result of the downwash induced vortices shed from the trailing edge of the wing. The induced drag is thus generated alongside lift. Because of this, the drag coefficient increases with lift coefficient, $C_{Lff} = \frac{2\pi R_A}{R_A+3}\alpha_{eff}$ in free flight (see equation 6.26). Consequently, the induced drag increases with the aerodynamic load factor.

Similar to the hydrodynamic lift induced drag on a planing hull bottom, the aerodynamic lift induced drag may also be given as

$$C_{Dff}{}^{ea} = C_{Lff}\tan(\alpha_{eff}) \tag{6.48a}$$

and for small angle approximation,

$$C_{Dff}{}^{ea} \cong \alpha_{eff} C_{Lff} \tag{6.48b}$$

According to classical wing theory, the induced drag coefficient of a wing with elliptical lift distribution in free flight is given by,

$$C_{Dff}{}^{ea} = K_{id}\left(C_{Lff}\right)^2 \tag{6.48c}$$

Equation 6.48c generally considers high aspect ratio wings about which air mainly flows in the longitudinal (chordwise) direction. As a result, the wings generate higher amount of aerodynamic lift. For low aspect ratio dihedral wing in ground effect, the airflow about the wings is more complicated. While the presence of the ground increases the aerodynamic pressure lift on the lower portion of the wings, the flow consisting of longitudinal, transverse and vertical flow components reduces the aerodynamic lift over the wings, and the lift distribution become non-elliptical. Hence, for a normal low aspect ratio dihedral wing in ground effect, the lift induced drag can be expressed in the form,

$$C_{Dff}{}^{ea} = K_{id}\left(C_{Lage}{}^{ea}\right)^{1.2} \tag{6.48d}$$

K_{id} is a proportionality factor regarded as the drag-due-to-lift factor and may be estimated from,

$$K_{id} = \frac{\alpha_{eff}}{C_{Lff}} \tag{6.49a}$$

Using the Oswald span efficiency method to account for the non-elliptical lift distribution on the low aspect ratio wings, K_{id} may be approximated as

$$K_{id} = \frac{1}{e\pi(R_A+3)} \tag{6.49b}$$

By comparing equations 6.49a and 6.49b, an approximate Oswald efficiency factor may be estimated as

$$e = \frac{C_{Lff}}{\pi(R_A+3)\alpha_{eff}} = \frac{2}{R_A} \tag{6.50}$$

Related Oswald efficiency factor proposed by other researchers include,

$e = 1.78\left(1 - 0.045{R_A}^{0.68}\right) - 0.64$ For straight wing

$e = 4.61\left(1 - 0.045{R_A}^{0.68}\right)(cos\Lambda_{LE})^{0.15} - 3.1$ For Swept wing

Generally, $0.7 < e < 0.85$ and swept angle Λ_{LE} of the wing at chord location where airfoil is thickest should be $\Lambda_{LE} > 30deg$.

e = 1 for elliptical wing as suggested by Maali Amiri (2015)

As the geometric aspect ratio of wing planform, R_A increases, the downwash speed, induced angle of attack and induced drag decreases. Hence, except there is a counteracting measure to reduce the induced drag, a relatively low aspect ratio wing is expected to have higher induced drag compared to a wing with higher aspect ratio. In the presence of ground effect, when the wing is moving close to the water surface, the downwash induced vortices interact with the water surface, thereby reducing the strength of the downwash and consequently lowering the induced drag.

Various empirical formulations for ground effect lift induced drag have been proposed by researchers such as Hubin (1992); Mantle (2016); Raymer (2006); Suh and Ostowari (1988); von Mises (1959) and Wieselsberger (1922). According to Wieselsberger (1922), the reduction in the free flight induced drag caused by the nearness of the wings to the ground or free surface may be expressed as

$${\Delta C_{Dige}}^{ea} = \frac{1-1.32\left(\frac{h_{te}}{b_a}\right)}{1.05+7.4\left(\frac{h_{te}}{b_a}\right)} \tag{6.51a}$$

More recently, Raymer (2006) expressed this ground influence coefficient as

$$\Delta {C_{Dige}}^{ea} = \frac{K_{ge}\left(\frac{h_{te}}{b_a}\right)^{1.5}}{1+\left(K_{ge}\frac{h_{te}}{b_a}\right)^{1.5}} \tag{6.51b}$$

Where, K_{ge} is a constant whose value equals 33.

An alternative ground influence factor implemented in this thesis is,

$$\Delta {C_{Dige}}^{ea} = 0.5 + \frac{K_{ge}\left(\frac{h_{te}}{b_a}\right)^{1.5}}{1+\left(K_{ge}\frac{h_{te}}{b_a}\right)^{1.5}} \tag{6.51c}$$

Where, K_{ge} is a factor that depends on the aspect ratio and relative ground clearance height of the wings. ground influence factor

Following from equations 6.48 to 6.51, the aerodynamic lift induced drag of an airborne WIGcraft becomes,

$${C_{Dige}}^{ea} = K_{id}\left(1 - \Delta {C_{Dige}}^{ea}\right)\left({C_{Lage}}^{ea}\right)^{1.2} \tag{6.52a}$$

By multiplying equation 6.52a by the equivalent hydrodynamic lift coefficient transformation factor, $\frac{{x_{ah}}^2}{R_A} = \frac{{b_a}^2}{{b_h}^2}\frac{\Upsilon}{R_A}$ in section 6.9.1, the aerodynamic lift induced drag on the water spray unaffected aerodynamic surfaces of a waterborne WIGcraft due to ground effect may be approximated as,

$${C_{Dige}}^{eha} = K_{id}\frac{{b_a}^2}{{b_h}^2}\frac{\Upsilon}{R_A}\left(1 - \Delta {C_{Dige}}^{ea}\right)\left({C_{Lage}}^{ea}\right)^{1.2} \tag{6.52b}$$

Based on the small angle approximation principle used in deriving Equation 6.52, the equation is valid for angle of attack or trim angle less than 10°.

Superscript eha denotes empirical hydrodynamic equivalent of the empirical aerodynamic drag component of equation 6.52a.

6.10.3 Parasitic drag

The viscous parasitic (zero lift) drag D_{P0A} for subsonic motion is majorly the sum of skin friction and the smaller value form drag (which gives the pressure drag due to viscous flow separation). The pressure drag is usually expressed as a percentage of the skin friction drag. Thus, the equivalent skin friction coefficient may be considered as the friction coefficient together with pressure drag expressed as percentage of the skin friction drag.

Lifting line and panel methods generally do not include viscous effect when used to estimate the parasitic drag. As a result, they tend to indicate linear relationship between angle of attack and lift. The parasitic drag is almost generally a parabolic function of the angle of attack. The value of the parasitic drag coefficient ${C_{Dpoa}}^{ma}$ may be deduced from experiments as the lowest point of the drag polar curve or it may be estimated by using the component build-up method or a rapid drag estimation method.

An approximate formula for preliminary determination of the parasitic drag on an airborne WIGcraft in Raymer (2006) may be given as

$${C_{Dpoa}}^{ea} = \frac{S_{wet} C_{fe}}{S_a} \tag{6.53a}$$

S_a is the reference wing area,

S_{wet} is the wetted area of the wing,

C_{fe} is determined from the look-up table in appendix B.

The hydrodynamic equivalent of ${C_{Dpoa}}^{ea}$ for a waterborne WIGcraft may be given as

$${C_{Dpoa}}^{eha} = \frac{{x_{ah}}^2}{R_A} {C_{Dpoa}}^{ea} \tag{6.53b}$$

Note:

$${D_{poa}}^{ea} = 0.5\rho_a S_a U^2 {C_{Dpoa}}^{ma} = 0.5\rho_w {b_h}^2 U^2 {C_{Dpoa}}^{eha} \tag{6.54}$$

6.10.4 Drag characteristics of wings near free surface water

This subsection examines the drag characteristics of an airborne WIGcraft near free surface water. The measured drag on the aerodynamic surfaces of the airborne WIGcraft near the free surface, consisting of the induced and parasitic drag and may be expressed as,

$${C_{Dage}}^{ma} = \frac{{D_{age}}^{ma}}{0.5\rho_a S_a U^2} \tag{6.55a}$$

Valid for airborne WIGcraft.

The hydrodynamic equivalent drag on the aerodynamic surface of the waterborne WIGcraft was determined to be,

$${C_{Dage}}^{ema} = \frac{{x_{ah}}^2}{R_A} {C_{Dage}}^{ma} = \frac{{D_{age}}^{ema}}{0.5\rho_w {b_h}^2 U^2} \tag{6.55b}$$

Applicable to waterborne WIGcraft when draught ≥ 0 and water spray does not impinge on its wings. Recall that, $\frac{{x_{ah}}^2}{R_A} = \frac{{b_a}^2}{{b_h}^2}\frac{\Upsilon}{R_A}$

${D_{age}}^{ema}$ is the measured drag of the WIGcraft model less the measured drag of the Outrigger model under operating conditions where there are no hull generated water spray impinging on its wings.

Generally, the ground effect induced drag on the airborne WIGcraft may be given as

$${C_{Dige}}^{ma} = \frac{{D_{ige}}^{ma}}{0.5\rho_a S_a U^2} \tag{6.56a}$$

However, it is not straightforward to experimentally measure the induced drag ${D_{ige}}^{ma}$ in isolation from the parasitic drag. The hydrodynamic equivalent of ${C_{Dige}}^{ma}$ may be expressed as,

$${C_{Dige}}^{ema} = \frac{{x_{ah}}^2}{R_A}{C_{Dige}}^{ma} = \frac{{D_{ige}}^{ma}}{0.5\rho_w {b_h}^2 U^2} \tag{6.56b}$$

Note:

$${D_{ige}}^{ma} = 0.5\rho_a S_a U^2 {C_{Dige}}^{ma} = 0.5\rho_w {b_h}^2 U^2 {C_{Dige}}^{ema} \tag{6.57}$$

Superscripts ma and ema are the measured aerodynamic lift induced drag on the aerodynamic surfaces and its equivalent hydrodynamic induced drag respectively.

The empirical expression for the drag coefficient on the airborne WIGcraft may be given as

$${C_{Dage}}^{ea} = {C_{Dige}}^{ea} + {C_{Dpoa}}^{ea} \tag{6.58a}$$

The hydrodynamic equivalent of ${C_{Dage}}^{ea}$ (the aerodynamic drag component) for the water borne WIGcraft without water spray drag may be approximated by

$${C_{Dage}}^{eha} = \frac{{x_{ah}}^2}{R_A}{C_{Dage}}^{ea} \tag{6.58b}$$

Valid for waterborne WIGcraft when draught ≥ 0 and water spray does not impinge on its wings.

As in the case of pure ground effect aerodynamic lift discussed earlier in section 6.9.4 of this Chapter, to isolate the drag due to the wing being nearer the ground (free surface water in this case) from the water spray drag on the wings, only experimental test cases where hull-generated water spray does not impinge on the wings of the WIGcraft are considered. These cases are

when the WIGcraft model is towed at zero draught and when the keel of the WIGcraft model is above the water surface by 6mm.

The lower part of Table 6.9 below shows the correlation between the results of the proposed empirical expression for the drag coefficient $C_{Dage}{}^{ea}$ and the measured drag coefficient $C_{Dage}{}^{ma}$ when the WIGcraft model is 6mm (h/c = 0.124) above the free surface water. The percentage differences between the results of the experiments and the proposed induced drag equation are in an order slightly above 10%. The table also shows similar magnitude of percentage differences between $C_{Dage}{}^{eha}$ and $C_{Dage}{}^{ma}$ when the WIGcraft model is at zero draught (h/c = 0.114). Since the proposed equation is dependent on the ground effect aerodynamic lift, $C_{Lage}{}^{ea}$, the relatively higher percentage differences may be partly attributed to the accumulation of errors transmitted from the computation of $C_{Lage}{}^{ea}$. Secondly, the uncertainties associated with the measured drag are relatively high for all trim angles at this draught position. From the uncertainty data for drag in Table A3, it is to be emphasized that the uncertainty associated with the measured data are higher and less reliable than that of the measured lift data.

Table 6.9 Drag coefficient of model WIGcraft due to pure ground effect.

Relative ground clearance height	Trim Angle (degrees)	K_{ge}	$\boldsymbol{C_{Dage}{}^{ema}}$	$\boldsymbol{C_{Dage}{}^{ema}}$	$\boldsymbol{C_{Dage}{}^{eha}}$	Difference (%)
0.114	0	24	2.417	0.026	Undefined	n.a
	2		1.556	0.016	0.019	15.19
	4		1.975	0.021	0.020	5.78
	6		4.000	0.043	0.025	43.74
0.124	0	13.5	n.a	$\boldsymbol{C_{Dage}{}^{ma}}$ 0.0164	$\boldsymbol{C_{Dage}{}^{ea}}$ Undefined	n.a
	2		n.a	0.0615	0.0549	10.61
	4		n.a	0.0855	0.0929	8.76

It is seen in Table 6.9, that the ground influence factor K_{ge}, varies with the relative ground clearance.

To further verify the validity of the empirical equation for ground effect drag of the air borne WIGcraft, equation 6.58a was applied to the experimental lift data of an anhedral trapezoidal wings from Fink and Lastinger (1961). Figure 6.17 compares the experimental lift data from Fink and Lastinger (1961) with the proposed empirical equation for two different aspect ratios

($R_A = 1, 2$) and relative clearance heights ($\frac{h_{te}}{c} = 0.042, 0.083, 0.167$) while Table 6.10 shows the percentage difference between their results. The Figure shows good correlation between the proposed semi-empirical expression and the measured results, especially at angles where the small angle approximation is valid (i.e., at AoA ≤10°)

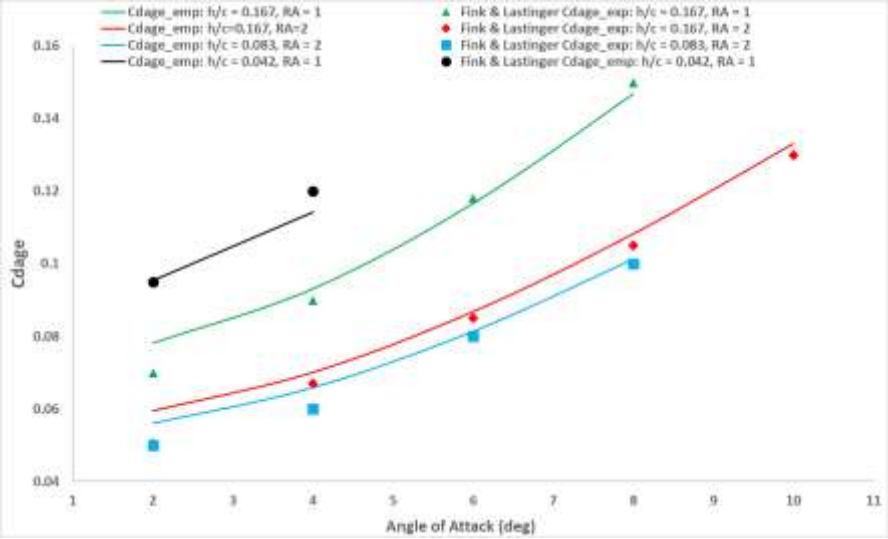

Figure 6.17 Comparison between Fink and Lastinger (1961) drag data and proposed empirical aerodynamic lift coefficients.

K_{ge} is a factor that depends on the aspect ratio and relative ground clearance height of the wings.

In both Tables 6.9 and 6.10, a clear pattern of K_{ge} with respect to the angle of attack and the relative ground clearance height of the wings trailing edge can be deduced from the Tables. The ground influence factor K_{ge}, is seen to be more strongly dependent on the relative ground clearance than it is on aspect ratio. A mathematical expression to fully describe this and other characteristics of K_{ge} is yet to be completed as at the time writing this thesis.

Table 6.10 Disparity in ground effect drag coefficient between Fink and Lastinger (1961) and the proposed empirical equation.

R. ground clearance height	Aspect Ratio	K_{ge}	Angle of Attack (deg)	Difference (%)	R. ground clearance height	Aspect Ratio	K_{ge}	Angle of Attack (deg)	Difference (%)
0.167	1	4.3	2	11.72	0.167	2	7	2	17.86
			4	3.53				4	4.72
			6	1.13				6	2.18
			8	2.13				8	3.12
			10	11.72				-	
0.043	1	72	2	0.32	0.083	2	25	2	12.14
			4	4.80				4	9.86
								6	1.69
								8	1.16

Nevertheless, it is to be stated that for flight dynamics purpose, the value of K_{ge} appears to be a multiple of the relative ground clearance. A higher value of K_{ge} is required to account for the increase in ground effect as the trailing edge of the wings of the WIGcraft approaches the ground. On the other hand, for WIGcraft design and performance prediction purposes, at a given relative ground clearance, the value of K_{ge} appears to be proportional to nearly twice the aspect ratio of the wings.

6.10.5 Hull-generated spray drag on wings

The measured drag of the waterborne WIGcraft less the drag generated by the Outrigger hull and the wing at equal ground clearance, gives a quantitative value of the spray drag factor for the waterborne WIGcraft. i.e.,

$$C_{Dsp}{}^{ma} = C_{DWIG}{}^{ma} - \left(C_{DOutrg}{}^{ma} + C_{Dage}{}^{eha}\right) \tag{6.59}$$

Where

$$C_{DWIG}{}^{ma} = \frac{D_{WIG}{}^{ma}}{0.5\rho_w U^2 {b_h}^2} \tag{6.60}$$

$$C_{DOutrg}{}^{ma} = \frac{D_{Outr}{}^{ma}}{0.5\rho_w U^2 {b_h}^2} \tag{6.61}$$

$C_{DWIG}{}^{ma}$ is the drag coefficient deduced from the measured drag on the waterborne WIGcraft model,

${C_{DOutr}}^{ma}$ is the drag coefficient deduced from the measured drag on the Outrigger model,

b_h is the beam of the WIGcraft hull at the operating draught,

The drag on the wings wetted by hull generated water spray on one hand may be considered to be analogous to spray drag on parts of the hull(s) wetted by hull generated spray described in detail in section 6.10.1. On the other, by replacing air with water spray, the drag on the wings wetted by hull generated water spray may be considered analogous to the wings subjected to water spray lift induced drag and water spray parasitic drag. In essence, the hull generated water spray consists of spray lift induced drag and water spray viscous drag components, i.e.,

$$ {C_{Dsp}}^{eha} = {C_{Dspi}}^{eha} + {C_{Dspv}}^{eha} \tag{6.62}$$

Following from equations 6.32 and 6.48b, the water spray lift induced drag is given as

$$ {C_{Dspi}}^{eha} \cong \alpha_{eff} {C_{Lsp}}^{eha} \tag{6.63}$$

Following from the concept of effective wetted area in Savitsky et al. (2007), the water spray viscous drag on the wings of the WIGcraft model may be approximated by the proposed empirical expression in a form similar to equation 6.40,

$$ {C_{Dspv}}^{ea} = \Delta R_{AS} {C_{fasr}}^{ea} \tag{6.64}$$

Where,

$$ {C_{fasr}}^{ea} = C_{fas} + C_{fr} \tag{6.65}$$

$$ {D_{WS}}^{ea} = 0.5 \rho_w {U_0}^2 \Delta R_{AS} {b_{aw}}^2 {C_{fasr}}^{ea} \tag{6.66}$$

ρ_w is reduced by 50% as earlier discussed in section 6.10.1 when calculating the Reynolds number and spray drag on wetted hulls.

U_0 is the velocity of the water spray over the wing, which is approximately equal to that over the hull surface as suggested in Savitsky et al. (2007).

C_{fasr} which consists of C_{fas} and C_{fr} may be estimated in similar manner as the whisker's spray drag in equation 6.40. However, the characteristic length is taken as the forward spray edge on the surface of the wing.

D_{WS} is total viscous force on the water spray area of the wings,

b_{aw} is the fraction of the span of the wing wetted by hull generated water spray,

$\Delta R_{AS} = f(\tau, \beta, f_{nB}, d/h_{te})$ is an experimentally determined spray quantity which accounts for the spray geometry, trajectory, wing location and other geometric considerations of the hull and wing.

$\Delta R_{AS} {b_{aw}}^2$ is the effective water spray wetted area on the wing. In this thesis, $\Delta R_{AS} {b_{aw}}^2$ can be estimated by using the approach suggested in ITTC (2017) for dynamic wetted surface area, in which the hull generated water spray wetted aerodynamic and hull surface areas of the physical model were estimated from the 3D CAD model in conjunction with above water photographs and video footages taken from each experimental run of the model.

The viscous drag coefficient of the water spray on wing may be expressed in the equivalent hydrodynamic terms as,

$$ {C_{fasr}}^{eha} = \frac{{D_{WS}}^{ea}}{0.5\rho_w U^2 {b_h}^2} \tag{6.67} $$

Figure 6.18 compares the results of semi-empirical expression (equation 6.62) for spray drag and that derived from the measured drag coefficient of the waterborne WIGcraft model (equation 6.59).

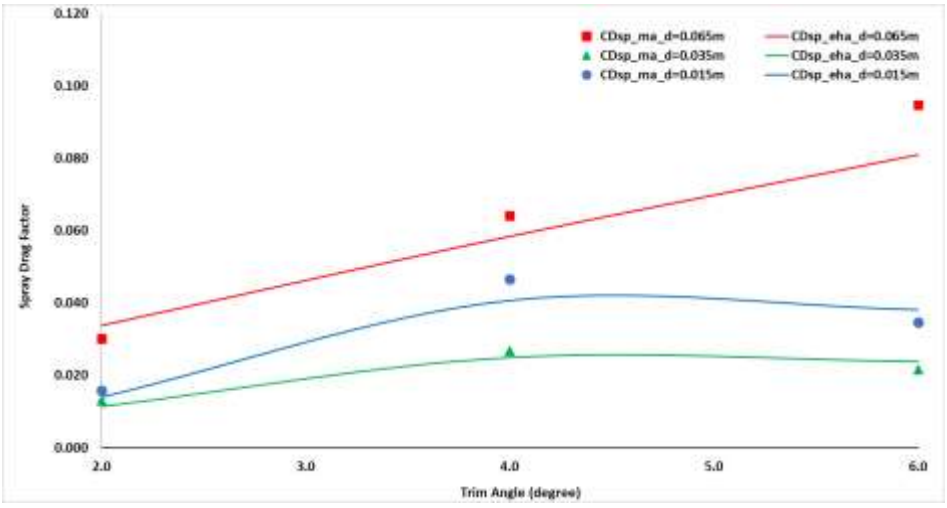

Figure 6.18 Spray drag on wings of WIGcraft model

The proposed semi-empirical expression generally underpredicts the spray drag coefficients at higher draughts where both the main hull and sponsons generate water spray that impinges on the wings. Nevertheless, results from the proposed semi-empirical expression show similar trend as the spray drag coefficient deduced from the measured drag on the wings. The disparity between the results is more or less than 10% as shown in Table 6.11. The discrepancies between

the results may be associated with the estimation of $\Delta R_{AS} {b_{aw}}^2$, where certain areas not wetted by solid water is unaccounted for. As noted in the ITTC (2017) recommended procedure. As stated in the ITTC report, the flow in the spray region is very complex and no known alternative practices are available.

Table 6.11 Comparison between ${C_{Dsp}}^{ma}$ and ${C_{Dsp}}^{eha}$

Draught (m)	Trim Angle (deg)	Difference (%)	Draught (m)	Trim Angle (deg)	Difference (%)
0.065	2	10.76	0.035	2	13.92
	4	9.72		4	7.50
	6	17.12		6	9.36
0.015	2	13.10	0	2	n.a
	4	14.54		4	n.a
	6	9.01		6	n.a

During the conduct of the experiments, no hull generated water spray impinged on the wings at zero draught for all the speed and trim angle range considered. Figure 6.18 shows that the spray drag increases with drag and trim angles. However, like the spray lift coefficient earlier described, it is noticed that there is a maximum limit of spray drag increment with trim angle before it begins to decrease. This characteristic of both the spray lift and drag coefficient reflects the characteristics of the high energy water spray volume with respect to trim angle (Morabito, 2010). As the trim angle is raised beyond a certain limit, parts of the hull(s) with lower deadrise angle impacts the free surface water, which reduces the spray volume of solid water impacting on the wings, and consequently reduces the spray drag on the wings. The proposed empirical model (equation 6.62) which is applicable for spray drag estimation irrespective of the WIGcraft configuration, however, was able to capture the nonlinear spray drag effects with respect to the attitude of the wings. This nonlinear relationship of the spray drag with the attitude of the vehicle is more noticeable at larger draught positions (i.e., at 0.065m and 0.035m draughts).

6.10.6 Drag characteristics of water spray influenced wings near free surface water

As in the case of the dynamic lift, the measured drag on the wings may be examined by computing the difference between the measured drag coefficients of the WIGcraft and the Outrigger model configurations.

$$C_{Dwing}{}^{ma} = C_{DWIG}{}^{ma} - C_{DOutrg}{}^{ma} \quad (6.68)$$

The drag on the wings of a waterborne WIGcraft subjected to hull-generated spray may be empirically estimated by

$$C_{Dwing}{}^{eha} = C_{Dage}{}^{eha} + C_{Dsp}{}^{eha} \quad (6.69)$$

Figure 6.19 compares the drag coefficient of the wings estimated from equations 6.68 and 6.69. Similar trend to Figure 6.18 is noticeable. However, from Table 6.12, it can be deduced that the percentage difference between the results of the proposed semi-empirical model for the drag on the wings and those derived from the experiments is relatively much larger (especially at zero draught) than the percentage difference in the other drag components calculated in this thesis. Besides the large experimental errors calculated for the drag coefficient at the zero-draught position (see table A3 of appendix A), this increase in difference between the results of the proposed model and that deduced from the experiments may be attributed to the accumulation of errors from both the spray drag and ground effect aerodynamic ground calculated using the semi-empirical equations, 6.62 and 6.58b.

Table 6.12 Comparison between $C_{Dwing}{}^{ma}$ and $C_{Dwing}{}^{eha}$

Draught (m)	Trim Angle (deg)	Difference (%)	Draught (m)	Trim Angle (deg)	Difference (%)
0.065	2	10.74	0.035	2	10.52
	4	7.97		4	6.13
	6	13.03		6	12.33
0.015	2	2.05	0	2	15.19
	4	11.75		4	5.78
	6	8.66		6	43.74

Comparison between Tables 6.9, 6.11 and 6.12 suggests that the spray drag on the wings is the major contributor to the total drag on the wing subjected to ground and water spray effects, and the near identical characteristics between Figures 6.18 and 6.19, similarly suggests the spray drag is the major contributor to the total drag on wings subjected to both hull generated water spray and ground effects. In other words, the aerodynamic induced drag and parasitic drag components contributes minimally to the total drag on the wings of the waterborne WIGcraft subjected to water spray effect. Figure 2.1 gives a pictorial view of the significance of hull-generated water spray on the wings and fuselage of the WIGcraft model tested in this study.

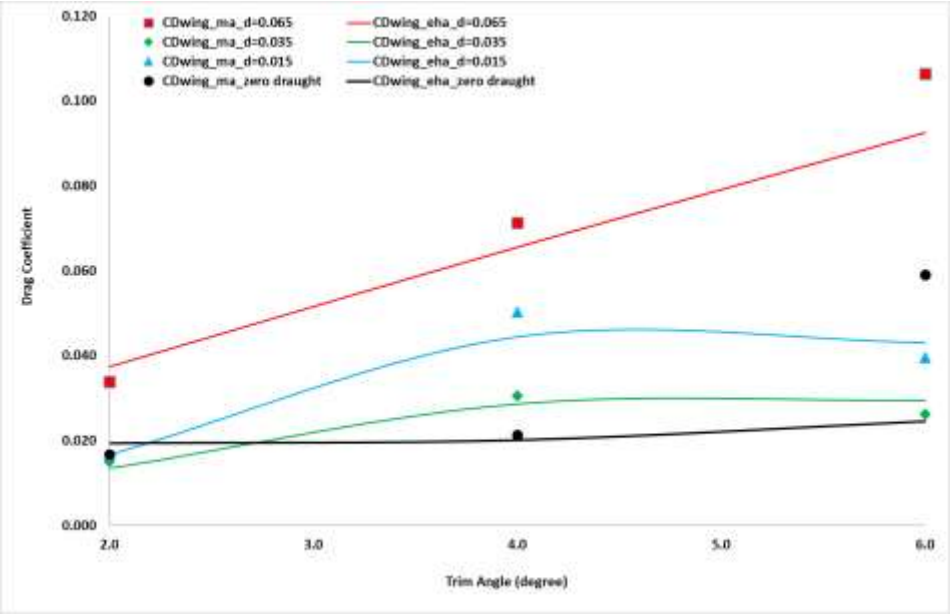

Figure 6.19 Measured ($C_{Dwing}{}^{ema}$) and calculated drag coefficients ($C_{Dwing}{}^{eha}$) on wings

From a preliminary design perspective, the dynamic efficiency of the model may be improved by locating the wings above the hull-generated spray apex. Hull generated spray trajectory can be estimated using the 2.5D numerical hydrodynamic model developed in chapter 3 of this thesis.

6.10.7 Total drag on the waterborne WIGcraft

The total drag on the water borne WIGcraft is composed of the drag components of the hull(s) (including the hydrodynamic lift induced drag, the hydrodynamic viscous drag and the whiskers viscous spray drag) and the drag components of the wings (including the aerodynamic lift induced drag due to ground effect, spray drag on the wings and the parasitic drag components). By combining these drag components already derived and described in this section of this thesis, the total drag on the waterborne WIGcraft may be approximated by simply summing equations 6.47 and 6.69,

$$C_{DWIG}{}^{eha} = C_{DOutrg}{}^{eha} + C_{Dwing}{}^{eha} \tag{6.70}$$

To examine if the formulated empirical model for estimating the total drag on a waterborne WIGcraft is satisfactory, the empirical equation 6.70 (i.e., $C_{DWIG}{}^{eha}$) is plotted against the drag coefficient ($C_{DWIG}{}^{ma}$) derived from the measured drag on the waterborne WIGcraft at various draught (see Figure 6.20).

The empirical model underpredicts the total drag on the water borne WIGcraft as can be seen in Figure 6.20. the model, however, is seen to capture the nonlinear behaviour of the WIGcraft drag characteristics and generally agrees with results of the experiments.

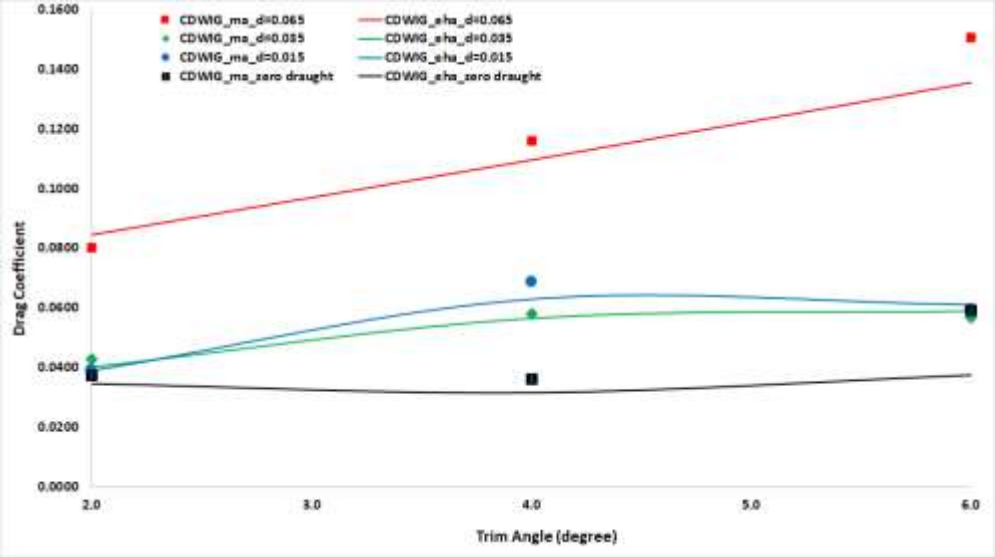

Figure 6.20 Measured WIGcraft model drag vs Empirical model drag

Except for the zero-draught condition, the discrepancies between the proposed semi-empirical expression and the experimental data are generally below 10% as shown in Table 6.13.

Table 6.13 Comparison between $C_{DWIG}{}^{eha}$ *and* $C_{DWIG}{}^{eha}$

Draught (m)	Trim Angle (deg)	Difference (%)	Draught (m)	Trim Angle (deg)	Difference (%)
0.065	2	5.36	0.035	2	6.08
	4	5.49		4	2.36
	6	10.01		6	3.59
0.015	2	0.33	0	2	7.59
	4	7.97		4	12.28
	6	2.62		6	36.83

The discrepancies between the results are mainly due to accumulation of errors from the drag components constituting the total drag on the waterborne WIGcraft. By comparing the almost identical characteristics of Figures 6.18, 6.19 and 6.20, it can be deduced that the spray drag is a major factor to consider when estimating the total drag on the water borne WIGcraft.

6.11 Maximum Dynamic Efficiency (*MED*)

Examination of Figure 6.21a reveals that the maximum dynamic efficiency is dependent on both trim angle and draught. As common with most planing hull forms, Figure 6.21a shows that the Outrigger model is generally inefficient when operating at larger draught. Related reasons for this occurrence are extensively discussed in Savitsky (2003). This inefficiency may be minimized by operating the Outrigger model at lower trim angle. Near the zero draught positions, the Outrigger model is most efficient when operating at higher trim angle. This result is consistent with the characteristics of most planing hullforms which must overcome hump drag as it changes attitude, and its centre of gravity is raised to near zero draught by dynamic lift. The increase in dynamic efficiency with trim angle is also consistent with typical planing hulls (Savitsky, 1964, 2003).

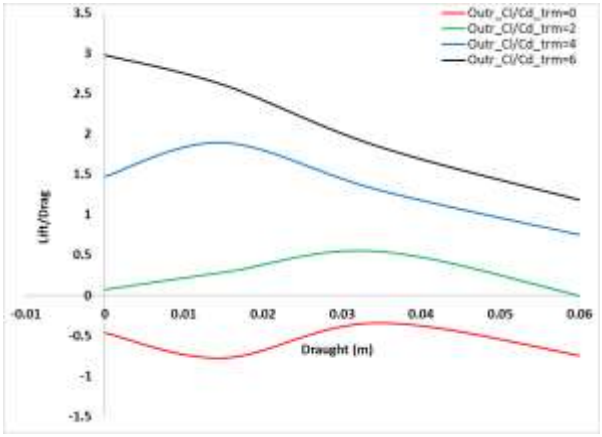

a. Outrigger model dynamic efficiency factors

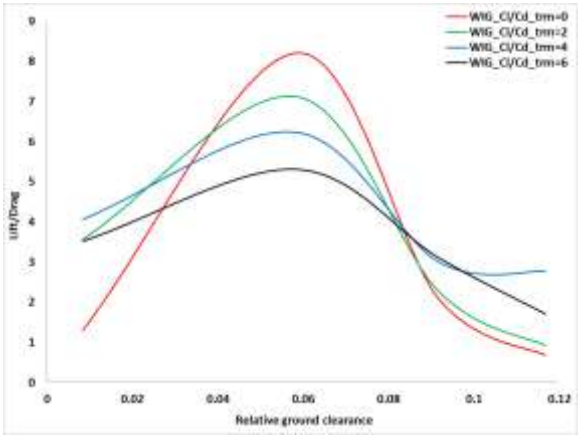

b. WIGcraft dynamic Efficiency factors

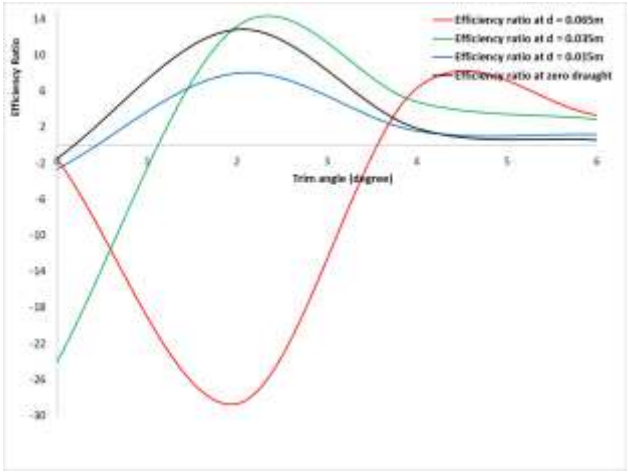

c. WIGcraft-Outrigger model efficiency ratio

Figure 6.21 Maximum dynamic efficiency (MED)

From the dynamic lift characteristics of the waterborne WIGcraft model shown in Figure 6.21b, it is seen that at all trim angles there is a particular draught position where the dynamic efficiency of the WIGcraft is maximum. This draught herein referred to as the *'Maximum Efficiency Draught (MED)'* of waterborne WIGcraft is a unique design and operation parameter that is crucial for successful installation of wings on any planing hull during the design and operation of a waterborne WGcraft. It is to be noted that this aero-hydrodynamic sweet spot is different from the aerodynamic alleviation zone (AAZ) indicated by Collu (2008, 2009). The magnitidue of the aerodynamic and hydrodynamic contributions are not necessarily equal. A water borne WIGcraft operating at the AAZ does not necessarily operates at its best efficiency. It can thus be argued that the need to establish an AAZ is more or less an academic exercise. A more practical requirement is to establish the MED which is crucial for a successful design and operation of a water borne WIGcraft. The MED plays analogous role as the maximum lift to drag ratio in aircraft design. Though, the MED has a relationship with trim angle, however, the trim angle is not necessarily needed to establish the MED. From Figure 6.21, it is seen that the lift to drag ratio is between 4.5 to 8 which is three or more times lesser than that of a typical free flight airplane with much larger aspect ratio ($7 \leq R_A \leq 17$) but more than double the lift to drag ratio of a typical planing watercraft.

The MED conspicuously increases almost linearly with trim angle as illustrated in Figure 6.21b. It can be stated that at each trim angle, the dynamic efficiency of the WIGcraft increases with relative ground clearance and approach the MED before asymptotically descending to the out of ground effect efficiency value as height is increased. In this study, it is seen that the water borne WIGcraft model in the presence of spray is not at its best efficiency when skimming on the water surface like a power boat or when operating at a displacement mode like conventional ships.

Figure 6.21b signifies the existence of a strong non-linear dynamic ground effects on the stability of the waterborne WIGcraft. A simple theoretical expression for estimating the point of maximum dynamic efficiency (MED) of the waterborne WIGcraft may be necessary for the design and optimal operation of the WIG-craft.

Figure 6.21 also show that the draught at which the Outrigger and WIGcraft models operates at maximum dynamic efficiency differs even though both models have the same hydrodynamic hull form. Interestingly, the efficiency of the WIGcraft at its design draught is superior to that of the Outrigger at is design draught.

At zero trim angle, a negative lift which tend towards positive lift as the draught is reduced to zero can be seen in Figure 6.21a. At the larger draught positions, the convex portion of the hull is submerged and possibly generate dynamic suction pressure forces (negative lift). By increasing the speed, the trim angle of the outrigger model increases resulting in a positive lift over time as the centre of gravity of the boat rises until the boat starts planing on the water surface. This nonlinear dynamic planing motion of the outrigger model cannot be attained if the trim angle of the boat is fixed at zero trim angle.

Owing to the inadequacy of the installed power to overcome its negative suction pressure force at the larger draught position, the boat may be unable to 'climb out of the sinkage created by the suction pressure (negative hydrodynamic force). In other words, while at lower draught positions, the installed power is sufficient to make the boat plane, at larger draught, the boat squats and remains non planing. The plaining boat design may be regarded as unsuccessful because it requires a prohibitive amount of installed power to make the boat plane.

Because there are no negative lifts at all draughts and trim angles for the WIGcraft (see Figure 6.21b), it can be stated that for a WIGcraft, the possibility of large draught hull-generated negative suction pressure force capable of inhibiting planing of the watercraft is overcome by the supplementary lift (aerodynamic) generated by the wing.

Figure 6.21c compares the dynamic efficiencies of the Outrigger and the WIGcraft model. The figure shows the WIGcraft maintains its highest dynamic efficiency over the Outrigger about 2° to 4° trim angles at its MED position. Figure 6.21c also shows that the WIGcraft model has poor dynamic efficiency when operated at larger draughts and below 2° trim angle.

It can be inferred from Figure 6.21 that equipping a planing hull does not necessarily translate to higher operational efficiency over hulls without wings. Figure 6.21 illustrates that hulls with wings will produce unsatisfactory outcome compared to unwinged planing hull if operated at the inappropriate draught and attitude.

6.12 Summary

The appropriateness and advantages of the experimental method used in this chapter for investigating a wide range of air and water borne WIGcraft behaviour has been demonstrated. New empirical models have been developed to estimate the dynamic lift and drag on a water borne WIGcraft with hull-generated water spray influence. In the course of formulating the lift

and drag empirical models, new semi-empirical relations were proposed to estimate the spray and ground effects on the aerodynamics of the isolated wings. The behaviour of a planing outrigger hull when coupled with wings was described. It was shown that the benefits of equipping a planing hull with wings largely depends on the location of the wings relative to the hull(s) and operating the draught, and to lesser extent, the trim angle. The significance of the hull-generated waterspray on the aerodynamic lift and drag force on the wings of the WIGcraft are well illustrated and discussed. An important finding from the experimental study presented in this chapter is the fact that a particular draught position referred to as Maximum Efficiency Draught (MED) (an 'aero-hydrodynamic sweet spot'), where coupling a wing to a planing hull is most beneficial do exist. At this draught position, the magnitudes of the aerodynamic and hydrodynamic contributions are not necessarily equal. In other words, to operate most efficiently, the waterborne WIGcraft does not need to operate at the aerodynamically alleviation zone (AAZ) indicated by Collu (2008, 2009).

Chapter 7: Validation of Numerical Models and Discussions on WIGcraft Dynamic Behaviour

7.1 Introduction

Unlike empirical and experiment-based investigations, the numerical models developed in chapters 3, 4 and 5 are less restrictive in predicting the behaviour of a waterborne WIGcraft. The numerical models developed in this study will find very useful application for WIGcraft structural design, location of wings, stability analysis and aero-hydrodynamic design of waterborne WIGcraft. However, before the proposed models can be put into beneficial use for the aforementioned applications, it is necessary that the models are validated.

In this chapter, the results from the simulation models developed in chapters 3, 4 and 5 will be validated against results derived from the experiments and Autowing code at the considered trim angles. The validation process for the hydrodynamic model developed in chapter 3 entails implementing the numerical model for the 0.035m draught case for all trim angles considered and comparing the coefficients of the lift and drag numerical results to those of the experiments described in chapter 6. Similarly, lift and drag results from the computational implementation of the numerical aero-hydrodynamic model for an airborne WIGcraft in Chapter 4 are compared to those generated by the AutoWing code and experiments for the $\frac{h_{te}}{c} = 0.113$ (or zero-draught) case. Comparison is also made between the lift and drag results of the numerical aero-hydrodynamic model for a waterborne WIGcraft developed in chapter 5 and the experimentally measured results of the waterborne WIGcraft model towed at the maximum efficiency draught (0.035m). For each of the proposed models developed in chapters 3, 4 and 5, the difference between the measured and numerical results are quantified, tabulated and possible causes of discrepancies are discussed.

Furthermore, comparison is made between the linear and nonlinear coupling of the aerodynamic and hydrodynamic components of the WIGcraft. The linear coupling of the aerodynamic and hydrodynamic components simply involves the summation of the results generated by the validated nonlinear hydrodynamic and nonlinear aerodynamic numerical models developed in Chapters 3 and 4 to predict the aero-hydrodynamic behaviour of a waterborne WIGcraft. The results of this linearly coupled nonlinearly models are compared to that of the nonlinear coupled aero-hydrodynamic numerical model developed in Chapter 5, and the inferences drawn from these comparative analyses are discussed. Also considered in this chapter, is the effects of the

hull generated water spray and the presence of water surface near the wings on the aerodynamic characteristics of the wings.

7.2 Validation of and Discussions on Proposed Hydrodynamic Model

The 3D CAD model employed for the numerical example is shown in Figure 6.1. For comparative purpose with the WIGcraft model experiments, the numerical computations carried out to evaluate hydrodynamics of the outrigger model are presented for the case where the WIGcraft model is towed at its *Maximum Efficiency Draught* (i.e., 0.035m) at the range of trim angles considered in the experiments. To simplify and keep track of the nodes of the boundary elements, each of the boundary segments of the Outrigger transverse sections are discretized into 25 elements.

The procedure described in chapter 3 was implemented in a MATLAB code using the above data as input. Comments on the various functions of the MATLAB code are presented in appendix C. The results of this computation are presented in the following subsections.

7.2.1 Total lift force on the Outrigger model

Figure 7.1 shows a comparison between the results from both the numerical model developed in chapter 3 and experiments at draught = 0.035m.

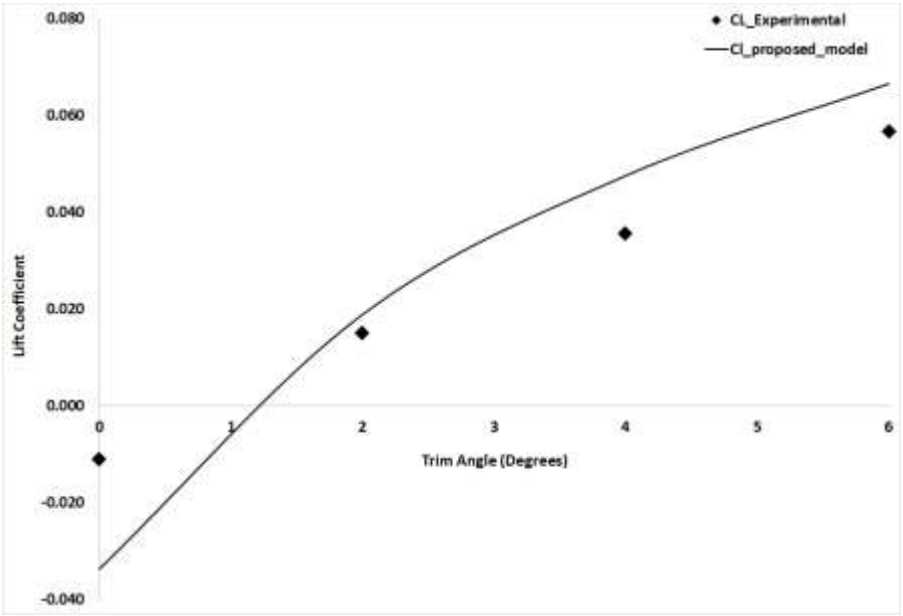

Figure 7.1 Hydrodynamic lift coefficient vs. trim angle (0.035m draught)

Table 7.1 shows that the discrepancies between the model and experimental results are below 20%, except at zero trim angle.

Table 7.1 Discrepancies between in numerical and experimental results at 0.035m draught

Trim Angle (deg)	Percentage Difference C_{Lhyd} (%)	Percentage Difference C_{DOutrg} (%)
0	146.15	22.57
2	17.88	8.94
4	19.54	5.96
6	16.07	11.08

Though the numerical model over-predicts the lift force, the numerical results show similar trend as the experimental data, especially at trim angle beyond 1°.

Since the uncertainties (see Table A2 of appendix A for uncertainty values) associated with the experimental data at the 0.035m draught are generally low except drag measurement at zero trim angle, the discrepancies between the numerical results and the experimental data for trim angles 2, 4 and 6 may be attributed to numerical inaccuracies related to the use of constant boundary element method, the correct placement of the dipole at free surface between the main and side hulls and other inherent limitations of the 2.5D theory associated with its application for multi-hull non-similar sections (Morabito, 2010; Zhao, 1997).

The discrepancies between the model and experimental results may also be attributed to the fact that the 2.5D numerical model does not sufficiently account for the three-dimensional (3-D) effect and neglects the effect of air-compressibility underneath the multi-hull during water entry. The 3-D effect which is a typical characteristics of planing hulls arises at the bow and chine due to the fact that the absence of gravity as noted in section 3.6.1a causes a sudden increment in the wetted areas near the bow and the start of the chine wetting position (x_c) which restrains the fluid energy within these limited regions. This causes variation in the pressure distribution downstream from these regions. Owing to the fact that there no 3D correction due to flow separation at the maximum beam section and that the Mackie (1963) near bow 3D effect analytical solution implemented in the 2.5D theory in this study does not accurately capture this pressure characteristics, the pressure lift forces are over-estimated.

The results may be improved by asymptotically matching the 2.5D theory with the near-bow 3D effect correction approach in Fontaine and Faltinsen (1997).

7.2.2 Total drag force on the Outrigger model

The drag results from the numerical model and experiments are presented in Figure 7.2 while the percentage differences between the results are shown in Table 7.1. It can be seen from the Figure that the numerical model slightly under-predicts the drag.

The shape of the drag coefficient curve is also seen to slightly differ. These differences may be attributed to the fact that the numerical model only accounts for the pressure drag force below the chine. Meanwhile, a close observation of the flow characteristics about the Outrigger model reveals that the hull-generated water spray wets other portions of the outrigger model beyond the chine region.

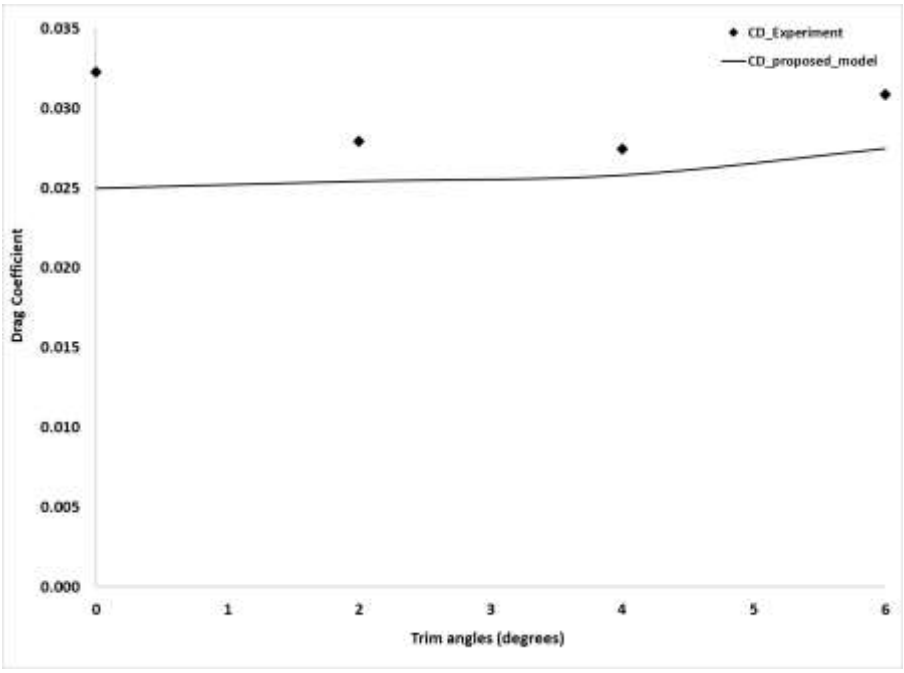

Figure. 7.2. Hydrodynamic drag coefficient vs. trim angle

Unfortunately, the numerical model as is, does not account for water spray drag beyond the chine. It is also important to note that whisker spray drag has significant contribution to the total drag on a planing watercraft, up to 15% according to Savitsky et al. (2007). The results of the numerical model may be improved by coupling a viscous flow model.

As with the results of the hydrodynamic lift discussed in subsection 7.2.1, at zero trim angle, a higher percentage difference between the results was observed for some unclear reasons (see Table 7.1). However, it is to be noted that the uncertainty percentages for measured drag shown in Table A3 of appendix A are relatively higher at the zero draught. Notwithstanding, errors made during the implementation of the numerical model, especially during the numerical treatments of the spray trajectory from the spray root, cannot also be completely ruled out as

contributing to the much higher difference between the experimental and numerical results at zero-degree trim angle.

Due to the re-entrant pointed (all-trailing) stern characteristics of the hulls used in this study (see water plane area shape in Figure 6.4), a sudden fluid flow separation occurs at the maximum beam section of the hull. Experiments have shown that beyond flow separation points, negative or suction hydrodynamic pressures can be generated (Maki et al., 2005, Faltinsen, 2001). Unlike the typical transom stern, a complicated balance between the hydrodynamic pressure and the hydrostatic ensues beyond the maximum beam section of the model used in this study, which tend to enforce reduction in the total pressure to zero or negative values towards the trailing edge of the stern. In so doing, the total hydrodynamic drag on the hull is reduced as noted in in Tulin (1982). Like the lift, the pressure drag beyond the maximum beam section is over-predicted by the 2.5D theory due to the 3-D effect. In Chapter 6, it was stated that the measured drag on the Outrigger model consists of other drag components which are not accounted for by the 2.5D theory. As a result, while the hydrodynamic pressure drag on the Outrigger model may well be over-predicted by the 2.5D theory, the total measured drag exceeds that predicted by the 2.5D hydrodynamic model.

The order of 10% difference (shown in Table 7.1) between the drag results of the numerical model and the measured drag represents a fair balance between the higher predicted drag due to 3D effect by the numerical model, the unaccounted viscous drag, contributions of numerical inaccuracies and experimental errors. The results in sections 7.2.1 and 7.2.2, affirms the applicability of the 2.5D theory to model and simulate the hydrodynamics of warped multi-hull high speed ships with reasonable transverse clearance (10 times its sponson beam) between its main hull and sponsons.

7.3 Validation of and Discussions on Proposed Aero-hydrodynamic Model for Air Borne WIGcraft

For the computational implementation of the aero-hydrodynamic model of an air borne WIGcraft near undisturbed free surface water, the case where the WIGcraft is at $\frac{h_{te}}{c} = 0.113$ for the range of trim angles is presented. The discretization scheme is similar to that of the hydrodynamic model. The dimension of the air-water interface boundary segment equals the span of the WIGcraft section as shown in Figure 4.2. The discretization of the far field segment

is similar to that described for the hydrodynamic model. Comments on the various functions of the MATLAB code are presented in appendix D.

The results of the numerical computation are compared to that of Autowing vortex lattice method-based code and the measured experimental data at $\frac{h_{te}}{c} = 0.113$.

7.3.1 Total lift on airborne WIGcraft model

In Figure 7.3, the results of the aerodynamic lift coefficient of the ground effect aerodynamic numerical model are compared with those from Autowing code and the experiments when the WIGcraft model is towed at constant at $\frac{h_{te}}{c} = 0.113$). The percentage differences between the results of proposed numerical method, the Autowing code and the experimental data are presented in Table 7.2.

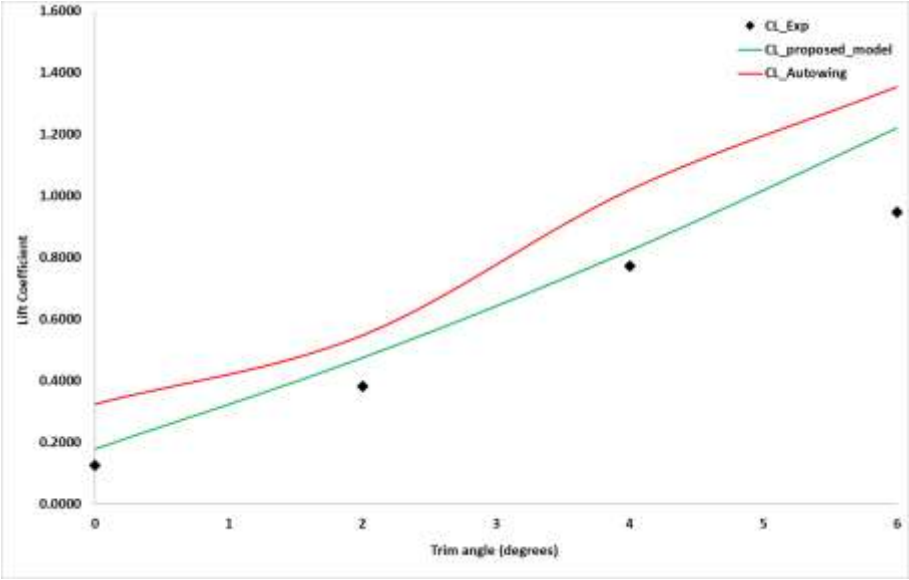

Figure 7.3 Ground effect aerodynamic lift coefficient vs. trim angle

From the figure, it is seen that the lift results of the Autowing code lies above the lift results from the proposed numerical model developed in chapter 4 and the experiments. The Autowing vortex lattice code is a robust code designed to predict the behaviour of WIGcraft. Though, the code over-predicts the dynamic lift of the WIGcraft model, in comparison with the 2.5D momentum transfer based slender wing theory proposed in this thesis, Figure 7.3 shows how well the Autowing code captured the nonlinearities in the lift characteristics of the wing in ground effect with respect to the experimental data. This success may be as a result of the high-

density transverse and longitudinal 3D lattice structure implemented in code (see appendix D). The code, however, depends on the method of images to predict ground effects. It is to be noted from Table 7.2 that the total lift results from the Autowing are considerably greater than the measured lift.

Table 7.2 Percentage differences between the numerical results and results of the experiment and AutoWing code at $\frac{h_{te}}{c} = 0.113$

Trim Angle (deg)	% Difference between Numerical C_{LWIG} & Experimental Data	% Difference between Autowing C_{LWIG} & Experimental Data	% Difference between Numerical C_{DWIG} & Experimental Data	% Difference between Autowing C_{DWIG} & Experimental Data
0	21.75	110.76	53.17	294.31
2	12.34	20.75	54.02	114.02
4	6.72	22.54	34.52	104.71
6	17.68	26.34	28.35	105.16

It is also seen from Figure 7.3 that the numerical model was able to capture some nonlinearities generally associated with ground effects, especially at the lower trim angles. Except at 2° trim angle, the proposed numerical model gives total lift values that are generally less than 18% of the measured data as can be seen in Table 7.2. The uncertainty values of the experimental lift data at 2° and $\frac{h_{te}}{c} = 0.113$ (zero draught) shown in Table A2 in appendix A, suggests that experimental errors contribute slightly to the discrepancy between the experimental data and the proposed numerical model. Apart from experimental errors, the discrepancies between the proposed model and the other two results may also be attributed to,

- Numerical inaccuracy related to the use of constant boundary element method.
- Presence of strong viscous effect at model scale. During the motion of the WIGcraft, boundary layer separation occurs near the leading edges of the dihedral wings of the WIGcraft. This results in free vorticities being shed which generates vortex lift (Drela, 2014). Owing to the inherent restricted use of the potential flow theory for ideal fluid flow, this increase in lift is not accounted for by the potential flow based 2.5D numerical model implemented in this thesis.
- The fact that the aspect ratio (1.333) of the WIGcraft model used may be described as ‘not-too-small. This suggests that the flow considered as transversal in the

numerical model also has a significant amount of longitudinal fluid flow components not adequately captured by the numerical model at higher trim angles.

- Thickness problem associated with the interaction between the downstream sections of the thick dihedral wings, and the wake introduces significant 3-D effect (Newman, 1982). Since the 2.5D theory does not adequately account for the 3D effect, it over-predicts the aerodynamic pressure lift.

7.3.2 Total drag on the airborne WIGcraft model

For the zero draught ($\frac{h_{te}}{c} = 0.114$) condition shown in Figure 7.3, it is seen that the drag coefficient results of the experiments, Autowing code and the proposed momentum transfer model based on 2.5D slender body theory increases nonlinearly with trim angle. However, the proposed model and the Autowing code generate drag coefficients that are far lesser (upto 54% and above 100% respectively) than the experimental values.

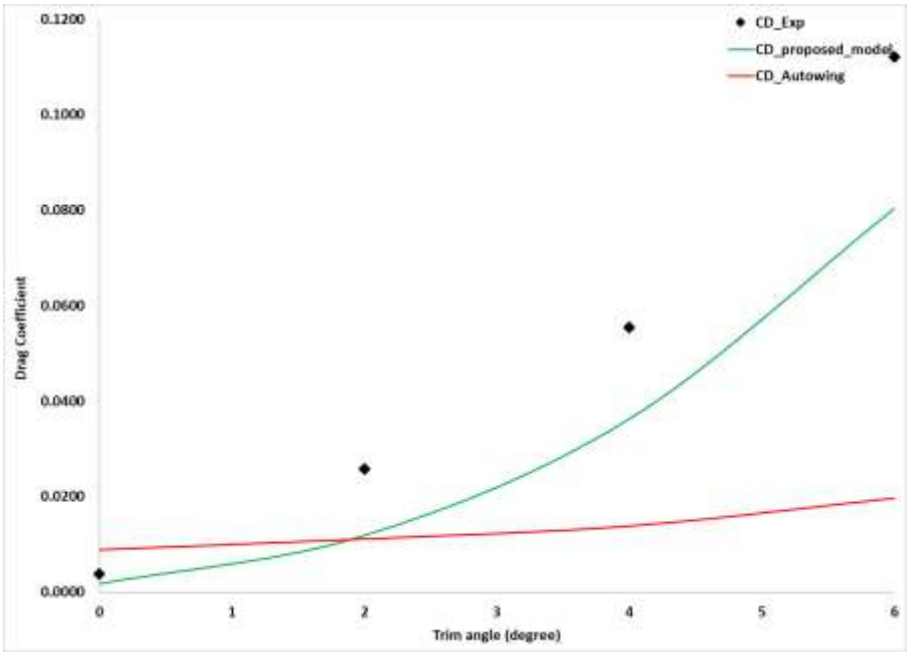

Figure 7.4 Aerodynamic drag coefficient vs. trim angle ($\frac{h_{te}}{c} = 0.114$)

Besides the inadequacies of the 2.5D previously stated subsection 7.3.1 and in other parts of this thesis, the discrepancy in drag between the experiments and the proposed model may be attributed to the fact that the proposed model does not account for the strong viscous force experienced by the WIGcrafts, especially at model scale (Yang et al., 2010). Secondly, it is to be emphasized that the percentage uncertainties (see Table A3 of appendix A) associated with measured drag are relatively higher than that computed for the measured lift at the zero-draught

condition, especially at zero trim angle. The uncertainties which is indicative of a relatively higher experimental errors may have significant impact on values of the measured drag data.

The flatness of the drag coefficient curve generated by the Autowing code is notable. Documentation of the Autowing code states that the code uses a boundary layer theory and viscous/inviscid interaction algorithm to account for viscous effect. At the time of writing this thesis, it is difficult to explain why the Autowing code generates far lesser drag coefficient than that of experiments at higher trim angles.

7.4 Validation of and Discussions on Proposed Aero-Hydrodynamic Model for the Water Borne WIGcraft model

To illustrate how the numerical model developed in chapter 5 compares with the experimental results, the case where the WIGcraft model was towed at its *Maximum Efficiency Draught* (draught = 0.035m) is presented. The discretization scheme used in this case is a combination of schemes used in sections 7.2 and 7.3. Further details of the discretization scheme and comments on the various functions of the MATLAB code are presented in appendix E.

7.4.1 Total lift on the water borne WIGcraft model

The total lift of a waterborne WIGcraft consists of buoyancy, hydrodynamic and aerodynamic lift components. However, for the fully constrained model, only the dynamic component of the total lift is measured. The contribution of each of the dynamic lift components are functions of speed, draught, trim angle and other geometric parameters of the watercraft.

The presence of ground effect and hull-generated water spray impingement on the wings complicates the fluid flow and dynamic force characteristics of a water borne WIGcraft compared to the flow about an Outrigger watercraft. The validity of the numerical model proposed in chapter 5 to predict the coupled aero-hydrodynamic lift of the water borne WIGcraft model is examined in this section. The hydrodynamic form of the lift coefficient discussed in chapter 6 is used for comparing the results from the numerical model and the experiments.

Figure 7.5 compares the results of the proposed model to that of the experiments at the Maximum Efficiency Draught position. The maximum percentage difference between the model and experimental lift and drag coefficient results is shown in Table 7.3 to be less than

20%. The proposed model shows a reasonable correlation with the experimental data even though it under-predicts the aero-hydrodynamic lift. This lower lift predicted by the model tends to contradict the results of the aerodynamic and hydrodynamic models which generally over-predicts their respective lift components.

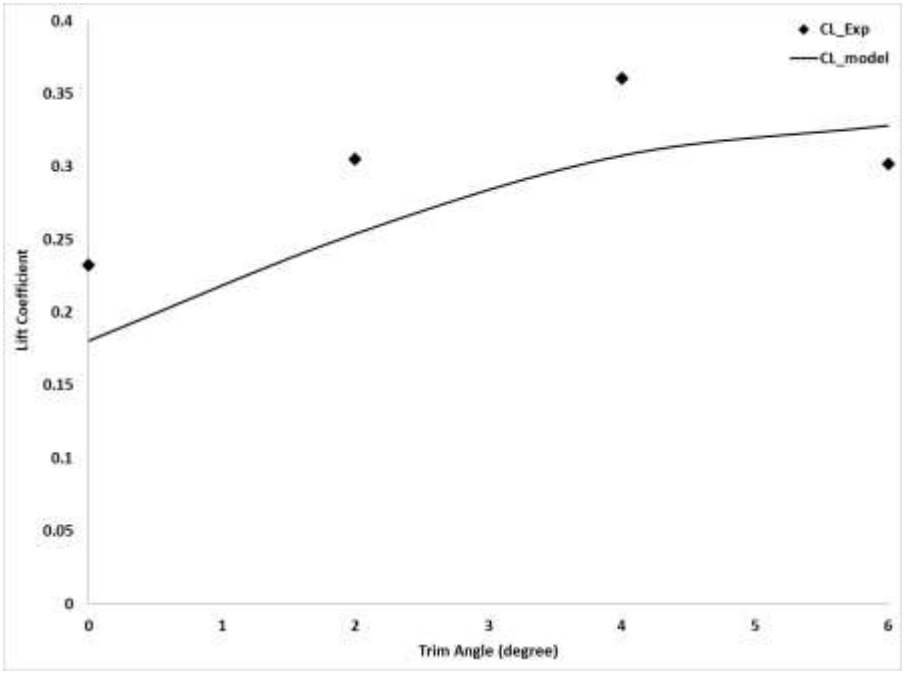

Figure 7.5 Aero-hydrodynamic lift coefficient characteristics at Maximum Efficiency Draught

Table 7.3 Percentage difference between the numerical and experiment results at MED

Trim Angle (deg)	% Difference in C_{LWIG}	% Difference in C_{LWIG} with spray lift	% Difference in C_{DWIG}
0	19.37	74.37	50.68
2	16.78	68.40	21.89
4	14.66	60.94	7.74
6	8.73	66.49	18.01

Almost similar trend was noted for cases where the WIGcraft model is towed at 0.065m and 0.015m. Figure7.6 illustrates the correlation between the experimental and the proposed model results at these draughts.

Given that the experimental uncertainties (shown in Table A3 of appendix A) at the 0.035m draught position are very minimal and suggests minimal experimental errors, the obvious reason for this lift under-prediction anomaly between the proposed numerical model and experimental results is that the aero-hydrodynamic model as is, does not account for hull-

generated water spray on the wings. In chapter 6, it was demonstrated that the hull-generated spray has a significant influence on the overall lift characteristics of a waterborne WIGcraft.

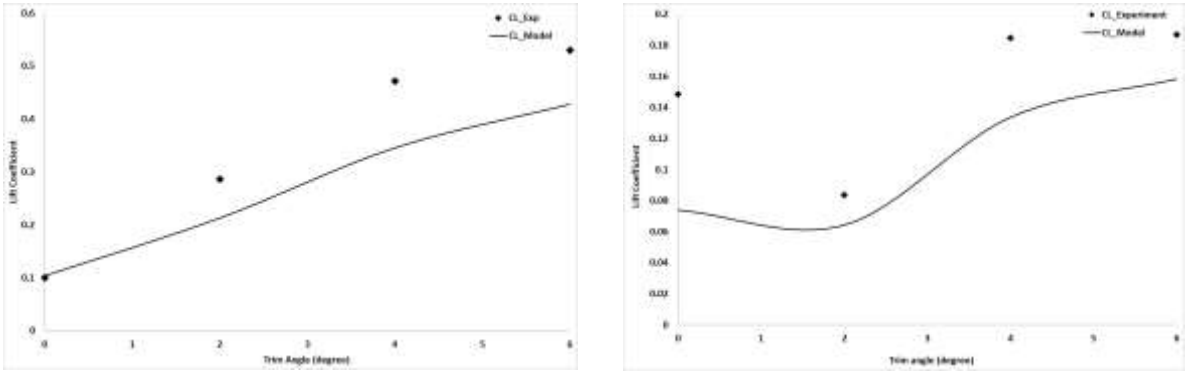

a.Draught = 0.065m *b. Draught = 0.015m*

Figure 7.6 Aero-hydrodynamic lift coefficient characteristics at 0.065 and 0.015 draught

An attempt made to linearly superimpose the measured spray factor calculated in chapter 6 is illustrated in Figure 7.7. It is seen that there is an improvement in the nonlinear characteristics of the proposed with respect to the experimental results, however, this improvement is accompanied by large increase in the lift coefficient. A possible reason for the large increase could be as a result of accumulation of the excess lift over-predicted by both the hydrodynamic (section 7.2.1) and aerodynamic (section 7.3.1) models together with the linear inclusion of spray factor. This finding further demonstrates how significant the hull generated water spray influence is on the WIGcraft dynamic lift.

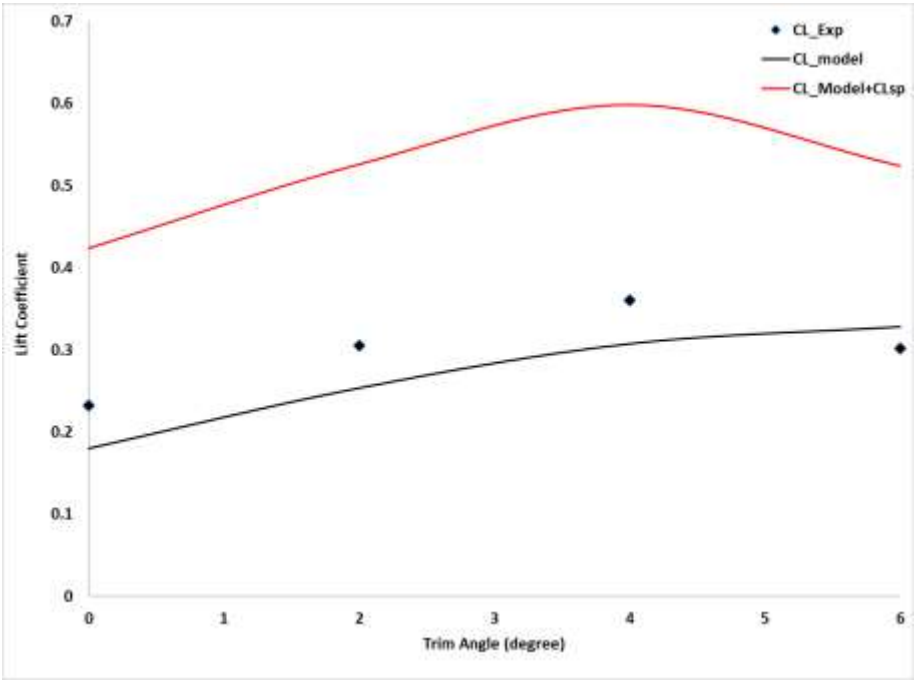

Figure 7.7 Aero-hydrodynamic lift coefficient vs. trim angle (with spray factor at MED)

On considering the lift characteristics of Figures 7.6 and 7.7, it can be inferred that the proposed aero-hydrodynamic model (without spray effects) will still over-predict the aero-hydrodynamic lift characteristics of the waterborne WIGcraft towed at a draught where hull generated spray does not impinge its wings.

Coupling a 3-D bow flow correction model and a more accurate water spray model in a nonlinear manner to the numerical model in its present state may possibly improve the accuracy of the proposed aero-hydrodynamic model.

7.4.2 Total drag on the waterborne WIGcraft model

For the case where the WIGcraft model is towed at its *MED*, the proposed numerical model shows similar trend as the experimental results as seen in Figure 7.8. It, however, generally under-predicts the drag with larger discrepancies noticeable at the zero trim angle position (see Table 7.3). The large discrepancy between the results was expected due to the fact the proposed model does not account for the hull-generated water spray viscous drag on the wings of the watercraft as well as the viscous drag on the hull(s).

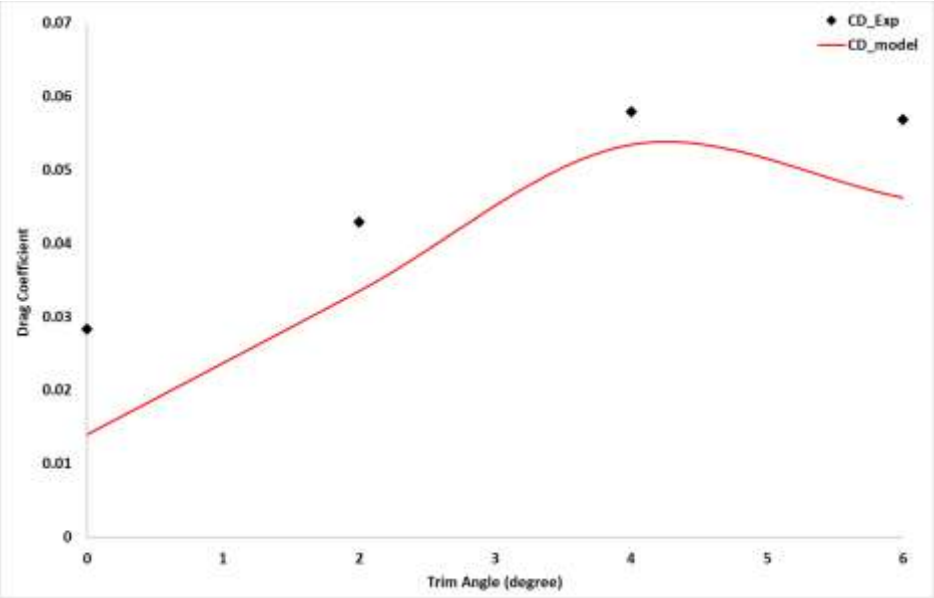

Figure 7.8 Aero-hydrodynamic drag coefficient characteristics at MED)

The significance of spray drag on the aerodynamic drag of the wings of the water borne WIGcraft has been discussed in chapter 6. The model results may be improved by coupling a viscous and water spray and 3D correction models.

7.5 Linear and Non-linear Coupled Aero-Hydrodynamics of the Water borne WIGcraft model

In this section, comparison is made between the results of the aero-hydrodynamic model and results derived from the linear superimposition of hydrodynamic and hydrodynamic models. This section examines if there are coupling effects not captured by implementing a linear coupling of hydrodynamic and aerodynamic forces (as carried out by Collu 2008, 2009) during stability analysis of a waterborne WIGcraft (AAMV). For this investigation, the aerodynamic, hydrodynamic and aero-hydrodynamic models are implemented for the WIGcraft at the *MED* for the range of trim angles considered in the experiments.

Figure 7.9 show that linearly coupling the aerodynamic and hydrodynamic models yields lift and drag coefficients that are slightly higher than when the aerodynamics and hydrodynamics of the waterborne WIGcraft are coupled using the momentum transfer theory implemented in the proposed aero-hydrodynamic model.

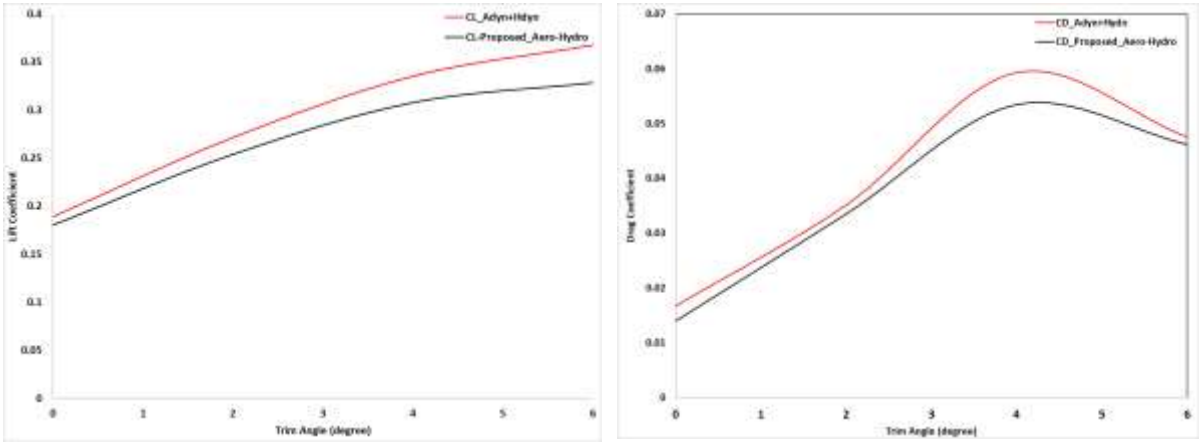

a. Lift coefficient variations *b. Drag coefficient variations*

Figure 7.9 Linearly coupled Aerohydrodynamic Lift vs proposed Aero-Hydrodynamic model

Table 7.4 shows that the percentage difference between the two coupling methods is in the order below 10%. The variations in the drag coefficient between the linear coupled and the proposed nonlinear coupled aero-hydrodynamic model are more significant than for lift. These differences regarded as aero-hydrodynamic coupling effect in this thesis, may not be considered insignificant when the vehicle operates at the air-water interface, where there is extreme dynamic instability due to dynamic ground effects.

Table 7.4 Percentage difference between Linear and Non-linear Aero-Hydrodynamic coupling

Trim Angle (deg)	% Difference in C_{LWIG}	% Difference in C_{DWIG}
0	5.49	20.35
2	7.04	5.86
4	9.14	11.13
6	11.89	3.09

7.6 Summary

The three numerical models developed in Chapters 3, 4 and 5 were validated in this Chapter by comparing their results with those from Autowing code and the captive model tests discussed in Chapter 6. The numerical results follow similar trends as the experimental results. 3D effects and other numerical inaccuracies may be liable for the percentage difference between the lift results of the numerical model and experimental data. The relatively large uncertainties calculated for the drag coefficients, especially at draught zero and -6mm positions, suggests experimental errors is partly responsible for the differences in the numerical and experimental drag results. Unaccounted viscous forces may also contribute significantly to the differences between the numerical and measured drag results. From the numerical models, it was deduced that there exist a not insignificant nonlinear effects which are unaccounted for when the aerodynamic and hydrodynamic forces are linearly coupled.

Chapter 8: Semi-empirical Simulation Model for WIGcraft Acceleration Motion to Take-off

8.1 Introduction

The acceleration to take-off (in calm water and rough seas) is a short duration but very important motion regime of an airborne WIGcraft. It is a pre-requisite for estimating the transport efficiency of a WIGcraft as a viable alternative to high-speed marine vehicles or low speed aircrafts used in conveying workers to and offshore oil and gas fields. The development of a simulation model based on results from constant speed captive model tests for a WIGcraft is imperative when in the absence of appropriate experimental test rig there is the need to investigate the attitude of the vehicle during its acceleration phase. Theoretical tools for investigating the characteristics of the acceleration phase of a WIG boat are uncommon and where they exist, they are almost unreliable, not been experimentally validated. Moreover, the cost associated with conducting such high-speed acceleration tests is huge. The test facilities are not readily available in most maritime engineering research institutions.

In Chapters 3 to 7, semi-empirical and numerical models have been proposed, developed and validated for a WIGcraft moving at a range of constant planing speeds for various sets of trim angle draught positions. In this chapter, a semi-empirical model will be developed to simulate the characteristics of the acceleration to take-off motion of the WIGcraft model by using the results of the captive model experiment. As against the use of the semi-empirical models developed in Chapter 6 for planing speed regime, a multivariate multiple regression method was used to develop model equations that fits the measured aero-hydro dynamic lift, drag and moment data as a function of draught, trim angle and planing speed range considered in this study. The hydrostatic and aero-hydrodynamic steady state forces and moments were combined into a state-space form and are solved in MATLAB. The state variables, the first and second derivatives of the states of the boat as well as the forces and moments acting on it are generated as output from the simulation model. Results from the simulation exercise are discussed with respect to the attitude of the WIGcraft, including crashing, excessive acceleration, time and power requirement during take-off.

8.2 Assumptions, Simplifications and Limitations of the Proposed Simulation Model

- Only vertical plane acceleration motion is considered.

- The experimental approach is developed to assess the performance of a WIGcraft accelerating in calm water only. In calm water operations, the attitude of boats propelled is generally maintained in the direction of thrust and trim angle settings. As such, this experimental approach ignores the unsteady forces and moments acting on the boat owing to ship motions which may attempt to push the boat out of equilibrium. The unsteady forces may play very significant role when the WIG boat accelerates to take-off in the presence of waves in the offshore environment.
- Since the tow point is at the centre of gravity of the WIGcraft model, it is assumed that thrust acts at the centre of gravity of the boat in a direction parallel to the calm water surface. As such, pitch moment and lift due to thrust force are taken as zero.
- All nonlinear terms are linearized.
- The success of this method depends largely on how the multivariate multiple regression results fit the experimental data.

8.3 Forces and Moment on the WIGcraft Model

Though the moving WIGcraft experiences forces in the horizontal and vertical planes, the acceleration to take-off motion mainly occurs in the vertical plane. As a result, it becomes necessary that vertical plane motion is decoupled from the horizontal plane motion and only the forces in the vertical plane are considered in this study. This approach reduces the equation of motion from 6 degree of freedom to a simpler 3 degrees of freedom.

8.3.1 Total steady state forces and moments

The total steady lift (L_{TSF}) and drag (D_{TSF}) forces, and moment (M_{TSF}) acting on the accelerating boat comprises of the hydrostatic restoring forces/moments, the aero-hydrodynamic damping force and moments as well as the added mass forces and moments at steady state conditions. These components of the total steady forces and moments are described and estimated below.

(a) Steady hydrostatic forces and moment

The prevailing steady components of the hydrostatic moment and forces are represented by the hydrostatic forces and moment on the submerged portion of the hull at a constant heave and pitch (or trim) position and the velocity is assumed constant at each time step during the vehicle's acceleration.

The hydrostatic force is a function of hullform parameters. The hydrostatic force may be stated as a function of the distance (z_d) of vertical centre of gravity from the calm water surface. The draught (d) is related to z_d by.

$$z_d = \text{VCG} - \text{d} \tag{8.1}$$

The hydrostatic force

$$L_{ZB} = f_{zB}(z_d) \tag{8.2}$$

The hydrostatic pitching moment is calculated as the product of the hydrostatic force and buoyancy moment arm whose length is the horizontal distance (x_{BM}) between the longitudinal centre of buoyancy and the centre of gravity from the aft.

The hydrostatic moment

$$M_{ZB} = f_{zB}(z_d, x_{BM}) \tag{8.3}$$

The restoring forces and moment in the same forward direction as the boat's acceleration are assumed negligible.

(b) Steady state aero-hydrodynamic forces and moment

The determination of the steady state aero-hydrodynamic damping forces and moments acting on the boat also follows a quasi-steady approach through forces and moments measurements of a fully constrained model tests towed at constant speed and at a range of constant draught, trim angle in a towing tank. The fully constrained model tests are conducted during this study are detailed in Chapter 6 of this thesis. The range of data considered in the experimental design for this simulation model are from 4.5m/s to 5.5m/s, where ground effect aerodynamics exists, 0º to 6º trim angles and 0.015m draught to zero or take-off draught).

Expressions that fit the measured aero-hydrodynamic lift (L_{AH}), drag (D_{AH}) and moment (M_{AH}) data as a function of draught, speed and trim angle can be derived from a multivariate multiple regression analysis. The equations are expressed as

$$D_{AH} = f_1(\dot{x}, z, \tau) \tag{8.4}$$

$$L_{AH} = f_3(\dot{x}, z, \tau) \tag{8.5}$$

$$M_{AH} = f_5(\dot{x}, z, \tau) \tag{8.6}$$

(c) Steady state aero-hydro dynamic added masses

During the constant forward acceleration to take-off, the WIGcraft model experiences aero-hydrodynamic inertial reaction forces in the x and z axis and about the y axis of the model. The steady components of the aero-hydrodynamic forces which is expressed in the form of the product of the added mass and the forward acceleration of the boat are given below.

Steady reaction in surge direction during constant forward acceleration:

$$R_{11} = -m_{11}\ddot{x} \tag{8.7}$$

Steady reaction in the surge direction during upward acceleration:

$$R_{31} = -m_{31}\ddot{x} \tag{8.8}$$

Steady reaction in surge direction during the pitch acceleration:

$$R_{51} = -m_{51}\ddot{x} \tag{8.9}$$

The unsteady components of the added masses ($m_{33}, m_{35}, m_{53}, m_{55}$) and damping forces ($b_{33}, b_{35}, b_{53}, b_{55}$) are neglected. Similarly, the added masses (m_{13} and m_{15}) and damping (b_{13} and b_{15}) in the surge direction due to heave and pitch motions are considered negligible. It should also be noted that the restoring force coefficients (c_{11}, c_{31} and c_{51}) in the surge direction are minute compared to the forward motion of the WIGcraft model and are thus neglected. These steady state aero-hydrodynamic added mass reaction forces and moment consists of the complex coupled interaction of aerodynamic and hydrodynamic components.

Unlike the aerodynamic and hydrodynamic added mass of aircraft or ships for which various formula and methods for their values are readily available in literature, mathematical and empirical formula for estimating these aero-hydrodynamic added mass reaction forces and moments is difficult to come by in existing literature. It is assumed in this work, that the aerodynamic components of the added mass coefficients are negligible compared to the hydrodynamic components. As a result, the aero-hydrodynamic steady state added mass coefficients in this study can be approximated from existing formula in ship hydrodynamics. In this study, the steady state added masses is determined following Dubrovsky et al. (2007),

$$m_{11} = \sum_i u_{11}^i \tag{8.10}$$

$$m_{31} = \sum_i u_{31}^i \tag{8.11}$$

$$m_{51} = \sum_i u_{51}^i + z_i u_{11}^i - x_i u_{31}^i \tag{8.12}$$

Where,

i (= 1,2,3) stands for the components (left and right sponsons and main hull) of the submerged part of the hull(s).

$x_i \; and \; z_i$ are the coordinates of each submerged hull relative to the centre of gravity of the main hull.

u_{11} is determined from Sargent and Kaplan (1974) empirical formula.

u_{51}^i and u_{31}^i are assumed negligible compared to u_{11}^i (Fossen, 2002). As such, Lewandowsky (2004) approximate formula for m_{51} holds true. i.e.

$$m_{51} \approx \sum_i z_i u_{11}^i \tag{8.13}$$

The principle of superposition of forces is a common method to combine the aerodynamic and hydrodynamic added masses of ships. However, it has been shown in section 7.5 of this thesis that superposition principle does not necessarily capture the complex aero-hydrodynamic interaction existing between the aerodynamic and hydrodynamic components of the WIGcraft model.

During the acceleration of the WIG boat,

Total Steady Drag Force

$$D_{TSF} = D_{AH} + R_{11} = (b_{11}\dot{x} + c_{13}z + c_{15}\tau) + R_{11} \tag{8.14}$$

Total Steady Lift Force

$$L_{TSF} = (L_{ZB} + L_{AH}) + R_{31} = (b_{31}\dot{x} + c_{33}z + c_{35}\tau) + R_{31} \tag{8.15}$$

Total Steady Pitch moment

$$M_{TSF} = M_{AH} - M_{ZB} + R_{51} = (b_{51}\dot{x} + c_{53}z + c_{55}\tau) - M_{ZB} + R_{51} \tag{8.16}$$

(d) Required thrust force T_F

Thrust force required to move the WIGcraft at constant acceleration must overcome the total steady forces and moments. As with drag forces, the thrust force required for constant acceleration of the boat is also a strong function of speed. This study does not focus on developing a precise model for the propulsion system of the WIGcraft. As such, a simple model approach which relates the thrust force to the speed of the boat is proposed as a general model for the thrust force during preliminary design. The thrust force relation is given as

$$T_F = K_T \rho U^{\gamma} \partial x \quad (8.17)$$

K_T is the propulsion constant, ρ is the density of water; U is speed of the boat; ∂x represents the engine throttle position, its value ranges between 0 and 1; γ represents the characteristics of the engine used. Highly efficient propulsion systems have γ = 1.

8.4 Model for Simulating the WIGcraft Acceleration

The WIGcraft model is considered to commence its motion at draught 0.015m with an attitude on water surface and on a straight course in the forward direction opposite the $x - axis$ direction in the space-fixed reference frame as shown in Figure 4.1. The steady state acceleration of the WIGcraft model and prevailing forces and moments acting on it are simulated using the equations below,

The Propulsion (Thrust) Equation:

$$m_d \ddot{x} = T_F cos(\tau + \varepsilon) - W_x - D_{TSF}) \quad (8.18)$$

The Sustention Equation:

$$m_d \ddot{z} = W_z - L_{TSF} - T_F sin(\tau + \epsilon) \quad (8.19)$$

The Pitch Moment Equation:

$$I\ddot{\theta} = M_{TSF} - M_T \quad (8.20)$$

Where,

x and z are respectively linear displacement in the x and z direction while θ is the angular displacement about the y axis of the coordinate system. The first and second derivatives of these displacements yield respectively their velocities and accelerations.

m_d is the mass displacement of the WIGcraft model,

W_x and W_z are respectively the components of the weight of WIGcraft model in the x and z direction of the coordinate system described in Chapter 4 of this thesis.

ε is the inclination of thrust line relative to keel.

M_T is moment of the thrust force.

I is moment of inertia of the boat about the y axis.

After substituting the appropriate parameters into equations (8.18) to (8.20), the resulting equations are expressed in matrix format thus,

$$[M]\langle\ddot{X}\rangle + [B]\langle\dot{X}\rangle + [C]\langle X\rangle = \langle F\rangle \quad (8.21)$$

Where,

$[M]$ is the mass matrix = $\begin{bmatrix} m_d + m_{11} & 0 & 0 \\ m_{31} & m & 0 \\ m_{51} & 0 & I \end{bmatrix}$

$[B]$ is the damping matrix = $\begin{bmatrix} b_{11} & 0 & 0 \\ b_{31} & 0 & 0 \\ b_{51} & 0 & 0 \end{bmatrix}$

$[C]$ is the restoring force matrix = $\begin{bmatrix} 0 & c_{13} & c_{15} \\ 0 & c_{33} & c_{35} \\ 0 & a_{53} & c_{55} \end{bmatrix}$

$\langle\ddot{X}\rangle$ is acceleration matrix = $\begin{bmatrix} \ddot{x} \\ \ddot{z} \\ \ddot{\tau} \end{bmatrix}$ $\langle\dot{X}\rangle$ is velocity matrix = $\begin{bmatrix} \dot{x} \\ \dot{z} \\ \dot{\tau} \end{bmatrix}$

$\langle X\rangle$ displacement matrix = $\begin{bmatrix} x \\ z \\ \tau \end{bmatrix}$ $\langle F\rangle$ is external force matrix = $\begin{bmatrix} F_x \\ F_z \\ M_y \end{bmatrix}$

The system of equations (8.21) is solved in Matlab. The running attitudes and the forces and moment experienced by the WIG boat model are derived from the simulation model. Suffice to say, this study focuses mainly on the simulation of the acceleration to take-off phase of the boat. It does not necessarily simulate the entire acceleration phase of the boat (i.e., from rest to take-off). The simulation was designed to terminate whenever the zero-draught mark (take-off point) is reached. This corresponds to a rise of the vertical centre of gravity (z_d) of the WIG-craft model from 0.05m at designed draught to 0.065m above the calm water surface.

8.5 Simulation Results and Discussion

The state variables and the first and second derivatives of the states of the WIGcraft as well as the forces and moments acting on it are generated as output from the simulation model. These results are plotted against each other to predict the running attitude of the WIGcraft.

The characteristics of acceleration to take-off is illustrated by Figures 8.1 to 8.3. The predicted take-off point is located where z_d = 0.065m in Figure. 8.1 and from which the corresponding drag and thrust required for take-off can be read.

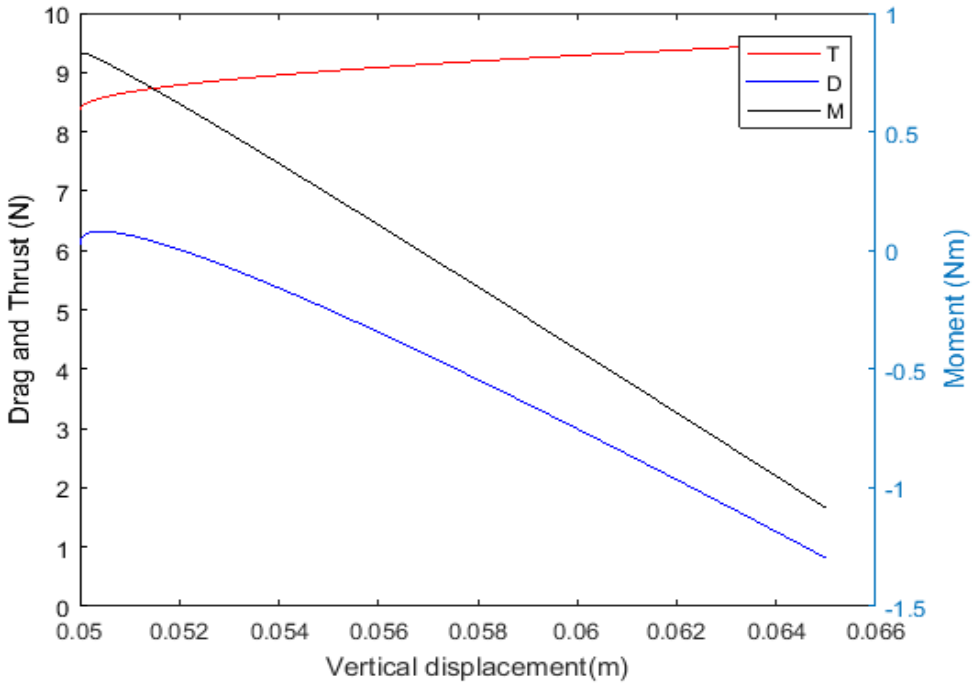

Figure 8.1. Variation of forces and moment during vertical displacement

During the preliminary design of the WIGcraft, a take-off speed of 5.1m/s was the target. The calculated take-off speed from the simulation suggests a lower take-off speed value of 4.55m/s as shown in Figure 8.2. The position of the hump drag prior to take-off was captured by the model at 4.15m/s where the difference between the thrust and the drag is minimal.

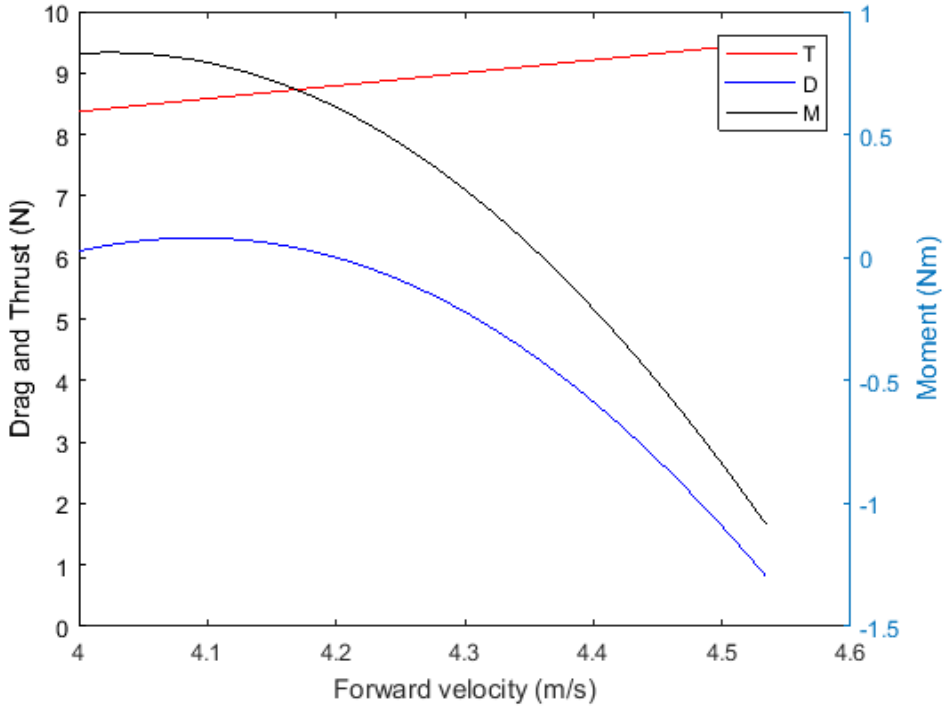

Figure 8.2 Prevailing forces and moment on accelerating WIGcraft

The maximum thrust point and the characteristic of Figure 8.2 determines the type and power rating of the propulsion engine to be installed. Beyond the maximum thrust power point, the drag of the boat reduces quickly to about 1N when it lifts off from the water surface. The engine becomes redundant, and the boat becomes commercially not viable. The cost associated with installing and operating a large engine at lower speed and power after the hump drag becomes prohibitive compared to other transport vehicles. Here-in lies the need to investigate the possibilities of developing humpless WIGcrafts or alternative utilization of the excess power of the engine.

The negative pitch moment and rapidly increasing margin between the thrust and the drag near the take off point (at vertical displacement z_a = 0.065m) in Figure 8.2. suggests the sudden take off from water and possible pitch down attitude the WIGcraft may experience without any control. There is also the likelihood of the model vehicle displaying submarining characteristics if it did not take-off from water.

Figure 8.3 reveal the swift time interval required for this take-off attitude to occur. In other words, it indicates the response effort and time needed to make the necessary thrust adjustment to overcome excessive acceleration and loss of longitudinal stability and subsequent crashing of the WIG boat.

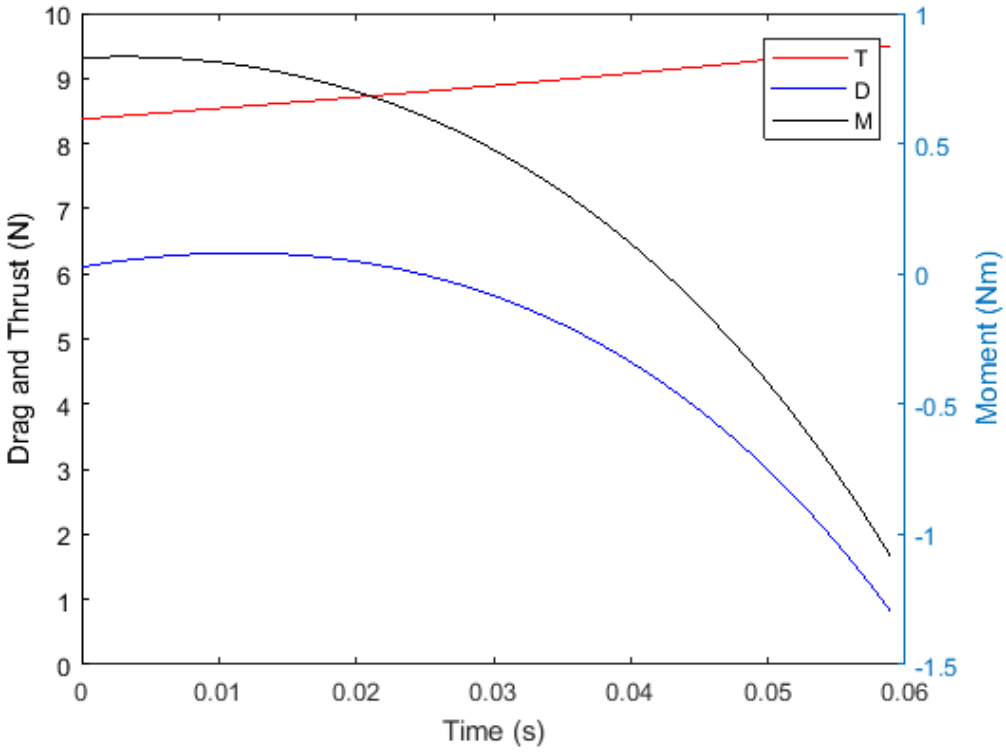

Figure 8.3. Take-off time for accelerating WIGcraft model

The steep reduction in drag after the hump drag leading to excessive acceleration of the boat can be attributed to the transition from hydrodynamic drag (as a result of reduced wetted surface after the hump drag) to aerodynamic drag. The management of this transition defines the success or failure in the design and operation of the boat.

This transition phase is unique to WIG-boats and is not found in high-speed boats or airplanes. As such, there is need for elaborate investigation to properly define its characteristics with a view to develop commercially viable WIGcrafts.

8.6 Summary

A semi-empirical model has been presented to simulate the acceleration to take-off phase of a WIGcraft. A multivariate multiple regression method was used to develop model equations that fits the measured aero-hydro dynamic lift, drag and moment data as a function of draught, speed and trim angle. The hydrostatic and aero-hydrodynamic steady state forces and moments were combined into a state-space form and are solved in MATLAB.

The state variables and the first and second derivatives of the states of the WIGcraft model, as well as the forces and moments acting on the model under steady running attitudes are generated as output from the simulation model. Though the simulation model proved successful in predicting the attitude of the WIGcraft including crashing and excessive acceleration and power requirement during take-off, the results from the model still need to be verified with CFD analysis, a full WIGcraft trial tests or with the expensive high speed towing tank capable of carrying out the full acceleration runs from rest to take-off. The method has the potential to be improved to account for the unsteady forces and moments that exists when the WIGcraft accelerates in offshore environment.

Chapter 9: Conclusion and Recommendation

9.1 Conclusion

The prediction of the coupled aero-hydrodynamic behaviour of a waterborne WIGcraft using numerical or empirical methods is a towering task that requires broad knowledge of aerodynamic and hydrodynamic theories, as well as the development of appropriate methods to couple these two disciplines. The fundamental parameters in aerodynamics and hydrodynamics to consider are many. The characteristics of the fluid flow about the vehicle are generally non-linear and require careful empirical and/or numerical treatments to obtain reasonable results. This thesis focuses on developing and validating tools to simulate and evaluate the behaviour of a water borne WIGcraft, including nonlinear effects such as ground effects, hull generated spray effects, coupling effects, acceleration etc.

Prior to the development of these numerical and semi-empirical tools, an extensive literature review on planing mono/multi hull watercrafts, air borne, and water borne WIGcrafts was carried out to better understand the behaviour of water borne WIGcrafts. A novel experimental approach based on ideas derived from ITTC (2017), Maskalik and Rozhdestvensky, (1998) and Belynsky and Zinchuk (1998) was implemented. The experiments involve fully captive model tests for quantitative measurement of the hydrodynamic, aerodynamic and aero-hydrodynamic forces on WIGcraft and Outrigger models moving with constant forward speed on calm water. An uncertainty analysis carried out to ascertain the accuracy and reliability of the experimental results shows that in most of the test cases the mean combined uncertainties in the measurement are generally below 10%. It was seen that the data acquisition system contributes more than 90% of the total uncertainty.

The analysis of the experimental results reveals that the dynamic characteristics of a WIGcraft are different from that of a typical single or multi-hull planing watercraft, irrespective of the fact that they have the same hull form. Both types of marine vehicles are to be operated differently. There exists an important design and operational parameter referred to as Maximum Efficiency Draught (MED), which is crucial for successful installation of wings on any planing hull during the design of a waterborne WIGcraft and its successful operation. The existence of the MED and further analysis of the experimental results suggests the following.

- High-speed Waterborne WIGcrafts if operated at the MED are more dynamically efficient than typical planing boats, airplanes and airborne WIGcrafts of equivalent size.

Their payload efficiency may be increased further where their speed-dependent hydrostatic lift force is considered.

- Equipping a high-speed watercraft with aerodynamic lift generating surfaces does not necessarily make the boat to possess acceptable higher operational efficiency over hulls without wings. The winged boat must satisfy the appropriate operational conditions, such as draught and trim angle.
- The suction forces generated by poorly designed planing may be offset by the aerodynamic lift generated from aerodynamic surfaces coupled to the boat. As a result, there is prospect of using less input power to overcome the squatting and non-planing characteristics of such poorly designed boats.

The experiments provided a database of forces which were used to validate the computational models developed in this thesis.

Three nonlinear numerical models based on 2.5D slender wing/body approximation and boundary element method were proposed, developed and validated for modelling and simulating the behaviour of a water borne WIGcraft model moving at constant forward speed in calm water. Semi-empirical models were also developed to predict the dynamic lift and drag characteristics of the water borne WIGcraft model, whose wings are subjected to hull-generated water spray.

The semi-empirical models were developed by first deriving semi-empirical expressions for the various components of the lift and drag coefficients before superposing the respective lift and drag components. This model development approach provides detailed insight into effects and contributions of the various geometric, hydrodynamic and aerodynamic parameters to the behaviour of a water borne WIGcraft.

In the course of formulating the semi-empirical models for the dynamic lift and drag on a water borne WIGcraft whose wings are subjected to hull-generated water spray:

- An equivalent coefficient transformation factor was formulated to transform calculated aerodynamic lift and drag force coefficients (generated from a given aerodynamic surface area) into their respective equivalent hydrodynamic lift and drag force coefficients of planing hull(s) with specified wetted beam. The thesis illustrates how implementing this transformation enabled the summation of force coefficients derived from fluid mediums of different densities (air, water, water spray sheet in this study) and lifting surfaces of inconsistent or different geometric configurations and parameters of the fluid borne vehicle.

- the expression for Savitsky (1964) lift coefficient was modified using a kind of trim angle independent block factor C_{∇}, to account for warped planing multihulls with re-entrant pointed (or all trailing) stern. A new expression for calculating an appropriate deadrise angle for the semi-empirical expressions was presented and implemented. The modified Savitsky (1964) dynamic lift semi-empirical expression developed in this thesis show good agreement with both the experimental results in this study and results of Model 250E tested by Wadlin and McGehee (1950b) to an order generally less than 10% difference.
- A new relation was derived to estimate the contribution of pure ground effect (without water spray) to the aerodynamic lift on the wings of the water borne WIGcraft. A new relation was also formulated to estimate the spray contribution to the aerodynamic lift on the wings of the water borne WIGcraft. Both models show agreement with their respectively experimentally deduced data to an order of 10% discrepancies. The proposed expression for the water spray lift coefficient was also shown to correlate to an order less than 10% difference from the experimental data of two different wing configurations in Fink and Lastinger (1961). These lift results reinforce the estimation of pure ground effect aerodynamic lift (with no water spray effect) on an air borne and water borne WIGcraft from towing tank experiments (Belynsky and Zinchuk, 1998). The significance of the hull-generated water spray on the aerodynamic lift on the wings of the WIGcraft are illustrated and discussed. As noted in Chapters 1 and 2, the calculated spray influenced aerodynamic lift in Chapter 6 will have a consequential impact on the motion behaviour and dynamic stability of the watercraft. For the water borne WIGcraft model operating at large draught (0.065 and 0.035), where its wings being closer to the free surface are subjected to both water spray and strong ground effects, it was found that the contribution of hydrodynamic lift and hull generated spray lift components to the total dynamic lift by far exceeds the lift contribution from ground effect. The induced and viscous drag on the hull(s) and water spray drag similarly exceed the drag contribution from ground effects. As a result, the ground effect of the wings in proximity to the free surface water may be regarded as secondary.
- The calculated lift and drag results from the proposed semi-empirical models show good correlation with experimental data conducted for waterborne WIGcraft model to an order below 10%. The semi-empirical models illustrate that the total dynamic lift and drag increases nonlinearly with trim angle and draught.

Three potential flows based 2D+t (2.5D) nonlinear numerical simulation models were developed in Chapters 3, 4 and 5 to determine respectively the hydrodynamic forces on planing warped single- and multi-hull Outrigger model; coupled ground effect aero-hydrodynamic forces on an air borne WIGcraft model and coupled ground effect aero-hydrodynamic forces on a water borne WIGcraft model with non-similar hull form sections. The development of these simulation models entails formulation of potential flow-based fluid dynamics problems, for which the velocity potentials and their normal drivatives were solved as an initial boundary value problem (IBVP) using the iterative constant boundary element method (IBEM). For the hydrodynamic model, careful numerical treatments of the free surface evolution and jet spray led to the convergence of the solution. For the coupled ground effect aero-hydrodynamic dynamic model of the air borne WIGcraft, a branch-cut was used to close the air and water domain boundaries to ensure a successful implementation of the boundary element method. In the coupled ground effect aero-hydrodynamic model of the water borne WIGcraft, a two-step iterative solution approach was formulated and implemented to integrate the proposed hydrodynamic and the ground effect aero-hydrodynamic models in a nonlinear manner. By solving the Bernoulli's equations in each of the numerical models with the aid of an acceleration potential, the pressure forces on the sections of the WIGcraft and Outrigger models were determined and integrated.

The results of the proposed numerical models were compared with those of Autowing code and captive model tests carried out during the study. All three numerical models under-predicted drag. The reason for the difference between the results can be attributed to the fact that the numerical models do not account for viscous forces. Though, the results of hydrodynamic model show similar trend in lift as those of the experiments, it over-predicted the lift by more than 10%. Since the Outrigger model drag and lift uncertainties are minimal for the maximum efficiency draught conditions that was simulated, the discrepancies between the experiments and the hydrodynamic model may be ascribed to numerical errors, the placement of the dipole at the free surface between the hulls as well as the 3-D effects that are neglected near the bow and the maximum beam sections. Similar trend was noted for the results of the coupled aero-hydrodynamic model with parts of its hull submerged, though with a smaller percentage difference from the experimental data. The differences between the results of the numerical model for the air borne WIGcraft and the experiments may be associated with 3D effect occurring between the wake and the downstream sections of the dihedral wings thick section. By coupling viscous flow models and 3D correction models to the proposed numerical models, the numerical models are expected to yield improved correlation with the experimental results.

From the numerical models, it was deduced that there exist a not insignificant nonlinear effects which are unaccounted for when the aerodynamic and hydrodynamic forces are linearly coupled. The results from the numerical model also reveal that,

- The 2.5D theory is applicable for modelling and simulating the hydrodynamic characteristics of non-similar monohull planing ships as well as multi-hull planing ships having appropriate lateral clearances between the hulls.
- The momentum transfer at the air-water interface is capable of capturing nonlinearities associated with the complicated air/water flow characteristics in the small gap underneath the wings of a WIGcraft.

Having proposed and developed both numerical and semi-empirical models for the dynamic lift and drag of a water borne vehicle, it can be stated that the semi-empirical models give a clearer and specific insight into the physics and how the various geometric, hydrodynamic and aerodynamic and operational parameters interact to influence the lift and drag characteristics of the vehicle. This property of the semi-empirical models is very useful for preliminary design and simulation of a waterborne WIGcraft. The simplified expressions of the semi-empirical model are very easy and time efficient to implement. As such, they are very handy tools for the development and running of real-time simulators on desktop computers. However, it is to be noted that the accuracy of the semi-empirical models is subject to their specified parameters' limits of application. Further validation from a more extensive sets of test data of waterborne WIGcraft of various configuration and operational range may improve the robustness of the semi-empirical models developed in this thesis.

On the other hand, the 2.5D nonlinear numerical models developed in this thesis are largely unrestricted to the configuration and operational range of the WIGcraft that can evaluate and simulate. The numerical models give physical insight into the nonlinearities, hydrodynamics and aerodynamics of a WIGcraft in air borne and water borne modes. Complex shaped WIGcraft configurations can be design and analysed using the proposed numerical models on desktop computers. As a result, they can be very useful for data-driven simulation model developments as well as for integrated simulation-based design and optimisation of waterborne WIGcraft.

A model to simulate the acceleration to take-off phase of a water borne WIGcraft was also developed from the experimental data. The draught, trim angle and all speed dependent expressions of the forces used in the Newton's equation of motion were derived from a

multivariate multiple regression analysis and supplemented by existing empirical formula for the calculation of the reaction forces associated with the model accelerations. The hydrostatic and aero-hydrodynamic steady state forces and moments were combined into a state-space form and are solved in MATLAB. The state variables, and the first and second derivatives of the states of the WIGcraft model as well as the forces and moments acting on it are generated as output from the simulation model. The simulation model illustrated the excessive acceleration and the reaction time needed by a WIGcraft pilot to avoid crashing during take-off. It also illustrated the excessive thrust power available for air borne cruise mode during take-off, which results in the large and expensive installed engines becoming redundant and inefficiently utilized, thereby increasing operational cost.

Finally, the information contained in the thesis is expected to enrich the scanty existing literature on water borne WIGcraft.

9.2 Recommendation

This study introduces the first part of an ongoing detailed study into the behaviour of a water borne WIGcraft whose wings are subjected to ground effects and hull-generated sprays. The numerical models developed in chapters 3, 4 and 5 and validated in chapter 7 are capable of evaluating in detail, the effects of the non-linear aero-hydrodynamic coupling on the free surface elevation, the effects of the non-linear aero-hydrodynamic coupling on the aerodynamic force distribution of the wing-fuselage and the effects of the non-linear aero-hydrodynamic coupling on hydrodynamic force distribution of the submerged hulls of the WIGcraft model. Due to time constraints, the detailed analyses of these nonlinear coupling effects as they relate to waterborne WIGcraft structural design and stability performance were reserved for future work and publications.

Previous studies have shown that the aerodynamic characteristics of the wings moving near water surface may be reasonably derived from fully captive experimental tests in a towing tank. Thus, it is believed that the lift and drag coefficients of the wings derived by subtracting the outrigger measured values from the WIGcraft measured values provides estimates of the coefficients accurate enough for engineering purposes. These estimates, however, may not represent the exact value of the lift and drag coefficients of the wings. It is therefore recommended that the wing-fuselage is further tested in wind tunnel to assure the certainty and reliability of the results from the towing tank.

The empirical expressions used to analyse the experimental results requires some extensive validation against benchmark experimental data to ascertain its usefulness for general application in the prediction of the behaviour of water borne WIGcraft of other geometry and configurations. This general validation process was not carried out in this thesis because experimental data for waterborne WIGcraft with spray influence are extremely difficult to find, if ever they exist.

The numerical models developed in chapters 3, 4 and 5 gave predictions of the forces on the watercraft that are similar in trend to the experimental data. The percentage differences between the models and the experimental results are generally below 18%. The numerical hydrodynamic model developed in chapter 3 made use of some fairly broad assumptions such as, no air compressibility underneath cross-structures of the hulls and the sponsons being far enough from the main hull for hull interference effects to be ignored. The accuracy of the hydrodynamic model may be improved by extending the model to include hull interference effects. The hull interference effects may be accounted for by asymptotically matching the evolving free surface boundaries adjacent to the main hull and each sponson. A further validation of the results of the proposed hydrodynamic model against drop (water entry) tests using multi-hull shaped wedge sections as the test models may also be necessary. The accuracy of the three proposed numerical models may be improved by considering the use of higher order boundary elements methods, coupling a viscous flow model and accounting for 3-D effects.

Finally, the experimental results, numerical and empirical models developed in this study would be very useful for such future studies by the author and other researchers in this discipline.

References

Abramowski, T. (2007) 'Numerical investigation of airfoil in ground proximity', *Journal of Theoretical and Applied Mechanics*, *45*, pp. 425–436.

Adams M.C. and Sears W.R. (1952) 'Slender body theory– review and extension', *Aerodynamic Session, Annual Summer Meeting, I.A.S.*

Adhynugraha, M. I. (2017) *Longitudinal dynamics of wing in ground effect craft in waves*. Cranfield University, UK.

Aframeev E.A. (1998) 'Conceptual bases of WIGcraft building: ideas, reality and outlook', *RTO AVT Symposium on Fluid Dynamic Problems of Vehicles Operating near or in the Air-Sea Interface*.

Alourdas, P. G. (2016) 'Planing Hull Resistance Calculation – The CAHI Method', *Presentation Made at SNAME Greek Section Meeting*.

Amiri, M. M., Dakhrabadi, M. T. and Seif, M. S. (2015) 'Development of a semi-empirical method for hydro-aerodynamic performance evaluation of an AAMV, in take-off phase', *Journal of the Brazilian Society of Mechanical Sciences and Engineering*, *37*(3), pp. 987–999. https://doi.org/10.1007/s40430-014-0217-0.

Anderson, J. D. (2016) *Fundamentals of aerodynamics* (6th ed.). McGraw-Hill, McGraw-Hill Education.

Ashley H. and Landahl M. (1965) *Aerodynamics of Wings and Bodies*. Addison-Wesley Publ. Co.

Axt, W. C. (1947) *The Effect of Scale, Surface Tension and Acceleration on the Main Spray Characteristics of Geometrically Similar Flying-Boat Hull Models.* Davidson Laboratory Technical Note No. 59.

Bannikov Ju M. and Lulashevsky V.A. (1976) 'Experimental investigation of the lift and drag of planing plates', *Proc. Central Aero-Hydrodynamic Institute (Uchenye Sapiski CAGI) VII, pp.117-123:* In Knud Benedict, Nikolai Kornev, Michael Meyer, Jost Ebert (2002) 'Complex mathematical model of the WIG motion including the take-off mode', *Ocean Engineering, 29(3), pp. 315-357.*

Bao, C. M., Wu, G. X. and Xu, G. D. (2016) 'Simulation of water entry of a two-dimension finite wedge with flow detachment', *Journal of Fluids and Structures*, *65*, pp. 44–59. https://doi.org/https://doi.org/10.1016/j.jfluidstructs.2016.05.010

Barber T.J. (2007) 'A study of water surface deformation due to tip vortices of a WIG', *Journal of Ship Resistance, 51*, pp. 182–186.

Beck, R. F. and Løken, A. E. (1989) 'Three-dimensional effects in ship relative-motion problems', *Journal of Ship Research*, *33*, pp. 261–268.

Belynsky, V. G. (1997) 'About movement of a wing above wavy surface of water', *AGARD FDP Workshop on High Speed Body Motion in Water. R-827.*

Benedict, K., Kornev, N., Meyer, M. and Ebert, J. (2002) 'Complex mathematical model of the WIG motion including the take-off mode', *Ocean Engineering*, *29*(3), pp. 315–357. https://doi.org/https://doi.org/10.1016/S0029-8018(01)00002-6

Bertorello, C. and Oliviero, L. (2007) 'Hydrodynamic resistance assessment of non-monohedral planing hull forms based on Savitsky's method', *Australian Journal of Mechanical Engineering*, *4*. https://doi.org/10.1080/14484846.2007.11464527

Betz, A. (1912) 'Lift and drag of a wing near a horizontal surface', *Zeitschrift Fur Flugtechnik Und Motorluftschiffahrt*, 217.

Blok, J. J. and Beukelman, W. (1984) 'The high-speed displacement ship systematic series hull forms-- seakeeping characteristics', *Transactions of the Society of Naval Architects and Marine Engineers*, *92*, pp. 125–150.

Blount, D. L. and Fox, D. L. (1976) 'Small-craft power prediction', *Marine Technology and SNAME News*, *13*(01), pp.14–45. https://doi.org/10.5957/mt1.1976.13.1.14

Bollay, W. (1939) 'A Non-linear wing theory and its application to rectangular wings of small aspect ratio', *Z. Angew. Math. Mech.*, *19*, pp. 21–35.

Boschetti, P. J., Quijada, G. M. and Cárdenas, E. M. (2017) 'Dynamic Ground Effect on the Aerodynamic Coefficients Using a Panel Method', *Journal of Aircraft*, *54*(2), pp. 838–844. https://doi.org/10.2514/1.C034098

Boschetti, P., Neves, C. and Gonzalez, P. (2022) 'Nonlinear Aerodynamic Model in Dynamic Ground Effect at High Angles of Attack', *Journal of Aircraft*, pp. 1–14. https://doi.org/10.2514/1.c036721

Byelinskyy V.G. (1998) 'Hydrodynamical characteristics of an Ekranoplane wing flying near the wavy sea surface', *Symposium on Fluid Dynamics Problems of Vehicles Operating near or in the Air-Sea Interface RTO-MP-15*.

Chu L. (1923) *Damping Coefficients Due to Tail Surfaces* in aircrafts. Massachusetts Institute of Technology, Report No. 13

Cointe, R., Geyer, P., King, B., Molin, B. and Tramoni, M. (1990) 'Nonlinear and linear motions of a rectangular barge in a perfect fluid', *Proceedings of 18th Symposium of Naval Hydrodynamics*.

Collu, M. (2008) *Dynamics of marine vehicles with aerodynamic surfaces* (PhD Thesis, Ed.). Cranfield University, UK.

Collu, M., Williams, Patel, M. and Trarieux, F. (2009) *Aerodynamically Alleviated Marine Vehicles (AAMV): Development of a Mathematical Framework to Design High Speed Marine Vehicles With Aerodynamic Surfaces.* Cranfield University, UK.

Cui, E. and Zhang, X. (2010) 'Ground Effect Aerodynamics', In *Encyclopedia of Aerospace Engineering*. John Wiley & Sons, Ltd. https://doi.org/https://doi.org/10.1002/9780470686652.eae022

Cummins, W. E. (1962) 'The Impulse Response Function and Ship Motions', *Schiffstechnik*, *47*, pp. 101–109.

DARPA/TTO. (2021) *Request for Information Design of Seaplane Wing-in-Ground Effect Vehicles*. Defense Advanced Research Projects Agency, Tactical Technology Office, USA: Vol. DARPA-SN-21-42.

de Luca, F. and Pensa, C. (2017) 'The Naples warped hard chine hulls systematic series', *Ocean Engineering, 139*.

Doctors, L.J. (1985) *Hydrodynamics of high-speed small craft.* University of Michigan, College of Engineering, Department of Naval Architecture and Marine Engineering, Report No. 292, January 1985, USA.

Dong, T., Minelli, G., Wang, J., Liang, X. and Krajnović, S. (2020) 'The effect of ground clearance on the aerodynamics of a generic high-speed train', *Journal of Fluids and Structures, 95*, 102990. https://doi.org/https://doi.org/10.1016/j.jfluidstructs.2020.102990

Drela M. (2014) *Flight Vehicle Aerodynamics*. MIT Press.

Dubrovsky V, Matveev K and Sutulo S (2007) *Small Waterplane Area Ships.* USA: Backbone Publishing Company.

Dundurs J. and Hamilton W.S (1954) *Liquid Jet Disintegration.* Hydraulics Laboratory, Northwestern University, Evanston, Illinois.

Dundurs J. and Hamilton W.S (1955) *Disintegration of Seaplane Spray and Flat Sheets*. Hydraulics Laboratory, Northwestern University, Evanston, Illinois.

Egorov Ivan Timofeevich, M. M. B. I. M. S. (1981) Propulsive Performance and Seaworthiness of Planing Vessels. *NAVSEA, 1965*.

Faltinsen O.M (2001) 'Steady and vertical dynamic behavior of prismatic planing hulls', In: *Proc. 22nd International Conference*, HADMAR, October 2001, Varna, Bulgaria.

Faltinsen, O. (2006) *Hydrodynamics of High-Speed Marine Vehicles*. Cambridge University Press.

Finkelstein A. (1957) 'The initial value problem for transient water wave', *Communications in Pure and Applied Mathematics, 10*, pp. 511–522.

Fontaine E. and Tulin M.P. (1998) 'On the prediction of nonlinear free-surface flows past slender h ulls u sing 2D+t theory: the evolution of an idea'. *RTO AVT Symposium on Fluid Dynamic Problems of Vehicles Operating near or in the Air-Sea Interface*.

Fontaine E. and Faltinsen O.M. (1997) 'Steady flow near a wedge-shaped bow'. *Twelfth International Workshop on Water Waves and Floating Bodies*, Carry-le-Rouet, France.

Fossen T.I. (2002) *Marine Control Systems, Guidance, Navigation and Control of Ships, Rigs and Underwater Vehicles*. Marine Cybernetics AS, Trondheim, Norway.

Fridsma G. (1969) *A Systematic Study of the Rough-Water Performance of Planing Boats*. NACA Report 1275.

Fu, T., O'Shea, T., Judge, C., Dommermuth, D., Brucker, K. and Wyatt, D. (2014) 'A detailed ssessment of Numerical Flow Analysis (NFA) to Predict the Hydrodynamics of a Deep-V Planing Hull', *International Shipbuilding Progress, 60*. https://doi.org/10.3233/ISP-130087

Garme, K. (2005) 'Improved time domain simulation of planing hulls in waves by correction of the near-transom lift', *International Shipbuilding Progress, 52*, pp. 201–230.

Garme, K. and Rosén, A. (2003) 'Time-domain simulations and full-scale trials on planing craft in waves', *International Shipbuilding Progress*, *50*, pp. 177–208.

Gerritsma, J. and Beukelman, W. (1967) 'Analysis of the Modified Strip Theory for the Calculation of Ship Motions and Wave Bending Moments' *SNAME Transaction*, pp. 319–337.

Gerritsma, J., Beukelman, W. and Glansdorp, C. C. (1974) 'The effects of beam on the hydrodynamic characteristics of ship hulls', *10th Symposium on Naval Hydrodynamics.*

Ghadimi, P., Dashtimanesh, A., Djeddi, R., and F. Maghrebi, Y. (2013) 'Development of a mathematical model for simultaneous heave, pitch and roll motions of planing vessel in regular waves', *International Journal of Scientific World, 1*. https://doi.org/10.14419/ijsw.v1i2.1056

Greco M. (2001) *A two-dimensional study of green water loading*. Norwegian University of Science and Technology.

Green, A. E. (1935) 'The gliding of a flat plate on a stream of finite depth part I', *Proceedings of the Cambridge Philosophical Society*, *31*.

Green, A. E. (1936a) 'Note on the gliding of a plate on the surface of a stream', *Proceedings of the Cambridge Philosophical Society*, *32*.

Green, A. E. (1936b) 'The gliding of a flat plate on a stream of finite depth, part II'. *Proceedings of the Cambridge Philosophical Society, 32*.

Grigoropoulos, G. J. and Loukakis, T. A. (1995) 'Effect of spray rails on the resistance of planing hulls. *FAST "95*.

Grundy I. H. (1986) 'Airfoils moving in air close to a dynamic water surface', *The Journal of the Australian Mathematical Society. Series B. Applied Mathematics*.

Han, S., Zhang, J., Xiong, X., Ji, P., Zhang, L., Sheridan, J. and Gao, G. (2022) 'Influence of high-speed maglev train speed on tunnel aerodynamic effects', *Building and Environment*, *223*, 109460. https://doi.org/https://doi.org/10.1016/j.buildenv.2022.109460

Hansman, R. J. and Craig, A. P. (1987) 'Low Reynolds Number Tests of NACA 64-210, NACA 0012, and Wortmann FX67-K170 Airfoils in Rain', *Journal of Aircraft*, *24*, pp. 559–566.

Hascoët, R., Jacques, N., Scolan, Y.M. and Tassin, A. (2019) 'A two-dimensional analytical model of vertical water entry for asymmetric bodies with flow separation', *Applied Ocean Research*, *92*, 101878. https://doi.org/https://doi.org/10.1016/j.apor.2019.101878

Hess, J. L. and Smith, A. M. O. (1967) 'Calculation of potential flow about arbitrary bodies', *Progress in Aerospace Sciences*, *8*, 1–138. https://doi.org/https://doi.org/10.1016/0376-0421(67)90003-6

Hicks, J. D., Troesch, A. and Jiang, C. (1993) 'Simulation and nonlinear dynamics analysis of planing hulls' *Journal of Offshore Mechanics and Arctic Engineering-Transactions of The Asme*, *117*, pp.38–45.

Hicks, J. D., Troesch, A. W., and Jiang, C. (1995) 'Simulation and nonlinear dynamics analysis of planing hulls', *Journal of Offshore Mechanics and Arctic Engineering*, *117*(1), pp.38–45. https://doi.org/10.1115/1.2826989

Hicks J.D. (1993) *Analysis Method for Planing Hull Vertical Motions*. University of Michigan, Ann Arbor, MI.

Holtrop, J., & Mennen, G. G. J. (1978) 'A statistical power prediction method', *International Shipbuilding Progress*, *25*, pp.253–256.

Holtrop, J. and Mennen, G. G. J. (1982) 'An approximate power prediction method', *International Shipbuilding Progress*, *29*, 166–170.

Hosseini, A., Tavakoli, S., Dashtimanesh, A., Sahoo, P. and Kõrgesaar, M. (2021) 'Performance prediction of a hard-chine planing hull by employing different CFD models. *Journal of Marine Science and Engineering*, *9*, 481. https://doi.org/10.3390/jmse9050481

Hubin W.N. (1992) 'The science of flight', In *The science of flight* (pp. 157–180). Iowa State University Press. Ames.

Hugli W.C. and Axt W.C. (1951) *Hydrodynamic investigation of a series of hull models suitable for small flying boats and amphibians.* NACA Technical Note 2503.

Im, Y.H. and Chang, K.S. (2000) 'Unsteady aerodynamics of a Wing-in-Ground-Effect airfoil flying over a wavy wall' *Journal of Aircraft*, *37*(4), pp. 690–696. https://doi.org/10.2514/2.2653

Irodov R.D. (1970) *Criteria of the Longitudinal Stability of the Ekranoplan*. National Technical Information Service

ISO (1995) *Guide to the expression of Uncertainty in Measurement (GUM),* International Organisation for Standardization, Geneve, Switzerland

ITTC. (1999) 'Uncertainty Analysis in EFD, Uncertainty Assessment Methodology', *22nd International Towing Tank Conference,* Seoul/Shanghai, ITTC Recommended Procedures and Guidelines, Procedure 7.5-02-01-01, Rev 00

ITTC. (1999) 'Density and Viscosity of Water,' *22nd International Towing Tank Conference*, Seoul/Shanghai, ITTC Recommended Procedures and Guidelines, Procedure 7.5-02-01-03, Rev 00

ITTC. (2002) *Recommended Procedure and Guidelines: Testing and Extrapolation Methods, Resistance Uncertainty Analysis, Example for Resistance Test.* ITTC, 7.5-02-02–02, Rev. 01.

ITTC. (2008) *The Specialist Committee of High-Speed Marine Vehicles.* Final Report and Recommendations to the 22nd ITTC.

ITTC. (2014a) *Recommended Procedure: Guide to the Expression of Uncertainty in Experimental Hydrodynamics*. 7.5-02-01–01, Revision 02.

ITTC. (2014b) *Recommended Procedure: General Guideline for Uncertainty Analysis in Resistance Tests*. 7.5-02-02–02, Revision 02.

ITTC. (2017) *Recommended Procedure and Guidelines: High Speed Marine Vehicles Resistance* 7.5-02-05–01, Revision 03.

James, D. and Collu, M. (2015) *Aerodynamically Alleviated Marine Vehicle (AAMV): Bridging the Maritime-to-Air Domain*. https://doi.org/10.5957/FAST-2015-019

Jean Ross (1961) *The Calculation of Lateral stability Derivatives of Slender Wings at Incidence, Including Fin Effectiveness and Correlation with Experiments.* Aeronautical Research Council Reports and Memoranda No. 3402.

Jones, R. T. (1946) *Properties of low-aspect-ratio pointed wings at speeds below and above the speed of sound*. NACA Report No. 835.

Jones R.T. (1941) *Corrections of the lifting line theory for the effect of chord.* NACA Tech Note 817, July 1941, Langley Aeronautical Laboratory, Virginia, US.

Kapryan, W. J. and Boyd, G. M. (1955). *Hydrodynamic Pressure Distributions Obtained During a Planing Investigation of Five Related Prismatic Surfaces*. NACA Technical Notes 3477

Kashiwagi M. (2018). *Wave-body interaction theory (Theory of ship waves)*. Lecture Note for Graduate Course, Lab of Seakeeping and Floating Body Dynamics in Waves. Dept of Naval Architecture and Ocean Engineering, Osaka University

Katz, J. (2019) 'Classical and potential flow-based aerodynamics - do we need them?' In *AIAA Scitech 2019 Forum*. https://doi.org/10.2514/6.2019-0864

Katz, J. and Plotkin, A. (2001) *Low-Speed Aerodynamics* (2nd edn.). Cambridge Aerospace Series). Cambridge: Cambridge University Press.

Keuning, J. A. (1994) *The nonlinear behaviour of fast monohulls in head waves*. Technische Universiteit.

KHMedia (2011) hydroplane amphibian Beriev Be-103 at Hydro Air Show 2010. Available at: https://www.youtube.com/watch?v=0m1YisSZCEY. (Accessed, 22 May 2023)

Khoo B.C. and Koe H. B. (2016) 'The hydrodynamics of the WIG (Wing-In-Ground) effect craft', *2016 IEEE International Conference on Underwater System Technology: Theory and Applications (USYS),* pp.195–200.

Kihara, H. (2004) 'Numerical Models of Water Impact', *Proc.4th Int. Conf. on High-Performance Marine Vehicles*, pp.200–214.

Kihara, H. (2006) 'A Computing Method for the Flow Analysis around a Prismatic Planing-Hull', *Proc.5th International Conference on High-Performance Marine Vehicles,* pp.262-272.

Kornev, N. (2019) 'On unsteady effects in WIGCraft aerodynamics', *International Journal of Aerospace Engineering, 2019,* 8351293. https://doi.org/10.1155/2019/8351293.

Kornev, N. and Matveev, K. (2003) 'Complex numerical modelling of dynamics and crashes of Wing-in-Ground vehicles', In *41st Aerospace Sciences Meeting and Exhibit*. https://doi.org/10.2514/6.2003-600.

Kornev, N. V, Kleinsorge, L. and Migeotte, G. (2010) 'Dynamics and stability of racing boats with air wings' *International Journal of Aerodynamics*, https://doi.org/10.1504/IJAD.2010.031700

Korvin-Kroukovsky, B. V. (1950) 'Lift of Planing Surfaces', *Journal of the Aeronautical Sciences, 17,* pp. 597–599.

Korvin-Kroukovsky, B. V. and Jacobs, W. R. (1957) 'Pitching and heaving motions of a ship in regular waves', *SNAME Transactions, 65*.

Kowalyshyn, D. H. and Metclaf, B. (2006) 'A USCG systematic series of high-speed planing hulls', *Trans. SNAME, 114*.

Kring D. (1978) *Investigation of the Zarnick Nonlinear Model of planing Craft Motions*. NACA Report No. 786.

Kumar, P. E. (1967) *Stability of ground effect wings; A preliminary survey of theoretical and experimental techniques*. CoA Report Aero No. 196.

Kwag, S.H. (2001) 'Lift/drag prediction of 3-dimensional WIG moving above free surface', *KSME International Journal, 15*, pp. 384–391. https://doi.org/10.1007/BF03185222

Lai, C. and Troesch, A. W. (1996) 'A vortex lattice method for high-speed planing' *International Journal for Numerical Methods in Fluids*, *22*(6), pp.495–513. https://doi.org/https://doi.org/10.1002/(SICI)1097-0363(19960330)22:6<495: AID-FLD353>3.0.CO;2-R

Latorre, R. (1983) 'Study of prismatic planing model spray and resistance components', *Journal of Ship Research*, *27*(3), pp.187–196.

Latorre, R., & Ryan, S. (1989) 'Dimensional and similitude analysis of spray blister sheet from prismatic planing models. *Ocean Engineering*, *16*(1), pp. 71–83.

Lewandowski E.M. *The dynamics of Marine Craft, Maneuvering and Seakeeping.* World Scientific Publishing Co. Pte Ltd, Singapore (2004).

Liang, H., Zong, Z. and Zou, L. (2013a) 'Nonlinear lifting theory for unsteady WIG in proximity to incident water waves. Part 1: Two-dimension', *Applied Ocean Research, 43*, pp. 99–111. https://doi.org/https://doi.org/10.1016/j.apor.2013.07.002

Liang, H., Zong, Z. and Zou, L. (2013b) 'Nonlinear lifting theory for unsteady WIG in proximity to incident water waves. Part 2: Three-dimension', *Applied Ocean Research, 43*, pp. 88–98. https://doi.org/https://doi.org/10.1016/j.apor.2013.07.003

Lin, W. C., & Day, W. G. (1974) 'The still-water resistance and powering characteristics of SWATH ships', In *AIAA/SNAME Advanced Marine Vehicle. Conf.: pp. 74-325*.

Locke, F. W. S. Jr. and B. H. L. (1943) *A Method for Making Qualitative Studies of the Main Spray Characteristics of Flying-Boat Hull Models*. NACA Report No. 232.

Locke F.W.S Jr. (1948). *Observations on British flying boat research and development*. NACA Report, No. 1048.

Longuet-Higgins, M. S. and Cokelet, E. D. (1976) 'The deformation of steep surface waves on water - A numerical method of computation', *Proceedings of the Royal Society of London. A. Mathematical and Physical Sciences*, *350*(1660), pp. 1–26. https://doi.org/10.1098/rspa.1976.0092

Lugni C., Colagrossi A., Landrini M. and Faltinsen O.M. (2004) 'Experimental and numerical study of semi-displacement monohull and catamaran in calm water and incident waves' *Proc. 25th Symposium on Naval Hydrodynamics*.

Maki K.J., Doctors L.J, Beck R.F. and Troesch A.W. (2005) 'Transom-stern flow for high speed craft', *proceeding of the eight international conference on Fast Sea Transportation (FAST 2005)*, Saint Petersburg, Russia.

Mackie, A. G. (1962) 'A linearized theory of the water entry problem', *Quarterly Journal of Mechanics and Applied Mathematics*, *15*, pp.137–151.

Mantle P.J. (2016) 'Induced drag of wings in ground effect' *The Aeronautical Journal. Royal Aeronautical Society*, *120*(1234), pp.1867–1890.

Martin, M. (1978) 'Theoretical prediction of motions of high-speed planing boats in waves', *Journal of Ship Research, 22*, pp.140–169.

Maskalik, A. I. and Rozhdestvensky, K. V. A. (1998) 'View of the present state of research in aero- and hydrodynamics of Ekranoplans', *RTO AVT Symposium on Fluid Dynamics Problems of Vehicles Operating near or in the Air-Sea Interface*.

McBride, E. E. (1956) *An experimental investigation of the scale relations for the impinging water spray generated by a planing surface.* NACA Technical Note 3615.

McGregor R.C., Chun H.H., Djatmiko E.B. and Jones A.H. (1990) 'On modelling the hydrodynamic behaviour of SWATH vessels', *Int. Conf. on Modelling~ and Control of Marine Vehicles*.

Mei, X., Liu, Y. and Yue, D. K. P. (1999) 'On the water impact of general two-dimensional sections' *Applied Ocean Research*, *21*(1), pp. 1–15. https://doi.org/https://doi.org/10.1016/S0141-1187(98)00034-0

Mercier, J. A. and Savitsky. D. (1973) *Resistance of transom stern craft in pre-planing regime.* Davidson Laboratory Report 1667.

Migeotte, G., Kornev, N., Hoppe, K. G. and Nesterova, A. V. (2005) 'Design of hydrofoil assisted catamarans using a non-linear vortex lattice method' *Journal of Marine Engineering, 1*(2).

Molina, J., Zhang, X. and Alomar, A. (2016) 'Aerodynamics of a pitching and heaving airfoil in ground effect', *AIAA Journal, 54*(4), pp.1158–1171. https://doi.org/10.2514/1.J053350

Morabito M.G. (2010) '*On the spray and bottom pressures of planing surfaces*. Stevens Institute of Technology.

Morino Luigi and Kuo Ching-Chiang (1974) 'Subsonic potential aerodynamics for complex configurations: A general theory. *AIAA Journal, 12*(2), pp. 191–197.

Munk M.M. (1924) *The aerodynamic forces on air-ship hulls.* NACA Technical Report 184.

Newman, J. (1982) 'Analysis of small-aspect-ratio lifting surfaces in ground effect', *Journal of Fluid Mechanics, 117*, pp. 305-314. doi:10.1017/S0022112082001645

Newman J. N. (2018) *Marine Hydrodynamics*. The MIT Press.

Ogilvie T.F. (1967) '*Nonlinear High Froude Number Free Surface Problems*', Journal of Engineering Mathematics 1, pp. 215–235

Orfanidis, S. J. (1996) *Introduction to Signal Processing*. Prentice-Hall.

Paek, C. S. (2006) *The viability of commercializing Wing-In-Ground (WIG) craft in connection with technical, economic and safety aspects followed by IMO legislation*. World Maritime University.

Panagiotis Zagklis (2017) *Orion 14*. Available at: https://www.youtube.com/watch?v=hMUTHXPnl_g. (Accessed, 22 May 2023).

Payne, P. R. (1974) 'Coupled pitch and heave porpoising instability in hydrodynamic planing' *Journal of Hydronautics, 8*(2), pp.58–71. https://doi.org/10.2514/3.62979.

Payne, P. R. (1994) 'Recent developments in "added mass" planing theory', *Ocean Engineering, 21*(3), pp. 257–309. https://doi.org/https://doi.org/10.1016/0029-8018(94)90002-7.

Payne, P. R. (1995) ‘Contributions to planing theory’, *Ocean Engineering*, *22*(7), pp. 699–729. https://doi.org/https://doi.org/10.1016/0029-8018(94)00033-4.

Pereowei Garrick O; Hu Z. and Song L. (2020) ‘Simulating the acceleration to take-off phase of a WIGcraft using results of a constrained experiment’, *Proceedings of the ASME 2020 39th International Conference on Ocean, Offshore and Arctic Engineering.* Ocean Engineering, Volume *6B:*(V06BT06A014. ASME).

Pereowei G.O. (2023) ‘On the maximum efficiency draught of waterborne IGcraft’, *Proceedings of the Thirty-third (2023) International Ocean and Polar Engineering (ISOPE) Conference*, Ottawa, Canada, June 19–23, 2022.

Peter Van Oossanen (1984) ‘Small-Waterplane-Area, Twin-Hull (Swath) Ships’, In *Status of hydrodynamic technology as related to model tests of high-speed marine vehicles (Section 3.1): Vol. Report 81/026*. DTNSRDC.

Pozrikidis, C. (2002) *A Practical Guide to Boundary Element Methods with the Software Library BEMLIB*. Chapman and Hall/CRC. CRC press LLC.

Radojčić, D. (2019) *Resistance and Dynamic Trim Predictions.* In *Reflections on Power Prediction Modeling of Conventional High-Speed Craft* (pp. 17–49). Springer International Publishing. https://doi.org/10.1007/978-3-319-94899-7_3

Radojcic, D. and Kalajdzic, M. (2017) ‘Resistance and trim modeling of Naples hard chine systematic series’, *The International Journal of Small Craft Technology, 160,* pp.31–41.

Radojcic, D., Morabito, M., Simić, A. and Zgradić, A. (2014) ‘Modeling with regression analysis and artificial neural networks the resistance and trim of series 50 experiments with V-bottom motorboats’ *Journal of Ship Production and Design*, *30*. https://doi.org/10.5957/JSPD.30.4.140011.

Raymer. D. (2006) *Aircraft design: A conceptual approach* (4th edn.). AIAA education series American Institute of Aeronautics and Astronautics.

Raymond A.E. (1921) *Ground Influence on Airfoils.* NACA Technical Report 265.

Razola, M., Rosén, A. and Garme, K. (2014) ‘Allen and Jones revisited’, *Ocean Engineering*, *89*, pp. 119–133. https://doi.org/https://doi.org/10.1016/j.oceaneng.2014.07.005

Renilson, M. (2007) ‘Predicting the hydrodynamic performance of very high-speed craft-a note on some of the problems’, *The International Journal of Small Craft Technology, 149*. https://doi.org/10.3940/rina.ijsct.2007.b1.6407

Rozhdestvensky, K. V. (2006) ‘Wing-in-ground effect vehicles’, *Progress in Aerospace Sciences*, *42*(3), pp. 211–283. https://doi.org/https://doi.org/10.1016/j.paerosci.2006.10.001

Ruscelli, D. (2009) *Dynamics of High-Speed Craft*. University of Genova.

Salvesen, N., Tuck, E. O. and Faltinsen, O. M. (1970) ‘Ship motions and sea loads’, *SNAME Transactions*.

Sargent T.P. and Kaplan P. (1974) *Modifications to Llyods Register of Shipping Strip Theory Computer Program (LR 2570)*, Technical Report 74-103 (1974), Oceanics Inc.

Tomotika, S., Nagamiya, T. and Takenouti, Y. (1933) 'The lift on a flat plate placed near a plane wall, with special reference to the effect of the ground upon the lift of a monoplane aerofoil', *Res. Inst.* Tokyo 97, 1–60

Savitsky, D. (1964) 'Hydrodynamic Design of Planing Hulls', *Marine Technology, 1*, pp. 71–95.

Savitsky D. (2003) *On the subject of high-speed monohulls*. Greek Session, SNAME.

Savitsky, D. and Breslin, J. (1958) *On the Main Spray Generated by Planing Surfaces. NACA* Report 678.

Savitsky, D., DeLorme, M. F. and Datla, R. (2007) 'Inclusion of whisker spray drag in performance prediction method for high-speed planing hulls. *Marine Technology and SNAME News*, *44*(01), pp. 35–56. https://doi.org/10.5957/mt1.2007.44.1.35

Savitsky, D. and Dingee, D. A. (1954) 'Some interference effects between two flat surfaces planing parallel to each other at high speed', *Journal of the Aeronautical Sciences*, *21*(6), pp.419–420. https://doi.org/10.2514/8.3057

Savitsky, D. and Morabito M.G. (2010) 'Origin and characteristics of the spray patterns generated by planing hulls', *Journal of Ship Production and Design*, *27*, pp. 63–83.

Serebriyskiy Ya M. (1939) *Experimental Study of vertical approach to a flat plate and indicial approach of a wing to the ground*. Ibid, No 442.

Shi, G., Xiao, Q. and Boulougouris, E. (2021) 'Ground effects on the propulsion of an undulating pectoral fin with various aspect ratios', *Journal of Fluids and Structures, 106*, 103388. https://doi.org/https://doi.org/10.1016/j.jfluidstructs.2021.103388

Shoemaker J. (1934) *Tank Tests of Flat and V-Bottom Planing Surfaces.* NACA Technical Notes, No. 509.

Shuford, C. L. (1957) *A theoretical and experimental study of planing surfaces including effects of cross section and plan form*. NACA Technical Notes, No. 3939.

Smiley, R. F. (1951a) *A Semiempirical Procedure for Computing the Water-Pressure Distribution on Flat and V-Bottom Prismatic Surfaces During Impact or Planing*. NACA Technical Notes, No. 2683

Smiley, R. F. (1951b) *An Experimental Study of the Water-Pressure Distributions During Landings and Planing of a Heavily Loaded Rectangular Flat-Plate Model*. NACA Technical Notes, No. 2453

Sottorf W. (1932) *Experiments with Planing Surfaces*. NACA Technical Notes, No. 661

Sottorf, W. (1944) *Analysis of experimental investigations of the planing process on the surface of water.* NACA Report, No. 1061.

Staufenbiel R.W. (1987) 'On the design of stable ram wing vehicles', *The Royal Aeronautical Society Symposium Proceedings*, pp.110–136.

Suh W.B. and Ostowari C. (1988) 'Drag reduction factor due to ground effect', *Journal of Aircraft, 25*(11).

Sun, H. and Faltinsen, O. M. (2007) 'The influence of gravity on the performance of planing vessels in calm water', *Journal of Engineering Mathematics*, *58*(1), pp. 91–107. https://doi.org/10.1007/s10665-006-9107-5

Tanizawa K. (1995) 'A nonlinear simulation method of 3-D body motions in waves', *Journal of the Society of Naval Architects of Japan*, 178, pp. 179–191.

Tanizawa, K. (1996) 'Long time fully nonlinear simulation of floating body motions with artificial damping zone', *Journal of the Society of Naval Architects of Japan, 180*, pp. 211–319.

Tassin, A., Korobkin, A. A. and Cooker, M. J. (2014) 'On analytical models of vertical water entry of a symmetric body with separation and cavity initiation', *Applied Ocean Research, 48*, pp.33–41. https://doi.org/https://doi.org/10.1016/j.apor.2014.07.008

Taylor, C. D. and Nicolas, D. P. (1989) 'An adaptive data-smoothing routine', *Computers in Physics*, *3*, pp.63–64.

Tuck, E. O. (1984). *Small-Gap Flows*. Report NAOE 84-1.

Tuck E.O. (1975) 'On airflow over free surfaces of stationary water', *Journal of Australian Mathematical Society, Series B, 19*, pp.66–80.

Tuck E.O. (1984) 'A simple one-dimensional theory for air-supported vehicles over water', *Journal of Ship Research, 28*, pp.290–292.

Tulin, M. P. (1957) 'The Theory of Slender Surfaces Planing at High Speeds', *Schiffstechnik, 4*, pp. 125–133.

Tulin, M.P. and Hsu, C.C. (1986) 'Theory of high-speed displacement ships with transom sterns', *Journal of Ship Research, 30*, pp.186-193.

Valentine, J. R. and Decker, R. A. (1995) 'A Lagrangian-Eulerian scheme for flow around an airfoil in rain', *International Journal of Multiphase Flow*, *21*(4), pp. 639–648. https://doi.org/https://doi.org/10.1016/0301-9322(95)00007-K

van Daalen E.F.G. (1993) *Numerical and theoretical studies of water waves and floating bodies*. Universiteit Twente.

Volker Bertram. (2012) *Practical Ship Hydrodynamics* (second). Butterworth-Heinemann publications.

von Karman T. (1930) *Calculation of Pressure Distribution on Airship Hulls.* NACA, T.M. NO. 574.

von Mises R. (1959) *Theory of flight*. New York: Dover Publications.

Vorus S. W. (2017) *Hydrodynamics of planing monohull watercraft*. Springer International Publishing.

Wadlin Kermeth L. and McGehee John R. (1950) *Planing characteristics of six surfaces representative of hydro-ski forms*. NACA RM L9L20.

Wadlin Kermeth L. and McGehee John R. (1950) *Planing characteristics of three surfaces representative of hydro-ski forms*. NACA L9C03.

Wagner, H. (1936) ‘Phenomena associated with impacts and sliding on liquid surfaces’, *NACA Library, Langley Aeronautical Laboratory. Translation of: Wagner, H., 1932. Über Stoß Und Gleitvorgänge an Der Oberfläche von Flüssigkeiten. Zeitschrift Für Angewandte Mathematik Und Mechanik*, *12*, pp.193–215.

Wang, Q.-X. (1991) ‘Flow around an unsteady thin wing close to curved ground’, *Journal of Fluid Mechanics*, *226*, pp. 175–187. https://doi.org/DOI: 10.1017/S0022112091002331

Wehausen J.V. (1960). ‘Surface Waves in Fluid Dynamics III’: In S. Flugge and C. Truesdell (Eds.), *Handbuch der Physik*, 9, pp. 446–778, Springer Verlag.

Weinstein I. and Kapryan W.J. (1953) *The high-speed planing craft characteristics of a rectangular flat plate over a wide range of trim angle and wetted length.* NACA Technical Report No. 2981.

Widnall S.E. and Barrow T.M. (1970) ‘An analytical solution for two- and three-dimensional wings in ground effect’, *Journal of Fluid Mechanics*, *41*, pp. 769–792.

Wieselsberger C. (1922). *Wing resistance near the ground.* NASA, NACA-TM-77.

Wu, G. X., Sun, H. and He, Y. S. (2004) ‘Numerical simulation and experimental study of water entry of a wedge in free fall motion’, *Journal of Fluids and Structures*, *19*(3), pp. 277–289. https://doi.org/https://doi.org/10.1016/j.jfluidstructs.2004.01.001

Wu G.X. and Taylor, E. R. (1996) ‘Transient motion of a floating body in steep water waves’, *Proc. 11th Int. Workshop on Water Waves and Floating Bodies*, 219–223. https://cir.nii.ac.jp/crid/1573950401090351488

Yang, W., Yang, Z. and Collu, M. (2015) ‘Longitudinal static stability requirements for wing in ground effect vehicle’ *International Journal of Naval Architecture and Ocean Engineering*, *7*(2), pp. 259–269. https://doi.org/https://doi.org/10.1515/ijnaoe-2015-0018

Yang, Z., Yang, W. and Qing, J. (2010) ‘Ground viscous effect on 2D flow of wing in ground proximity. *Engineering Applications of Computational Fluid Mechanics*, *4*, pp. 521–531. https://doi.org/10.1080/19942060.2010.11015338

Yettou, E.M., Desrochers, A. and Champoux, Y. (2007) ‘A new analytical model for pressure estimation of symmetrical water impact of a rigid wedge at variable velocities’, *Journal of Fluids and Structures*, *23*(3), pp. 501–522. https://doi.org/https://doi.org/10.1016/j.jfluidstructs.2006.10.001

Yun, L., Bliault, A. and Doo, J. (2010) *WIG Craft and Ekranoplan*. Springer International Publishing

Zaghi, S., Broglia, R. and di Mascio, A. (2011) ‘Analysis of the interference effects for high-speed catamarans by model tests and numerical simulations’ *Ocean Engineering*, *38*(17), pp. 2110–2122. https://doi.org/https://doi.org/10.1016/j.oceaneng.2011.09.037

Zarnick, E. E. (1978). *A nonlinear mathematical model of motions of a planing boat in regular waves*. David W. Taylor Naval Ship Research and Development Center

Zhang, R.M. and Cao, Y. (2010) ‘Study of aerodynamic characteristics of an airfoil in rain’, *Hangkong Dongli Xuebao, Journal of Aerospace Power*, *25*, pp. 2064–2069.

Zhao, R. and Faltinsen, O. (1993) ‘Water entry of two-dimensional bodies’, *Journal of Fluid Mechanics*, *246*, pp. 593–612. https://doi.org/DOI: 10.1017/S002211209300028X

Zhao, R., Faltinsen, O. M. and Aarsnes, J. (1996) ‘Water entry of arbitrary two-dimensional sections with and without flow separation’, *Proceedings of the 21st Symposium on Naval Hydrodynamics*.

Zhao, R., Faltinsen, O. M. and Haslum, H. (1997) ‘A simplified non-linear analysis of a high-speed planing craft in calm water’, *Proc. FAST’97*.

Zhukov V.I. (1993) ‘Specific Features of Dynamics of Ekranoplan’, *Proceedings of the 1st International Conference of Ekranoplans*.

Zong, Z., Liang, H. and Zhou, L. (2012) ‘Lifting line theory for wing-in-ground effect in proximity to a free surface’, *Journal of Engineering Mathematics*, *74*(1), pp. 143–158. https://doi.org/10.1007/s10665-011-9497-x

Appendices

Appendix A

Table A1 Experimental Matrices

Stand. Order	Run Order	Speed	Trim Angle	Designation	Stand. Order	Run Order	Speed	Trim Angle	Designation
6mm above Free Surface									
1	2	5.0	4	CMT_S50T4D-6	4	4	5.0	0	CMT_S50T0D-6
2	1	5.5	4	CMT_S55T4D-6	5	6	5.0	2	CMT_S50T2D-6
3	3	5.5	0	CMT_S55T0D-6	6	5	5.5	2	CMT_S55T2D-6
Draught = 0mm									
1	1	4.5	0	CMT_S45T0D0	7	7	5.5	6	CMT_S55T6D0
2	3	5	0	CMT_S50T0D0	8	9	5	6	CMT_S50T6D0
3	2	5.5	0	CMT_S55T0D0	9	8	4.5	6	CMT_S45T6D0
4	4	5.5	4	CMT_S55T4D0	10	10	5.5	2	CMT_S55T2D0
5	5	4.5	4	CMT_S45T4D0	11	11	4.5	2	CMT_S45T2D0
6	6	5	4	CMT_S50T4D0	12	12	5	2	CMT_S50T2D0
Draught = 15mm									
1	1	4.5	0	CMT_S45T0D15	9	9	5.5	6	CMT_S55T6D15
2	4	4.0	0	CMT_S40T0D15	10	12	4.0	6	CMT_S40T6D15
3	2	5.5	0	CMT_S55T0D15	11	10	4.5	6	CMT_S45T6D15
4	3	5.0	0	CMT_S50T0D15	12	11	5.0	6	CMT_S50T6D15
5	8	4.0	4	CMT_S40T4D15	13	16	4.0	2	CMT_S40T2D15
6	5	5.5	4	CMT_S55T4D15	14	13	5.5	2	CMT_S55T2D15
7	7	5.0	4	CMT_S50T4D15	15	14	4.5	2	CMT_S45T2D15
8	6	4.5	4	CMT_S45T4D15	16	15	5.0	2	CMT_S50T2D15
Draught = 35mm									
1	1	4.5	0	CMT_S45T0D35	15	15	5.5	6	CMT_S55T6D35
2	3	2.5	0	CMT_S25T0D35	16	18	4.5	6	CMT_S45T6D35
3	7	5.5	0	CMT_S55T0D35	17	16	3.0	6	CMT_S30T6D35
4	6	3.0	0	CMT_S30T0D35	18	21	2.0	6	CMT_S20T6D35
5	4	5.0	0	CMT_S50T0D35	19	19	5.0	6	CMT_S50T6D35
6	2	2.0	0	CMT_S20T0D35	20	17	2.5	6	CMT_S25T6D35
7	5	4.0	0	CMT_S40T0D35	21	20	4.0	6	CMT_S40T6D35
8	8	5.5	4	CMT_S55T4D35	22	22	5.5	2	CMT_S55T2D35
9	12	4.5	4	CMT_S45T4D35	23	23	2	2	CMT_S20T2D25
10	14	3.0	4	CMT_S30T4D35	24	27	2.5	2	CMT_S25T2D35
11	10	2.0	4	CMT_S20T4D35	25	28	3	2	CMT_S30T2D35
12	5	5.0	4	CMT_S50T4D35	26	26	4	2	CMT_S40T2D35
13	9	2.5	4	CMT_S25T4D35	27	25	4.5	2	CMT_S45T2D35
14	11	4.0	4	CMT_S40T4D35	28	24	5	2	CMT_S50T2D35
Draught = 65mm									
1	6	3.0	0	CMT_S30T0D65	15	21	2.0	6	CMT_S20T6D65
2	7	5.5	0	CMT_S55T0D65	16	16	3.0	6	CMT_S30T6D65

3	4	5.0	0	CMT_S50T0D65	17	19	5.0	6	CMT_S50T6D65
4	5	4.0	0	CMT_S40T0D65	18	20	4.0	6	CMT_S40T6D65
5	1	4.5	0	CMT_S45T0D65	19	15	5.5	6	CMT_S55T6D65
6	3	2.5	0	CMT_S25T0D65	20	18	4.5	6	CMT_S45T6D65
7	2	2.0	0	CMT_S20T0D65	21	17	2.5	6	CMT_S25T6D65
8	10	2.0	4	CMT_S20T4D65	22	28	3.0	2	CMT_S30T2D65
9	12	4.5	4	CMT_S45T4D65	23	23	2.0	2	CMT_S20T2D65
10	8	5.5	4	CMT_S55T4D65	24	22	5.5	2	CMT_S55T2D65
11	11	4.0	4	CMT_S40T4D65	25	24	5.0	2	CMT_S50T2D65
12	14	3.0	4	CMT_S30T4D65	26	27	2.5	2	CMT_S25T2D65
13	5	5.0	4	CMT_S50T4D65	27	26	4.0	2	CMT_S40T2D65
14	9	2.5	4	CMT_S25T4D65	28	25	4.5	2	CMT_S45T2D65

Table A2. Uncertainty in measured lift coefficients of WIGcraft and Outrigger models

WIGcraft Model Lift Coefficient				**Outrigger Model Lift Coefficient**		
Relative Ground clearance height, h/c	Draught (m)	Trim Angle (deg)	Mean Combined Uncertainty (%)	Draught (m)	Trim Angle (deg)	Mean Combined Uncertainty (%)
0.000117	0.065	0	5.30	0.065	0	4.22
		2	1.81		2	5.87
		4	1.06		4	2.82
		6	0.93		6	3.55
0.057096	0.035	0	1.67	0.035	0	15.05
		2	1.87		2	6.62
		4	2.31		4	2.35
		6	1.61		6	2.03
0.090	0.015	0	13.54	0.015	0	6.16
		2	19.72		2	15.59
		4	5.45		4	2.91
		6	2.78		6	1.52
0.114	0	0	111.12	0	0	39.68
		2	22.89		2	30.42
		4	10.86		4	8.13
		6	6.73		6	2.70
0.124	-0.006	0	95.99	-0.006	0	67.37
		2	23.82		2	27.99
		4	7.40		4	9.67

Table A3. Uncertainties in measured drag coefficients of WIGcraft and Outrigger models.

WIGcraft Model Drag Coefficient				**Outrigger Model Drag Coefficient**		
Relative Ground clearance height, h/c	Draught (m)	Trim Angle (deg)	Mean Combined Uncertainty (%)	Draught (m)	Trim Angle (deg)	Mean Combined Uncertainty (%)
0.000117	0.065	0	4.58	0.065	0	0.34
		2	3.31		2	1.01
		4	1.75		4	1.40
		6	1.28		6	1.59
0.057096	0.035	0	5.10	0.035	0	4.35
		2	7.59		2	4.41
		4	7.71		4	2.87
		6	5.86		6	3.81
0.090	0.015	0	15.49	0.015	0	6.16
		2	18.57		2	9.76
		4	6.627		4	10.78
		6	5.47		6	9.27
0.114	0	0	35.20	0	0	33.02
		2	7.35		2	39.72
		4	18.13		4	27.11
		6	8.43		6	19.79
0.124	-0.006	0	79.26	-0.006	0	69.10
		2	45.56		2	55.86
		4	36.33		4	46.74

Appendix B

Table B.1 C_{fe} values (Raymer, 2012)

Vehicle	C_{fe}
Bomber and civil transport	0.0030
High upsweep fuselage military cargo	0.0035
Airforce Fighter	0.0035
Navy Fighter	0.0040
Single engine light airplane	0.0055
Twin engine light airplane	0.0045
Propeller seaplane	0.0065
Jet seaplane	0.0040

Appendix C: Comments on the Computer Code for the Hydrodynamic model

The length of the Outrigger model was discretized such that the space between adjacent sections is 1cm apart. This small interval was used to allow the program to capture the geometric variations of the hull sections during the implementation of the 2D+t theory. To simplify and keep track of the nodes of the boundary elements, each of the boundary segments of the Outrigger transverse sections are discretized into 25 elements.

The current version of the main program and various functions implemented in the hydrodynamic model code to solve the BVP are briefly described below.

outrg.m

The outrg.m is the main program of the hydrodynamic code that calls the other functions when needed. The main programme reads the data files (including geometric and boundary conditions) of each boundary segment and distinguishes between when monohull (draught $\leq$ 0.015m) and multi-hull (draught $\geq$ 0.015m) analysis are to be carried out. This program also keeps track of each transverse section domain boundary (or station along ship model) analysed and calls in the next station to be analysed. The outrg.m ensures that the BEM requirements are met, and all boundary segments are properly linked. In this program, all the nodes of each element are given identification numbers to keep track of the values of the unit normal, size of elements between nodes, velocity potential and its normal derivative at the collocation points as well as track evolution of the free surface. The free surface evolution, numerical treatments on the spray jet, regridding and smoothing of the free surface contour as well as calculation of the pressure distribution. and total force on the hull section domain boundaries are carried out in this program.

genmsh.m

This function takes geometric input data of the segments and discretises each segment of the monohull or multihull section domain boundary into a desired number of elements.

outrgbc.m

This program assigns the specified boundary conditions stated in chapter to collocation point of each element, segment by segment. The program is capable of distinguishing between a monohull and a multihull when assigning the boundary conditions.

outrgfrm.m

This program takes the boundary conditions specified on the elements from the o*utrgbc.m* and calculates the influence coefficients of the Neumann and Dirichlet boundary elements stated in chapter 3. The influence coefficients are arranged in a matrix format.

potout.m

This function calculates the unknown potentials and normal derivatives of the potentials on the Neumann and Dirichlet boundary elements on the hull and free surface using a linsolve.m function in MATLAB.

fsevo.m

This function considers the coordinates of the collocation points, the velocity potential and its normal derivative at the collocation point of each element of the free surface segment. It calculates the y and z coordinate derivatives of the velocity potential on the free surface segment before handing its output to the main program to calculate the free surface evolution and the pressure distribution on the hull section domain boundary.

Appendix D: Comments on the Computer Code for the Ground Effect Aerodynamic model

The discretization scheme used on the airborne WIGraft in the aerodynamic code is similar to that described for the hydrodynamic model except that the entire WIGcraft model is discretised as against only the submerged portion of the hull in the hydrodynamic model. Spaces between adjacent transverse sections are 1cm apart. The segment of the WIGcraft follows that described in chapter 4 with each segment also discretized into 25 elements.

The discretization of the free surface is similar to that in the hydrodynamic code. However, it is more straightforward in absence of the submerged hull section. To implement the procedure described in chapter 4, two main programs (*airdm.m* and *waterdm.m*) and a mother program (*intdm.m*) were written.

waterdm.m

This code as the main code to the solve the BVP in the water domain performs similar function as the *outrg.m,* except that portion of the o*utrg.m* which includes hull section segments are excluded. The *genmsh.m* function was used to discretize the segments of the water domain boundaries as stated in chapter 3. The *wadmbc.m* function is a replica of the outrgbc function in the hydrodynamic code. It assigns the specified boundary conditions to the nodes of the elements on each segment of the domain. The *wafrm.m* calculates the influence coefficients in the water domain while *wapot.m* calculates the unknown potentials and normal derivatives of the potential. The *fsevo.m* is used to determine the y and z derivatives of the velocity potential which are then returned to the main program *waterdm.m* to calculate the free surface evolution on the free surface domain boundary.

airdmbc.m

This is the main program that solves the BVP in the air domain. It performs similar function as the main code in the hydrodynamic model. The location of the far field boundary segment beneath the wings in the air domain is used to control the relative clearance height of the WIGcraft from the water domain. The *airdmbc.m* hosts functions similar to *genmsh.m, outrgfrm.m* and *potout.m* in the hydrodynamic model. The *airpot.m* returns the calculated potentials and its normal derivatives to the *airdmbc.m* main program to calculate the pressure

distribution and total force on the upper and lower portion of the WIGcraft section domain boundary.

intdm.m

The *intdm.m* is the mother code that integrates the *airdm.m* and *waterdm.m* at the air-water interface. The momentum transfer or exchange process between the air domain and water domain stated in chapter 4 is implemented in the code. At each time step, the *intdm.m* takes the output from both *airpot.m* and *wapot* to solve equation 4.17 in an iterative manner.

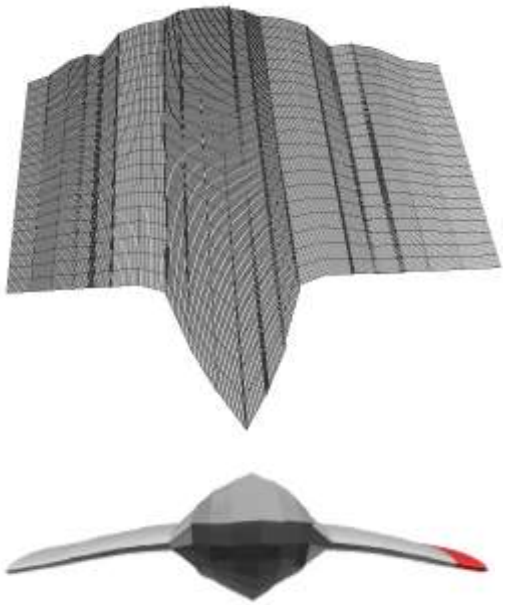

D1. Autowing model

Appendix E: Comments on the Computer Code for the Aero-Hydrodynamic model

The aero-hydrodynamic computer code is very similar to the aerodynamic code except the *waterdm.m* code is replaced by the main function of the hydrodynamic code, *outrg.m*. The mother code, *intdm.m* integrates both the a*irpot.m and potout.m* functions as noted on the comments on the aerodynamic model.